

Rational Design of Novel Antibody Decorated Nanoparticles Targeting Breast Cancer Cells

A thesis submitted for the degree of
Philosophiae Doctor in Cardiff
University
By

Saeed Mohammed Tayeb

January 2022
Cardiff School of Pharmacy and
Pharmaceutical Sciences
Cardiff University

Abstract

Every year there are over 50,000 new cases of breast cancer in UK, which represents the most common UK cancer (CR-UK). Despite significant advances in anti-breast cancer treatments, there is still a need for improved therapeutics to overcome drug resistance. HER2 (Human Epidermal Growth Factor Receptor 2) is a transmembrane oncoprotein encoded by the HER2/neu gene and overexpressed in approximately 20 to 30% of invasive breast cancers. Tumours overexpressing HER2 are more aggressive and carry a poor prognosis; thus, the receptor is a priority therapeutic target. One targeting entity is Trastuzumab (Tz), a monoclonal antibody recognized as one of the most effective agents against HER2+ breast cancer and has also been attached to chemotherapeutics to form antibody-drug conjugate (ADC). These ADCs, such as Kadcyła®, require cell binding to HER2 and access to the cell interior by endocytosis to release the payload. HER2 is, however, commonly termed the "endocytosis deficient" member of the HER family of receptors, thus challenging attempts to design ADCs that need access to lysosomes for drug release and activity.

Previous studies in the laboratory showed that HER2 endocytosis was significantly promoted with concomitant lysosomal delivery and degradation via Tz-mediated crosslinking, and this presented work lies under the hypothesis that nanoparticles (NPs) decorated with sufficient numbers of Tz could also cause HER2 cross-linking, endocytosis, and HER2 degradation. Later data showed that HER2 crosslinking induced a form of endocytosis termed macropinocytosis to drive cell entry. The work presented initially investigated macropinocytosis as a process in different cell types and ways to inhibit this process using inhibitors targeting the sodium proton exchanger (NHE1) as a regulator of intracellular pH and this endocytic process. EIPA (5-(N-Ethyl-N-isopropyl) amiloride) as a macropinocytosis inhibitor, surprisingly significantly increased the internalisation of HER2; a result not observed with other NHE1 inhibitors amiloride and the more selective NHE1 inhibitor cariporide. EIPA was also shown to increase the uptake of the fluid phase and macropinocytosis marker dextran but had no effect on endocytosis of transferrin via clathrin-coated vesicles. The results suggest that EIPA targets need further analysis as modulators of HER2 internalisation and targets for breast cancer therapy.

Fluorescently labelled Tz- decorated Poly (lactic glycolic acid) NPs were then generated and found to be highly selective for HER2 expressing breast cancer cells over controls. Upon incubation with cells, the decorated NPs rapidly accumulated on the cell surface and also appeared as large intracellular structures suggestive of macropinosomes. Rhodamine and Doxorubicin encapsulated Tz-PLGA NPs were synthesised, showing their capacity to drive internalisation of the fluorophore and cytotoxic drug into vesicular structures, with the later formulation enhancing the cytotoxicity of the drug over its soluble counterpart.

Acknowledgement

First and foremost, I would like to express my gratitude to my primary advisor, Professor Arwyn Jones, for his continuous support, guidance, inspiration, encouragement, and patience during my PhD study. I am appreciative of his constant encouragement and vast expertise in the subject of cell biology, which enabled me to accomplish my research project.

I am particularly thankful to my co-supervisors, Professor. Andrew Westwell and Dr Youcef Mehellou, whose assistance and contributions have enriched the project.

The support and assistance provided by fellow lab members and friends: Dr Edd Sayers and Dr Jennifer Wymant, have been invaluable to the success of this project, and I am extremely grateful to both of them.

I would like to thank Dr Jared Whitehead, Dr Rohan Naryan, Carwyn Hughes, and Maria Edwards, and other researchers who I have met in Arwyn Jones group.

Thanks also to my colleagues from the School of Pharmacy, whose friendship, support, advice, and technical assistance have been essential to me on a personal and academic level.

Thanks, are also extended to Dr Pete Watson and his group, whose participation in lab meetings has been invaluable for troubleshooting and guiding the research. Special thanks to the Saudi Embassy in London and Umm Al-Qura University for funding my PhD project and for being so supportive during the entire course of my studies.

Finally, I would like to express my gratitude to Cardiff University and School of Pharmacy and pharmaceutical science for allowing me to pursue my PhD degree in higher education.

Table of Contents

Chapter 1 : General Introduction.....	1
1.1 Cancer	2
1.2 Breast Cancer (BC)	2
1.2.1 Epidemiology	2
1.2.2 Pathophysiology	3
1.2.3 BC Classification.....	5
1.2.4 Aetiology.....	7
1.2.5 Receptor Tyrosine Kinase and BC-The HER1-4 family	8
1.2.6 Human Epidermal Growth Factor Receptor 2:.....	12
1.2.7 HER2 and Cell Signalling.....	14
1.2.8 Treatment	15
1.2.8.1 Antibodies targeting HER2.....	19
1.2.9 HER2 Clustering	24
1.3 Endocytosis.....	25
1.3.1 Clathrin-mediated endocytosis (CME).....	26
1.3.2 Clathrin-independent endocytosis (CIE).....	29
1.3.2.1 Macropinocytosis.....	31
1.3.3 Endocytic Probes.....	32
Dextran.....	32
Transferrin.....	33

1.3.4 Chemical inhibitors of endocytosis	36
1.4 Nanoparticles	39
1.4.1 Nanoparticle Delivery Systems	39
1.4.2 Efficacy of Passive Nanoparticle Targeting	42
1.4.3 Nanoparticle targeted BC.....	44
1.4.4 Tz decorated NPs targeting BC.....	44
1.4.5 Materials for making NPs.....	44
1.5 Hypothesis, Aims, and Objectives	45
1.5.1 Hypothesis	45
1.5.2 Main aims, and objectives proposed for the project	48
1.5.3 Main experimental methods proposed for the project	48
Chapter 2 : Materials and Methods	49
2.1 Materials.....	50
2.2 Cell Culture	53
2.2.1 Routine Cell Maintenance	53
2.2.2 Freezing Cells.....	53
2.2.3 Thawing cells	54
2.2.4 Media.....	54
2.3 Live Cell Uptake Analysis	54
2.3.1 Cell Culture	54
2.3.2 Confocal Microscopy.....	55

Chapter 3 methodology.....	55
2.3.3 DEX uptake experiments as a fluid phase marker +/- Inhibitors	55
2.3.4 Transferrin Experiments as a marker for Clathrin Mediated Endocytosis	56
2.3.5 Fluorescence-Activated Cell Sorting (FACS)	56
2.3.6 DEX uptake experiments in the presence of macropinocytosis	56
2.3.7 Transferrin uptake in the presence of macropinocytosis inhibitors.	57
2.3.8 FACS Analysis	58
2.3.9 Dextran Uptake in BT474 and Clone5 BT474 cells	58
2.3.10 Transferrin uptake and recycling in BT474 and Clone5 BT474 cells.	59
Chapter 4 methodology.....	59
2.3.11 Generation and characterisation of fluorescent Alexa488 conjugated Tz	59
2.3.12 Analysis of Tz concentration	61
2.3.13 Tz488 binding HER2 downregulation and method optimization.....	62
2.3.14 Cell uptake of Tz488 in the presence of EIPA	62
2.3.15 Cell Mask +/- EIPA.....	63
2.3.16 Metabolic Activity Assays.....	63
Analysis of Metabolic Activity	63
Chapter 5 methodology.....	65
2.3.17 Synthesis of Rhodamine B (RhoB) / Doxorubicin (DOX) encapsulated Tz conjugated Poly (lactic-co-glycolic acid) (PLGA) nanoparticles.	65

2.3.17.1 RhoB encapsulated PLGA nanoparticles.	65
2.3.17.2 Doxorubicin (DOX) encapsulated PLGA nanoparticles.....	66
2.3.17.3 Tz conjugated PLGA NPs encapsulated RhoB/DOX.....	66
2.3.17.4 Dynamic Light Scattering (DLS) – Zeta Sizer.	67
2.3.17.5 DOX Encapsulation Efficiency (EE%)	68
2.3.17.6 Live cell imaging confocal analysis of NP binding and endocytosis.	69
2.3.17.7 Viability assay in cells incubated with PLGA NPs.....	69
2.3.18 Western blotting (W.B)	70
2.3.18.1 Cell culture.....	70
2.3.18.2 Lysate collection	70
2.3.18.3 Standard SDS-PAGE gel preparation	71
2.3.18.4 Protein transfer and ponceau staining.....	72
2.3.18.5 Protein detection by immunoblotting	73
2.3.18.6 Quantifications of Western Blots with ImageJ	73
2.4 Statistical Analysis.....	74
Chapter 3 : In Vitro studies of HER 2-internalisation	75
3.1 Introduction	76
3.1.1 Overview of HER 2 Internalisation	76
3.1.2 Macropinocytosis analysis using DEX prob in BC cell lines.....	77
3.1.3 Analysis of Clathrin Mediated Endocytosis in BC cell lines.....	78

3.1.4 Macropinocytosis inhibitors.....	79
3.1.4.1 F-actin-depolymerizing Agents.....	80
3.1.4.2 Inhibitors of Phosphoinositide Metabolism	81
3.1.4.3 Sodium Hydrogen Exchanger (NHE) inhibitor agents.....	81
3.2 Results and Discussion.....	84
3.2.1 Effect of amiloride on DEX 10 kDa internalisation in BC cell lines	84
3.2.2 Effect of EIPA on DEX 10 kDa internalisation in BC cell lines	87
3.2.3 Effect of EIPA on DEX 70 kDa internalisation in BC cell lines	90
3.2.4 Effect of cariporide on DEX 10 kDa in BC cell lines.....	96
3.2.5 Effect of amiloride on Transferrin in BC cell lines	98
3.2.6 Effect of EIPA on Tf in BC cell lines	100
3.2.7 Effect of cariporide on Tf in BC cell lines.....	102
3.2.8 Metabolic Activity Assays in BC cell lines treated with NHE1 inhibitors.	104
3.2.9 Metabolic Activity Assay (Solvents) in BC cell lines.....	107
3.2.10 Comparative analysis of CME, recycling, and fluid phase endocytosis in BT474 and Clone5 BT474 cells.....	110
3.2.11 CME and recycling of Transferrin in BT474 and Clone5 BT474 cells	110
3.2.12 Differences between BT474 and Clone5 BT474 in Dex uptake	113
3.3 Summary.....	117
Chapter 4 : Effects of Trastuzumab on Breast Cancer Cells	120

4.1 Introduction.....	121
4.1.1 Trastuzumab.....	122
4.1.2 Mechanism of Action of Tz.....	123
4.1.2.1 Tz and HER2 Dimerization.....	123
4.1.2.2 Tz, HER2 downregulation, and degradation.....	123
4.1.2.3 Tz and Cell Signalling	124
4.1.2.4 Tz and Cell Cycle.....	124
4.1.2.5 Tz and antibody-dependent cell-mediated cytotoxicity (ADCC).....	124
4.1.3 Tz Resistance	125
4.2 Results and Discussion.....	127
4.2.1 Tz conjugated Alexa 647.....	127
4.2.1.1 Amine crosslinker reactive groups	127
4.2.2 Tz488 binding and internalisation in BC cells	130
4.2.3 Time dependant Tz488 uptake and plasma membrane ruffling in BC cell lines.....	133
4.2.4 EIPA enhances Tz488 internalisation.....	136
4.2.4.1 Tz +/- EIPA in BC cell lines (Methods Optimized)	136
4.2.4.2 Method C: EIPA/Tz488 co-incubation.....	139
4.2.5 Cellular profile of CellMask in EIPA treated BC cell lines	143
4.2.6 Tz +/- Amiloride or cariporide co-incubated in BC cell lines.....	145
4.2.7 Metabolic Activity Assay (EIPA and Tz)	148

4.3 Summary	153
Chapter 5: Synthesis and in vitro analysis of Trastuzumab conjugated PLGA nanoparticles for targeting HER2	156
5.1 Introduction	157
5.1.1 Nanoparticles and Cancer.....	158
5.1.2 Polymeric nanoparticles	159
5.1.3 Poly (lactic-co-glycolic acid) – (PLGA).....	160
5.1.4 PLGA conjugated Tz.....	162
5.2 Results and Discussion.	166
5.2.1 Nanoparticles Preparations.....	166
5.2.2 Cellular uptake study	175
5.2.3 PLGA-RhoB-Tz488 binding and internalisation in BC cells	175
5.2.4 NP studies and plasma membrane labelling with CellMask.....	181
5.2.5 Influence of PLGA-T z NPs on HER2 Degradation	186
5.2.6 Metabolic Activity assay of PLGA-Tz488.....	189
5.2.7 PLGA encapsulated DOX attached to Tz	192
5.2.8 Metabolic activity of BC cells incubated with PLGA-DOX-Tz	202
5.3 Summary.....	204
Chapter 6: General Discussion	205
References.....	215
Appendix.....	245

List of Figures

Figure 1.1: Anatomy of Breast and BC Metastasis. Most breast cancers develop in the lactiferous (milk) ducts or lobules	4
Figure 1.2: HER family structure, differences, conformation change, and dimerization	10
Figure 1.3: HER2 promotes cancer cell proliferation, invasion, metastasis, and angiogenesis by activating the PI3K/Akt and Ras/Raf/MEK/ERK signalling cascades	15
Figure 1.4: Structure of HER2, binding sites of Tz and Pertuzumab	20
Figure 1.5: Tz Antibody increases ADCC's ability to destroy cancer cells	21
Figure 1.6: Biotinylated Antibody and Streptavidin complexes formation on cells	24
Figure 1.7: Different types of endocytosis mechanisms at the cell membrane, CME, CIE.....	26
Figure 1.8: EGFR receptor trafficking via Rabs.....	28
Figure 1.9: The process of macropinocytosis.....	31
Figure 1.10: TfR1 and Tf cycle of iron absorption via CME.	35
Figure 1.11: A schematic representation of the various nanoparticle properties that have been studied in cancer therapy to promote drug delivery	45
Figure 1.12: A schematic model of the hypothesised mechanism behind NP-mediated clustering of HER2	47
Figure 2.1: Protocol for RhoB/DOX encapsulated Tz conjugated Poly (lactic-co-glycolic acid) (PLGA) NPs.....	67
Figure 2.2: The chemical structures and the synthetic steps of PLGA conjugated Tz antibody using EDC/NHS chemistry.....	68

Figure 3.1: NHE inhibitor structures of amiloride, amiloride analogues and cariporide.....	84
Figure 3.2: Confocal microscopy and FACS of DEX488 10kDa uptake +/- amiloride in BC cell lines.....	86
Figure 3.3: Confocal microscopy and FACS of DEX488 10kDa uptake +/- EIPA in BC cell lines.....	88
Figure 3.4: Confocal microscopy and FACS of DEX TMR 70kDa uptake +/- EIPA in BC cell lines	91
Figure 3.5: Expression of NHE1 from Human Protein Atlas depository	95
Figure 3.6: Confocal microscopy and FACS of DEXTMR 70kDa uptake +/- cariporide in BC cell lines.....	97
Figure 3.7: MCF7 digital zoomed images were used to confirm no differences in intracellular localisation was observed between VC and cariporide treated cells.	98
Figure 3.8: Confocal microscopy and Flow cytometry of Tf488 uptake +/- amiloride in BC cell lines.....	99
Figure 3.9: Confocal microscopy and Flow cytometry of Tf488 uptake +/- EIPA in BC cell lines.....	101
Figure 3.10: Confocal microscopy and Flow cytometry of Tf488 uptake +/- cariporide in BC cell lines.....	103
Figure 3.11: Amiloride, EIPA and cariporide Cytotoxicity assays in BC cell lines	106
Figure 3.12: DMSO, MeOH and PBS Cytotoxicity assays in BC cell lines.....	109
Figure 3.13: Tf uptake and recycling in BT474 and Clone5 BT474 cells	112
Figure 3.14: Tf recycling in BT474 and Clone5 BT474 cells.....	113

Figure 3.15: Differences between BT474 and Clone5 BT474 in DEX uptake...	115
Figure 3.16: Dextran uptake in BT474 and Clone5 BT474 cells.....	116
Figure 4.1: The history of Tz, from discovering HER2 to the evidence of its therapeutic benefits	121
Figure 4.2: NHS esters react with the primary amino groups of a protein at a pH range of 7.0 to 9.0.....	128
Figure 4.3: Characteristics of Tz conjugated to Alexa 647	129
Figure 4.4: Tz488 binding and internalisation in BC cells.....	132
Figure 4.5: Tz treatment enhances HER2 plasma membrane ruffling in HER2 BC cells	135
Figure 4.6: The effects of EIPA on HER2 endocytosis and Plasma ruffles in BC cells (Method A).....	137
Figure 4.7: EIPA increases HER2 endocytosis and Plasma ruffles in HER2 BC cells (Method B).....	138
Figure 4.8: Co-incubation analysis of EIPA and TZ488 in BC cells to monitor Tz488 uptake and plasma membrane dynamics (Method C)	142
Figure 4.9: Incubation of BC cells with EIPA and CellMask Deep Red.....	144
Figure 4.10: Structures of pyrazinoylguanidine (Amiloride and EIPA) and benzoylguanidine (cariporide).....	146
Figure 4.11: Effects of amiloride on Tz binding and internalisation in BC cells .	146
Figure 4.12: Effects of cariporide on Tz binding and internalisation in BC cells	147
Figure 4.13: EIPA enhances BC cells toxicity with different concentrations of Tz	150
Figure 4.14: BC Metabolic Activity in the presence of different concentrations of EIPA and 50nM Tz.....	151

Figure 5.1: Selectivity of the Tz decorated NP for HER2 expressing BC cells..	176
Figure 5.2: Cell binding of PLGA-RhoB-Tz488, Tz488 and Tf488 incubated with BC cells for 1 hr on Ice.....	177
Figure 5.3:High selectively for HER2 expression of PLGA-RhoB-Tz488 incubated with BT474 cells for 5 hrs.....	180
Figure 5.4:High selectively for HER2 expression of PLGA-RhoB-Tz488 incubated with Clone5 BT474 cells for 5 hrs	180
Figure 5.5: Lack of binding to MCF7 cells of PLGA-RhoB-Tz488 after 5 hrs ...	182
Figure 5.6: Selectivity of PLGA-RhoB-Tz488 for HER2 after incubation in SKBR3 cells for 5 hrs	183
Figure 5.7: Selectivity of PLGA-RhoB-Tz488 for HER2 after incubation in BT474 cells for 5 hrs	184
Figure 5.8: Selectivity of PLGA-RhoB-Tz488 for HER2 after incubation in Clone 5 BT474 cells for 5 hrs.....	185
Figure 5.9: Analysis of HER 2 expression BT474 and Clone5 BT474 cells incubated for 7 hrs.....	188
Figure 5.10: Metabolic Activity of BC cells incubated with PLGA or PLGA-Tz..	191
Figure 5.11: DOX distribution in PLGA-DOX-Tz incubated BC cells showing different spatial subcellular distribution compared with DOX alone	194
Figure 5.12: DOX distribution in PLGA-DOX-Tz incubated MCF7 cells for 5 hrs showing no evidence of vesicular labelling	195
Figure 5.13: DOX distribution in PLGA-DOX-Tz incubated SKBR3 cells highlighting appearance of vacuole like structures.....	198
Figure 5.14: DOX distribution in PLGA-DOX-Tz incubated BT474 cells highlighting appearance of vacuole like structures	199

Figure 5.15: DOX distribution in PLGA-DOX-Tz incubated Clone5 BT474 cells highlighting appearance of vacuole like structures
Figure 5.16: Max projection images of PLGA-DOX-Tz effects on Metabolic Activity of BC cells 201
Figure 5.17: PLGA-DOX-Tz effects on Metabolic Activity of BC cells..... 203

List of tables

Table 1.1: Four Biomarkers for BC Classification into Five Intrinsic subtypes, ER, PR, HER2 and KI67 (Proliferation, prognostic and predictive markers)	7
Table 1.2: HER Receptors and their cognate ligands.....	12
Table 1.3: The most often used chemotherapeutic and Endocrine medicines to treat BC and the mechanisms of action of these agents	18
Table 1.4: Targeted therapy for HER2 BC	22
Table 1.5: Examples of Endocytosis inhibitors	37
Table 1.6: Examples of ligands conjugated NPs for cancer targeting.....	41
Table 2.1: BC Cell lines used in this study.	50
Table 2.2: Different methods in the project for metabolic activity assay.....	64
Table 2.3: Preparation of Lysis Buffer (50ml):	71
Table 2.4: Preparation of Sample Buffer (50ml):	71
Table 4.1: IC ₅₀ calculations after cells were treated with EIPA, Tz or EIPA+Tz for 7 hrs.	152
Table 5.1: The table shows different studies used PLGA conjugated/Encapsulated Tz.	163
Table 5.2: Nanoparticle Preparations and formulations.....	170
Table 5.3: The Pearson correlation coefficient (r) between DOX and Hoechst in PLGA-DOX-Tz compared with DOX treatment.....	197
Table 6.1: Examples of NPs for chemotherapy delivery for BC treatment approved for clinical studies.....	212

Abbreviations

AR	Amphiregulin
AP2	Adaptor Protein-2
ADCC	Antibody-Dependent Cellular Cytotoxicity
ADC	Antibody-Drug Conjugate
ATCC	American Type Culture Collection
ALND	Axillary Lymph Node Dissection
BSA	Bovine Serum Albumin
BC	Breast Cancer
BTC	Betacellulin
BCMPG	Breast Cancer Molecular Pharmacology Group
BCA	Bicinchoninic Acid Assay
BAR	Bin, amphiphysin and Rvs
CME	Clathrin-mediated endocytosis
CIE	Clathrin-independent endocytosis
CCPs	Clathrin-Coated Pits
CHCs	Clathrin Heavy Chains
CLCs	Clathrin Light Chains
CCVs	Clathrin-Coated Vesicles
CytD	Cytochalasin D
Dex	Dextran
Dex488	Dextran attached to alexa 488
DEX 10/70 kDa	Dextran 10 or 70 kilodalton
DAT	Dopamine Transporter
DMT1	Divalent Metal Transporter 1
DM1	Derivative of Maytansine 1
dH ₂ O	Distal Water
DOX	Doxorubicin
DMSO	Dimethyl sulfoxide
DMEM	Dulbecco's modified eagle media
DTT	Dithiothreitol
DNA	Deoxyribonucleic Acid
ERRB2	erb-b2 receptor tyrosine kinase 2 gene
EPS	Exopolysaccharide
EAPs	Endocytic Accessory Proteins
EGFR	Epidermal Growth Factor Receptor
EGF	Epidermal Growth Factor
EP	Epiregulin
EIPA	5-(N-Ethyl-N-isopropyl) amiloride
EE	Encapsulation efficiency
ECL	Enhanced Chemiluminescence
EPR	Enhanced Permeability and Retention
FBS	Foetal Bovine Serum
FLOT1	Flotillin 1
FCHO1/2	F-BAR domain only protein 1 and 2 complex
GAK	Cyclin-G-associated Kinase

GEF	Guanine Nucleotide Exchange Factor
GAP	GTPase Activating Protein
Grb2	Growth factor receptor-bound protein 2
HSC70	Heat Shock Congate 70
HB-EGF	Heparin-Binding Epidermal Growth Factor
HR+	Hormone Receptor Positive
HER1-4	Human Epidermal Growth Factor Receptors 1-4
hrs	Hours
hcAb	Heavy-Chain Antibodies
MAPK	Mitogen-Activated Protein Kinase
MAPKK	MAPK Kinase
mTOR	Mammalian Target Of Rapamycin
MHC class I	Major histocompatibility complex
mins	Minutes
mAbs	Monoclonal Antibodies
N α FB	Nuclear factor α B
NRG1-4	Neuregulin 1-4
NCME	Non-Clathrin Mediated Endocytosis
NPs	Nanoparticles
nTPM	Normalised Transcript Per Million
PLGA	Poly (lactic-co-glycolic acid)
PLGA-DOX	Poly (lactic-co-glycolic acid)-Doxorubicin
PLGA-DOX-Tz	Poly (lactic-co-glycolic acid)-Doxorubicin-Trastuzumab
PTEN	Phosphatase And Tensin Homolog
PLC	Phospholipase C
PKC	Protein Kinase C
PI3K	Phosphatidylinositol 3-Kinase
PTEN	Phosphatase and Tensin Homolog)
PBS	Phosphate-buffered saline
pHi	Intracellular pH
RhoB	Rhodamine B
RTKs	Receptor Tyrosine Kinases
STEAP3	Six-Transmembrane Epithelial Antigen of the Prostate 3
SFM	Serum Free media
SA	Streptavidin
SEM	Scanning electron microscopy
SDS-PAGE	Sodium Dodecyl Sulfate–Polyacrylamide Gel Electrophoresis
SERMs	Selective Oestrogen Receptor Modulators
TMR	Tetramethylrhodamine
Tz	Trastuzumab
T-DM1	Ado-trastuzumab emtansine
Tf	Human Transferrin
TfR1-2	Human Transferrin Receptors 1-2
Tf488	Alexa 488 attached to Transferrin
TGF- α	Transforming growth factor- α

Chapter 1 : General Introduction

1.1 Cancer

Cancer is the name given to a group of conditions involving uncontrolled division of abnormal cells, which can potentially migrate to other parts of the body. Cancer mortality can be decreased by early detection and treatment, but this disease has a substantial societal and economic effect that is growing, and its yearly economic impact was projected to be US\$ 1.16 trillion in 2010 (WHO. 2021). Worldwide, 2020 witnessed an estimated 19.3 million new cancer diagnoses and about 10.0 million cancer deaths. In 2040, the worldwide cancer burden is projected to reach 28.4 million cases and is considered the primary or second major cause of mortality before the age of 70 years in 112 of 183 countries (Sung et al. 2021). There are about 375,000 new cancer cases in the UK every year, equivalent to about 1,000 new cases every day (2016-2018), and every two mins, someone in the UK is diagnosed with cancer. The United Kingdom has a ranking of cancer mortality in the top 30% of countries in the world and a higher ranking of cancer incidence in the top 10% (CR-UK. 2021).

1.2 Breast Cancer (BC)

1.2.1 Epidemiology

In recent years, BC mortality and morbidity rates have increased significantly worldwide. Approximately 2 million people around the world were affected by BC in 2018, while over 600,000 deaths were attributed to this group of diseases (Bray et al. 2018).

BC has passed lung cancer as the leading cause of cancer incidence worldwide in 2020, and it is the most commonly diagnosed malignant disease among females (Sung et al. 2021). It overtook lung cancer as the most frequently diagnosed cancer, with an estimated 2.3 million new cases globally, representing

11.7% of all cancer cases, and is the most often diagnosed type of cancer in women and the major cause of death. Every woman in the United States has a lifetime risk of developing BC of 12.4%, or one in every eight women. BC incidence is expected to reach 3.2 million by 2050 worldwide. BC was the second leading cause of mortality in developed countries, followed by lung cancer (Momenimovahed and Salehiniya 2019). It is the most frequent type of cancer in the United Kingdom, accounting for 15% of new cancer cases. Each year, about 55,900 new cases of BC are diagnosed, or more than 150 each day (2016-2018). Each year, over 11,500 women die of BC in the United Kingdom (CR-UK. 2021). BC incidence is expected to increase by 2% in the UK between 2014 and 2035, to 210 incidences per 100,000 females by 2035.

1.2.2 Pathophysiology

The breast consists of two distinct types of tissues: glandular and stromal (supporting). Glandular tissues include the milk-producing glands (lobules) and ducts (milk tubes), whereas stromal tissues contain the breast's fatty and fibrous connective tissues. Additionally, the breast has a lymphatic immune system that eliminates cellular fluids and waste (Sharma et al. 2010).

BC is classified as invasive or non-invasive based on its relationship to the basement membrane. Breast non-invasive neoplasms are generally classified into lobular carcinoma and ductal carcinoma. Lobular carcinoma conforms to the typical lobule's shape, with enlarged and filled acini. Ductal carcinoma is more morphologically heterogeneous than Lobular carcinoma, and pathologists classify it into four distinct subtypes: papillary, cribriform, solid, and comedo. Papillary and cribriform lesions are often lower grade, while solid and comedo lesions are usually of higher grade. Ductal carcinoma, if not treated, usually transforms into

invasive cancer. Invasive ductal cancer, alternatively referred to as ductal carcinoma, is the most frequent BC, responsible for 50% to 70% of all invasive BC. Invasive lobular carcinoma is responsible for 10% of BC (Alkabban and Ferguson 2021) (Figure 1.1).

BC can be categorised into four stages, represented by Stages 1 and 2 as early progression, which means the tumour is small and localized inside the breast tissue, or it may be discovered in nearby lymph nodes. Stage 3 cancer refers to when cancer has progressed to a lymph node, the breast surface, or the chest wall. Stage 4 cancer indicates that cancer has spread to another part of the body (CR-UK. 2021).

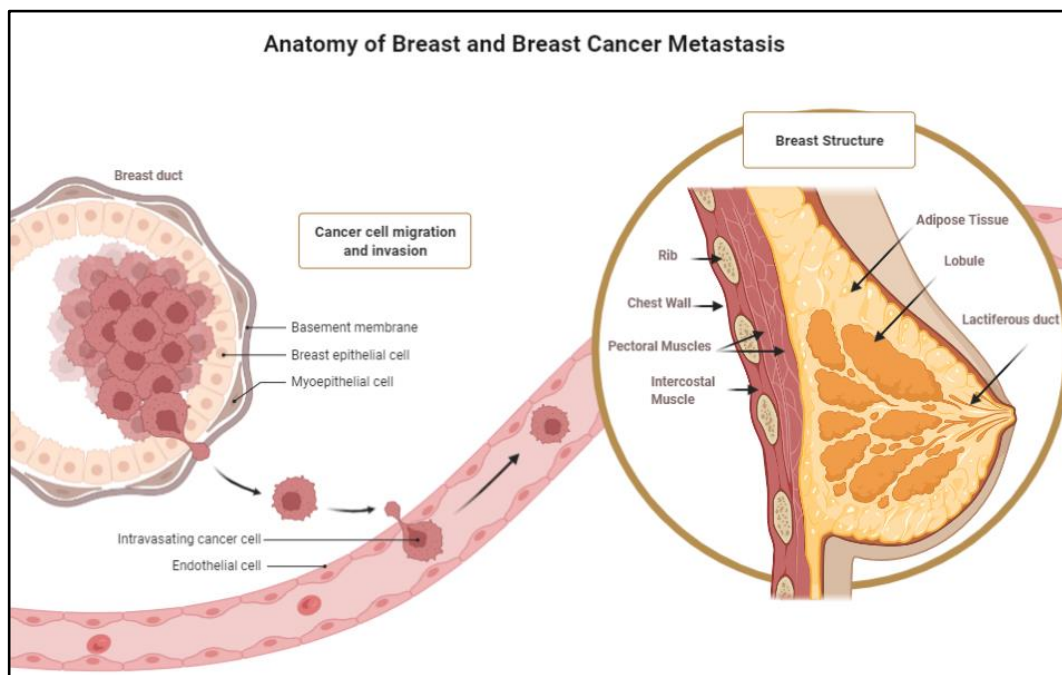


Figure 1.1: Anatomy of Breast and BC Metastasis. Most breast cancers develop in the lactiferous (milk) ducts or lobules. Tumours will spread through the breast tissue as the disease advances, either outward to the skin or inside towards and/or through the chest wall. Very invasive breast tumours will expand to lymph nodes and/or blood arteries before metastasizing to other organs. Prepared using BioRender.

1.2.3 BC Classification

Biomarkers are useful in BC diagnosis for determining the prognosis at the time of initial diagnosis, selecting an effective systemic treatment, postoperative surveillance, and monitoring therapy in advanced disease (Duffy et al. 2015).

Biomarkers can be used to evaluate the biological condition of a cancer, which can then be used to identify the type of tumour, its progression, or treatment responses, so helping in the management of BC (Afzal et al. 2022). BC is categorised, selectively targeted and treated on the basis of the overexpression of three proteins: oestrogen receptor (ER), progesterone receptor (PR), and HER2 receptors; these biomarkers are routinely tested clinic pathological features (Toss and Cristofanilli 2015).

As shown in table 1.1, breast tumours can be classified according to the expression of specific biomarkers into the following five types: Luminal A and Luminal B which expresses ER or PR, those with HER2 over-expression, basal, and normal-like tumours (Dai et al. 2015).

Biomarkers in BC can be divided into two categories: prognostic biomarkers and predictive biomarkers (for targeting) (Janes et al. 2015). The overexpression of receptors (biomarkers in Table 1.1) can initiate downstream signaling and increase proliferation in BC cells have been extensively studied and are major targets for therapeutics (Masoud and Pagès 2017). These BC biomarkers play an important role in the management of BC disease (Wu and Chu 2021). They are also used for subtyping BC and predicting BC susceptibility. Several other biomarkers have been identified and validated with BRCA gene mutations being

very well established (Wang et al. 2021). However, the majority have only been validated in mouse models or preclinical trials (Li et al. 2017; Wu and Chu 2021).

The basal-like, known as triple negative, is a type of BC characterised by negative expression of ER, PR, and HER2. As there are no specific proteins to target, it also has worse prognosis compared to Luminal A, Luminal B and HER2 classes (Dai et al. 2015). Studies indicates that triple negative BC can be further subdivided into several subclasses with different clinical features. For instance, some triple negative BC types overexpress EGFR and may benefit from anti-EGFR treatment (Foulkes et al. 2010). Chemotherapy is the primary treatment option for triple negative BC and identified biomarkers for this type including common genetic mutations like BRCA1 and BRCA2, CHEK2, PTEN, and TP53 (Walsh et al. 2016). BC with these mutations are more likely to become resistant to treatment, and they account for about 10% of all BC cases (Afzal et al. 2022).

Table 1.1: Four Biomarkers for BC Classification into Five Intrinsic subtypes, ER, PR, HER2 and KI67 (Proliferation, prognostic and predictive markers) (Yerushalmi et al. 2010; Dai et al. 2015).

Intrinsic Subtype	Immunohistochemistry (IHC) Status					Prevalence
	ER	PR	HER2	KI67	Basal Marker	
Luminal A	+	+	-	-		23.7 %
Luminal B	+	+	-	+		38.8 %
	+	+	+	+		14 %
HER2 overexpression	-	-	+			11.2 %
Basal	-	-	-	-	+	12.3 %
Normal-like	+	+	-	-		7.8 %

1.2.4 Aetiology

Mutations in genes are the most common cause of all malignancies, including BC (Tomasetti and Vogelstein 2017). BC is quite variable in terms of pathological features, with some tumours growing slowly and having a good prognosis while others are aggressive. Current projections and statistics indicate that breast cancer's global incidence and death are increasing (Sung et al. 2021).

Epigenetic traits of the disease and the risk of BC are often important for promoting cancer prevention at three levels, first by identifying risk factors and their mode of action, second by establishing markers of early disease and third

by establishing markers of disease progression and drug resistance (Tao et al. 2015).

BC is associated with a number of risk factors. Gender, age, and blood group are examples of demographic factors; reproductive factors such as menarche age, menopause age, full-term pregnancy, and pregnancy characteristics. Additionally, there are factors associated with hormonal replacement therapy, such as hormonal contraceptives, ovulation-stimulating medicines, and postmenopausal hormone replacement therapy. Factors related to hereditary and genetic characteristics breast-related factors such as lactation and lifestyle factors such as obesity and being overweight, alcohol consumption, smoking, poor diet, and of physical exercise have been linked to BC. Other risk factors, such as diabetes and radiation, must also be considered (Momenimovahed and Salehiniya 2019; Mavaddat et al. 2010).

1.2.5 Receptor Tyrosine Kinase and BC-The HER1-4 family

Human epidermal growth factor receptors consist of four receptors, EGFR (HER1/ERBB1), HER2 (ERBB2), HER3 (ERBB3), and HER4 (ERBB4), and all have been implicated in promoting the growth of cancer cells (Arienti et al. 2019). These four molecules are members of the type I group of 20 families of plasma membrane receptor tyrosine kinases (RTKs), which control various cellular metabolic activities. These receptors are called tyrosine kinase receptors due to a tyrosine residue in the intracellular domain capable of catalyzing the phosphorylation of the receptor itself or other proteins. Tyrosine Kinase Receptors play a crucial role in cell proliferation, survival, migration, differentiation, and apoptosis (Yamaoka et al. 2018).

HER family members (except HER2) are generally activated by extracellular ligand binding (See table 1.2), which results in a conformational change accompanied by homo- or heterodimerization, therefore activating an intracellular signalling cascade (Mitchell et al. 2018).

Despite the fact that HERs have a large number of common structural similarities, each family member shows distinct characteristics that may impart nonredundant modes of action. For example, HER3 lacks intramembrane kinase activity, whereas HER2 lacks a ligand binding site and, thus, a natural ligand (Figure 1.2) (Lyu et al. 2018; Barros et al. 2010). These receptors contain an extracellular domain for ligand binding, a single hydrophobic transmembrane domain, and a C-terminal cytoplasmic domain with enzymatic activity. Each dimer demonstrates conjugate ligands necessary to induce cell transformation. Ligand activation via the extracellular domain then stimulates receptor homo- or heterodimerisation. However, in the absence of a ligand, HER2 has a conformation that always resembles the ligand-activated state with a protruding dimerization loop (Wee and Wang 2017).

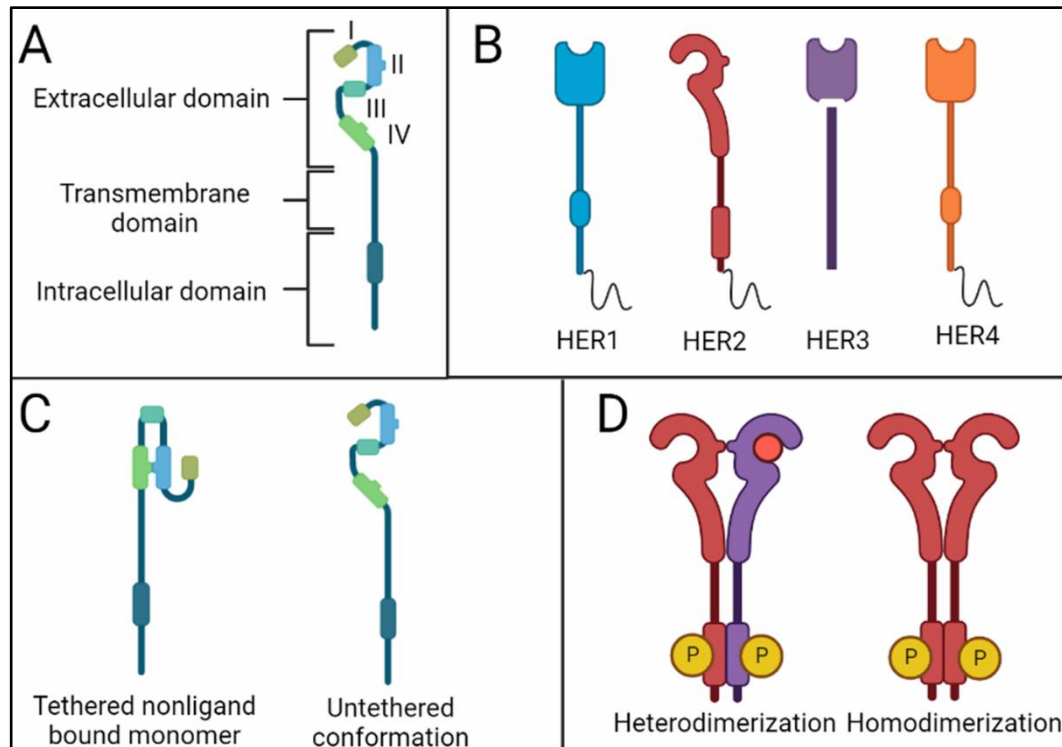


Figure 1.2: HER family structure, differences, conformation change, and dimerization. (A) HER domains include extracellular, transmembrane, and cytoplasmic/intracellular domains. Both ligand binding domains (I and III) and cysteine-rich domains (II and IV) are present in the extracellular component. The lipophilic transmembrane domain is followed by the cytoplasmic region that contains the kinase domain and the carboxy-terminal tail (Mitchell et al. 2018). (B) Diagram of the four HER family members illustrate their variations and similarities. HER2 is the single member of this family without a ligand-binding site. On the other hand, HER3 lacks an internal domain-localized tyrosine kinase (TK) region. Both the epidermal growth factor receptor (EGFR) (1) and the human epidermal growth factor receptor (HER4) (4) include a ligand binding site and TK. The receptor tyrosine kinase is a conserved area found in all families except HER3 that requires the other members to form a dimer and activate downstream pathways (Barros et al. 2010). (C) Nonligand bound monomer tethered (Closed conformation) and untethered conformations (open conformation). The untethered conformation can be bound by ligands linkage at domains I and III, stabilising it for dimerization and downstream TK activation (Patel et al. 2015). (D) Homodimerization of HER2 with another HER2 and heterodimerization of HER2 with other family members, particularly HER3. Prepared using BioRender.

When inactive, HERs reside in a monomeric tethered configuration; however, upon ligand engagement, the receptor extends, revealing a dimerization arm. Interaction with another open conformation receptor leads to the receptor dimer's formation, which results in another conformational change in the receptor complex's intracellular domain. This conformational change results in a transphosphorylation event, during which the donor receptor transfers numerous phosphate groups into the acceptor receptor's C-terminal tail, enabling attachment and activation of the downstream signalling cascade. The conventional wisdom that HER family receptors exist exclusively in a monomeric state prior to ligand binding has been challenged by evidence indicating HER can exist in an inactive dimerized form prior to ligand stimulation (Maruyama 2014). Dephosphorylation, receptor internalisation via endocytosis, and lysosomal degradation or recycling of the receptor contribute to signal deactivation (Kumar et al. 2020).

Table 1.2: HER Receptors and their cognate ligands (Arienti et al. 2019). Full names of abbreviations here can be found in the abbreviations list.

Receptors	Cognates Ligands
HER1	AR BTC EGF EP EPIGEN HB-EGF TGF- α
HER2	None-identified
HER3	NRG1 NRG2
HER4	BTC HB-EGF NRG1 NRG2 NRG3 NRG4 EP

All HER family members have been implicated in several different cancers (Sareyeldin et al. 2019), and overexpression of HER1, HER2, and HER3 have all been shown to lead to a poorer prognosis in BC patients, whereas overexpression of HER4 has illustrated a protective effect (Wang et al. 2016). As the subject area of this thesis is HER2, the other family members will not be discussed in any detail.

1.2.6 Human Epidermal Growth Factor Receptor 2:

The HER2 receptor is encoded by the HER2/neu gene and is overexpressed in approximately 20% of invasive breast cancers (Wahdan-Alaswad et al. 2020). HER2 overexpression occurs in other types of malignancies as well, including those of the stomach (Modi et al. 2020), lung (Pillai et al. 2017), bladder (Haque 2018), oesophagus (Rahman et al. 2018), uterine cervix (Varshney et al. 2020), colon (Raghav 2018) and ovarian carcinomas (Khalil et al. 2016). HER2

overexpression constitutes a predictive factor of inadequate response to chemotherapy and endocrine therapy (Mosly et al. 2018; Wang et al. 2019; Montagna and Colleoni. 2019)

Heterodimer complexes of HER2, especially HER2/HER3 heterodimers, are more stable at the cell membrane compared with homo or heterodimers of other family members (Fichter et al. 2018). Thus, HER2 stays at the cell membrane for a longer time, with a lower endocytosis uptake rate than other HER members (Devarajan and Dandekar 2019). The binding of EGF to EGFR induces cell signalling, its endocytosis and degradation in lysosomes or recycling to the cell surface (Tomas et al. 2014). HER2 has no ligand, and this represents another reason for it being more permanent at the plasma and with it always been in an active conformation, it is continuously driving cell growth and division. If endocytosed it is recycled to the cell surface, ready for another activation cycle and further augmenting growth factor signalling (Shramova et al. 2018).

It has been demonstrated that HER2 is localized to plasma membrane protrusions and this is defined as an endocytosis-resistant receptor (Bertelsen and Stang 2014). A study showed that HER2 expression inhibits the creation of clathrin-coated pits in the plasma membrane (Cortese et al. 2013), thus the HER2 recycles persistently (Austin et al. 2004). HER2 recycling to plasma membrane allows repeated stimulation and prolonged signalling. Because HER2 is the preferred dimerisation partner for all members of the HER family, this can also enhance downregulation resistance to partner receptors (Theos et al. 2005).

Overexpression of HER3 is common in HER2 breast tumours but in comparison to other HER family members, HER3 is not carcinogenic when overexpressed

alone (Drago et al. 2022). While HER3 does not induce cancer on its own, HER2:HER3 heterodimers have the highest transforming capacity of any HER family dimer and HER3 is required for HER2-mediated carcinogenesis in a variety of tumour types (Haikala and Jänne 2021)

1.2.7 HER2 and Cell Signalling

A large body of laboratory data has accumulated to suggest that HER2 family members perform cell signalling by forming heterodimers (e.g., HER1: HER2 or HER4:HER2). Notably, the formation of these heterodimers may occur even in situations when only a single member of the pair binds its ligand (Roskoski 2014). Additionally, the literature indicates that heterodimers, when comparatively examined against homodimers, are associated with stronger downstream signalling activation (Furrer et al. 2018).

Homo- or heterodimerization of HER2 results in autophosphorylation of tyrosine residues within the receptor's cytoplasmic domain, activating a variety of signalling pathways, most notably the mitogen-activated protein kinase (MAPK), phosphatidylinositol-4,5-bisphosphate 3-kinase (PI3K), and protein kinase C (PKC), resulting in cell proliferation (Figure 1.3) (Hsu and Hung 2016). Because of its open conformation, HER2 is the preferred dimerization partner for the family members. The HER2-HER3 heterodimer is the most effective activator of downstream signalling pathways, most notably PI3K/Akt, regarded as the master regulator of cell growth and survival (Iqbal and Iqbal 2014).

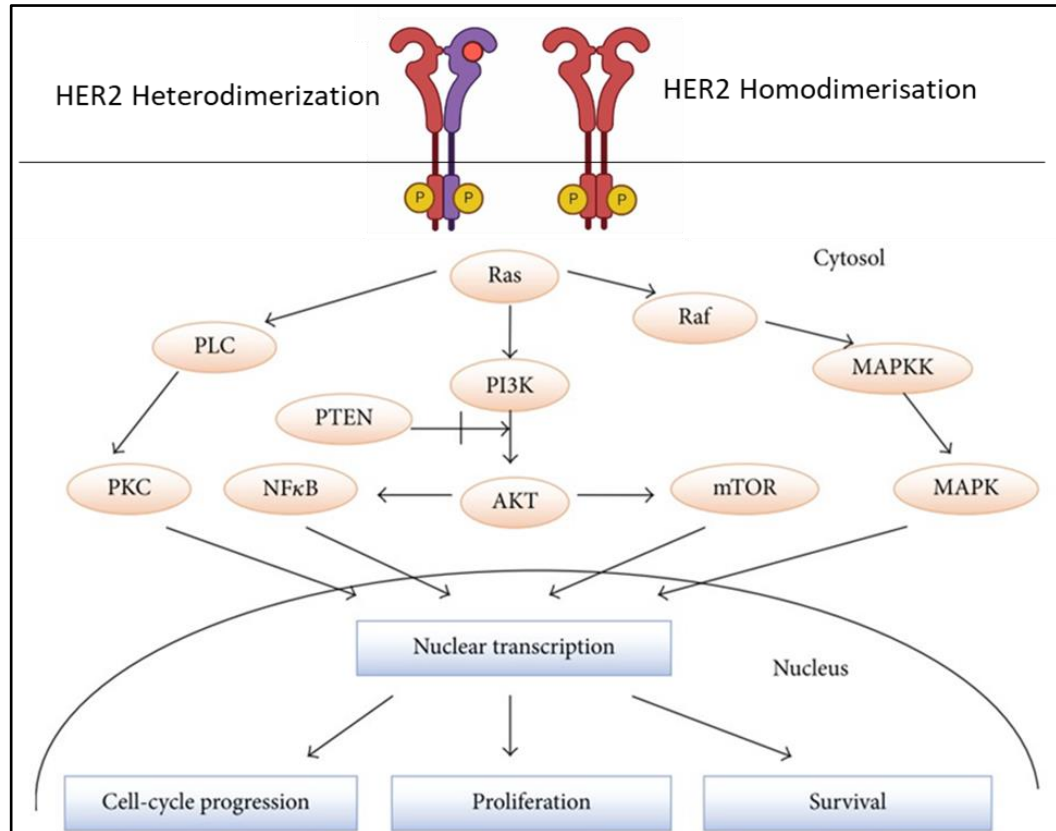


Figure 1.3: HER2 promotes cancer cell proliferation, invasion, metastasis, and angiogenesis by activating the PI3K/Akt and Ras/Raf/MEK/ERK signalling cascades. The two most important well-studied downstream signalling pathways activated by HER receptors. Ras functions as a self-inactivating signal transducer at the top of these cascades. PKC, which is triggered by PLC, is a third critical factor in the network. Adapted from (Iqbal and Iqbal 2014). (AKT) Protein kinase B; (PLC) Phospholipase C; (PKC) Protein Kinase C; (PI3K) Phosphatidylinositol 3-Kinase; (PTEN) Phosphatase and Tensin Homolog; (NFκB) nuclear factor κB; (mTOR) Mammalian Target of Rapamycin; (MAPK) Mitogen-Activated Protein Kinase; (MAPKK) MAPK kinase.

1.2.8 Treatment

BC is treated in various ways, and there is no unique treatment for BC. For patients with nonmetastatic BC, the primary aims of therapy are to eradicate the tumour from the breast and regional lymph nodes and prevent a metastatic recurrence.

Non-metastatic BC is often treated with a combination of local and systemic treatment. Local therapy is often initiated with surgery, considered the main treatment option for BC, followed by postoperative radiation. The surgical options vary from extensive local excision (lumpectomy) to radical mastectomy and Axillary lymph node dissection (ALND), which includes the removal of the breast, chest wall muscles, and lymph nodes. Systemic therapy may be preoperative (neoadjuvant), postoperative (adjuvant), or both, depending on BC subtype.

Metastatic BC is considered incurable in almost all patients. The therapy aims for metastatic BC are to prolong life and relieve symptoms. Systemic treatment is utilised in metastatic BC, and Local therapeutic techniques (surgery and radiation) are generally reserved for metastatic disease BC (Waks and Winer 2019).

Radiotherapy has been utilised as a therapeutic method for over a century and is presently employed as a stand-alone or adjunctive modality for cancer. This therapy aims to eradicate cancer cells while protecting normal tissue, and the treatment modality is determined by the tumour's anatomical location, size, and type.

In radiotherapy, there are two basic forms of treatment: electromagnetic radiation, which includes x-rays and gamma-ray, and particle radiation, which includes electrons, neutrons, and protons. Radiotherapy involves using Ionizing radiation, which acts directly on biological molecules by transferring energy through deoxyribonucleic acid (DNA) strand breaks or indirectly on tumour cells by producing free radicals and reactive oxygen species (Robinson and Holloway 2019).

According to the American Medical Association (2019), BC treatment is categorised into hormone receptor-positive (HR+), receptor tyrosine-protein kinase positive (HER2+), and triple-negative subtypes. The therapy of HER+ will be explained in detail later. Standard endocrine therapy for non-invasive HR+ BC consists of daily oral anti-Oestrogen therapy for five years to avoid recurrence. Endocrine treatment may include tamoxifen or aromatase inhibitors (anastrozole, exemestane, and letrozole) (Table 1.3). Clinicians may also choose to combine chemotherapy in patients with HR+/HER- BC, depending on the anatomic stage and grade of the tumour. In early BC, various neoadjuvant and adjuvant chemotherapy regimens may be explored. The regimens docetaxel/cyclophosphamide, adriamycin/cyclophosphamide, and cyclophosphamide/methotrexate/5-fluorouracil are all appropriate alternatives for low-risk patients, and toxicities are a primary concern. Chemotherapy regimens that include anthracyclines and taxanes provide the highest risk reduction and continue to be the optimal choice for high-risk patients. The Food and Drug Administration (FDA) has authorised only chemotherapeutic medicines to treat nonmetastatic triple-negative cancers (Waks and Winer 2019).

Table 1.3: The most often used chemotherapeutic and endocrine medicines to treat BC and the mechanisms of action of these agents. Table compiled from the following sources: (Visovsky 2014; Waks and Winer 2019; Wind and Holen 2011; CR-UK 2021).

Drug Name	Classification of the drug	Mechanism of Action
Endocrine Hormonal Drugs:		
Tamoxifen	selective Oestrogen receptor modulators (SERMs).	Competitively prevents Oestrogen binding to Oestrogen receptor
Anastrozole, Exemestane, and Letrozole	Aromatase Inhibitors	Decreases the conversion of androgens to Oestrogen
Fulvestrant	Oestrogen receptor antagonist	Prevents Oestrogen binding and down-regulate Oestrogen receptors.
Chemotherapeutic Agents		
Cyclophosphamide	Alkylating agent	Prevents protein synthesis by cross-linking strands of DNA and RNA
Doxorubicin	Anthracyclines	Triggers DNA cleavage by topoisomerase II inhibition resulting in cell death
Paclitaxel	Taxane	Mitotic inhibitor; interferes with the normal function of microtubule breakdown. Also induces apoptosis
Docetaxel	Taxane	Interferes with microtubule breakdown
Methotrexate	Anti-metabolites	Acts specifically during DNA and RNA synthesis, and thus it is cytotoxic during the S-phase of the cell cycle
Fluorouracil (5FU)	Anti-metabolite	Metabolised to cytotoxic metabolites which are incorporated into DNA and RNA, inducing cell cycle arrest and apoptosis
Carboplatin	Alkylating agent	Cross-links DNA and disrupts DNA replication

1.2.8.1 Antibodies targeting HER2

An example of a therapeutic that can stop HER2 signalling effectively is a humanised monoclonal antibody medicine known as Trastuzumab (Tz), with the brand name Herceptin. Tz is commonly recognised as one of the most effective HER2+ cancer treatments representing a significant therapeutic agent against HER2+ BC (Wu et al. 2022; Kreutzfeldt et al. 2020; Maximiano et al. 2016). Tz targets a variable region of HER2 at the extracellular juxtamembrane domain (39 amino acids), specifically binding to amino acids present in domain 4 (Figure 1.4) (Hudis 2007; Park et al. 2022). The antibody can act as a competitive antagonist to EGF protein by blocking the ligand-independent HER2–HER3 dimerization. This blockade inhibits receptor stimulation and activation by EGF and prevents conformational change required for dimerization. Tz can stop the signalling of the MAPK, PI3K, and AKT/mTOR pathways that lead to cell division, as mentioned previously (Hervent and De Keulenaer 2012; Nami et al. 2018). Tz can also stimulate immune-mediated responses against HER2-overexpressing cells leading to antibody-dependent cellular cytotoxicity (Listinsky et al. 2013). It also has an antiangiogenic effect and lowers the proapoptotic threshold for chemotherapy. Therefore, Tz has been demonstrated to possess a synergistic effect with chemotherapeutics such as doxorubicin, epirubicin, paclitaxel carboplatin, docetaxel, and gemcitabine (Gajria and Chandarlapaty 2011). Tz also has had success by administration with another HER2 targeting monoclonal antibody pertuzumab, i.e., dual HER2 targeting therapy and taxane therapy for first-line metastatic HER2+ BC disease (Bachelot et al. 2019). General resistance mechanisms to Tz can arise and are a major clinical problem, mainly owing to signalling through an alternate receptor and/or pathway (Nahta and Esteva

2006). HER2+ BC with activating mutations of the PIK3CA gene and deletions of the PTEN gene can also develop Tz resistance (Kim et al. 2017). A recent study suggests that PIK3CA (Phosphatidylinositol-4,5-bisphosphate 3-kinase), gene mutations transcribed into the p110 subunit have a significant role in promoting cancer through enhanced signalling of the PI3K/AKT/mTOR survival pathway (Willis et al. 2020). As a lipid kinase PIK3CA is involved in many signalling cascades often leading to cell growth (Conti and Guerrini 2017).

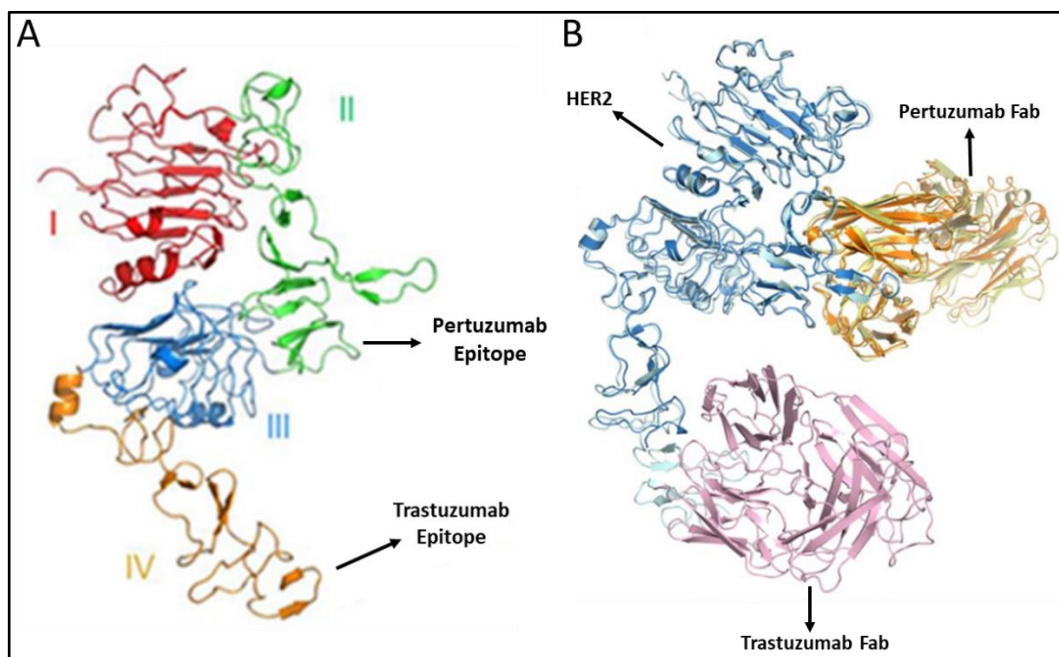


Figure 1.4 Structure of HER2, binding sites of Tz and Pertuzumab. A. The HER2 subdomains I through IV are coloured sequentially in red, green, blue, and orange. The epitopes of Pertuzumab and Tz are represented by arrows. B: Structures of HER2, Trastuzumab Fab and Pertuzumab Fab are shown in cyan, pink and yellow respectively. Adapted from (Oganesyan et al. 2018; Hao et al. 2019).

Another mechanism of Tz resistance is a failure to trigger the immune-mediated mechanisms that destroy tumour cells. Specifically, Tz is an IgG subtype and can be affected by the Fc receptor located in the membranes of certain immune cells. These cells can produce off tumour site ADCC responses (antibody-dependent cellular cytotoxicity) (Figure 1.5) during Tz treatment while significantly impairing clinical response rates and progression-free survival of patients treated with Tz

(Nami et al. 2018; Pohlmann et al. 2009). The accumulation of a truncated extracellular form of the HER2 receptor p95-HER2 has also been regarded as a mechanism driving Tz resistance, as this will bind to the antibody away from the tumour/cancer cell sites. Lastly, Tz can activate downstream signalling and upregulate HER2 downstream signalling pathways lead to increased cell proliferation (Gajria and Chandarlapaty 2011). Further information on Tz will be provided in Chapter 4.

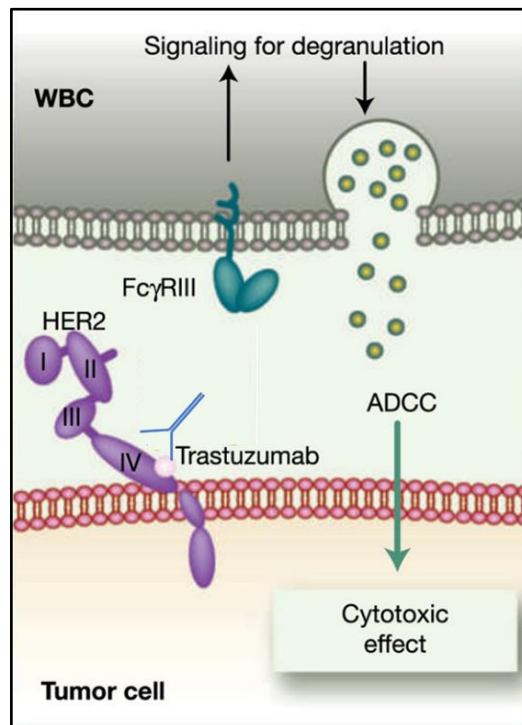


Figure 1.5: Tz antibody increases ADCC's ability to destroy cancer cells. The Fab part of an antibody attaches to its cognate antigen on a target cell (i.e., cancer cell), while the Fc part of the antibody interacts with the Fc receptor on an effector cell from the immune system. This mechanism is known as antibody-dependent cell-mediated cytotoxicity (ADCC). This mechanism initiates the release of cytotoxic granules from the effector cell toward the target cell and results in the apoptosis of the target cell. WBC; White Blood Cell. Adapted from (Pohlmann et al. 2009).

Despite the fact that HER2 is endocytosis deficient, Tz has been conjugated to cytotoxic drugs (Xu et al. 2019). This conjugation is required to be delivered to lysosomes for degradation and release the drug from the antibody (García-Alonso et al. 2020). These are termed Antibody Drug Conjugates (ADCs), and a

clinically approved version of the second type is Kadcylla, also known as Tz emtansine (T-DM1). Several small molecule drugs targeting HER2 have also been described in (Table 1.4).

Table 1.4: Targeted therapy for HER2 BC.

Drug Name	Classifications	General Information
Lapatinib	Tyrosine Kinase Inhibitor (TKI)	Lapatinib has been targeted reversibly against the activity of both HER2 and EGFR receptors by inhibiting tyrosine autophosphorylation and downstream signalling such as PI3K and MAPK (Spector et al. 2005). It also promotes cell cancer apoptosis through anti-HER2 antibodies (Xia et al. 2005). Furthermore, lapatinib has been demonstrated to inhibit the growth of HER2 that was previously seen to be Tz-resistant. Thus, this indication suggests using lapatinib as dual therapy with Tz for patients experiencing Tz resistance (Azim and Azim 2012).
Pertuzumab	Humanised monoclonal antibody	Pertuzumab targets the extracellular dimerisation domain II region. This leads to inhibition of homo- heterodimerisation of HER2–HER3 dimer formation in a ligand-induced fashion and inhibition of the downstream signalling pathways (Di Modica et al. 2017). Moreover, pertuzumab has also indicated the triggering of ADCC against cancer cells (Capelan et al. 2013). Consequently, pertuzumab dual therapy with Tz and chemotherapy is now used as a first-line treatment for metastatic BC disease (Gianni 2018).
Tz-emtansine	antibody-drug conjugate (ADC)	Tz emtansine incorporates the HER2-targeted anti-tumour properties of Tz alongside the cytotoxic activity of the microtubule-inhibitory agent DM1 (a derivative of maytansine). This drug is released from lysosomes once the ADC has been delivered by endocytosis. The antibody and the cytotoxic agent are conjugated by a stable linker, and lysosomal proteases degrade the antibody allowing the drug to escape across the lysosomal membrane to reach its cytosolic target (Barok et al. 2014).

		Thus, T-DM1 allows intracellular drug delivery specifically to HER2-overexpressing cells, thereby improving the therapeutic index and minimising the exposure of normal tissues (Verma et al. 2012).
Neratinib	Tyrosine Kinase Inhibitor (TKI)	Neratinib is irreversible inhibitor of HER1, HER2 and HER4. It is authorised as adjuvant therapy of patients with HER2+ early-stage BC who have previously been treated with a Tz-based adjuvant regimen in the United States. Neratinib inhibits autophosphorylation of HER2 and EGFR and signals of MAPK and AKT pathways. Neratinib indicated synergistic efficacy when used with Tz for the treatment of HER2 BC (Deeks 2017).
Margetuximab	Monoclonal Antibody	Margetuximab has identical Tz epitope-binding properties, but its designed Fc domain is different (Tarantino et al. 2021). The changes to Fc have no effect on antigen recognition or antiproliferative activity. The antibody is engineered for enhanced binding to Fc receptor IIIA (CD16A). Margetuximab was registered in the United States in 2020 for use with chemotherapy in patients with HER2+metastatic breast cancer who had received two or more previous anti-HER2 regimens (Markham 2021).
Tz-Deruxtecan	antibody-drug conjugate (ADC)	Tz-Deruxtecan was recently approved by FDA in August 2022 (FDA.GOV). Tz antibody conjugated to topoisomerase I inhibitor induces DNA damage and apoptosis. Deruxtecan is released as a result of Tz internalisation and intracellular cleavage by lysosomal enzymes, whereas Tz is expected to be destroyed. Tz-Deruxtecan is recommended to use for recurrent HER2 BC (Nguyen et al. 2021).

1.2.9 HER2 Clustering

Receptor activity can be downregulated via for example ligand binding, endocytosis to lysosomes and degradation. HER2 has very low intrinsic internalisation rates and is known to recycle back the plasma membrane where it can continue to activate signalling.

Our previous studies showed that HER2 endocytosis was significantly promoted with concomitant lysosomal delivery and degradation via Tz-mediated cross-linking by adding biotinylated Tz to breast cancer cells. We could force HER2 clustering by adding streptavidin that can bind 4 biotin molecules (Figure 1.6) (Moody et al. 2015).

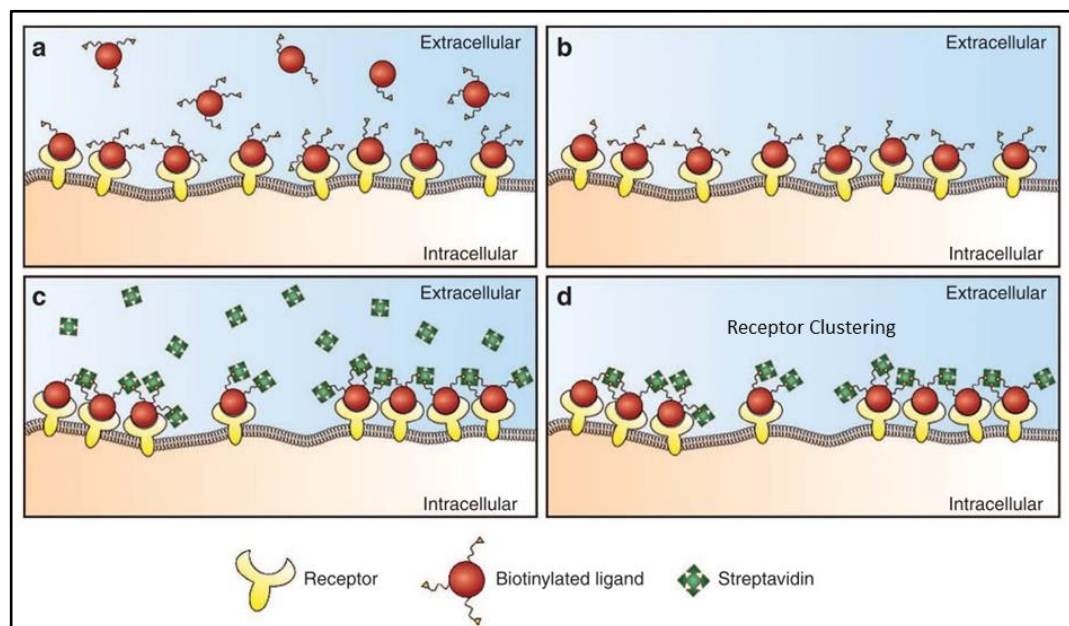


Figure 1.6: Biotinylated antibody and streptavidin complexes formation on cells adapted from (Moody et al. 2015). (a) Cells are treated with exogenous biotinylated protein. (b) Washing is used to remove excess unbound protein. (c) Cells are incubated with streptavidin, which clusters receptors via the creation of prolonged cross-links between receptor:ligand–biotin complexes. (d) Excess streptavidin is removed.

Later, using Scanning Electron Microscopy (SEM), the same experiment was repeated with a short time treatment on HER2 overexpressed cells to explore in detail the cellular processes underlying endocytosis and plasma membrane morphology. Significant membrane ruffling of the plasma membrane was rapidly observed suggesting that this effect was initiating macropinocytosis (Wymant et al. 2020). Later studies have shown that other mechanisms of driving HER2 clustering, either via using one antibody targeting two HER2 epitopes or a combination of antibodies binding to different epitopes also have the same effects (Szymanska et al. 2016).

1.3 Endocytosis

A range of mechanisms have arisen within mammalian cells due to evolutionary processes, several of which facilitate the internalisation of small molecules, macromolecules, and particles. Furthermore, mechanisms exist within mammalian cells, which allow them to target these molecules to specific sealed organelles inside the cytoplasm. The group of processes associated with this function is referred to as endocytosis, a term proposed by (Malt 1964). Broadly speaking, endocytosis regulates how cells interact with their environment and incorporates a range of methods and processes that synthesize internal membranes from the plasma membrane lipid bilayer and contribute to the uptake of extracellular material. Endocytosis is integral to many cell processes, including mitosis, nutrient uptake, cell shape, transcellular transport, plasma membrane receptor downregulation and cell migration (Khan and Steeg 2021). Additionally, pathogens such as viruses and bacteria use endocytic pathways to facilitate their uptake into cells (Figure 1.7) (Doherty and McMahon 2009; Cossart and Helenius 2014).

The most well-studied and possibly common internalisation pathway is Clathrin-mediated endocytosis (CME); however Clathrin-independent endocytosis (CIE), pathways and macropinocytosis also fall under pinocytosis with phagocytosis representing the final mechanism of cell uptake (Dutta and Donaldson 2012).

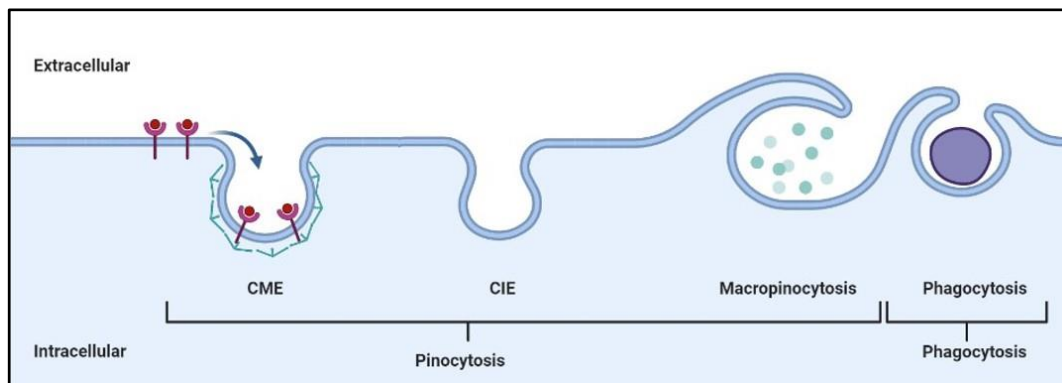


Figure 1.7: Different types of endocytosis mechanisms at the cell membrane, CME, CIE. Adapted and modified by BioRender.

1.3.1 Clathrin-mediated endocytosis (CME)

Numerous endocytic mechanisms have been identified in eukaryotic cells; however, the main endocytic pathway for the internalisation of a wide variety of cargoes is CME (Bitsikas et al. 2014). CME is named after one key component of the clathrin protein's endocytic machinery.

CME occurs via clathrin-coated pits (CCPs), which are generated by the formation of the main coat proteins, clathrin triskelia, which consists of three clathrin heavy chains (CHCs) with strongly linked clathrin light chains (CLCs), and the adaptor protein-2 (AP2). CME can be divided into four steps: initiation, stabilisation, maturation, and membrane fission. The following stages involve the uncoating and fusion of clathrin-coated vesicles (CCVs) with cargo destined for early endosomes (Mettlen et al. 2018). Clathrin coats on the plasma membrane were first identified using electron microscopy in the 1960s (Roth and Porter

1964). Now it is understood that the formation of clathrin-coated endocytic vesicles requires around 60 additional cytosolic proteins (Weinberg and Drubin 2012). Currently, there is still a need for a full understanding of how all of these proteins promote vesicle formation; for example, it is unclear whether cargo molecules are required to begin an endocytic process or are more passive passengers recruited after the initiation. The full molecular processes underlying the initiation of the endocytic site are not entirely known (Armstrong and Olson 2022; Prichard et al. 2022).

CME is triggered by the BAR domain proteins F-BAR domain only protein 1 (FCHO1) and FCHO2, that bind to small curvatures on the plasma membrane and are required for the progression of the clathrin-coated pits (Kaksonen and Roux 2018; Henne et al. 2010). The Adaptor Protein-2 (AP2) complex attaches to cytosolic domains on plasma membrane receptors and attracts other scaffold proteins, which subsequently enclose the membrane-bound adaptors, forming the endocytic site. Following this, clathrin and other coat-associated proteins are recruited, effectively extending the coat, and endocytic vesicles in mammals generally have a diameter of around 100 nm (Kaksonen and Roux 2018). Dynamin is a GTP binding protein that orchestrates the breaking of the vesicle's connection with the plasma membrane to free the invagination from the plasma membrane to form a new clathrin-coated vesicle that will fuse with the early endosome that is then sorted to other cellular destinations including recycling back to the plasma membrane (Preta et al. 2015). For example, a receptor may enter the early endosome via one of three pathways: rapid or delayed recycling or degradation (Figure 1.8) (Cullen and Steinberg 2018).

Following internalisation, sorting in the early endosome segregates molecules for recycling via rapid (Rab4, Rab14, Rab15) and slow recycling channels (Rab11a, Rab15, Rab22a). In addition to the more ubiquitous Rab4, Rab5, and Rab11 GTPases, epithelia feature specific recycling circuits that employ Rab17 and Rab25 (Agola et al. 2011). Through Rab6 and the retromer complex, which may interact with Rab7, early endosomes also govern the return to the Golgi (Seaman 2004). Rab9 regulates the return of late endosomes to the Golgi. Endocytosed and phagocytosed cargo intended for destruction is transported from early to late endosomes via a Rab7-dependent mechanism that requires fusion with lysosomes (Vanlandingham and Ceresa 2009).

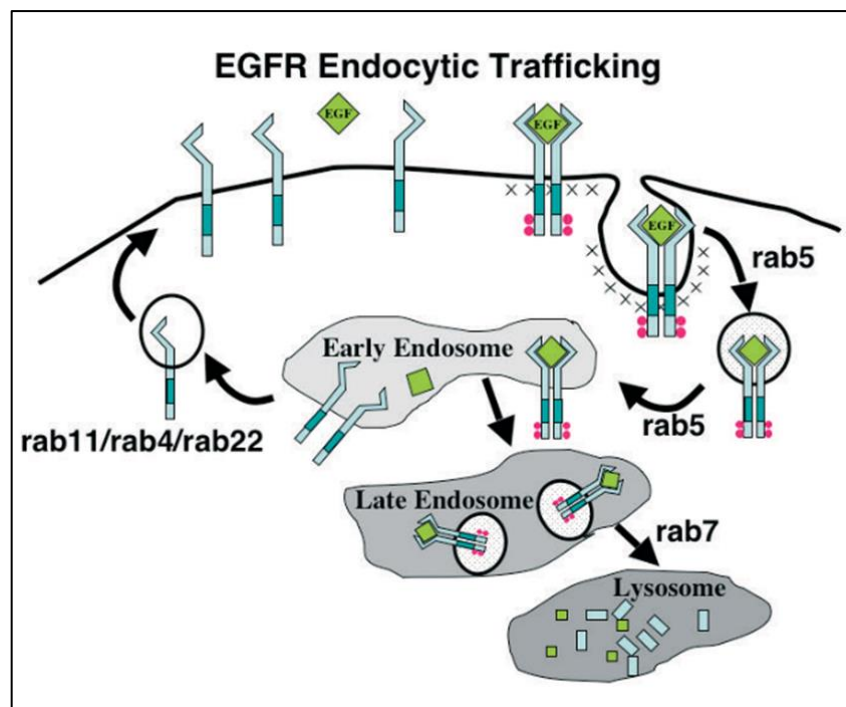


Figure 1.8: EGFR receptor trafficking via Rabs. The ligand-bound receptor translocates to plasma membrane areas containing an intracellular clathrin lattice. The clathrin lattice invaginates to create a clathrin-coated pit, which then pinches off to produce a clathrin-coated vesicle. Once the EGFR enters the early endosome, it either proceeds along a degradation process or is recycled back to the plasma membrane. Adapted from (Ceresa 2006).

1.3.2 Clathrin-independent endocytosis (CIE)

CIE is composed of numerous parallel pathways, each of which has a unique method to produce endocytic carriers. It is generally accepted that all known CIE routes deliver their payload to early endosomes; consequently, the distinctions between them lie in the initial plasma membrane stages (Ferreira and Boucrot 2018).

CIE, alternatively referred to as non-clathrin mediated endocytosis NCME, occurs along with CME and has been observed in a number of cell types in vitro. CIE includes a nonselective bulk entry process referred to as 'pinocytosis' with the 'macro' or 'micro' prefix indicating the size of the vacuole formed (Johannes et al. 2015). However, it should be noted that all endocytic uptake mechanisms have the capacity to internalise fluid.

Named clathrin-independent uptake routes are often based on the proteins that regulate them, including caveolae-mediated endocytosis, Arf6-dependent, flotillin-1-dependent, Cdc42- dependent, and RhoA-dependent endocytosis which results in the formation of membrane structures with very different sizes and morphologies to clathrin-coated vesicles (Mayor et al. 2014). For example, membrane ruffles can fold back over the plasma membrane to generate large (0.2 to >10 μm) endocytic vacuoles called macropinosomes (Watanabe & Boucrot 2017). See section 1.3.2.1.

Caveolin was identified in 1950 and consists of three distinct isoforms and are now known to be engaged in and contributing to endocytic events (Feng et al. 2013). These proteins as different isoforms functions in CIE located in cholesterol- and sphingolipid-rich nanodomains on the plasma membrane

measuring 50–100 nm in diameter and resembling endocytic carriers prior to scission. For example uptake via caveolae was shown to be involved in transporting proteins and lipids like LDLs, albumin, and insulin from the blood vessels (endothelial cells) to the opposite face and vice versa (Transcytosis) (Cheng and Nichols 2016).

The first evidence for flotillins mediating endocytosis was published in 2006, showing that Flotillin 1 is needed for internalisation of cholera toxin and endocytosis of a GPI-linked protein CD59 (Glebov et al. 2006). Two flotillin isoforms were hypothesized to arrange cholesterol-enriched membrane microdomains, or rafts, that generally do not contain caveolin and were found to be regulators of dopamine transporter (Sorkina et al. 2013). Very few subsequent studies have in fact identified a role for these proteins in endocytosis rather than plasma membrane organisation.

ARF6 is a small GTPase found in the plasma membrane and endosomes, where it affects endocytic membrane trafficking and actin remodelling. As ARF6 cycles between active and inactive states, it enables ligand uptake at the cell surface and subsequent trafficking down the endocytic pathway (Grossmann et al. 2019). Similarly, RhoA, Cdc42, and Rac1 are GTPases involved in vesicle trafficking and endocytosis. Cdc42 is involved in vesicle trafficking from the cell surface to the Golgi, transport between the ER and the Golgi, post-Golgi transport, and exocytosis. Rac1 is involved in both endocytosis and exocytosis, whereas RhoA is primarily involved in endocytosis (Chi et al. 2013).

1.3.2.1 Macropinocytosis

Macropinocytosis, an essential process of endocytosis, occurs continuously in extracellular (i.e., plasma) membranes within most, if not all, cells. The process is initiated via protrusive movements of actin-rich membrane folds known as ruffles that engulf fluid and solutes via structures called macropinosomes that are then internalised to form distinct organelles (King and Kay 2019). Macropinocytosis has a characteristic morphology in which the plasma membrane's active region protrudes into the surrounding environment via actin filaments rather than invaginating (Jones 2007). Of note is that macropinosomes, once inside cells, can follow two pathways of cargo delivery. They can recycle to the plasma membrane or deliver to lysosomes, where the cargo is degraded; degradation products can be transported into the cytosol for anabolic metabolism (Swanson et al. 2019) (Figure 1.9).

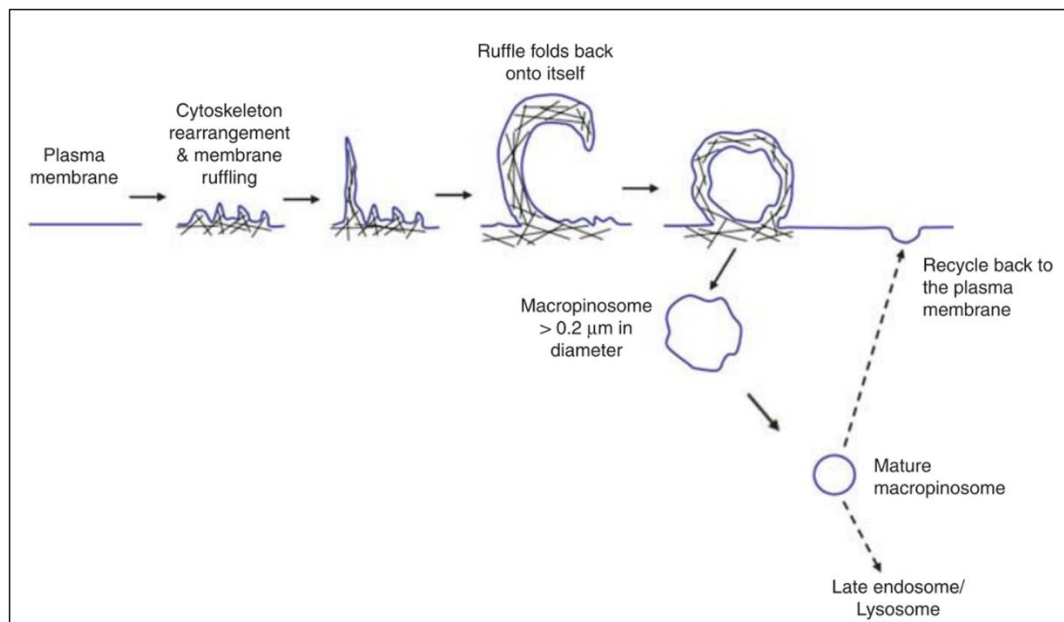


Figure 1.9: The process of macropinocytosis. Macropinocytosis includes remodelling the actin cytoskeleton at the plasma membrane, which results in the creation of membrane ruffles. Ruffles can refold and fuse at the base of the plasma membrane. Early development of macropinosomes producing a more spherical shape of macropinosomes.

The macropinosomes contents are then degraded or recycled to the plasma membrane. Adapted from (Lim and Gleeson 2011).

Macropinocytosis is driven by actin, which is an important component of endocytic membrane traffic. It is manifested in "ruffling" and is also a characteristic of cell motility (Bohdanowicz and Grinstein 2022).

The term macropinocytosis was coined by Warren Lewis, who described it as a process in which macrophages engulf liquid and other components (Lewis 1937). Now macropinocytosis is classed as a subset of CIE (Donaldson 2019). A number of cellular functions have been ascribed to this process, including in antigen-presenting immune cells (e.g., immature dendritic cells or macrophages). These cells have high levels of macropinocytosis for sampling their environment for antigens, which stimulates immune responses by naive T cells (Liu and Roche 2015). Macropinocytosis is also hijacked by intracellular pathogens such as bacteria and viruses but can also be exploited for vaccine delivery (Zeng et al. 2020; Rennick et al. 2021). With this in mind, it is promising to note findings in the literature show that, due to the efficient way macropinocytosis delivers extracellular macromolecules to targets within specific cells, it could be capitalised on for drug delivery by, for example nanotherapeutics (Li and Pang 2021).

1.3.3 Endocytic Probes

Dextran

Dextran (DEX) is a natural linear polymer of D-glucose and an exopolysaccharide (EPS) generated by lactic acid bacteria or their enzymes in the presence of sucrose. There are no known receptors for DEX in human cells, and as an inert and easy to manipulate molecule, for the last 40 years has been used as the

classical marker for fluid-phase endocytosis, with the majority reaching lysosomes in vitro. In a review of the literature, researchers have mostly studied DEXs with molecular weights ranging from 3 to 70 kDa as markers of clathrin-independent endocytosis, including macropinocytosis (Yoo et al. 2020; Al Soraj et al. 2012) or fluid-phase endocytosis (micropinocytosis) (Frost et al. 2009; Cao et al. 2007). Recently, it was shown that the size of DEXs has a significant effect on their endocytosis profiles (Li et al. 2015). The size of fluid cargoes determines their entry into cells, confirming a size-based sorting for endocytic pathways.

Now commercial DEXs of different molecular weights labelled with a library of different fluorophores are available for conducting cell-based endocytosis studies that rely upon detection of fluorescence via flow cytometry or microscopy.

Transferrin

Transferrin (Tf) is the main iron-transport glycoprotein of serum blood with a molecular weight 80-kDa and is mainly synthesized in the liver (Talukder 2021). It is composed of two lobes at the N- and C-terminus, which have a high degree of similarity and are linked by a brief connecting region. Each lobe can attach to a single metal ion of iron (Gomme et al. 2005). Iron is absorbed from the gastrointestinal tract and as the ferric (Fe^{+3}) ion, can be stably bonded and transferred from the blood to the cells via holo-Tf forms (Tf-bound diferric iron). Thus, one Tf molecule can contain two ferric ions (Fe^{+3}). Holo-Tf binds to Tf receptors (TfR) categorised as TfR1 or TfR2. TfR2 is expressed in hepatocytes, whereas TfR1 is the most widely expressed receptor for Tf and iron transporter in the majority of cells (Kawabata 2019). Fe^{+3} and Tf interact in a pH-dependent manner; Fe^{+3} binds effectively to Tf at pH 7.4 and dissociates from Tf at acidic pH, such as that seen in endosomes (pH 5.5) (Gkouvatsos et al. 2012).

In the extracellular environment at pH 7.4, holo-Tf binds TfR1, which triggers the complex's internalisation via CME (Deng et al. 2018; Ogun and Adeyinka 2021 ; Tortorella and Karagiannis 2014; Richard and Verdier 2020) (Figure 1.10). Fe^{+3} dissociates then from Tf (apo-Tf) in the acidic environment of the endosome. Six-transmembrane epithelial antigen of the prostate 3 (STEAP3) then convert Fe^{+3} to Fe^{+2} and subsequently transport it into the cytosol via divalent metal transporter 1 (DMT1) (Tabuchi et al. 2000). The recycling endosome then transports the Tf/TfR1 complex to the cell surface, where apo-Tf is discharged into the circulation (De Domenico et al. 2008). Thus, cells efficiently assimilate serum iron via the Tf/TfR1 system, and both TfR1 and Tf are utilised in another cycle of iron absorption by cells (Maxfield and McGraw 2004). Furthermore, it is important to highlight that Tf continues to associate with TfR as the endocytic cycle from the plasma membrane to endosomes and back to the plasma membrane again. Apotransferrin, however, has a weak affinity for TfR at pH7.2, thus it dissociates from the receptor upon entering the plasma membrane, allowing the receptor to bind to another iron-loaded Tf (Maxfield and McGraw 2004; Ogun and Adeyinka 2021).

Due to the increased iron requirement of cancer cells and the fact that CME mediates TfR, it has been found that TfR can be efficiently targeted in cancer treatment, and several Tf conjugates are used to deliver medications (Shimosaki et al. 2017).

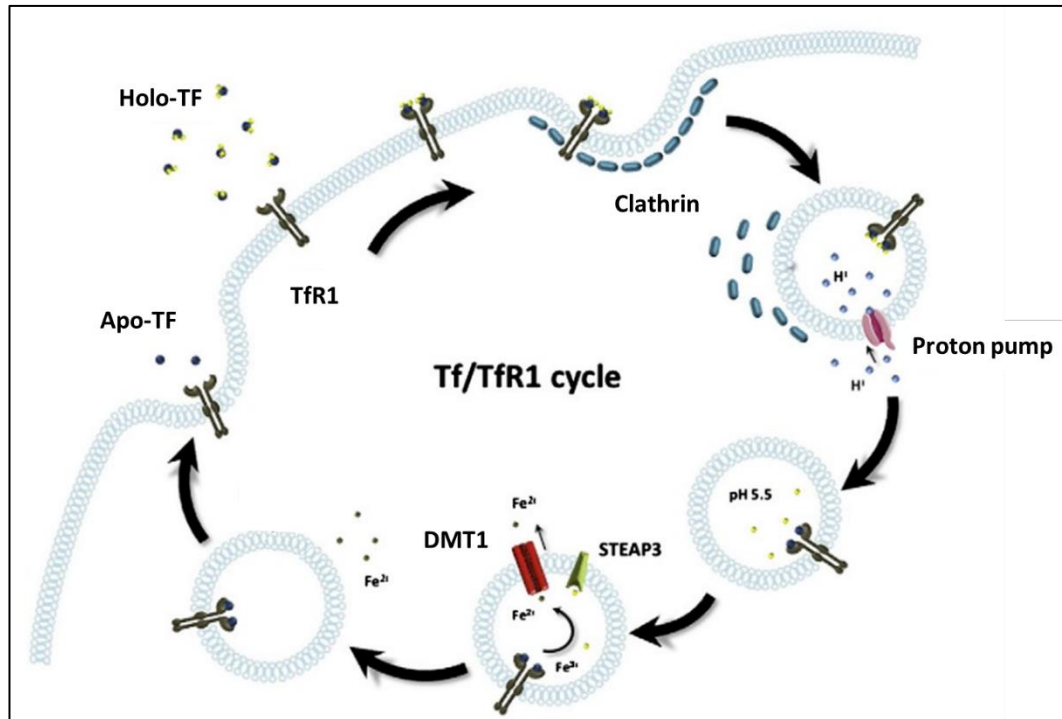


Figure 1.10: TfR1 and Tf cycle of iron absorption via CME. Tf binds to its cell surface Tf receptor (TfR), and CME is initiated by forming clathrin-coated pits and continues with the internalisation of the vesicle into the cytoplasm. Reduced pH to 5.5 by hydrogen ion proton pumps (H⁺ ATPase) in the endosome results in the dissociation of iron bound Tf vesicles, which release their iron ions. At a neutral pH, apo Tf dissociates from its receptor and enters the bloodstream, where it repeats the cycle. Apo Tf remains bonded to its receptor and is recycled to the plasma membrane. Adapted from (Gkouvatzos et al. 2012).

DEX and Tf represent endocytic probes used in this study, but several other probes have been used to identify other uptake routes, including lactosylceramide, which was identified to be internalized via caveolae with albumin and also shown to be endocytosed via this pathway (Kaźmierczak et al. 2020), and a number of different molecules shown to be internalized via CIE including interleukin 2 and receptors such as MHC Class 1 (Mayor et al. 2014). There is however an important shortage in having probes as selective as Tf for other pathways and ligand/receptors that have been shown to enter via only one pathway.

1.3.4 Chemical inhibitors of endocytosis

There has been considerable interest in discovering a chemical agent that would selectively inhibit a distinct endocytic pathway, thus allowing researchers to then investigate which pathways are used by ligands and receptors for cell entry and also drug delivery vectors. In order to comprehend endocytosis processes in cell biology, endocytosis inhibitors have been produced. Understanding the manner of uptake can provide crucial information regarding delivery efficiency and therapeutic efficacy. For instance, endocytosis is the primary uptake for nanoparticles to enter the cell (Rennick et al. 2021). Those discovered (Table 1.5) have been extremely popular for analysing endocytosis for several reasons. First of all, pharmacological inhibitors have an effect on all eukaryotic cells, and it is possible to titrate and quantify these effects in a relatively straightforward manner. Secondly, Cells and endocytosis are often exposed to inhibitors for a short time, preventing the development of delayed side effects or compensatory mechanisms. Thirdly, pharmacological inhibitors are still the most effective options for in vivo research. Finally, approaches utilising chemical inhibitors are the least time- and labour-intensive, and they are the most cost-effective. However, despite their popularity in the cell biology and drug delivery field, several reviews have pointed out that significant caution should be taken when interpreting data from studies using these agents and by far the main concern regards their lack of specificity and selectivity for any particular pathway (Ivanov 2008).

Table 1.5: Examples of Endocytosis inhibitors (Rennick et al. 2021; Dutta and Donaldson 2012; Ivanov 2008)

Targeted Pathway	Endocytosis inhibitors	Mechanism of Action	Off target effect
CME	Hypertonic sucrose	-Inhibit clathrin in micro cages. -Block protein internalisation.	Macropinocytosis can be inhibited.
	Potassium depletion	Block clathrin-coated pit	Interact with actin.
	Cytosol acidification	Inhibit cytosolic pH	Macropinocytosis can be inhibited.
	Chlorpromazine	Inhibit clathrin and AP2 complex	CIE can be inhibited in some cells.
	Chloroquine	Affects the function of clathrin-coated vesicles.	
	Dynasore	Blocks GTPase activity of dynamin.	Interact with actin.
Lipid Raft/Caveolae-Mediated	Methyl-beta-cyclodextrin	Inhibit cholesterol from the Plasma	CME and Fluid phase endocytosis.

Endocytosis		membrane.	
	Filipin and nystatin	Interact with cholesterol.	Has little effects on CME and Macropinocytosis.
Macropinocytosis	Amiloride/EIPA	Inhibit NHE exchange.	May also block CME.
Macropinocytosis and Phagocytosis	Cytochalasin D	Depolymerizes F-actin.	Interact with actin polymerization and may inhibit multiple pathways

In this project, only macropinocytosis inhibitors were studied and details on these are given in the Introduction to Chapter 3.

1.4 Nanoparticles

1.4.1 Nanoparticle Delivery Systems

This study focuses on NP designed to induce internalisation of HER2 via following their design, physical and finally biological characterization in HER2 positive and negative BC cell lines. Here a brief introduction will be given to NP as drug delivery systems, and as this is a huge field of literature; major focus will be given to those that have been conjugated to Tz. Here a NP is defined as a structure ranging between 10-300 nm in diameter though other measurements have also been used to define this term (Alirezai et al. 2022; Kobayashi et al. 2014) .

During the past twenty years, there has been considerable development in the nanomedicine field, particularly in relation to its potential use for treating cancer and more recently as vaccines (Neek et al. 2019; Davodabadi et al. 2022). In this capacity, nanomedical research often focuses on developing systems whereby a generated NP is synthesised to enclose a bioactive agent such as a small molecule drug, for example an anti-cancer agent, or a biological molecule such as mRNA or siRNA (Kon et al. 2022; Ashrafizadeh et al. 2021; Montané et al. 2020; Jin et al. 2020). This branch of research explores multiple NP formulations based on for example polymers or liposomes that vary in size and charge (Figure 1.11) (Sun et al. 2014; Joy et al. 2022). NPs also offer the capacity to encapsulate drugs of low solubility; some of these are effective compounds but are pharmacokinetically poor, which has traditionally limited their efficiency and use. By incorporating them into NPs, these compounds adopt a different biodistribution and pharmacokinetic profile, improving their efficacy and safety (Guo and Huang 2014). NPs can also address problems of low therapeutic

indexes, drug resistance, drug toxicity, and the efficacy of medications approved to treat cancer (Manzari et al. 2021). Furthermore, NPs enhance both the selectivity and specificity of anti-cancer agents. For NPs carrying small molecule drugs can avoid P-glycoprotein recognition, which has been identified as a fundamental drug resistance mechanism for small molecule drugs (Niazi et al. 2016). In efforts to circumvent toxic anti-cancer agents distributing throughout the body they can be encapsulated into NPs that are then decorated with ligands such as antibodies for specifically targeting receptors that are overexpressed on the surface of cancer cells (Gavas et al. 2021; Peng et al. 2019; Alasvand et al. 2017).

Conventional chemotherapy is most often associated with poor selectivity for cancer cells following systemic administration and they must cross to number of biological barriers, including blood vessels, tissues, organs, cells, and even subcellular compartments to reach their targets. The majority of these issues could potentially be overcome and intratumoural accumulation increased by NPs decorated with active ligand (Toporkiewicz et al. 2015). Monoclonal antibodies (mAbs), which are the main focus of this research, are one example of this. In numerous studies, Tz-decorated NPs have been employed to specifically target HER2 and deliver cytotoxicity (Sakhi et al. 2022; Choi et al. 2018; Zhang et al. 2019). HER2 was also targeted by antibody fragments, such as affibody protein (8kDa) conjugated PLGA using carbodiimide chemistry (Shipunova et al. 2021). Nanobody is a Fab fraction of conventional antibodies or single-domain antibody with a molecular weight of only 15 kDa targeted HER2 as well (Altunay et al. 2021).

Via modifications in surface chemistry NPs can be tailored for attachment to ligands that can result in delivering a therapeutic to target cancer cells overexpressing plasma membrane receptors (Yang et al. 2022). Several different ligands have now been attached to the surface of NPs to selectively target receptors in cancer cells (Table 1.6). Once decorated nano formulations bind to a specific receptor. There is, in the vast majority of cases, a need for endocytosis and by default the receptor must also internalise. However, while NPs offer many advantages as drug carrier systems, a range of limitations have yet to be solved, including poor oral bioavailability, instability in circulation, inadequate tissue distribution, and toxicity (Rajan and Sahu 2020; Cho et al. 2008; Mitchell et al. 2021).

Table 1.6: Examples of ligands conjugated NPs for cancer targeting.

Ligand name (active targeting)	Ligand classifications	Cancer receptor targeted	Reference
Cetuximab	Monoclonal Antibodies	EGFR	(Su et al. 2022)
Pertuzumab	Monoclonal Antibodies	HER2	(Fisusi et al. 2020)
Tz	Monoclonal Antibodies	HER2	(Fisusi et al. 2020)
Hyaluronic Acid	Polysaccharides	CD44	(Hayward et al. 2016)
Transferrin	Glycoprotein	Tf receptor	(Bhagwat et al. 2020)

Folic acid	Vitamin	Folic acid receptor	(Bahrami et al. 2015; Alirezai et al. 2022)
sgc8c and TDO5	Aptamers	PTK 7 receptors and IgG receptors	(Bamrungsap et al. 2012)
sp204	Peptide	Androgen receptor	(Yeh et al. 2016)
Z HER2:342	Affibody	HER2	(Satpathy et al. 2014)
HER2 Nanobodies	Nanobody	HER2	(Altunay et al. 2021)
Lectin	Carbohydrate	Sialic acid glycans receptors	(Martínez-Carmona et al. 2018)

1.4.2 Efficacy of Passive Nanoparticle Targeting

Depending on the size of a particular NP injected into a human vein, it may not be able to escape outside the blood vessels to reach a particular cancer tissue. It is known since 1984 that tumour vasculature is leaky and within the tumour environment there is poor lymphatic drainage and this is the basis of the Enhanced Permeability and Retention (EPR) of formulations such as NPs (Matsumoto et al. 1984). Further evidence was published two years later to support the EPR effect in the context of tumour targeting (Maeda and Matsumura 1986). The existence of significant gaps between endothelial cells on the walls of the tumour vasculature was verified using direct visualisation methods, including optical microscopy and electron microscopy (Hashizume et al. 2000), and the EPR effect is still highlighted as a means to more selectively deliver NPs to tumours. However, there is also evidence that significant differences exist with respect to the extent of EPR in different tumours (Hashida 2022; Shi et al. 2020;

Jahan et al. 2021). NPs once injected into the body, face both physical and biological barriers such as diffusion, flow and shear forces, aggregation, protein adsorption, phagocytic sequestration, and renal clearance. All have the potential to influence the proportion of administered NP reaching cancer cells (Lazarovits et al. 2015).

The potential that NPs could be engineered to selectively detect and destroy cancer cells in the body remains an interesting concept (Min et al. 2015). For EPR effects, large gaps in tumour vessels enhance permeability of the tumour vasculature, which is the result of fast and disorganized angiogenesis (Hobbs et al. 1998). A recent study by Sindhvani and colleagues indicates that NPs can penetrate the tumour vasculature (endothelial cell lining) mostly through a transcytosis process (Sindhvani et al. 2020). NP parameters that affect interactions with biological barriers include material composition, geometry, surface chemistry, charge, and mechanical properties (Blanco et al. 2015). EPR parameters are also affected by for example the type of tumour, anatomical location and its stage (Shi et al. 2017).

A review of analysis of research (2006-2016) into NP delivery and accumulation in tumours indicated that only 0.7% of the administered NP dose is found to be delivered to a solid tumour (Willhelm et al. 2016). It highlighted the extensive use of in vitro (cell culture) models and in vivo models (such as murine) models; that did not result in promising clinical translation. In 2020 less than 10 anticancer drug delivery systems were entering phase III or IV clinical studies or had regulatory approval in Europe and the United States (de Lázaro and Mooney 2020).

1.4.3 Nanoparticle targeted BC

Numerous NP materials and BC targeting by ligands have been investigated. Through receptor-mediated endocytosis, the presence of ligand on NPs surfacers improves drug delivery. Overexpression of receptors in BC cells is the basis for ligand-targeted therapy. These receptors include EGFR, Folic acid, HER2, Oestrogen receptor, CD44, Tf, Biotin, $\alpha\beta3$, luteinizing hormone releasing hormone receptor (LHRH) and ETC (Jahan et al. 2021).

1.4.4 Tz decorated NPs targeting BC

One aim of this project is to generate NP decorated with Tz that contains a chemotherapeutic agent and then study its dynamics in cells in addition to its capacity to drive HER2 endocytosis via its clustering at the plasma membrane. Multivalent Tz NPs could initiate HER2 clustering by conjugating several Tz molecules at the particle's surface; this can enhance the antiproliferative effect and inhibit Tz resistance (Truffi et al. 2018). Thus, the formulation would have dual capacity in reducing the expression of HER2, and therefore its signalling capacity, and deliver the chemotherapeutic payload to inhibit cell division.

1.4.5 Materials for making NPs

It is beyond the scope of this thesis to discuss all the materials that have been used for making NPs for the purpose of drug delivery. These include for example those based on polymers, lipids, proteins, and combinations of these to eventually generate a nanostructure that is fit for purpose (Alasvand et al. 2017; Gavas et al. 2021; Montané et al. 2020). The main categories with reviews for each type is presented in table 1.6 and focus will then be given to polylactic-co-glycolic acid (PLGA) that will used in this thesis to generate a HER2 targeting

formulation. More information on PLGA and PLGA drug delivery system is given in Chapter 5.

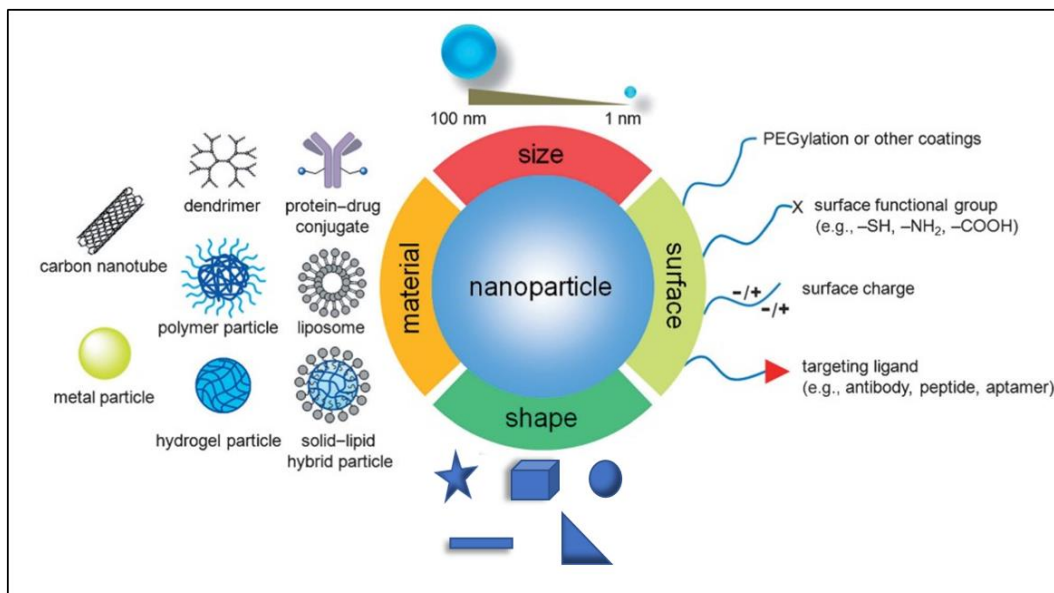


Figure 1.11: A schematic representation of the various nanoparticle properties that have been studied in cancer therapy to promote drug delivery (Sun et al. 2014).

1.5 Hypothesis, Aims, and Objectives

1.5.1 Hypothesis

This work is based on the hypothesis that Tz decorated NPs can be generated to specifically induce HER2 clustering to stimulate macropinocytosis, its delivery to lysosomes and degradation. This strategy will also allow co-delivery of small molecule drugs encapsulated within the NP.

1.5.2 Main aims, and objectives proposed for the project

As discussed above, HER2 overexpression has been identified in 20-30% of all breast cancers, and this has been linked to the oncogenesis-development-progression process for aggressive cases. HER2+ BC prognosis is typically negative, and the receptor represents a crucial target for treatment interventions.

For this particular type of BC, Tz is the primary treatment option, but it is worth emphasising that therapeutic resistance undermines the degree to which it is clinically effective. This is partly due to the status of Tz as a weak driver of HER2 downregulation/internalisation, and as a consequence of this, the therapeutic agent is considered an inefficient way in which to facilitate intracellular cytotoxic delivery. Once Tz as the ADC Kadcyla and conjugated to emtansine binds to the plasma membrane, it needs to be endocytosed and delivered to the late endosomes and lysosomes to allow proteases to degrade the antibody allowing the drug to then escape to reach the microtubules (Fu et al. 2020). Since endocytosis does not downregulate HER2 in an efficient manner, and since HER2 hinders endocytosis of HER1, 3 and 4 following heterodimerisation with them, it is referred to as the endocytosis deficient member of the HER family of receptors. Thus, new mechanisms are needed to promote endocytosis of HER2.

An initial aim of this project was to study the selectivity of NHE1 inhibitors EIPA, amiloride and cariporide for different endocytic pathways to consolidate earlier studies in the laboratory showing that EIPA may induce uptake of Tz-HER2 rather than inhibition. A major project aim was to then generate a NP platform for conjugation to Tz to test the hypothesis that this could lead to HER2 targeting and clustering, endocytosis and co-delivery of therapeutics. More widely the project aims to advance BC research, specifically by allowing future researchers to establish multifunctional formulations to target various plasma membrane receptors.

A major objective was to utilise the NHE1 inhibitors together with confocal microscopy and flow cytometry to test their selectivity for inhibiting the endocytic uptake of the macropinocytosis probe DEX and also probes such as Tf that enter

via different pathways. This would lead to analysis of NHE1 inhibition in the presence of the targeting NPs to investigate whether they, as hypothesised, stimulate macropinocytosis to gain entry to the cell. The project's other main objective was to generate and physically characterise PLGA NPs decorated with Tz and enclosing a small molecule label and/or drug (Figure 1.12). By labelling the antibody, binding and internalisation of the NP in BC cells could be measured along with their capacity to drive HER2 degradation and deliver a cytotoxic drug to inhibit cell viability.

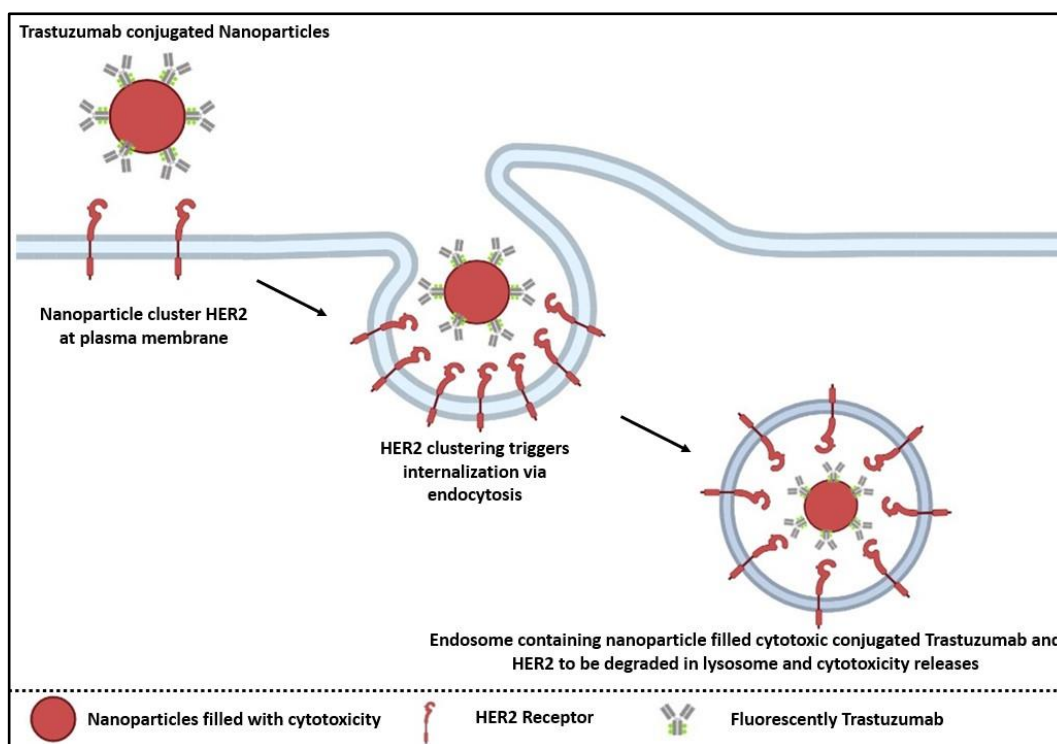


Figure 1.12: A schematic model of the hypothesised mechanism behind NP-mediated clustering of HER2. The conjugated NP becomes internalised along with the receptor. It is speculated that if the NPs have several Tz molecules bound to it, the NP will imitate HER2 cross-linking and clustering, thus triggering HER2 endocytosis. The intracellular trafficking mechanism of HER2/NP endosomes has not yet been elucidated. However, if comparable to the mechanism described in Moody et al., lysosomal degradation of HER2 and the NP would result in cytotoxic drug being released into the cell. Prepared using BioRender.

1.5.2 Main experimental methods proposed for the project

- (1) Cell culturing for BC cell lines and analysis of cell viability
- (2) High Content analysis of BC cell models via live cell imaging confocal microscopy
- (3) Flow cytometry to quantify the BC cell internalisation of endocytic probes
- (4) Western blots for assessing HER2 expression in BC cells
- (5) Synthesis and physical characterisation of Tz decorated PLGA NPs
- (6) Apply methods 1-5 for analysing the dynamics of NPs in BC cells

Chapter 2 : Materials and Methods

2.1 Materials

Four BC cell lines were used in this study, and all were originally purchased from American Type Culture Collection (ATCC) and selected based on their expression of HER2. MCF7 and BT474 human BC cells were gifted at low passage (P9) from the Breast Cancer Molecular Pharmacology Group (BCMPG), Cardiff University UK. Tz as prescription medicine ontruzant 150 mg - (LOT: F1803047) was generously provided by the Velindre Cancer Centre in Cardiff, UK. BC SKBR3 and Clone5 BT474 were purchased from (ATCC).

Table 2.1: BC Cell lines used in this study.

Cell lines	Catalogue number	Classification (Garcia et al. 2020).	ER	PR	HER2
BT474	#HTB-20	Luminal B	+	+	+
Clone5 BT474	#CRL-3247	Luminal B	+	+	+
SKBR3	#HTB30	HER2+	-	-	+
MCF7	#HTB22	Luminal A	+	+	-

Life Technologies (Paisley, UK):

DMEM Low sugar (#21885), DMEM high Sugar (#21875), FBS (#16000-044) - 0.05% Trypsin EDTA (#25300062), Hoechst 33342 (#H3570), Transferrin Alexa 488 (#T-13342), CellMask™ Plasma Membrane Stain (#C10046).

Sigma Aldrich (Poole, UK):

Triton X-100 (#X100), BSA (#A7906), Bicinchoninic Acid solution (#B9643), Copper (II) Sulphate solution (#C2284), Ponceau S solution (#P7170), Tween 20 (#P1379), cOmplete(TM), Mini Protease Inhibitor Cocktail, Tablets provided in a glass vial (#11836-153001), N-(3-Dimethylaminopropyl)-N'-ethylcarbodiimide hydrochloride (#E7750), N-Hydroxysuccinimide, 98% (#130672), Carboxylic acid-poly(ethylene glycol)-b-poly(lactide-co-glycolide)(#902071), Poly(D,L-lactide-co-glycolide), lactide:glycolide (50:50), mol wt 30,000-60,000 (#P2191), Rhodamine B, ≥95%(HPLC)(#R6626), Poly(vinyl alcohol), Mw 89,000-98,000, 99+% hydrolyzed (#341584), Invitrogen Goat Anti-Rabbit (#32460), EIPA (#A3085), Cariporide (#SML1360).

VWR International Ltd (Leicestershire, UK)

Amiloride HCL (#129876-100), Microspatulas (#231-0296).

Promega (Loughborough, UK):

CellTitre Blue viability assay (#G8080).

Bio-rad (Hemel Hempstead, UK):

Clarity Western ECL substrate (#170-5060), Any kD Mini-PROTEAN TGX Precast Protein Gels, 10-well, 50 µl (#4569034).

Fisher Scientific (Loughborough, UK):

Coverslips No. 1 circle 16mm diameter (#12313138), PVDF membrane (#10344661), Invitrogen™ NP40 Cell Lysis Buffer (#10069262), Thermo Scientific™ SuperSignal™ West Femto Maximum Sensitivity Substrate (#11859290), Molecular Probes™ Alexa Fluor™ 488 NHS Ester (Succinimidyl Ester)(#10266262), Invitrogen™ Transferrin From Human Serum, Alexa Fluor™ 488 Conjugate (#11550756), Fisherbrand™ Snap Cap Vial, Clear Glass (#10749644), Invitrogen™ Molecular Probes™ DEX, Alexa Fluor™ 488; 10,000 MW, Anionic, Fixable (#D22910), Zeba™ Spin desalting columns (#WB319157), PBS, pH 7.2-500 MI (#20012019).

Insight Direct UK Ltd (Sheffield, UK)

Trans-Blot Turbo Transfer Pack, PVDF, 7 x 8.5 cm (#170-4156).

Strattech Scientific Ltd (Suffolk, UK):

Doxorubicin (#A3966-APE).

Cell Signalling Technology

Rabbit—HER2 antibody (#2242).

Abcam

Mouse—Tubulin HRP (#ab-21058).

2.2 Cell Culture

2.2.1 Routine Cell Maintenance

Cells were passaged every 3-5 days and added to the cell culture plate, usually a T-75 flask with low confluency, and split when the confluency reached 80%. The media was aspirated, cells washed with 8 to 10 mL PBS. This was then removed, and 2 mL of Trypsin EDTA (ethylene diamine tetraacetic acid) (0.05%) was added to detach the cells. Cells were then incubated for 5-10 minutes (mins) under tissue culture conditions (37°C/5% CO₂) until detached from the plate surface. Media (10 mL) was then added, and the suspended cell solution was transferred to a 15 mL falcon tube and centrifuged at 400 x g for 3 mins. Following removal of the supernatant, cells were diluted in an appropriate volume of fresh media with aliquots passing on to new flasks to achieve 20-30% confluency. Cells were not passaged more than 30 times to avoid phenotypic drift.

2.2.2 Freezing Cells

Frozen cell stocks were seeded in a T-175 cm² flask and prepared by freezing down 80% confluent cells in a freezing media. The freezing media was made 1-2 days prior to the experiment and included 85% DMEM, 10% FBS, and 5% DMSO and was stored in the refrigerator at 2° to 8°C. Media was aspirated and cells were washed 2x with PBS. Cells were then detached with 0.05% w/v Trypsin, and the flask was incubated for 10 mins under tissue culture conditions (37°C/5% CO₂). After deactivating trypsin with 10 mL of warmed media, the total number of cells was measured using a Scepter 2.0 Cell Counter (Thermo Fisher Scientific, Loughborough, UK). The cell suspension was then centrifuged for 3 mins at 400 x g, resuspended in cold freezing media at a cell density of ~1 x 10⁶/mL, and

aliquoted (1mL) into each cryovial. Each vial was labelled with a permanent marker to indicate the cell type, passage number, person name, and date. Cryovials were frozen at -20°C in a Mr. Frosty™ freezing container with isopropanol at a rate of 1°C per min. Cell vials were initially stored at -20°C for 5 hrs and then at -80°C for 24 hrs before being transferred to liquid nitrogen for long-term storage.

2.2.3 Thawing cells

Cells preserved in liquid nitrogen were thawed rapidly by immersing cryogenic vials in a 37°C water bath. Once thoroughly defrosted, cells were transferred to a clean 15 mL tube containing 10 mL complete media and centrifuged for 3 mins at 400 x g to eliminate any residues of DMSO. After discarding the supernatant, the cell pellet was resuspended in a 15 mL complete media and placed in a sterile T-75 tissue culture flask. After overnight incubation to allow the cells to attach, the media in the flask was changed with new complete media to remove dead cells that floated.

2.2.4 Media

All BC cell lines were cultured in DMEM (Dulbecco's Modified Eagle Media), with high glucose used for SKBR3 and BT474, and low glucose for Clone5 BT474 and MCF7. All media contained phenol red and was supplemented with 10% v/v FBS.

2.3 Live Cell Uptake Analysis

2.3.1 Cell Culture

Cells (2.5×10^5 – 3×10^5) were seeded with 2 mL of media in 35 mm glass-bottomed imaging dishes (MatTek) and incubated at 37°C in a 5% CO₂ humidified atmosphere for 60 hrs to allow them to reach 70-80% confluency at

the start of the experiment. **For all experiments employing endocytic probes or endocytosis inhibitors controls were set up under identical conditions employing diluent solutions (e.g., DMSO/PBS) rather than the probes/inhibitors. All cell incubations at 37°C were performed under tissue culture conditions of 5% CO₂ and 37°C.**

2.3.2 Confocal Microscopy

Confocal microscopy was performed with a Leica TCS SP5 Confocal Microscope (Leica Microsystems Ltd, Buckinghamshire, UK) using the 405, 488, and 633 nm lasers and utilizing the heated platform and CO₂ chamber. The microscope was equipped with a 40, 65x oil-immersion objective. Both gain and offset setting were adjusted and improved for each imaging well within a vehicle control in each experiment. Images were recorded using the sequential scanning mode in some experiments to prevent fluorescence channel crosstalk/bleed through Images were scanned at 200 Hz with a line average of three to reduce noise and captured using the Leica LAS AF software on the system. Images were processed using ImageJ software and further details are provided in Appendix A.

Chapter 3 methodology

2.3.3 DEX uptake experiments as a fluid phase marker +/- Inhibitors

All experiments contained vehicle control assays and treatment conditions. DEX70 kDa Tetramethylrhodamine (TMR) or DEX10 kDa (alexa 488) from a stock concentration of 5 mg/mL was diluted with dH₂O for drug-free treatment in 600 µL of complete media to give a final concentration of 0.5mg/mL +/- 50 µM inhibitors (amiloride, EIPA, and cariporide). All cells were then incubated for 2 hrs under tissue culture conditions. After aspirating the media from the dishes, the

cells were washed twice with 1 mL of PBS and resuspended in 600 μ L of serum-free media (SFM) (Phenol red free) for confocal imaging. Experimental points were staggered (20 mins) to allow for confocal imaging.

2.3.4 Transferrin Experiments as a marker for Clathrin Mediated Endocytosis

Control and treatment cells were washed twice with PBS and then pre-incubated for 30 mins under tissue culture conditions in 0.2 % BSA (Bovine serum albumin) diluted in SFM; this to deplete the cells of bovine Tf. Cells were washed twice with PBS and then incubated for 1 hr with 50 nM Tf-Alexa488 (Tf- from a stock concentration of (5mg/mL conjugate = approx 62.5 μ M Tf) and 50 μ M inhibitors in 600 μ L of SFM. The cells were then washed and imaged.

2.3.5 Fluorescence-Activated Cell Sorting (FACS)

FACS was performed with (FACSCalibur, Becton Dickinson, Heidelberg, Germany) to provide more quantitative analysis of the cell uptake of the two probes in the presence of the inhibitors.

2.3.6 Dextran uptake experiment in the presence of macropinocytosis

Cells were seeded in 12-well plates at $1.2 - 1.5 \times 10^5$ cells/well and incubated under tissue culture conditions for 60 hrs. They were then washed with 2x PBS and then incubated for 2 hrs in 400 μ L complete media containing 0.5 mg/mL of the 70 or 10KDa fluorescent DEX's. The media was then removed, and cells washed 2x with PBS before by adding 250 μ L of Trypsin-EDTA per well and incubated for 5 mins at 37°C. The culture plates were then put on ice, and cold 10% FBS in PBS was added to deactivate the Trypsin. Cells were transferred to the Eppendorf tube on ice and centrifuged at 400 x g 4°C for 3 mins. The

supernatant was then removed, and cells were resuspended in 1 mL fresh cold PBS and centrifuged at 400 x g 4°C for 3 mins. This step was repeated twice more. Finally, 500 µl of cold PBS was added, and cells were placed on ice prior to FACS.

2.3.7 Transferrin uptake in the presence of macropinocytosis inhibitors.

Cells were seeded at a density of $1.2 - 1.5 \times 10^5$ cells per well in 12-well plates and incubated under tissue culture conditions for 60 hrs. They were then washed twice with PBS and then pre-incubated with 0.2% (w/v) BSA (SFM/BSA) for 30 mins to deplete the plasma membrane and endosomes of bovine Tf (Moody et al. 2015). Cells were then incubated for 1 hr with 50nM Tf488 in 400 µl SFM/BSA containing the inhibitors at 50µM or diluent control. Cells were washed 2x with PBS, followed by a 1-min incubation in acid wash (0.2M acetic acid, 0.2M NaCl, pH 2.0) to remove any remaining surface Tf (Al Soraj et al. 2012). Cells were then washed 2x with PBS, followed by 5 mins of trypsinisation at 37°C. Following that, cold 10% FBS in PBS was added to deactivate the Trypsin and cells placed on ice to stop further uptake. Cells were transferred to the Eppendorf tube and centrifuged (4°C) at 400 x g for 3 mins. The supernatant was then removed, and cells were resuspended in 1 mL fresh cold PBS and centrifuged at 400 x g 4°C for 3 mins. This step was repeated twice. Finally, 500 µl of cold PBS was added, and cells were placed on ice for FACS analysis.

2.3.8 FACS Analysis

The fluorescence of DEX488/Tf488 in cells was measured using a 488 nm laser on a BD FACSCanto™ II flow cytometer system. Cells/well were counted between 7,000 and 10,000. The FACS analysis differed according to the cell type, detection parameters, and cell gating. To eliminate dead cells and debris, cells were gated using FSC-A/SSC-A, followed by FITC-A/FSC-A. In this thesis FACS analysis is abbreviated as FACS.

2.3.9 Dextran Uptake in BT474 and Clone5 BT474 cells

For live cell confocal imaging, cells were seeded in MatTek dishes until they reached the desired confluency of 80%. They were then washed 2x in PBS and incubated under tissue culture conditions with 0.5 mg/mL DEX488 in complete media (600 µl) for either 30 min or 4h. Cells were then treated as in section 2.3.2 for live cell imaging confocal microscopy and image analysis.

For quantifying DEX uptake, the cells were washed 2x in PBS, and incubated under tissue culture conditions with 0.5 mg/mL DEX488 for, 30 min, 1h, 2h, or 4h. Cells were then washed 2x with PBS and incubated for 5 min in 200 µL pre-warmed 0.25% Trypsin-EDTA. Ice-cold 10 % FBS in PBS (500 µL) was added and the cell solution transferred to the pre-chilled 1.5 mL Eppendorf tubes. Cells were centrifuged twice for 3 mins at 400 x g, and this step was repeated twice before the supernatant was removed and resuspended pellet in 500 µL fresh, ice-cold PBS and Performed for FACS.

2.3.10 Transferrin uptake and recycling in BT474 and Clone5 BT474 cells.

For live cell imaging confocal microscopy, cells were seeded in MatTek dishes according to section 2.2.1. On the day of experiment, cells were washed with PBS x2 and 600 μ L of 0.2 % BSA/SFM was added for 1 hr (Starvation). Cells were then treated with 50 nM Tf488 for 15 mins (pulse) under tissue culture conditions. The cells were then 'chased' for 10 mins and 90 mins with 600 μ L of complete media. The cells were then processed for confocal analysis as described in section 2.3.2.

For FACS analysis, cells were seeded in 24 wells until they reached the desired confluency, and then cells were washed twice in PBS. Cells were then incubated for 1 h in 0.2% BSA in SFM (Starve) washed and then incubated in 250 μ L of 50 nM Tf488 in SFM 15 min (pulse) washed two times in PBS, and then chased for either 0 min, 10 mins, 20 mins, 30 mins 1h and 1.5 hrs. The cells were then washed and treated with acid and analysed by FACS as described in section 2.3.8.

Chapter 4 methodology

2.3.11 Generation and characterisation of fluorescent Alexa488 conjugated Tz

For buffer exchange, clinical formulated Tz solution was prepared and contained: 21mg/ml Tz, L-histidine HCl, with L-histidine, α,α -trehalose dehydrate, and polysorbate. For labelling, this clinical formulation (1.5 mL, 32 mg Tz) was passed through two 10 mL Zeba™ Spin desalting columns, equilibrated in PBS pH 7.4 before being used in the in vitro studies, as previously described (Wymant et al.

2020). Of the 1.7 mL eluted from the column, 1.5 mL of Tz (30 mg) was added directly to 1 mg NHS-Alexa647 or NHS-Alexa488.

Two Zeba columns were employed following the manufacturer's procedure for centrifuge balance and to filter the Tz solution twice through the column. The bottom closure of the column or the bottom sealing material of the plate was twisted off, and the columns' cap was loosened but not removed. After inserting the column into the collection tube (50 mL centrifuge tube), the column was centrifuged at 1000 x g for three mins to remove the storage solution. After discarding the storage solution, PBS was placed on the resin and the tube centrifuged at 1000 x g for three mins to collect flow through. The storage solution was then discarded, and this step was performed twice. After each spin, the resin was checked to ensure that there was no evidence of fluorescence. Tz was then added to one of the columns, and an equal volume of PBS was added to the other column for balance. Both columns were then centrifuged at 1000 x g for three mins. After discarding the PBS, Tz 1st purified solution (storage solution) was added along with an equal volume of PBS for the column used for the first flow of Tz. The concentration of Tz was then calculated following the Bicinchoninic acid assay (BCA) assay. Both columns were centrifuged again, and Tz (2nd purified solution) was collected and stored in -20 for further uses.

Tz (30 mg/mL) from the previous eluted solution was added to 1 mg NHS-Alexa488 (w/v). At room temperature, the conjugation was processed in a dark place and the reaction was allowed to run for 1 hr.

Any excess of unbound alexa488 was purified and eliminated using Zeba Spin desalting columns. The previous method for Tz purification was followed here,

and the Tz488 solution was run through the column twice. The Tz488 was then filtered with a 0.2-micron filter, aliquoted into 0.5 mL Eppendorf tubes, and stored at -20 °C. The number of fluorophores per antibody of Tz was then calculated using a Jasco V-650 UV-Vis spectrophotometer.

2.3.12 Analysis of Tz concentration

The bicinchoninic acid (BCA) assay was used to determine the concentration of Tz. BSA protein standards were produced in PBS at concentrations ranging from 0 to 10 mg/mL utilizing BSA as the protein source. Because the sample absorbance values were within the assay's linear range, the Tz solution was diluted at 1:6 and 1:10 in PBS buffer before being used. Next, the BCA working solution was necessary to mix 49 parts bicinchoninic acid with 1 part copper sulphate pentahydrate. A total of 200 µL of working BCA solution was pipetted into a 96-well plate with a flat bottom. A sufficient BSA and copper sulphate solution was prepared to allow for the total collection of duplicate measurements for BSA standards and triple measures for Tz samples. The standards/samples (20 µL) were added to the appropriate number of measurement wells, and the mixture was mixed well. The plate was incubated at 37°C for 30 mins before the absorbance at 562 nm was measured using a plate reader.

The absorbance values were plotted against the known BSA standard concentrations to produce a calibration curve, which was then used to build the curve. The unknown was determined using the equation of the line of best fit for the calibration graph, which was then used to find the unknown.

2.3.13 Tz488 binding HER2 downregulation and method optimization

Tz conjugated Alexa 488 selectivity for binding to HER2 was tested in 4 BC cell lines using confocal microscopy. Cells were seeded in 35 mm (MatTek) dishes until they reached 80% confluency and incubated with (50nM) in 600 μ L of complete media under tissue culture conditions for 30mins, 1h, 3h, 5h or 7h. After aspirating the media from the dishes, the cells were washed twice with 1 mL of BPS and resuspended in 600 μ L of SFM for confocal imaging.

2.3.14 Cell uptake of Tz488 in the presence of EIPA.

Some method optimisation was required for this analysis, described as methods A,B and C

1- Method A

Two conditions were set up for each time point: vehicle control and Tz-488 treatment. Cells were cultured in a 35 mm (MatTek) dish until they reached a confluency of 80% and then washed with PBS. Cells were then treated with 50 nM Tz488 for 1 hr followed by 50 micromolar (μ M) EIPA for 1 hr or the cells treated with 50 nM Tz488 for 5 hrs followed by 50 μ M EIPA treatment for 1 hr. Cells were then washed in PBS before analysis by live cell imaging confocal microscopy.

2- Method B

Cells were seeded in a 35 mm (MatTek) dish until they achieved 80% confluency and then washed with PBS. They were then treated with 50 μ M EIPA for 1 hr followed by 50 nM Tz488 for 1 hr, or with 50 μ M EIPA for 5 hrs followed by 50 nM Tz488 for 1 hr. Cells were then washed in PBS before analysis by live cell imaging confocal microscopy.

3- Method C

Cells were seeded in a 35 mm (MatTek) dish until they achieved 80% confluency and then washed with PBS. They were then co-incubated with 50 nM Tz488 and 50 μ M EIPA / Inhibitors for 2 or 5 hrs, washed 2x with PBS before analysis by live cell imaging confocal microscopy.

2.3.15 Cell Mask +/- EIPA

Cells were cultured in a 35 mm (MatTek) dish until they reached 80% confluency, washed with PBS and co-incubated with 50 μ M EIPA and CellMask for 5 hrs under tissue culture conditions. Cells were then washed with PBS twice before analysis by live cell imaging confocal microscopy.

2.3.16 Metabolic Activity Assays

Analysis of Metabolic Activity

The viability of the cells was evaluated using the CellTiter-Blue® assay, performed according to the manufacturer's instructions. In a 96-well plate, 11000 cells/well were seeded for SKBR3 and BT474, and 8500 cells/well for CLONE5 BT474 and MCF7 (Corning 3603, Black Plate, clear bottom). Cells were then incubated, in the presence or absence of external compounds such as drugs and Tz, under tissue culture conditions for 7 or 24 hrs. To minimise cell loss, cells were seeded in 100 μ L of media for 48 hrs and then supplemented with an additional 100 μ L of media containing agents on the treatment day. Under control conditions of growth, the number of cells in each well was expected to reach 15,000 cells/well. The fluorescence (544Ex/590Em) in each well was examined using a Fluostar Optima fluorescence plate reader after 4-hr incubation with 20 μ l

of CellTiter-Blue reagent. Each assay contained the following conditions in either duplicate or triplicate (Table 2.2):

- i. No-Cell Control: wells containing all reagents but no cells
- ii. Untreated Controls: cells incubated during the experimental period in complete media alone
- iii. Vehicle Controls: Cells incubated during the experimental period in complete media containing the equivalent volume of diluent for each respective compound
- iv. Test Compound: Cells incubated during the experimental period in complete media containing the test compound
- v. Cytotoxicity Control: Cells incubated during the experimental period in complete media containing 0.2 % v/v Triton X-100 to permeabilise the plasma membrane (Sayers et al. 2022).

Table 2.2: Different methods in the project for metabolic activity assay

Metabolic Activity Assays					
Section	Method descriptor	Agent or diluent	Concentration - Incubation time	Cell Titer Blue	Information
2.3.16.1	Macropinocytosis Inhibitors	Amiloride	0- 500 μ M for 24 hrs	4 hrs	
		EIPA	0- 500 μ M for 24 hrs	4 hrs	
		Cariporide	0- 500 μ M for 24 hrs	4 hrs	
2.3.16.2	EIPA and Tz (Protocol 1)	EIPA	0- 500 μ M for 7 hrs	4 hrs	cells were co-incubated with EIPA and Tz
		Tz	0-500 nM for 7 hrs	4 hrs	
2.3.16.3	EIPA and Tz Protocol 2	EIPA	0- 500 μ M for 24 hrs	4 hrs	
		Tz	50 nM for 24 hrs	4 hrs	
2.3.16.4	Solvents cytotoxicity	PBS	0- 10% for 24 hrs	4 hrs	
		MeOH	0- 10% for 24 hrs	4 hrs	
		DMSO	0- 10% for 24 hrs	4 hrs	

2.3.16.5	PLGA-Tz cytotoxicity	PLGA	0- 500 µg/mL for 24 hrs	4 hrs	
		PLGA-Tz	0- 500 µg/mL for 24 hrs	4 hrs	
2.3.16.6	PLGA-DOX-Tz cytotoxicity	DOX	0- 10 µM for 24 hrs	4 hrs	Concentration based on DOX encapsulation in NP.
		PLGA- DOX-Tz	0- 10 µM for 24 hrs	4 hrs	

Chapter 5 methodology

2.3.17 Synthesis of Rhodamine B (RhoB) / Doxorubicin (DOX) encapsulated Tz conjugated Poly (lactic-co-glycolic acid) (PLGA) nanoparticles.

2.3.17.1 RhoB encapsulated PLGA nanoparticles.

An oil in water (O/W) emulsion-solvent evaporation method was used to prepare PLGA NPs based on literature protocols (Yu et al. 2016; Prabhuraj et al. 2020; Rezvantab et al. 2018). As the organic phase, (12 mg, 0.26 µmol (micromole)) of non-functionalized PLGA Lactide: Glycolide (50:50), (12 mg, 0.8 µmol) of Carboxylic acid-PLGA Lactide: Glycolide (50:50), and (1 mg, 2.08 µmol) of RhoB were dissolved in 8 mL of Acetone. The aqueous phase was 2% of Poly Vinyl Alcohol PVA dissolved in water (2% w/v), and 14 mL of the aqueous solution was added to a 50 mL conical flask with a magnetic stirrer in the fume cupboard. The organic phase was added dropwise to the aqueous phase, and the resulting emulsion was then stirred overnight to allow the organic solvent to evaporate. The obtained material was washed to remove any remaining unencapsulated RhoB and centrifuged at 15000 xg for 15 mins at 4°C. Washing was performed until no RhoB could be seen in the supernatant. The collected NPs (pellet) were then resuspended in 1 mL of water and sonicated twice at a 30-second interval

for 1 min each time using a probe sonicator (Soniprep 150) operating at 300W. This material was either stored at 4°C or immediately used for the next step.

2.3.17.2 Doxorubicin (DOX) encapsulated PLGA nanoparticles

Two different protocols were investigated, the first based on the previously described PLGA-RhoB encapsulation method. PLGA and (1 mg, 1.83 μmol) of DOX were dissolved in 8 mL of acetone as the organic phase, and the organic phase was then dropped wise into the aqueous phase. The same experiment steps were then followed as previously indicated in 2.3.17.1.

For the second protocol DOX (1 mg) was dissolved in 0.07 mL of DMSO, and 13.93 mL of PVA in water (2% w/v) was then added. The organic phase containing PLGA was added dropwise to DOX-PVA-water (aqueous phase). The same experiment steps were then followed as previously describe in 2.3.16.

2.3.17.3 Tz conjugated PLGA NPs encapsulated RhoB/DOX

This method described here was applied to generate NP decorated with both unlabeled and Alexa-488 labelled Tz (Figure 2.1). The NP surface was modified by the covalent attachment of Tz through the formation of a stable amide linkage. To activate the terminal carboxyl groups on the NPs, (5.7mg, 49.52 μmol) N-hydroxysuccinimide (NHS) (50 mM final concentration) and (19.2 mg, 100.15 μmol) N-(3-dimethyl aminopropyl)-N'-ethyl carbodiimide hydrochloride (EDC) (100 mM final concentration) were added to 1 mL of the previously prepared PLGA NPs (Figure 2.2). This solution was then transferred to a 50 mL conical flask with a magnetic stirrer bar and sealed with a rubber cap. The flask was then filled with N_2 using a balloon. To the flask Tz (in PBS), 89 μL (from 5.7 mg/mL Tz stock concentration (38.0 μM) was then added of 1 mL of (Final concentration

500 µg/mL). The flask was then filled with N₂ using a balloon, and solutions were allowed to react at room temperature for 3 hrs.

The Tz conjugated NPs were then washed twice with water via centrifugation at 15000 xg for 15 mins at 4° C to remove any free Tz in the solution. The resulting conjugate was then resuspended in 1 mL of water and stored at 4° C.

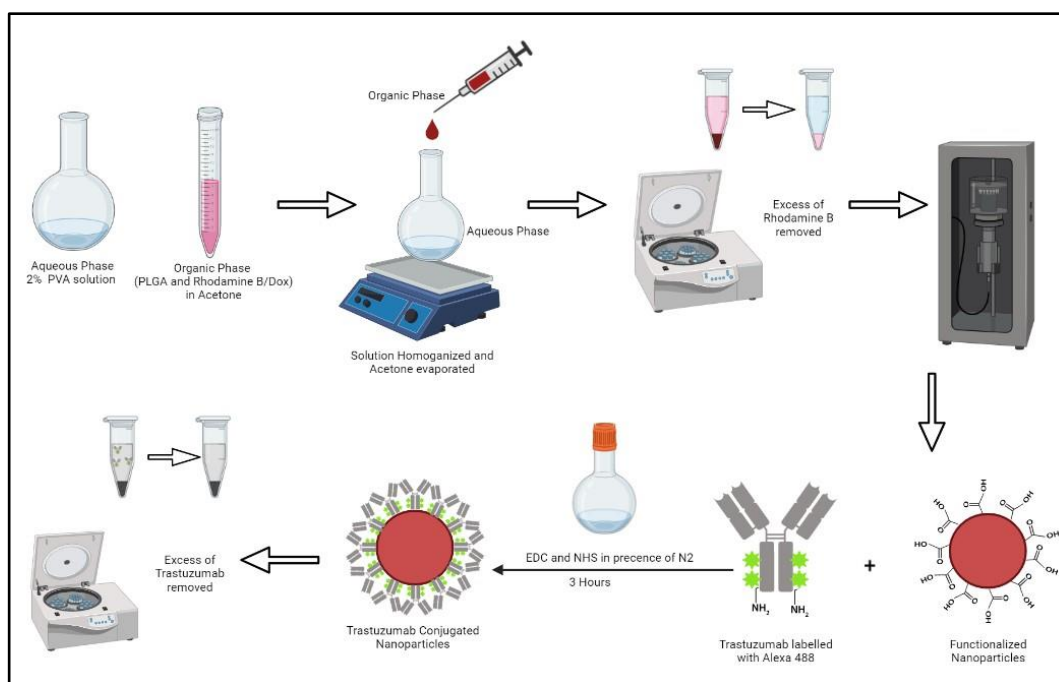


Figure 2.1 Protocol for RhoB/DOX encapsulated Tz conjugated Poly (lactic-co-glycolic acid) (PLGA) NPs.

2.3.17.4 Dynamic Light Scattering (DLS) – Zeta Sizer.

A Zeta sizer cuvette (70 µL) with 8.5 mm center height and 1 cm path length was used to analyze the size of the NPs. The NPs solution (20 µL) dissolved in 180 µL of purified water and added to zeta sizer cuvette. The DLS setting was set as above.

2.3.17.5 DOX Encapsulation Efficiency (EE%)

The concentration of DOX in PLGA was determined using a standard curve prepared with known DOX concentrations ranging from 0 mg/mL to 1 mg/mL. DOX standard concentration was first dissolved in 0.5% of DMSO (5 μ L) and then added 99.5% of dH₂O (995 μ L). PLGA encapsulated DOX NPs in 1mL of dH₂O was first centrifuged at 15000 xg for 15 mins, and the supernatant was aspirated. PLGA-DOX was then dissolved in 0.5% of DMSO (5 μ L), and 99.5% of dH₂O (995 μ L) was then added. This solution (200 μ L) was added in triplicate to a 96-well transparent plate. To generate a calibration curve, absorbance readings at 488 were plotted using DOX at 0 mg/mL to 1 mg/mL. The following formula was used to obtain the encapsulation efficiency (EE%) = $(Wt/Wi) \times 100$ where (Wt) is the total amount of drug in the nanovesicle suspension and (Wi) is the total quantity of drug added initially during preparation.

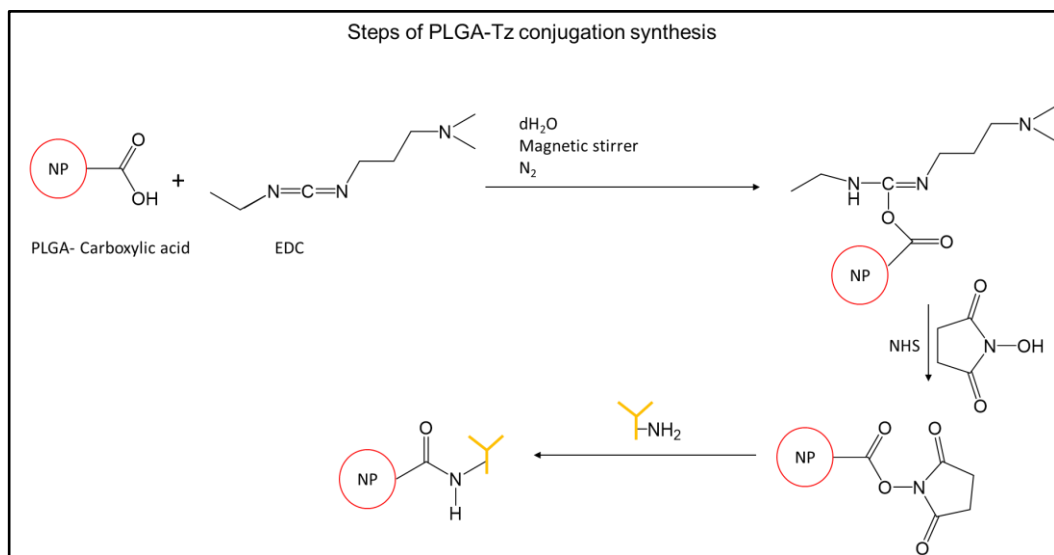


Figure 2.2: The chemical structures and the synthetic steps of PLGA conjugated Tz antibody using EDC/NHS chemistry. A reactive ester was produced from a carboxyl group in PLGA. Primary amine was then present in an introduced antibody react and covalently bind to the ester (Jazayeri et al. 2016). Prepared using ChemDraw.

2.3.17.6 Live cell imaging confocal analysis of NP binding and endocytosis.

Four types of NP formulations were investigated including Tz488 alone always at a concentration of 50nM. BC cells were seeded in 2 mL of media in MatTek wells and incubated for 60 hrs until they were 80% confluent. 0.1 to 1 mg/mL of the NPs were added to 600 μ L of complete media and solutions or Tz488 were incubated with the cells for 1, 3, 5 and 7hrs under tissue culture conditions. Media from the dishes were then aspirated, and the cells were washed 2x with 1 mL of BPS and incubated in 600 μ L of imaging media for live cell imaging confocal microscopy using the 488 nm laser for DOX and 543nm laser for RhoB. As before gain and offset setting were adjusted and improved for each imaging well within an experiment. Images were recorded using the sequential scanning mode to prevent fluorescence channel crosstalk/bleed through. Images were scanned at 200 Hz with a line average of three to reduce noise. Captured images were processed using ImageJ.

2.3.17.7 Viability assay in cells incubated with PLGA NPs

Cells were treated with NPs at final concentrations of 0 – 500 μ g/mL. Concentrations of Tz ranged from 0 – 500 nM. DOX alone control were treated cells at final concentrations of 0-10 μ M. PLGA-DOX-Tz was added to equivalent concentration of DOX in the NPs at final concentrations of 0-10 μ M. The cells were then Incubated for 24 hrs before performing viability assays as described in Section 2.3.16.

2.3.18 Western blotting (W.B)

2.3.18.1 Cell culture

Cells (MCF7: 220,000, Clone5 BT474: 220,000, BT474: 300,000, SKBR3: 300,000) were seeded on 6-well plates and cultured in complete media until 80-90% confluent on the day of lysate collection. The variation in the number of cultured cell lines is due to the growth rates of MCF7 and Clone5 BT474 are faster than SKBR3 and BT474.

Cells were in six wells plate prepared as described in section 2.2.1. Cells were treated with 50nM of Tz, or 500 µg/mL of PLGA, PLGA-Tz and PLGA-RB-Tz for 7 hrs.

The following analysis for HER2 expression follows that published from previous work in our laboratory (Wymant et al. 2020).

2.3.18.2 Lysate collection

At the end of the experiment, cells were washed twice with ice-cold PBS after the cell culture plates were placed on ice and the media was aspirated from the wells. Lysis solution (150 µL) containing protease inhibitors was then added to each well. The plate on ice was placed on a lateral, rotating shaker for 15 mins, and the lysates were scraped from the surface and transferred to pre-cooled Eppendorf tubes. The samples were centrifuged at 13000 x g for 10 mins at 4°C. The supernatants were aspirated and transferred to a new Eppendorf tube and the protein concentrations of the samples was determined using the BCA assay as previously described in section 2.3.12.

Table 2.3: Preparation of Lysis Buffer (50ml):

Chemical:	Amount:
NaCl (150mM)	438.3mg
Tris-Base (50mM)	302.85mg
dH ₂ O	To 45mL
pH to 8.0 then top up to 49.5mL with dH ₂ O	
NP-40 (1%)	500µl

2.3.18.3 Standard SDS-PAGE gel preparation

Sample Preparation

The cell lysates (10-50 µg) were prepared 1x sample buffer (from a 3x sample buffer stock) containing 2M DTT that was then heated to 96 °C for 10 mins.

Table 2.4: Preparation of Sample Buffer (50ml):

Chemical:	Amount:
SDS	4g
Glycerol	25g (weighed out)
Bromophenol Blue	4ml
Tris-HCL	1.97g
dH ₂ O	To 38ml
pH to 6.8 then top up to 40ml with dH ₂ O	

Sample loading and SDS-PAGE

Mini-PROTEAN TGX Precast Protein Gels contained 4–15% of TGX (Tris-Glycine Extended) precast gel were used by removing the comb and green stripe at the bottom of the gel. The "stuffer gel" was secured in a clamp with the plates facing each other, ensuring a tight fit between the two plates.

The central reservoir was filled with 1 x Running (100mL of 10x Running buffer was diluted to 1L of dH₂O and was gently mixed). The inner lip and any leaks were checked, indicating a loose clamp.

Using gel loading tips, the gel was loaded with 20 µg/well of protein; 6 µL and 2 µL of molecular weight marker were added on both edges of the gel. The tank was then filled with 1x Running Buffer and proteins separated at 200 V for 30-45 min using (Powerpac basic, BIO-RAD, USA).

2.3.18.4 Protein transfer and ponceau staining.

Here proteins were transferred to PVDF membranes between two blotting sheets utilising the (Trans-Blot Turbo™, BIO-RAD, USA) transfer system. The following options were selected in the machine: List> BIO-RAD> 1 MINI GEL> Std M.W/High M.W or (Mixed M.W) (Optimized).

After that, the membrane was gently rinsed with dH₂O before being immersed in ponceau S solution for 1 min. Following this, the membrane was washed in dH₂O multiple times, and the staining was checked to confirm that the samples had transferred and that the transfer was equal. The membrane was then washed three times, 5 mins each time, with 0.025 % Tween20 (PBST).

2.3.18.5 Protein detection by immunoblotting

The membrane was then blocked for 1 hr at room temperature in 5% milk powder in PBS containing 0.025 % Tween20 (PBST). The membrane was then incubated overnight at 4°C with the primary antibody (Rabbit—HER2 antibody), diluted in PBST 2% milk powder.

The membrane was then washed three times for five mins in PBST, and 2nd antibody (Goat Anti-Rabbit antibody) in 2% of Milk PBST was added and incubated with the membrane for 1 hr. The membrane was then washed three times for five mins in PBST.

For control, the membrane was then washed three times for five mins in PBST and incubated with (Mouse—Tubulin HRP) for 1 hr. The membrane was then washed three times for five mins in PBST.

Equal amounts of enhanced chemiluminescence (ECL) reagents were mixed together and placed on a PVDF membrane for 5 mins and any excess solution was removed. (ChemiDoc™ XRS+, BIO-RAD, Universal Hood II, USA) system was then used to image the membrane. Clarity™ Western ECL was utilised for the majority of the Western blotting methods, however, SuperSignal West Femto was employed for low level expression (as specified) in some cases.

2.3.18.6 Quantifications of Western Blots with ImageJ

ImageJ software was used to quantify the band intensities obtained as digital images. It was first necessary to create a tall and narrow box around the first band, which represented the expression level of a particular protein of interest. This was done using the rectangular selection tool. In order to determine lane "1," the Analyze>Gels>Select First Lane command was selected.

The following command was used to outline the subsequent lanes with equal-sized rectangles, which were then highlighted and allocated lane numbers using the following command: Analyze>Gels>Choose the Next Lane. Then, using the Analyze>Gels>Plot Lane's command, we were able to generate profile plots. The resultant plots depicted the relative density within each of the highlighted lanes. Width of the peaks corresponds to the size/area of the bands. It was necessary to draw a line across the base of each peak in order to measure the area beneath each peak with minimal or no background noise; thus, the Straight-Line tool was utilised to do this. The data was then exported to Excel and the test bands (HER2) intensity: loading control ratios were determined to identify and experimental differences in HER2 expression.

2.4 Statistical Analysis

FACS data are presented from duplicate samples of three or four independent experiments. Statistical analysis was performed using the GraphPad software. The mean for both control and treatment were calculated to form three independent experiments separately. Statistical analysis for FACS experiments complexity was observed one-way analysis of variance (vehicle control) to compare with treatment for each cell line. Student's independent T-test was used to determine the significant differences between the two groups. Statistical significance was attributes for values $p < 0.05$. The differences between Clone5 BT474 and BT474 were determined using a two-way variance analysis ANOVA (Sidak's multiple comparisons test).

**Chapter 3 : In Vitro studies of HER 2-
internalisation**

3.1 Introduction

Since the publication of (Moody et al. 2015) showed that HER2 clustering by Tz could induce HER2 endocytosis and downregulation, further work in the laboratory focused on understanding how this is occurring. Since then, Scanning Electron microscopy (SEM) studies have shown clustering of HER2 induced membrane ruffling indicative of macropinocytosis (Wymant et al. 2020). This study also demonstrated that clustering HER2 by Tz also induces HER3 but not EGFR downregulation. Surprisingly, early studies performed by Wymant in the laboratory showed that preincubation with the macropinocytosis inhibitor, EIPA stimulated rather than inhibited HER2 endocytosis in the absence of clustering (data not shown). It is unknown whether this also leads to HER2 degradation or whether this effect is selective for HER2 over other plasma membrane receptors.

3.1.1 Overview of HER 2 Internalisation

Following HER receptor activation, phosphorylation of particular tyrosine residues and subsequent recruitment and activation of downstream signalling proteins activates downstream signalling pathways that promote cell proliferation, survival, migration, adhesion, angiogenesis, and differentiation (Trenker and Jura 2020). The Phosphatidylinositol 3-kinase (PI3K)-Akt pathway and the Ras/Raf/MEK/ERK pathway (also known as extracellular signal-regulated kinase/mitogen-activated protein kinase (ERK/MAPK) pathway are the two most important and well-characterized downstream signalling pathways activated by HER receptors (Liu et al. 2019; Yarden and Sliwkowski 2001). Downstream signalling cascades regulate cell cycle, cell growth and survival, apoptosis, metabolism, and angiogenesis (Bartholomeusz and Gonzalez-Angulo 2012). Signalling from HER

receptors is then halted by endocytosis, and Internalized receptors are then recycled to the plasma membrane (HER2) or destroyed (EGFR) (Furrer et al. 2018).

3.1.2 Macropinocytosis analysis using DEX prob in BC cell lines.

As noted, macropinocytosis is a type of endocytosis that allows for the efficient uptake of non-selective extracellular proteins, liquids, and particles. This endocytic process can be activated via growth factor signalling pathways manifest as the cell internalising external solutes and nutrients into irregular endocytic vesicles called macropinosomes. Macropinosomes are then immediately coated with the early endosome associated with Rab5 and then the late endosome associated with Rab7 during maturation towards lysosomal degradation (Palm 2019).

Macropinocytosis is critical for the feeding of cancer cells. Cancer cells are frequently depleted of oxygen and nutrients due to their fast proliferation and the abnormal vascular microenvironment. As a result, they must alter their metabolism in order to live and grow. To meet their energy requirements, cancer cells increase macropinocytosis activity. The process is deeply linked with actin cytoskeleton remodelling, and the mechanism by which macropinosomes are generated includes plasma membrane ruffling (Xiao et al. 2021). Macropinosomes are bigger than other endocytic vesicles and, in cell studies, can be labelled with high molecular weight DEX that, upon internalisation, will be located in vesicles with a diameter of $\geq 0.2 \mu\text{m}$ (Commisso 2014). In this chapter, DEX will be used as a marker of macropinocytosis, but the cells were not stimulated with a growth factor.

Amiloride, as an NHE inhibitor, has been shown to block the DEX probe, which has previously been related to fluid phase and Macropinocytosis (Li et al. 2015). The evidence suggests that amiloride can be considered a potassium-sparing diuretic that selectively blocks sodium transport, thereby suppressing NHE. Amiloride is used in clinical settings for oedema and arterial hypertension patients. In addition, amiloride is utilised for hypokalaemia patients and is often administered alongside diuretic medications that can cause potassium depletion (Vidt 1981). Cariporide belongs to a different class than amiloride, and its NHE1 inhibition is more powerful than amiloride, yet it is not FDA-approved. Cariporide is believed to have anticancer activity and is capable of causing considerable intracellular acidity in cancer cells (Koltai 2020). Cariporide, a selective inhibitor of NHE1, has been demonstrated to be non-toxic to mammalian cells. The NHE1 is responsible for maintaining the acidic tumour microenvironment via stimulating extracellular Na⁺ reabsorption and intracellular H⁺ efflux. The rise in extracellular acidity that results contributes to the chemoresistance of malignant tumours (Lee et al. 2017). However, preclinical research revealed that cariporide causes cardiac arrest as a severe adverse effect (Gazmuri et al. 2019).

3.1.3 Analysis of Clathrin Mediated Endocytosis in BC cell lines.

A Tf uptake analysis can be used to determine CME as, to date, this protein has only been shown to enter via this pathway (Trofimenko et al. 2021). CME occurs across every eukaryotic cell. It is the main mechanism for sorting and internalising different macromolecules, proteins, and lipids, as well as regulating the activation of signalling pathways. Additionally, it plays a key role in nutrient uptake, signal transduction, synaptic vesicle recycling, and cell polarity maintenance. CME can be classified into five distinct phases: nucleation, cargo

selection, coat formation, vesicle scission, and uncoating, which can be explained by evaluating the cargo internalisation process. EGFRs are implicated, as are binding domains for PI(4,5)P₂, which is thought to play a role in endocytic protein recruitment to the membrane in CME mechanism (Prichard et al. 2022).

A commercial and fluorescent conjugate of Tf was utilised to analyse CME. The half time required for the formation of coated pits and coated vesicle budding of the Tf receptor is 3-5 mins (Hopkins et al. 1985; Maxfield and McGraw 2004; Morris and Schmid 1995).

Initially, Tf was used to evaluate CME in BC cell lines in the presence and absence of macropinocytosis inhibitors in order to validate that the inhibitors have no effect on CME and to determine if there is a correlation between CME and HER2 overexpression. This utilised both largely qualitative live cell confocal microscopy analysis and FACS.

Another study was conducted to compare BT474 and Clone5 BT474 (Tz-resistant cell line) with regard to macropinocytosis (DEX) and CME (Tf). The results reveal statistically significant differences between two cell lines in terms of uptake as measured by Confocal Microscopy as a quantitative approach, FACS as a qualitative way and a second confirmation.

3.1.4 Macropinocytosis inhibitors

Pharmacological inhibitors for macropinocytosis can be categorised into the following types, including F-actin-depolymerising drugs (e.g., cytochalasin D and latrunculins); sodium hydrogen exchanger (NHE) inhibitor agents (e.g., amiloride and its analogue, 5- (N-ethyl-N-isopropyl) amiloride (EIPA)); and inhibitors of phosphoinositide kinases (e.g., Wortmannin).

3.1.4.1 F-actin-depolymerizing Agents

As macropinocytosis is an actin driven process, interest has been placed on drugs that affect action polymerisation and depolymerization. Cytochalasin D and latrunculins are commonly used examples, including in the drug delivery field. Since many features of NP trafficking within cells are still completely unclear, Deville conducted a study to determine how stained polystyrene NPs can penetrate and react with A549 Lung epithelial cells. They identified that microtubules and actin microfilaments both play roles in the intracellular trafficking of NPs in vesicles and cell organelles. Nocodazole and latrunculin A were introduced to the cells following NP internalisation to conduct the experiment. Interfering with the polymerization of the tubulin and actin cytoskeletons, nocodazole, and Latrunculin A considerably reduces the trafficking they facilitate (Deville et al. 2015). Another study by Stack was conducted to use actin depolymerizing agent Latrunculin A in vivo after 24 hrs of injected NPs to reach the tumour cells. This is done to block the mononuclear phagocyte system (MPS) macropinocytosis, which is considered one of the major barriers for NPs to reach their targets (Stack et al. 2021). NPs are often eliminated by MPS prior to reaching their intended targets. The study found that Latrunculin inhibits macropinocytosis of MPS and increases the accumulation of folate-receptor targeting NPs in tumour. A similar study used latrunculin A co-administered with NPs to inhibit MPS cells macropinocytosis and phagocytosis. The study also found that NPs were accumulated in tumour due to Latrunculin A administration.

A series of conducted research projects, including (Kaksonen et al. 2006; Merrifield 2004), have reported an evidence to suggest that the actin cytoskeleton plays a role in regulating various endocytic pathways. For example, confocal

microscopy imaging investigations of living cells have shown that clathrin-coated pits and caveolae internalisation and formation are linked to the actin skeleton. There is then evidence indicating that when actin polymerisation is inhibited using pharmacological agents, endocytosis via these two pathways is inhibited. Based on these findings, it is reasonable to conclude that Latrunculins and cytochalasin D globally and non-selectively inhibit every internalisation pathway, as opposed to serving as specific obstructers of macropinocytosis.

3.1.4.2 Inhibitors of Phosphoinositide Metabolism

Both phosphoinositide 3-kinase (PI3K) and phosphatidylinositol-specific phospholipase C (PI-PLC) enzymes can regulate and organise the actin cytoskeleton that is involved in the acceleration of fluid-phase endocytosis. These enzymes are then considered as targets for agent inhibitors that can affect fibre disruption, cortical actin recruitment, ruffling, and macropinosome formation (Amyere et al. 2000). As an example, for this class, wortmannin has been used for blocking PI3K and the inhibition of fluid-phase pinocytosis. It has also been shown to affect other endocytic processes, including receptor-mediated internalisation (Araki et al. 1996).

3.1.4.3 Sodium Hydrogen Exchanger (NHE) inhibitor agents

Amiloride represents the initial NHE inhibitor used to investigate macropinocytosis. For example, it was observed that activation of EGFR by EGF induced membrane ruffling and macropinocytosis could be blocked by EIPA (amiloride derivatives) (Chiasson-Mackenzie et al. 2018). Amiloride is not selective for NHE1 and can inhibit other NHE isoforms and conductive Na⁺ channels and Na⁺/Ca²⁺ exchangers. As noted by Masereel, a range of amiloride derivatives have since been described that are more selective towards NHE1

(Masereel et al. 2003). More recently, one of these derivatives, EIPA has taken over as being the most widely used macropinocytosis inhibitor that is used on cell culture lines at concentrations ranging between 50 and 100 μ M (Ivanov 2008). Several drug delivery researchers have used EIPA to investigate the uptake of their vectors and for example, Chemical inhibitors, such as amiloride as a macropinocytosis inhibitor, have been used to evaluate multiple endocytosis routes as attempts to characterise routes NPs uptake into cells (Manzanares and Ceña 2020). A study by (Vollrath et al. 2013) investigated the uptake of NPs by the HeLa and L929 cell lines. They utilised different inhibitors for clathrin-dependent (chlorpromazine), caveolin-dependent (filipin III), and macropinocytosis (EIPA). They found that NPs with a size of 200 nm were internalised by CME, but NPs with a size more than 300 nm were internalised via macropinocytosis. Other research evaluated corona NPs (200 nm) in HeLa cell line uptake with various endocytosis inhibitors, including EIPA, chlorpromazine, methylcyclodextrin, dynasore, cytochalasin D, and nocodazole. EIPA decreased the uptake of NPs by 50% to 80%, indicating that macropinocytosis is involved in the uptake of NPs (Francia et al. 2019). In another study, MCF7 or MCF-10A cells were treated with paclitaxel-PLGA-NPs and endocytosis inhibitors; Amiloride and cytochalasin D used to inhibit macropinocytosis, phenylarsine oxide used for CME, and nystatin used for caveolin-mediated endocytosis. Macropinocytosis was inhibited significantly by amiloride in both cell lines treated with PLGA NPs Loaded with Paclitaxel.

Although the evidence indicates that macropinocytosis is susceptible to inhibition via the blocking of Na^+/H^+ exchange, the functional relationship between Na^+/H^+ exchange and macropinosome formation remains unknown. It has been stated

that macropinocytosis and NHE in A431 can be activated by EGF stimulation through elevating cytosolic pH and stimulating Na⁺ influx (Koivusalo et al. 2010).

Amiloride and its analogues (Figure 3.1) are identified as NHE blockers, but they are also considered nonselective compounds that interact with many membrane receptors, ion transporters, and other membrane proteins (Gao and Ijzerman 2000; Garritsen et al. 1992; Kleyman and Cragoe 1988; Dai et al. 2007). They have been shown to interact differently with for example Adenosine-A receptor, B adrenoreceptor, dopamine, histamine, muscarine, and serotonin receptors (Garritsen et al. 1991).

Amiloride and EIPA both contain a pyrazinoylguanidine, and the main difference between them lies in the functional group (R₂) of ethyl isopropyl in EIPA substituted to replace the amine group in amiloride (Figure 3.1). This substitution was shown to enhance the activity of EIPA against NHEs (Blair et al. 2021) that have 12 transmembrane domains in NHE with domains 4 and 9 being responsible for binding and inhibition of amiloride and amiloride analogues (Torres-López et al. 2013). Amiloride's unsubstituted guanidino group is important for the molecule's activity, as its substitution results in inactivity (Laeckmann et al. 2002). Amiloride compounds with substituted molecules containing 5 or 6 carbon alkyl groups at positions R₂ (Figure 3.1) show high inhibitory potency such as hexamethylene amiloride (HMA) (Harris and Fliegel 1999). However, substitution of the carbonyl guanidinium moiety decreases the potency of the molecule (Frelin et al. 1988).

In an approach to selectively inhibit NHE1 a benzoylguanidine termed Cariporide was designed by replacing the 6-chloro- moiety of amiloride with a sulfomethyl group and the 2-amino group with a -H group (Mondal and Ilies 2020).

Chemical structures of amiloride, amiloride analogues and cariporide						
Compound	R	R ₁	R ₂	R ₃	X	Y
Amiloride	H	NH ₂	NH ₂	CL	N	N
EIPA (Amiloride analogue)	H	NH ₂		CL	N	N
Dimethyl amiloride (Amiloride analogue)	H	NH ₂		CL	N	N
hexamethylene amiloride (Amiloride analogue)	H	NH ₂		CL	N	N
Cariporide	H	H	(CH ₃) ₂ CH	SO ₂ CH ₃	CH	CH

Figure 3.1: NHE inhibitor structures of amiloride, amiloride analogues and cariporide. Adapted from (Laeckmann et al. 2002; Asher et al. 1987; Frelin et al. 1988). Prepared by ChemDraw.

3.2 Results and Discussion

3.2.1 Effect of amiloride on DEX 10 kDa internalisation in BC cell lines

Initial experiments focused on studying the effects of amiloride on the two named HER2 expressing BC cell lines and HER2 BC cell line as a control. These cells were treated with vehicle control or amiloride and analysed for endocytic uptake of DEX via live cell imaging confocal microscopy or FACS.

For microscopy analysis, each cell line was treated with amiloride and microscope settings for vehicle control (VC) and drug treatment were identical for analysis within each cell line but different between cell lines. This would explain

why DEX fluorescence in BT474 cells (VC) appear to be higher than in other cell lines.

Confocal microscopy data in figure 3.2 (A1-C1) show the DEX labelling vesicular structures in the three cell lines with evidence of an amiloride inhibitory effect in all three cell lines. However, FACS analysis shows a general decrease in DEX uptake in all three lines, with this being statistically significant in BT474 (p -value= 0.0444) and MCF7 cells; (p -value= 0.0045).

The results obtained with the BT474 and MCF7 FACS are consistent with other studies in different cell types revealing that amiloride and its derivative EIPA decrease DEX uptake and macropinocytosis (Cortese et al. 2008; Koivusalo et al. 2010; Nazere et al. 2022).

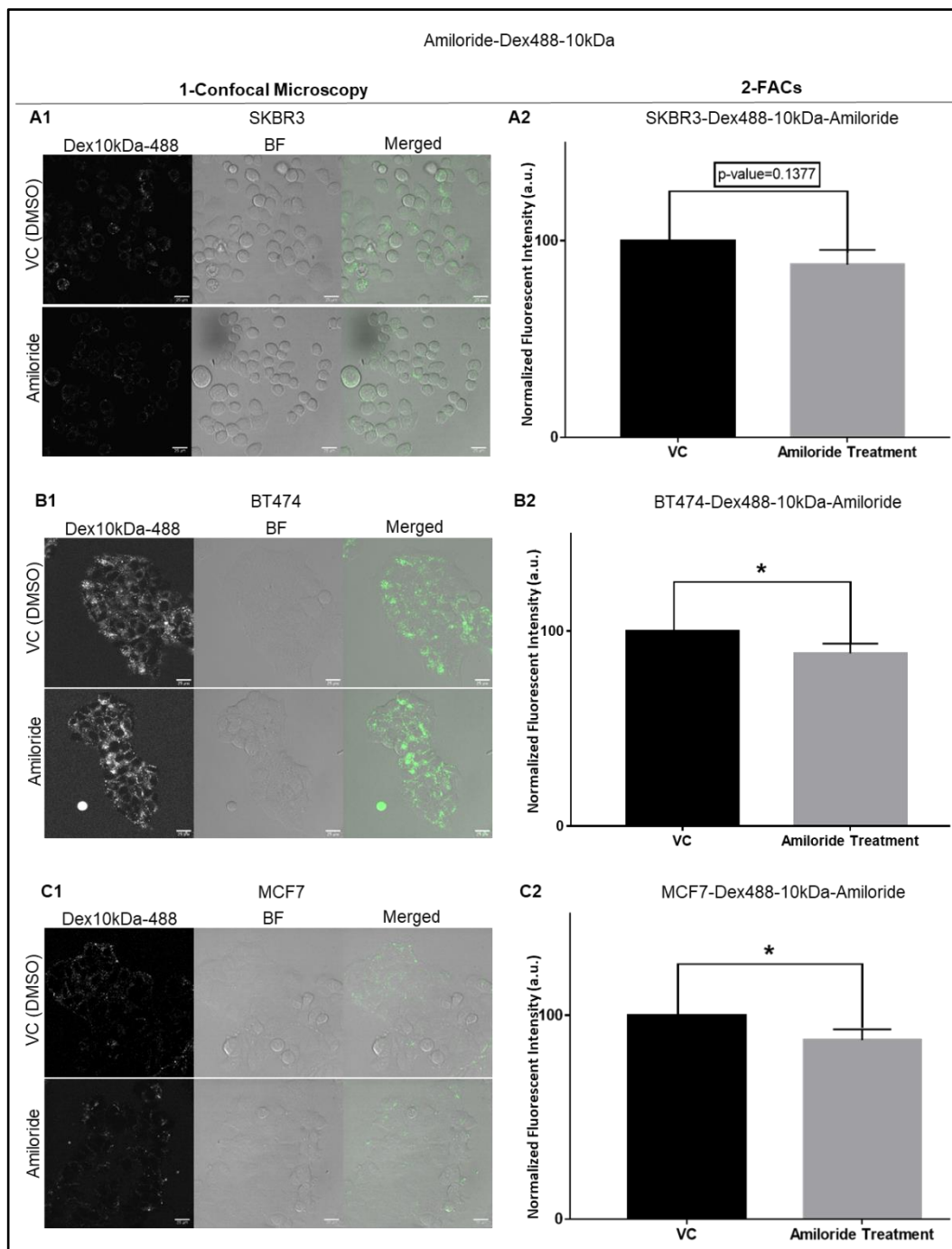


Figure 3.2: Confocal microscopy and FACS of DEX488 10kDa uptake +/- amiloride in BC cell lines. Cells plated on MatTek dishes (A1-C1) or 12 well plates (A2-C 2) were incubated with vehicle control (DMSO) or amiloride in the presence of 10kDa Alexa488 for 2 hrs, washed, and processed for analysis by confocal microscopy and FACS. Data in A2, B2 and C2 represent means, and standard error of the means from three independent experiments performed in triplicate. Scale bars 25µm, BF: Bright Field.

3.2.2 Effect of EIPA on DEX 10 kDa internalisation in BC cell lines

The same experiment was then performed, replacing amiloride with EIPA as the macropinocytosis inhibitor, figure 3.3, however, shows that opposite effects were seen with this reagent in the two HER2 expressing cells, SKBR3 and BT474 showed significant differences between treatment and VC, with p-values of 0.0008 (***) and 0.0056 (**), respectively. Interestingly, MCF7 FACS demonstrate no difference between treatment and VC. Confocal microscopy also indicated that DEX appeared to be localised close to or on the surface of the cells in contrast to EIPA treatment, where DEX was clearly intracellular. Thus these studies do not agree with the previously mentioned studies (Cortese et al. 2008; Koivusalo et al. 2010; Nazere et al. 2022).

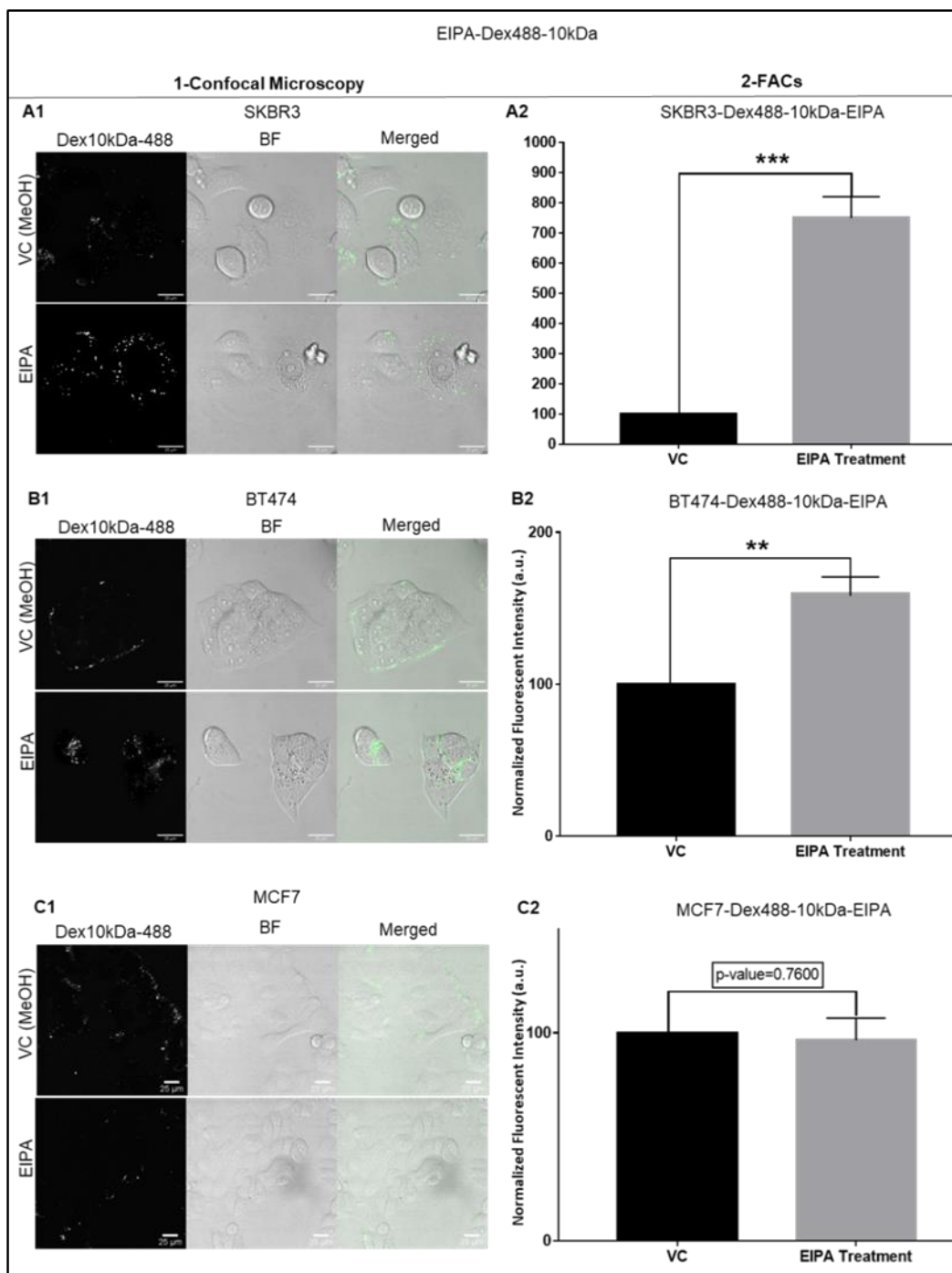


Figure 3.3: Confocal microscopy and FACS of DEX488 10kDa uptake +/- EIPA in BC cell lines. Cells plated on MatTek dishes (A1-C1) or 12 well plates (A2-C2) were incubated with vehicle control (MeOH) or EIPA in the presence of 10kDa Alexa488 for 2 hrs, washed, and processed for analysis by confocal microscopy and FACS. Data in A2, B2 and C2 represent means, and standard error of the means from three independent experiments performed in triplicate Scale bars 25µm, BF: Bright Field.

It is very difficult to interpret these findings as both drugs, amiloride and EIPA, are known to affect other NHEs isoforms (11 isoforms) (Fuster and Alexander 2014), i.e are not selective for the macropinocytosis regulator NHE1. Comparative analysis of NHE1 expression, could be investigated using SDS PAGE and Western Blotting to identify whether the observed effects relate to this. As already mentioned, (Section 3.1.4.3) EIPA also can interact with other membrane receptors, ion transporters, and other membrane proteins.

In other studies different size DEX and Alexa dyes of different spectral were investigated suggesting that 70kDa endocytosis is mostly driven by macropinocytosis, whereas DEX10 kDa endocytosis is driven by both macropinocytosis and micropinocytosis (Li et al. 2015; Lambies and Commisso 2022). In view of this and the rather unexpected data obtained with 10KDa DEX, a 70 KDa TMR variant was investigated under the same experimental conditions using EIPA as an inhibitor; this particular DEX variant has been labelled a macropinocytosis marker in a number of different studies (Tejeda-Muñoz et al. 2019; Maeda et al. 2021; Xiao et al. 2021).

3.2.3 Effect of EIPA on DEX 70 kDa internalisation in BC cell lines

The confocal microscopy data in figure 3.4 show a cell line dependant increase in DEX70 kDa uptake that was particularly prominent in SKBR3 cells that had low control uptake; but the same trend was apparent in the other cell lines. The uptake data for this cell line was confirmed using FACS (p-value = 0.0104), but there were no significant effects of EIPA in the other two cell lines. With regards to culture of these cells and comparison between confocal microscopy, each has unique growing characteristics with BT474 cells growing tower-like and clumping (Figure 3.4 B1). This makes confocal microscopy challenging, as does separating them to individual cells for FACS. As indicated in DEX 10 kDa in previous section 3.2.1, BT474 are easily removed from the plastic representing a challenge when washing after addition of endocytic probes thus a greater fraction may have remained in association with the plasma membrane rather than being inside the cells. However, there is good evidence that intracellular fluorescence is also higher in this cell line compared with the others suggesting a higher capacity for fluid phase endocytosis.

In general, with and without EIPA, uptake of this probe was comparatively low noting that microscopy conditions were exactly the same for all experiments.

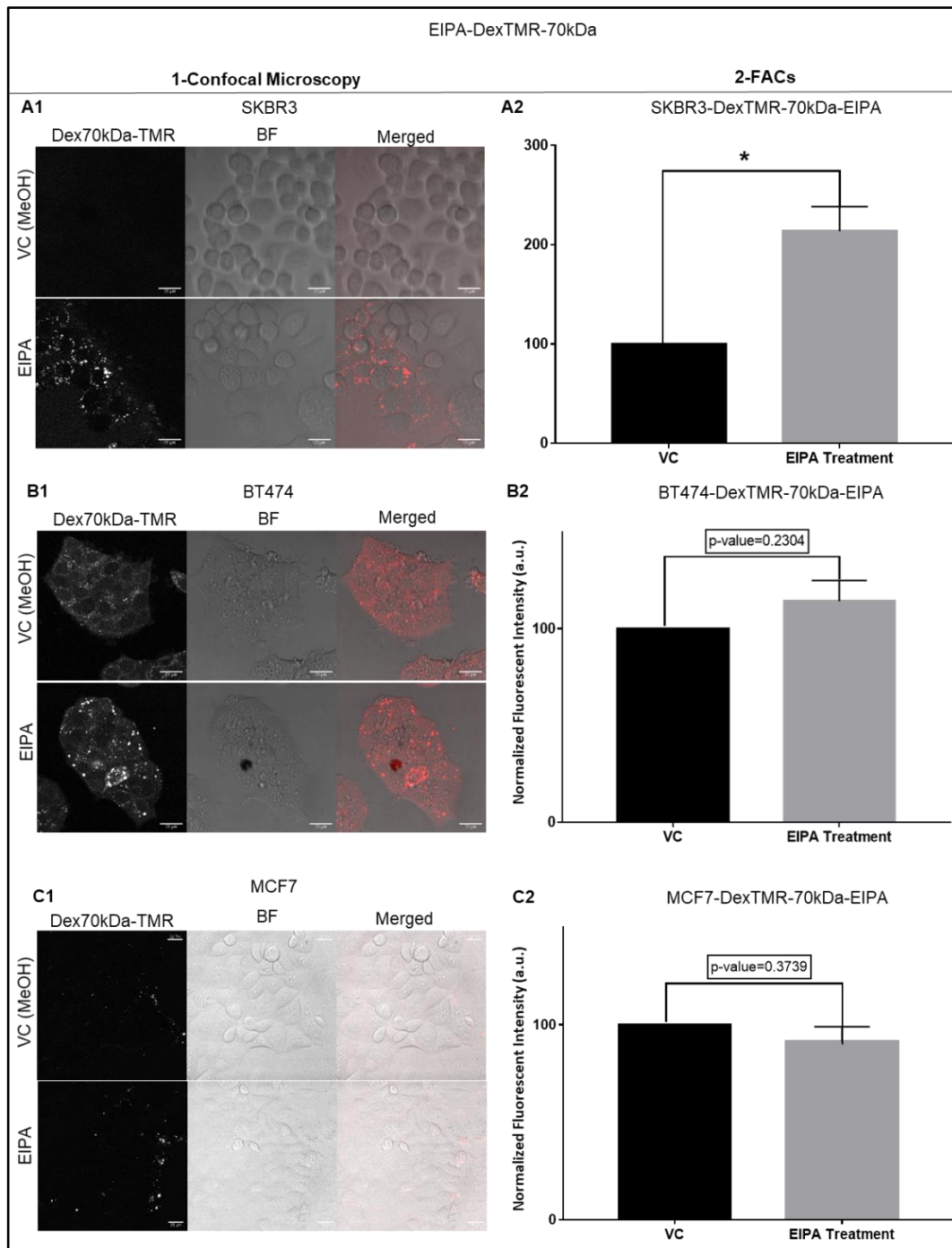


Figure 3.4: Confocal microscopy and FACS of DEX TMR 70kDa uptake +/- EIPA in BC cell lines. Cells plated on MatTek dishes (A1-C1) or 12 well plates (A2-C2) were incubated with vehicle control (MeOH) or EIPA in the presence of DEXTMR 70kDa for 2 hrs, washed, and processed for analysis by confocal microscopy and FACS. Data in A2, B2 and C2 represent means, and standard error of the means from three independent experiments performed in triplicate Scale bars 25µm, BF: Bright Field.

In general, EIPA increase in DEX uptake did appear to be more apparent in HER2 expressing cells, but it is very difficult to understand why this is the case and draw conclusions from or the mechanism by which this is happening. It may be that much depending on the expression of different NHE subtypes that may be differentially sensitive to EIPA. It is difficult also to compare this data with others that have shown opposite effects with both these drugs (Tejeda-Muñoz et al. 2019; Recouvreux and Commisso 2017; Xiao et al. 2021; Feng et al. 2013). Macropinocytosis process is often triggered when growth factor signalling pathways such as those involving EGFR Ras and PI3K are activated. This regulates actin-driven membrane ruffling and macropinosome (Palm 2019), and it remains to be determined if HER2 (also a signalling receptor) is somehow activated by EIPA. However, the difference between the three cell lines is likely to expand well beyond HER2 expression levels.

Another explanation may be due to the relationship between macropinocytosis and intracellular pH. It was demonstrated that acidifying the cytosol, via amiloride-induced blockage of NHEs, significantly inhibited micropinocytosis (Recouvreux and Commisso 2017). Changes in pH caused by NHE (from pH = 7.8 to 6.8) appeared to influence the recruitment and activation of proteins that cause membrane ruffles. A separate study by Koivusalo et al. (2010) suggested that the acidification shown in presence of inhibitors had no effect on receptor engagement or phosphorylation. However, it was shown that activation of GTPases involved in actin remodelling is acutely sensitive to submembranous pH. This sensitivity endows macropinocytosis with a susceptibility to Na⁺/H⁺ exchange inhibitors, that could have caused the effects seen in figure 3.4.

NHE1 is highly expressed in various cancer cell lines and is the most extensively studied isoform including for macropinocytosis studies (Granja et al. 2017). A study by (Cardone et al. 2015) showed a correlation between EGFR and NHE1 expression in cancer invasion. In pancreatic adenocarcinoma cell lines, a high correlation between the epidermal growth factor receptor (EGFR) and NHE1 was observed, implying that NHE1 plays a critical role in transducing the EGFR signal, contributing to the induction of metastasis.

In view of this, we probed the Human Protein Atlas depository that provides RNA expression data on commonly used cell lines with NHE1 (also known as Solute Carrier 9 Member A1) represented by the expression of gene SLC9A1 (<https://www.proteinatlas.org/>) (Figure 3.5). Only two of the cell lines used in this study were listed, having comparatively modest expression of this protein with SKBR3 having higher expression compared with MCF7. However, the picture is more complicated than this, noting that both amiloride and EIPA may have other targets. On this note, amiloride and amiloride analogues have been examined in various cancer contexts for their anticancer potential (Harguindey et al. 2013). Recent research showed that EIPA hindered DNA replication, inhibited proliferation and migration, and promoted apoptosis, therefore lowering hepatocellular carcinoma invasion and motility (Yang et al. 2010). It is also stated that in DOX-resistant colon cancer cells, co-administration of EIPA boosted the intracellular accumulation of co-administered doxorubicin (Matthews et al. 2011). This suggests it may have an activity on the plasma membrane to allow this drug to enter cells. NHEs as a family contribute to both normal and pathological cellular processes. Tumours acidify their microenvironment due to the action of proton pumps and transporters, becoming more aggressive and resistant to

therapy (Granja et al. 2017). NHE-1 is the isoform implicated in cancer's pH regulation (Ariyoshi et al. 2017). NHE1 also regulates cell volume and pH homeostasis, promoting cell transformation, proliferation, motility, migration, resistance to chemotherapy in vitro, tumour development, metastasis, and perhaps spontaneous tumour regression (Cardone et al. 2005). Several investigations demonstrated that NHE1 is involved in various types of neoplastic growth in cancer. For example, Amith's group demonstrated that blocking NHE1 caused MDA-MB-231 cells to be more susceptible to paclitaxel (Amith et al. 2015).

Cariporide is not a member of the amiloride family of drugs, but was shown to be more selective to NHE1 over other NHE isoforms (Granja et al. 2017). The drug has noted side effects, mostly related to drug accumulation and cerebrovascular problems. However, cariporide may become a novel, and effective anticancer drug for several human cancers (Harguindey et al. 2013). Another study also considered cariporide is not harmful to mammalian cells (Wong et al. 2002). Thus, and in line with its higher selectivity for NHE1, this drug was evaluated for effects on the uptake of DEX and Tf.

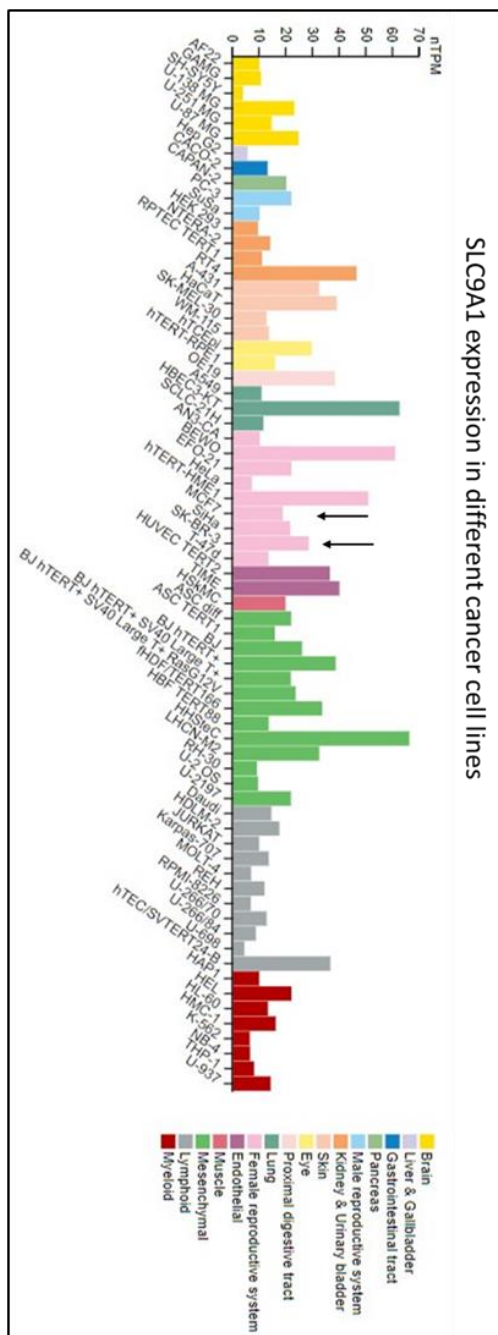


Figure 3.5: Expression of NHE1 from Human Protein Atlas depository. RNA expression data for tissue culture cell lines are represented as normalised transcript per million (nTPM) values. The studied cell lines are classified into 16 colour-coded categories based on the tissue type. SKBR3 shows a 28.4 in SLC9A1 RNA expression compared to MCF7, 18.7. The webpage does not provide an analysis of the BT474 cells or Clone5 BT474.

3.2.4 Effect of cariporide on DEX 10 kDa in BC cell lines

Experiments performed with amiloride and EIPA were repeated with cariporide, and both confocal microscopy and FACS in figure 3.6 clearly demonstrate that it did not significantly affect the uptake of DEX in BT474 or SKBR3. A small but significant (p.value= 0.0140) inhibition was observed in the lower NHE1 expressing MCF7 cells, and interestingly the drug also changed the subcellular localisation of the probe, manifest as more polar juxtannuclear fluorescence (Figure 3.7).

The next studies focused on performing the same kind of microscopy and FACS analysis with these drugs but using Tf as a probe for CME.

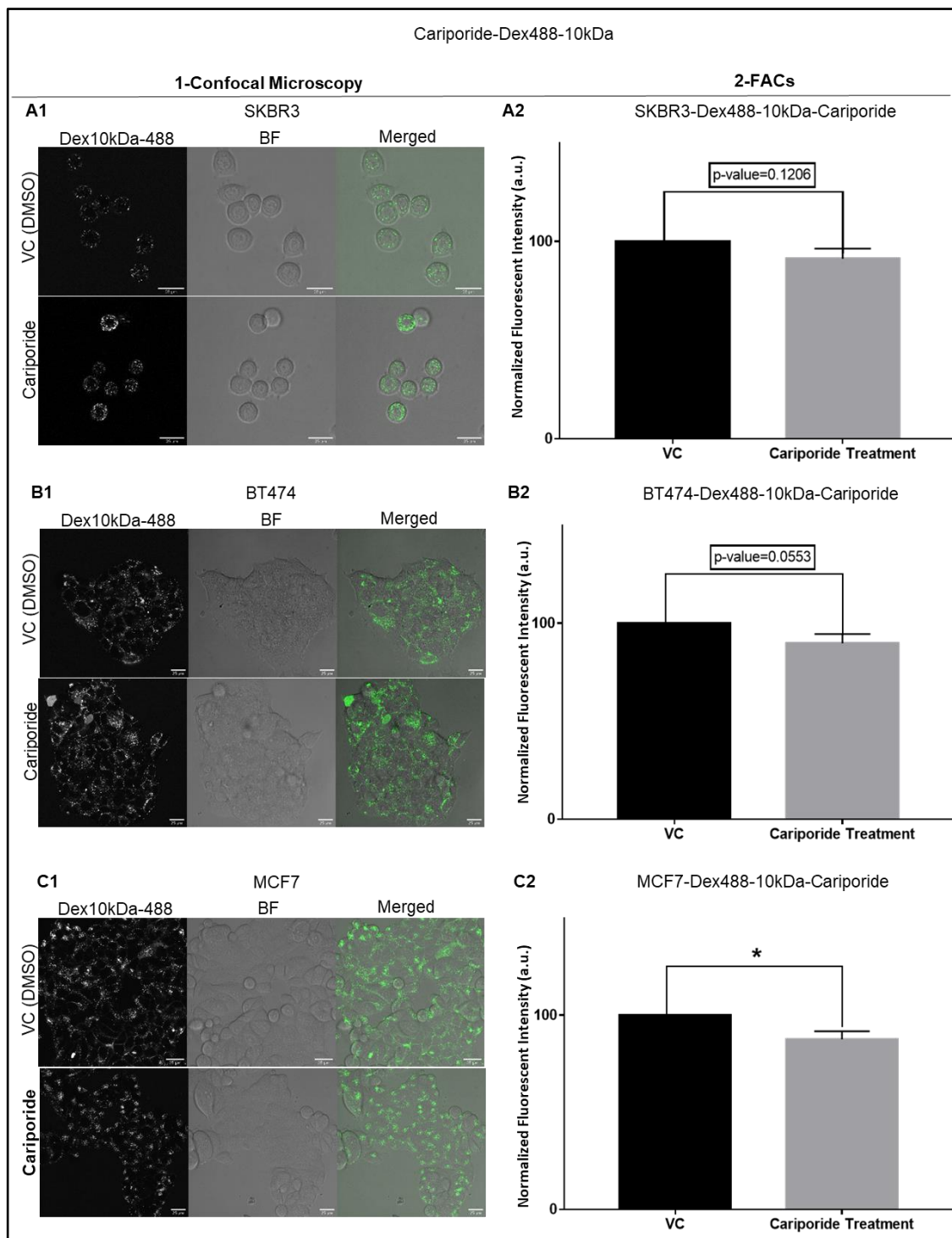


Figure 3.6: Confocal microscopy and FACS of DEXTMR 70kDa uptake +/- cariporide in BC cell lines. Cells plated on MatTek dishes (A1-C1) or 12 well plates (A2-C2) were incubated with vehicle control (DMSO) or cariporide in the presence of 10kDa Alexa488 for 2 hrs, washed, and processed for analysis by confocal microscopy and FACS. Data in

A2, B2 and C2 represent means, and standard error of the means from three independent experiments performed in triplicate Scale bars 25µm, BF: Bright Field.

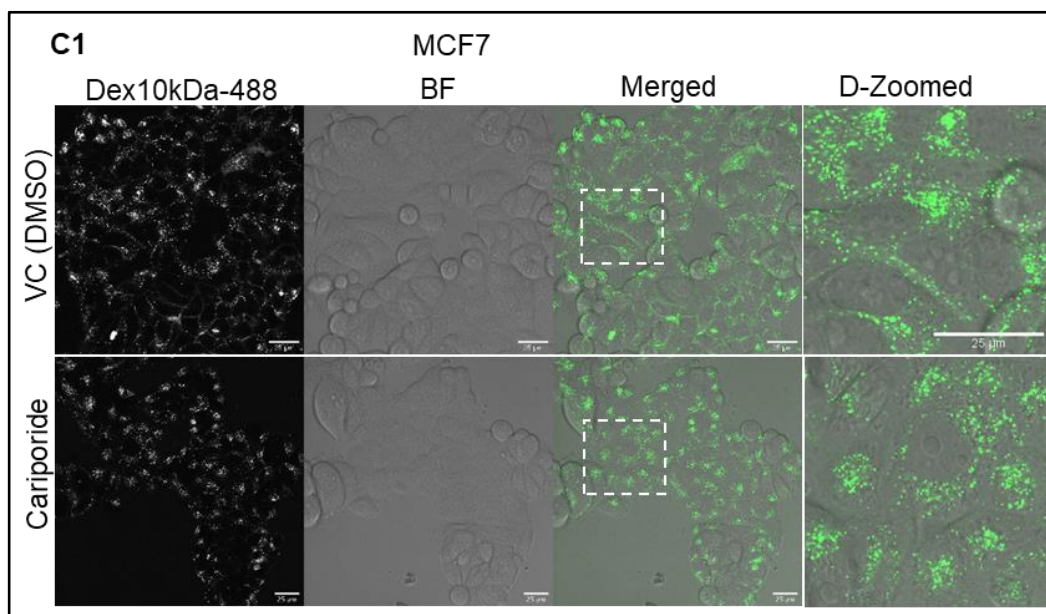


Figure 3.7: MCF7 digital zoomed images were used to confirm no differences in intracellular localisation was observed between VC and cariporide treated cells.

3.2.5 Effect of amiloride on Transferrin in BC cell lines

Data in figure 3.8 clearly show that by microscopy and flow cytometry, that amiloride has no effect on Tf uptake and, therefore CME. This agrees with previous studies (West et al. 1989; Cortese et al. 2008; Wang et al. 2019; Wiranowska et al. 2011). However, other investigators show that amiloride inhibits CME, including junctional protein complexes in epithelial cells (Chang et al. 2014). Amiloride and EIPA were also shown to significantly inhibit albumin uptake via receptor-mediated in renal proximal tubule-derived epithelial cells (Drumm et al. 2003; Gekle et al. 2001).

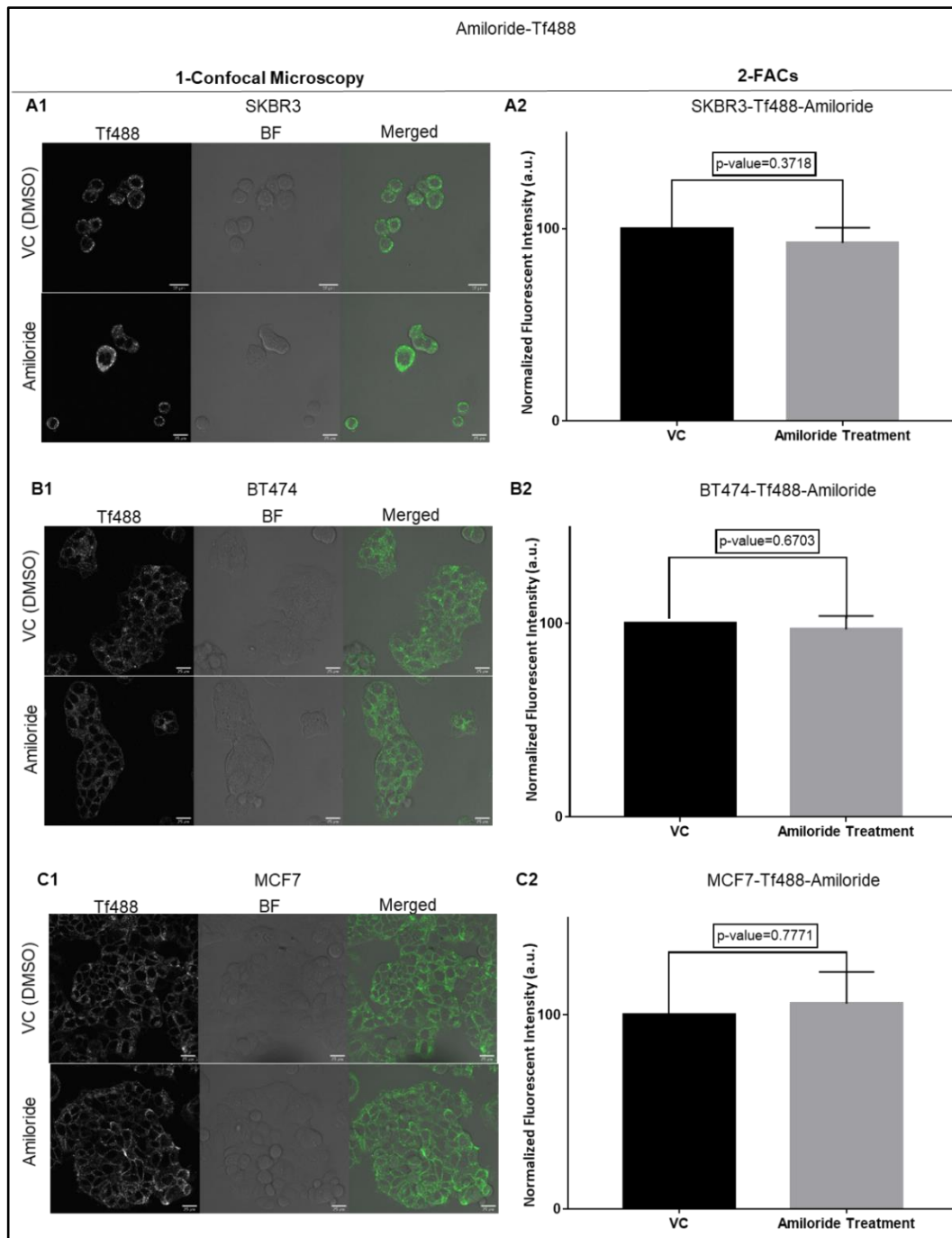


Figure 3.8: Confocal microscopy and Flow cytometry of Tf488 uptake +/- amiloride in BC cell lines. Cells plated on MatTek dishes (A1-C1) or 12 well plates (A2-C2) were incubated with vehicle control (DMSO) or Amiloride in the presence of Tf488 for 1 hr, washed, and processed for analysis by confocal microscopy and FACS. Data in A2, B2 and C2 represent means and standard error of the means from three independent experiments performed in triplicate Scale bars 25µm, BF: Bright Field.

3.2.6 Effect of EIPA on Tf in BC cell lines

Previous data (Figure 3.8) showed that amiloride had no effect on Tf uptake and data in figure 3.9 shows that the same is true for EIPA giving median p-values for SKBR3, BT474, and MCF7 of 0.4120, 0.7396, and 0.0908, respectively. However, there was less evidence that EIPA was causing mislocalisation of the Tf compared with effects seen with DEX in MCF7 cells and effects that the Jones laboratory has previously reported for EIPA and amiloride for endocytic markers such as EEA1 in fixed cells and cell penetrating peptides in live cells (Fretz et al. 2006).

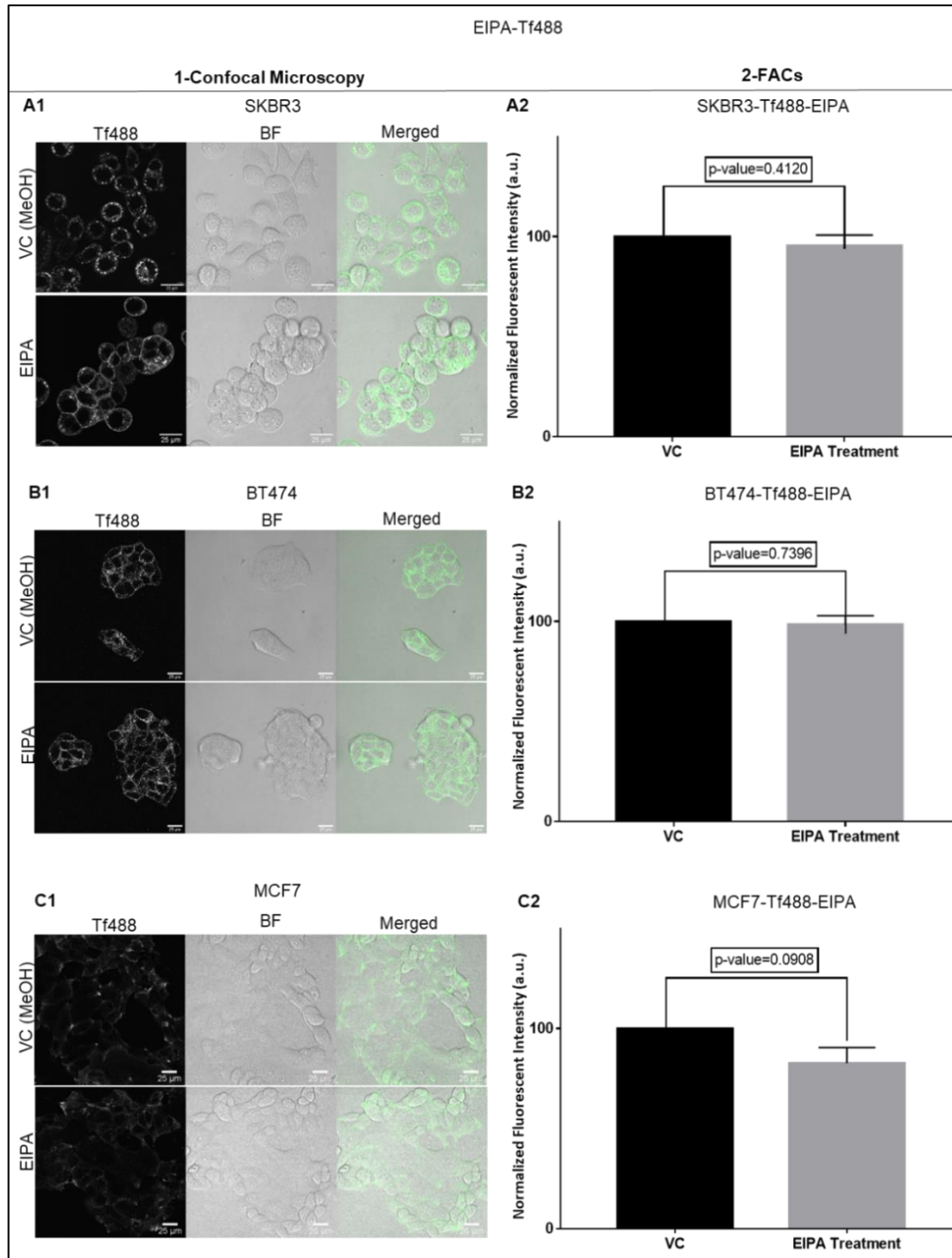


Figure 3.9: Confocal microscopy and Flow cytometry of Tf488 uptake +/- EIPA in BC cell lines. Cells plated on MatTek dishes (A1-C1) or 12 well plates (A2-C2) were incubated with vehicle control (MeOH) or EIPA in the presence of Tf488 for 1 hr, washed, and processed for analysis by confocal microscopy and FACS. Data in A2, B2 and C2 represent means and standard error of the means from three independent experiments performed in triplicate Scale bars 25µm, BF: Bright Field.

3.2.7 Effect of cariporide on Tf in BC cell lines

Unsurprisingly the same data trend was observed in cells treated with cariporide that lowered Tf uptake marginally but not significantly (p-value = 0.0553) in SKBR3 compared to BT474 and MCF7, which have p-values of 0.2530 and 0.2000, respectively. Confocal Microscopy also supported FACS with no evidence that the drugs were causing mislocalisation of the protein (Figure 3.10).

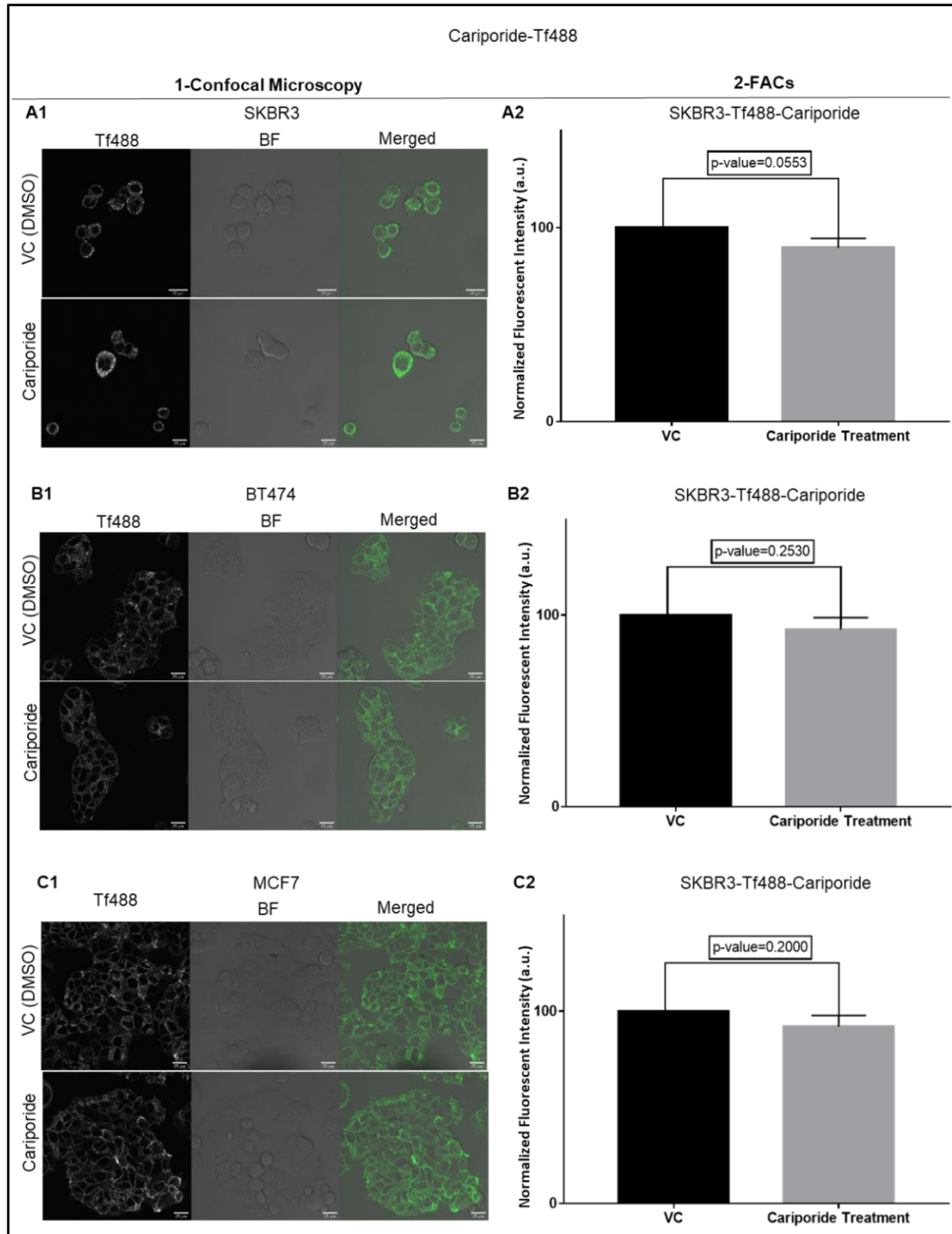


Figure 3.10: Confocal microscopy and Flow cytometry of Tf488 uptake +/- cariporide in BC cell lines. Cells plated on MatTek dishes (A1-C1) or 12 well plates (A2-C2) were incubated with vehicle control (DMSO) or cariporide in the presence of Tf488 for 1 hr, washed, and processed for analysis by confocal microscopy and FACS. Data in A2, B2 and C2 represent means and standard error of the means from three independent experiments performed in triplicate Scale bars 25µm, BF: Bright Field.

3.2.8 Metabolic Activity Assays in BC cell lines treated with NHE1 inhibitors.

Cell viability and cytotoxicity assays are generally based analysing for example membrane permeability, mitochondrial enzyme activity, ATP production, cell adherence and numbers. Currently, these assays are commonly used in cancer cell biology research to assess toxicity of compounds such as anti-cancer drugs (Aslantürk 2018).

Generally, metabolic and viability assays are employed to evaluate the overall metabolism occurring in a cellular model. It is important to differentiate between cells that have for a particular reason, a low metabolic rate and dead cells. In several studies, this difference is ignored, which results in directly linking cell growth to metabolic activity (Braissant et al. 2020). The CellTitre blue assay used in this thesis measures metabolic activity and not cell viability, thus the term metabolic activity assay was used.

Due to the very different effects of these drugs on endocytosis, the next experiments focused on performing a comparative analysis of their potential cytotoxicity in the BC cell lines, including the Tz resistant Clone 5 BT474 cell line. For this, the cells were incubated for 24 hrs in the continuous presence of the drug. As illustrated in figure 3.11, EIPA was the most toxic agent in all four cell lines reducing metabolic activity to <40% at 150µM and being highly toxic at higher concentrations. Amiloride and cariporide were, but to a lesser extent, toxic in a concentration dependent manner in all cell lines.

Numerous investigations have established that EIPA and amiloride are effective at doses ranging from 10 to 100 μM as macropinocytosis inhibitors (Kamei et al. 2019; Fretz et al. 2006; Haspot et al. 2012). The study by (Fretz et al. 2006) in KG1a leukaemia cells demonstrated that 0–50 μM EIPA had no impact on viability, 100 μM indicated 5% to 25% cytotoxicity, and increased to 40–50% at 200 μM . The experiments performed with amiloride concentrations up to 200 μM revealed no toxicity.

Cariporide was not toxic to BC MCF7 or MDA-MB231 cell lines at a concentration of 80 μM at varying pHs of 7.4 to 5.9. (Wong et al. 2002). Another study investigated cariporide's effect on the viability of human malignant mesothelioma H-2452 cells compared to same cell line but has acid-tolerable at concentrations ranging from 40 μM to 360 μM . They found that the cariporide treatment significantly inhibited the growth of H-2452AcT cells at a concentration at which H-2452 cells exhibited no notable toxicity (Lee et al. 2017).

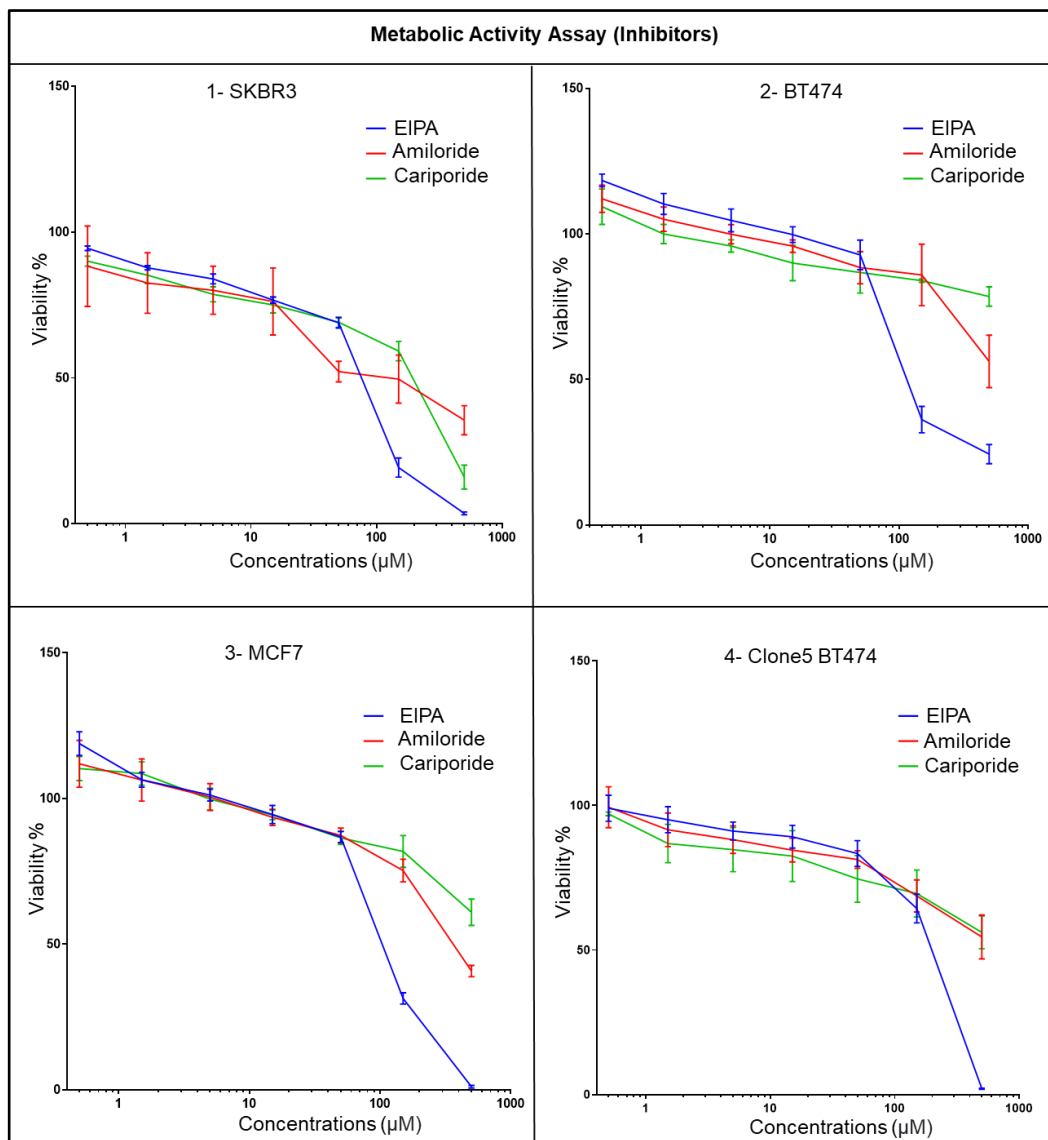


Figure 3.11: Amiloride, EIPA and cariporide Cytotoxicity assays in BC cell lines. Cells were seeded and cultured for 48 hrs, and then were treated with the inhibitors for an additional 24 hrs prior to performing CellTiter Blue metabolic activity assays. Data show SEM from three independent experiments performed in duplicate.

3.2.9 Metabolic Activity Assay (Solvents) in BC cell lines

In order to rule out the possibility that the solutes used to dissolve the drugs were having nonselective toxic effects, they were explored in the absence of the drugs. It would have been challenging to perform this analysis at the same time as investigating the drugs. Here, amiloride and cariporide were dissolved in DMSO, and EIPA was dissolved in MeOH.

In figure 3.12, 500 μ M (the highest concentration used) equates to 1% v/v DMSO and 1% v/v MeOH.

Figure 3.12 shows that none of the solvents at the highest concentrations inhibited metabolic activity by >40%. However, in SKBR3 and BT474 lines there was some clear effects of DMSO or DMSO/MeOH respectively. But for all experiments in this thesis their concentrations on cells did not exceed 1%.

DMSO is used to dissolve a range of polar and nonpolar compounds that are generally insoluble. This, in conjunction with its perceived low toxicity at concentrations of less than 10% (Pelzel et al. 2010; Burugula et al. 2011), has led to its extensive usage as a solvent for drugs, as used in this thesis. Other reports indicate that DMSO concentrations of more than 10% (v/v) induce cellular damage (Julien et al. 2012; Hanslick et al. 2009). Another study by Galvao's group demonstrated that DMSO was toxic to Retinal Ganglion -5 cells, and 90.5% of cells died at 10% of DMSO treatment. They stated that "The IC₅₀ was also calculated after 24 h and was found to be at 2.14% DMSO" (Galvao et al. 2014) and this equates to 245 μ M. I was not able to find similar studies for the BC cell lines studies here.

In line with research conducted by Nguyen et al. (2020) that compared DMSO and MeOH in several cancer cell lines. Methanol at 10% v/v had considerable cytotoxicity in all cell lines, and at 5 % significantly affected cells such as HepG2 and MCF7; determined and measured by recording the change in the impedance of electron flow caused by adherent cells. They noted that DMSO should be employed as a solvent at concentrations between 0.15- 0.6% v/v and methanol between 0.15 and 1.25 % v/v, the study agreed with data in figure 3.12, Methanol had a less effect compared to DMSO at the concentrations used to dissolve the drugs to the required concentrations.

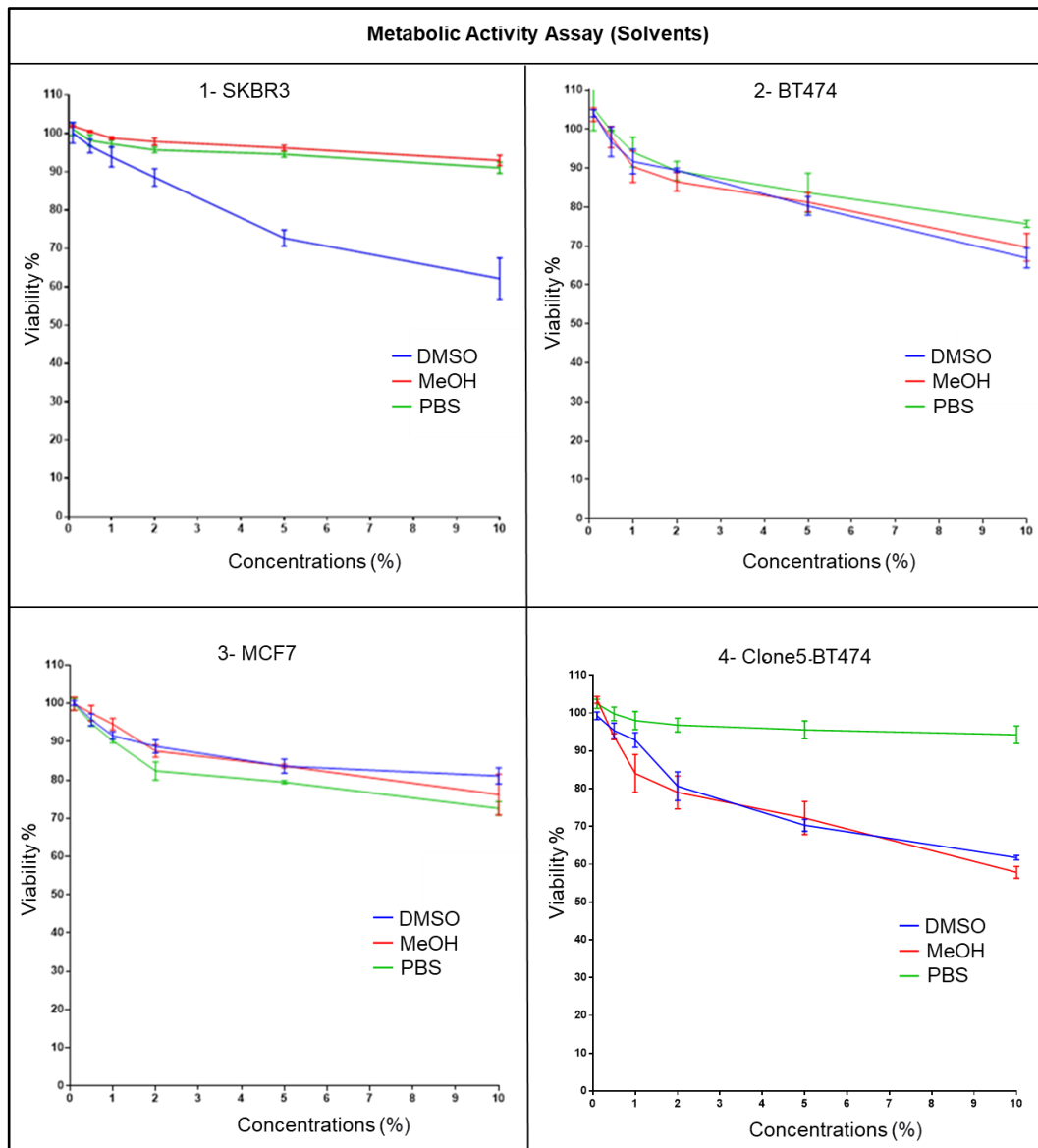


Figure 3.12: DMSO, MeOH and PBS Cytotoxicity assays in BC cell lines. Cells were seeded and cultured for 48 hrs, and then were treated with the inhibitors for an additional 24 hrs prior to performing CellTiter Blue metabolic activity assays. Data show mean SEM from three independent experiments performed in duplicate.

3.2.10 Comparative analysis of CME, recycling, and fluid phase endocytosis in BT474 and Clone5 BT474 cells

As noted in Chapter 2, BT474 is an epithelial-like cell line derived from a solid, invasive ductal carcinoma that overexpresses HER2 (Subik et al. 2010). As noted in the Introduction resistance of HER2 cells to Tz represents a significant clinical challenge. The Clone5 BT474 cell line was generated by continuously incubating BT474 cells with Tz until they became unresponsive to this agent (Kute et al. 2004). Citations of this article confirm the resistance of this line to Tz (Paroni et al. 2019). Recent work in the Jones laboratory showed that HER2 in these cells does not respond to crosslinking by entering cells, i.e. as noted for BT474 and SKBR3 (Wymant et al. 2020), and here further analysis was performed on the endocytic properties of this starting with analysis of CME of Tf and it's recycling out of the cells.

3.2.11 CME and recycling of Transferrin in BT474 and Clone5 BT474 cells

In these assays, the cells were initially incubated in serum free media (SFM) to minimise the effects of bovine Tf in the serum. They were then incubated with human Tf488 for 15 mins, and this represents the pulse period as the probe is binding to TfR and being internalised into early and recycling endosomes. There follows for different periods of time a 'chase' period whereby the Tf progressively recycle out of the cells with the possibility that some could re-enter. This process can be analysed using live cell imaging confocal microscopy and FACS. Though largely qualitative, the confocal microscopy in figure 3.13 suggests that Tf fluorescence is higher in BT474 than in Clone5 BT474 pre and after the chase period. Measured here and not via FACS is the plasma membrane bound

fraction. The FACS data in figure 3.14 using ANOVA confirm the confocal results showing lower fluorescence at experimental time points: 0 min, 10 mins, 20 mins, 30 mins, and 1 h, giving p-values (****) 0.0001, (**) 0.0012, (**) 0.0042, (**) 0.0014, and (**) 0.0061, respectively. There was also a similar reduction in fluorescence 1.5 h, but this was non-significant, with a p-value of 0.3711.

Studies were then initiated investigating the fluid phase uptake of DEX that is known to be trafficked to lysosomes in the absence of a receptor. Here the experiment was simpler and more conducted by simply incubating the cells with the probe and measuring fluorescence using confocal microscopy and FACS at different time points.

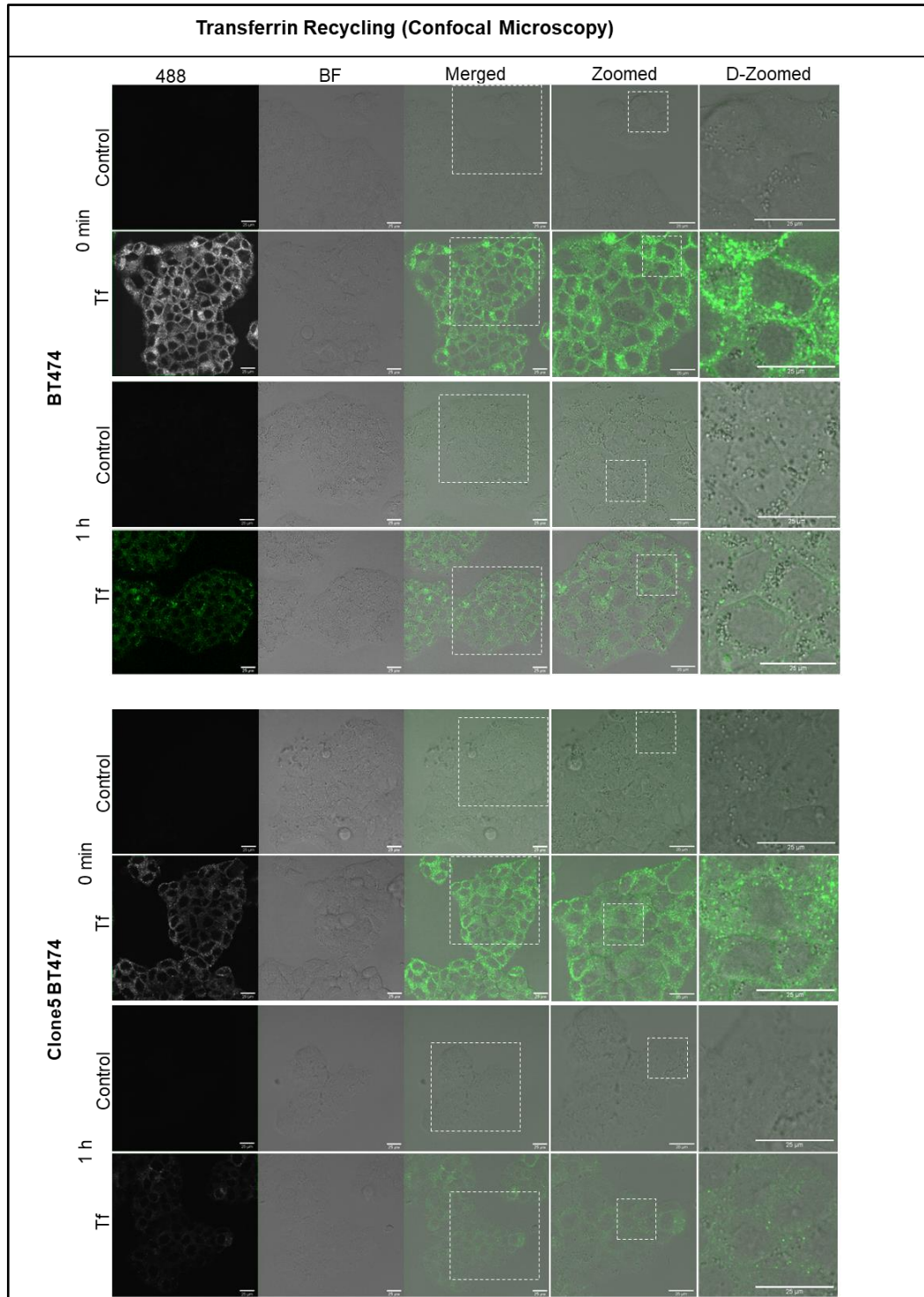


Figure 3.13: Tf uptake and recycling in BT474 and Clone5 BT474 cells. SFM starved cells were incubated for 60 mins and then treated with 50nM Tf488 for 15 mins and then either imaged or further incubated for 60 mins (chase) and then imaged by live cell confocal microscopy. Control represents cells that were not incubated with Tf488 but otherwise treated the same.

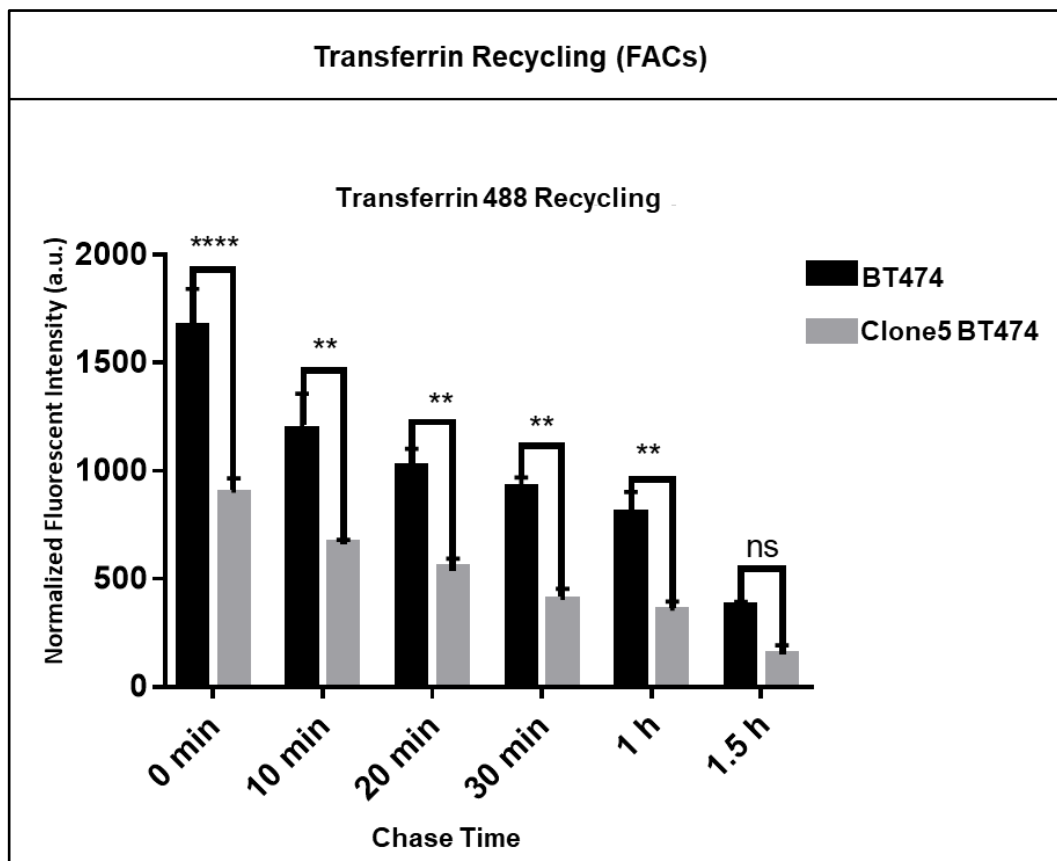


Figure 3.14: Tf recycling in BT474 and Clone5 BT474 cells. Cells were washed and starved for 1h in SFM. Cells were then incubated with Tf488 for 15 mins. Cells were then chased for Tf recycling for 0min, 10mins, 20 mins, 30 mins, 1h, and 1.5hrs prior to processing for and analysis by FACS. Data as means and SEM represents three independent experiments performed in duplicate.

3.2.12 Differences between BT474 and Clone5 BT474 in Dex uptake

Interestingly the results followed the same trend as that seen for Tf with FACS showing significant (≥ 30 mins) increases in the uptake of this probe in the BT474 cells compared with the Clone 5 BT474 variant; this was confirmed using confocal microscopy (figure 3.15) for 30, 60, 120 and 240 mins p-values were (*) 0.0121, (*) 0.0179, (****) 0.0001, and (****) 0.0001, respectively (figure 3.16).

Overall, the data highlight that the differences in the behaviours of the Clone 5 BT474 cells to Tz is not due to deficiency in either fluid phase endocytosis or

CME. However, other endocytic pathways exist, their analysis is more complex than these two pathways that have appropriate probes for their studies. Pathways such as those organised by caveolin -1, Flotillin-1, and ARF6 still lack good selective markers and the exact mechanism by which HER2 enters cells is unknown.

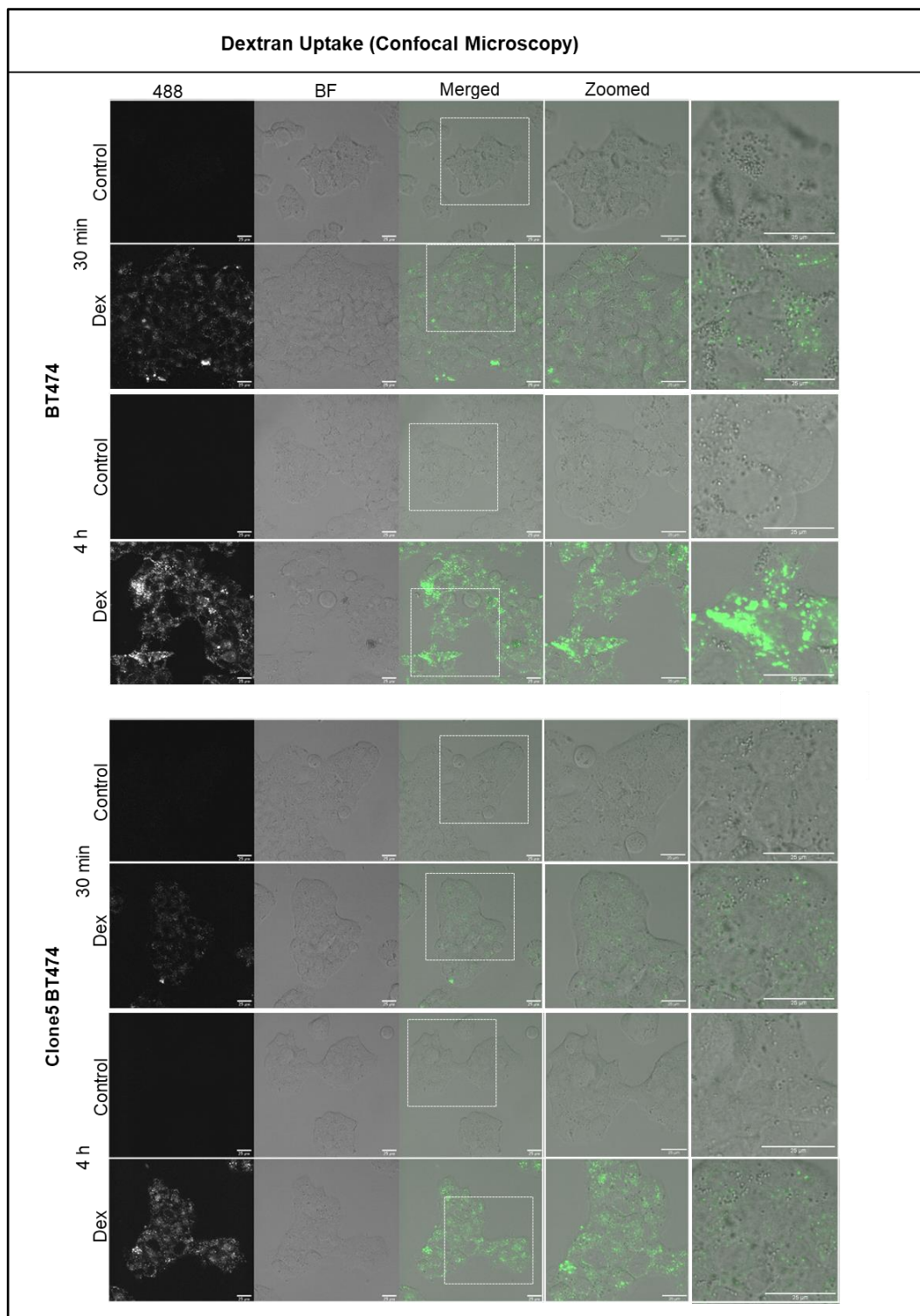


Figure 3.15: Differences between BT474 and Clone5 BT474 in DEX uptake. Cells were washed in PBS twice, and DEX488 (0.5 mg/ μ L) or dH₂O in complete media was added to the relevant wells and incubated for 30 min and 4h.

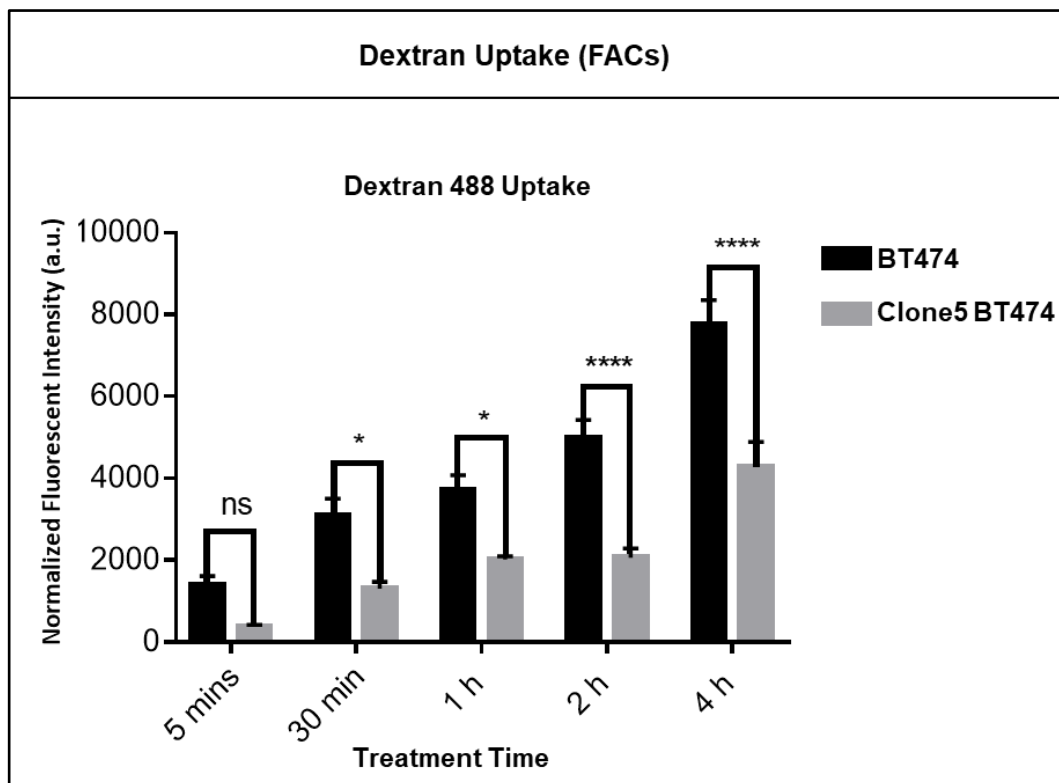


Figure 3.16: Dextran uptake in BT474 and Clone5 BT474 cells. Cells were washed and incubated with DEX488 in complete for 5min, 30 min, 1h, 2h, and 4h prior to processing and analysis by FACS. Data as means and SEM represents three independent experiments performed in duplicate.

3.3 Summary

For models to test HER2 receptor and Tz uptake internalisation, High (BT474, SKBR3), and low (MCF7) HER2 expressing variants were used to investigate a role for macropinocytosis; three different NHE inhibitors were employed. EIPA has been identified as a well-characterised macropinocytosis inhibitor, largely overtaking the initial use of amiloride (West et al. 1989; Veithen et al. 1996; Meier et al. 2002). In this thesis, we find rather surprisingly that EIPA could also increase the uptake of a well-characterized macropinocytosis probe in the form of Dex and that this effect was not dependent on Dex size or choice of the fluorophore. This effect occurred in SKBR3 and BT474 (HER2+) cell lines but not in MCF7 cells (HER2-). As earlier discussed, there are many reasons for this, but the results contradict those reported in the literature, which indicate that EIPA is a macropinocytosis inhibitor based on the definition that this is how Dex enters cells as opposed to constitutive fluid phase endocytosis. A study by Li et al. (2015) suggested that uptake of Dex in HeLa cells was size dependent. Based on inhibitor studies with amiloride and the PI 3-kinase inhibitor, Wortmannin Dex 70 kDa was thought to be a more effective probe for the monitoring of fluid uptake via macropinocytosis, while Dex 10kDa, could be used to analyse general fluid-phase endocytosis (including macropinocytosis and micropinocytic processes). Interestingly the inhibitory effects of EIPA and amiloride were suggested to be nonselective on distinct endocytic pathways but via effects on the actin cytoskeleton that could affect numerous endocytic pathways and processes (Chang et al. 2014; Ivanov et al. 2008). Additionally, attenuation of internalisation via lipid rafts was attributed to amiloride (Wadia et al. 2004), while studies from the Arwyn Jones laboratory showed EIPA was affecting morphology

and the intracellular distribution of both early and late endosomes (Fretz et al. 2006).

In this thesis, cariporide was then used as a more selective inhibitor of NHE1; to my knowledge, this drug has not yet been investigated as a potential endocytosis inhibitor. Here, Tf was also included as a marker for CME. The findings show that cariporide or amiloride had no effect on the uptake of either Dex in the cells studied and Tf uptake in all cell lines was normal in the presence of all three inhibitors. This strongly suggests that the observed effects of EIPA are not dependent on NHE1 inhibition and due to other undetermined effects.

Metabolic activity assays were then performed to analyse the cytotoxicity of the inhibitors, and findings revealed that EIPA, compared to amiloride and cariporide, was more toxic but at levels higher than used for the earlier studies that were performed at a much shorter time point. However, it does raise the challenge of interpreting endocytosis data with this drug.

In summarising the results with the inhibitors, it is interesting to note that with the exception of cariporide, the so-called macropinocytosis inhibitors had significant and sometimes unexpected effects on the uptake of endocytic probes such as DEX. The biological or indeed clinical significance (Amiloride is an approved drug) of this is difficult to interpret as the results were often cell line dependent and the in vitro data here may not translate to the in vivo setting. However, the data does raise significant issues regarding their use as agents to study distinct endocytic pathways and specific proteins regulating these events.

Finally, preliminary experiments in the Clone5 BT474 Tz resistant cell line further highlighted that its endocytic profile is different to the parental BT474 line

(Wymant et al. 2020), and further comparative analysis of these lines is presented in Chapters 4 and 5 when cell uptake of Tz as a soluble antibody or decorating PLGA NPs is investigated.

Chapter 4 : Effects of Trastuzumab on Breast Cancer Cells

4.1 Introduction

In 1984, a gene named neu was isolated and found to encode a protein with a M.W. of 185 kDa (Schechter et al. 1984). The gene was later found localised to the human chromosome 17 q21 region (Coussens et al. 1985). It was later termed HER2 and proposed to function as a cell surface receptor and a kinase (Drebin et al. 1986) (Figure 4.1). Since then, there has been considerable interest in targeting this protein with drugs including Tyrosine Kinase Inhibitors (TKI) (Schlam and Swain. 2021), and monoclonal antibodies targeting such as Tz and Pertuzumab and antibody-drug conjugates such as Tz Emtansine (Bose et al. 2021). HER2 neu gene was identified in 1985 (Hetzl 1992). HER2 overexpression is caused by mutations that change amino acids in the transmembrane and juxtamembrane domains. This causes autophosphorylation of tyrosine residues in the cytoplasmic domain of the heterodimer, which initiates a number of signalling pathways that lead to cell growth and tumourigenesis (Oh and Bang 2020).

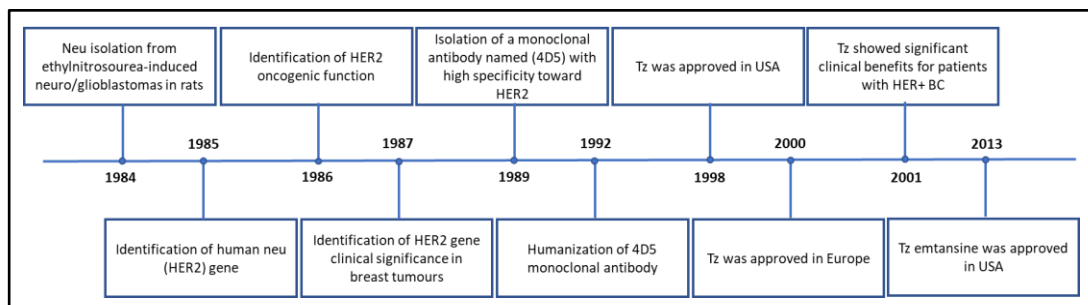


Figure 4.1: The history of Tz, from discovering HER2 to the evidence of its therapeutic benefits. Adapted from (Maadi et al. 2021).

4.1.1 Trastuzumab

This monoclonal antibody has been introduced in the introduction, and several significant trials have now been conducted utilising Tz in many forms, including the very large Hera Trial (5102 patients) that compared Tz to standard therapy and also its assessment as an adjuvant to chemotherapy such as DOX (Piccart-Gebhart et al. 2005). However, the drug had been FDA approved since 1998, but this trial was the most significant in identifying the positive value of this antibody. Several studies have demonstrated that adjuvant Tz therapy significantly improved disease-free survival in women with operable HER2+ BC (Gaibar et al. 2022; Loibl and Gianni 2017; Di Modica et al. 2017). Tz with Pertuzumab combined with paclitaxel or docetaxel is recommended first-line therapy for HER2+ metastatic BC (Martínez-Sáez and Prat 2021; Loibl and Gianni. 2017).

Despite the therapeutic effectiveness of Tz, resistance to this antibody following treatment represents a significant clinical challenge to the drug's usage and is identified as a major obstacle to successfully treating BC (Bose et al. 2021). It has been stated that the efficacy of Tz for patients with HER2+BC in its early stages varies between 30 and 50 %, with the majority of patients developing resistance to this therapy within one year. Therefore, overcoming Tz resistance would represent a major step forward, and continuous efforts are being made to do this (Rezaei et al. 2019). Tz resistance is covered in more detail in section 4.1.3.

4.1.2 Mechanism of Action of Tz

4.1.2.1 Tz and HER2 Dimerization

Until now, Tz's exact mechanism of action remains controversial, and several potential mechanisms have been proposed (Maadi et al. 2021). Initial research demonstrated that Tz reduces tumour development by preventing the dimerization of HER2 with other HER receptors, such as HER3. Tz, as immunoglobulin G (IgG), can bind through electrostatic and hydrophobic interaction to HER2 (Wei et al. 2017). However, studies have produced contradictory findings regarding the effects of Tz on HER2 homodimerization – but studies have also shown that Tz increases HER2 homodimerization in a dose- and time-dependent manner (Maadi et al. 2018). Thus these findings suggest that Tz stimulates HER2 homodimerization and inhibits HER2 heterodimerization in a ligand-independent manner (Richard et al. 2016).

4.1.2.2 Tz, HER2 downregulation, and degradation

Tz's effects in promoting HER2 endocytosis and degradation are also debatable. Some research indicates that Tz downregulates HER2 (Yang et al. 2017), whereas others show no impact (Bagnato et al. 2017). In general, research has indicated that long-term treatment with Tz downregulates HER2; however, the mechanism for this has not been identified. Several studies have shown that Tz suppresses the expression of other HER receptors, including HER3 and EGFR (Dokmanovic et al. 2014). Our data reveal that Tz induces plasma membrane ruffling in HER2 BC cell lines after 5 to 7 hrs of treatment (Figures 4.4 and 4.5).

4.1.2.3 Tz and Cell Signalling

The MAPK signalling cascade has been extensively studied and plays a crucial role in various cellular activities, including cell proliferation, differentiation, apoptosis, migration, and stress responses (Guo et al. 2020; Wang et al. 2018). Additionally, this pathway is highly active in several cancer types (Korzeniecki and Priefer 2021). Investigations have demonstrated that Tz inhibits both threonine and serine AKT phosphorylation (Yu et al. 2017; Watanabe et al. 2019). Tz can also enhance the separation of Src (a nonreceptor tyrosine kinase) from HER2, hence inhibiting its activity. PI3K/Akt and mammalian target of rapamycin (mTOR) would therefore be suppressed (Derakhshani et al. 2020). Other studies have shown that Tz has limited effects on HER2-mediated intracellular signalling and phosphorylation of ERK and AKT, and they demonstrated that it did not inhibit phosphorylation of ERK and AKT in CHO-K6 cells (Maadi et al. 2018).

4.1.2.4 Tz and Cell Cycle

Tz inhibits cell proliferation and stimulates cytostatic action, arresting the cell cycle in the G1 phase (Weissenstein et al. 2016; Valabrega et al. 2007). The cell cycle is arrested by inhibiting the production of proteins associated with the cleavage of the cyclin dependent kinase (CDK) inhibitor p27kip1 (Derakhshani et al. 2020).

4.1.2.5 Tz and antibody-dependent cell-mediated cytotoxicity (ADCC)

ADCC is a crucial Tz mechanism regulated by effector immune components such as NK cells (Kim et al. 2017). The binding of fragment crystallizable receptors (FcγRs) to the Fc region of Tz activates the ADCC process, which concludes with the release of perforin and granzymes from immune effector cells (Treffers et al.

2019). Perforin can facilitate the formation of holes in tumour cells, hence facilitating granzyme diffusion into the cytoplasm. This enhances apoptosis and lysis of tumour cells (Prager et al. 2019). Tumour cell lysis improves tumour antigen presentation in the tumour microenvironment and subsequently promotes antigen-presenting cell activation and T cell polarisation (Rainone et al. 2016). In addition, research indicates that Tz enhances other immune responses against HER2+BC cells. Tz stimulates HER2 uptake by dendritic cells (DC) when co-cultured with HER2+SKBR3 and BT474 BC cells (Gall et al. 2017).

4.1.3 Tz Resistance

As mentioned, The Food and Drug Administration (FDA) officially authorised the clinical use of Tz for HER2-overexpressing metastatic BC in 1998, and since then, it has significantly increased the life expectancy of BC patients with HER2+status. Nevertheless, up to 70% of patients do not respond to Tz, and Tz resistance develops in most patients within a year (Yu et al. 2017). The mechanisms behind Tz resistance are still quite under study and summarised here.

Many mechanisms have been proposed to explain how BC cells develop resistance to Tz. Studies have shown that low expression of PTEN Levels and PIK3CA mutations may contribute to Tz resistance (Rimawi et al. 2019; Yokoyama et al. 2021). Resistance may be further enhanced by chronic activation of the PI3K/AKT signalling pathway (Figure 1.3). A method that prevents Tz from binding to HER2 relates to the plasma membrane truncation of HER2 at the extracellular domain, thus resulting in 'epitope masking' (Scaltriti et al. 2007). Additionally, hyperactivation of other tyrosine kinase receptors, such as

the insulin-like growth factor-I receptor (IGF-IR), compensates for suppressing the HER2 downstream signalling pathway by Tz (Saisana et al. 2016).

As mentioned in Chapter 1 HER2 possesses characteristics that prevent it from being endocytosed, starting with the fact that it does not have a natural ligand, like EGF for EGFR, that could drive dimerization and activate internalisation. Austin et al. (2004) conducted detailed research on Tz's effect on the endocytosis of HER2. They demonstrated that Tz did not affect the HER2 distribution being internalised and did not drive HER2 endocytosis. However, Tz entered recycling endosomes and trafficked back to the plasma membrane rather than into the lysosomes for degradation. This HER2 internalisation aspect is highly significant for the project presented in this thesis.

Currently, Tz is not the standard of care as a monotherapy, and to overcome Tz resistance, it is administered with other therapies (Martínez-Sáez and Prat 2021; Bapat et al. 2021). Examples of combinational therapies include adding another antibody that binds to HER2 at a different site, such as Pertuzumab, or adding another small molecule drug, such as lapatinib, that inhibits the tyrosine kinase activity of the receptor to overcome Tz resistance (Wang and Xu 2019; Barok al. 2014).

Tz has been conjugated to a very toxic drug known as emtansine (T-DM1) to form an ADC, with the drug inhibiting microtubule assembly in the cytosol. This treatment has been demonstrated to improve the clinical results of HER2 BC patients (Maadi et al. 2021). Based on the information on HER2 and endocytosis, it is important to note that for emtansine to reach the tubulin target, it needs access to the cells and the lysosome for the enzymes to degrade the antibody

and release the drug to the cytosol (Barok et al. 2014). It is likely that what is known about HER2 endocytosis and recycling is counterproductive to the success of this ADC in the clinic. Currently, T-DM1 monotherapy is regarded as the standard second-line treatment (Martínez-Sáez and Prat 2021).

Based on results in chapter 3 relating to some unexpected findings associated with the effects of EIPA and other macropinocytosis inhibitors on the internalisation of endocytic probes, this chapter investigated the cell binding and internalisation of a fluorescent Tz conjugate in the presence and absence of macropinocytosis inhibitors. Materials and methods were described in Chapter 2.

4.2 Results and Discussion

4.2.1 Tz conjugated Alexa 647

4.2.1.1 Amine crosslinker reactive groups

A method for labelling Tz with an Alexa fluorophore has been previously used in the laboratory to demonstrate low inherent internalisation unless it can be used to crosslink HER2 (Moody et al. 2015; Wymant et al. 2020).

Amine-reactive crosslinker reactive group of N-hydroxy succinimide (NHS) ester is considered one of the most popular and straightforward methods for labelling a protein such as an antibody by utilising NHS ester to react with primary amines ($-NH_2$) (Figure 4.2). Primary amine (N-terminus) is present in a variety of proteins, are positively charged at physiologic pH; consequently, they are located mainly on the exterior surfaces of tertiary protein structures, where they are readily accessible to conjugation reagents introduced into an aqueous media. Moreover, among the functional groups often present in biological or protein samples, primary amines are the most nucleophilic, making them easier to target for

conjugation. A limitation of this method is that it is often generic since conjugation can occur at any accessible primary amine (Nanda and Lorsch 2014).

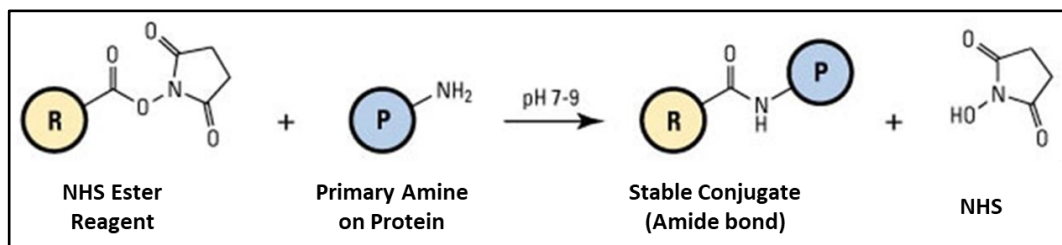


Figure 4.2: NHS esters react with the primary amino groups of a protein at a pH range of 7.0 to 9.0. This reaction generates a stable amide bond between the primary amines and the NHS conjugate. Adapted from (ThermoFisher).

Tz488 utilised in this study was prepared and kindly donated by Dr. Edward Sayers in our laboratory. The protocol of (Wymant et al. 2020) was then followed and used to prepare Tz488, and data in figure 4.3 shows the characteristics of this conjugate, giving an average number of close to three fluorophores per antibody; comparable to the Wymant publication.

In another study (Obaid et al. 2017), eight molecules of Alexa Fluor 700 per antibody were calculated. In contrast to our 1 mg/mL concentration, they employed 10 mg/mL of Alexa flour to conjugate the antibody.

Based on the suitability of the available Tz conjugates (488 and 647), with respect to other fluorescence probe that are used in the laboratory it was determined that further experiments would be performed with the 488 variant.

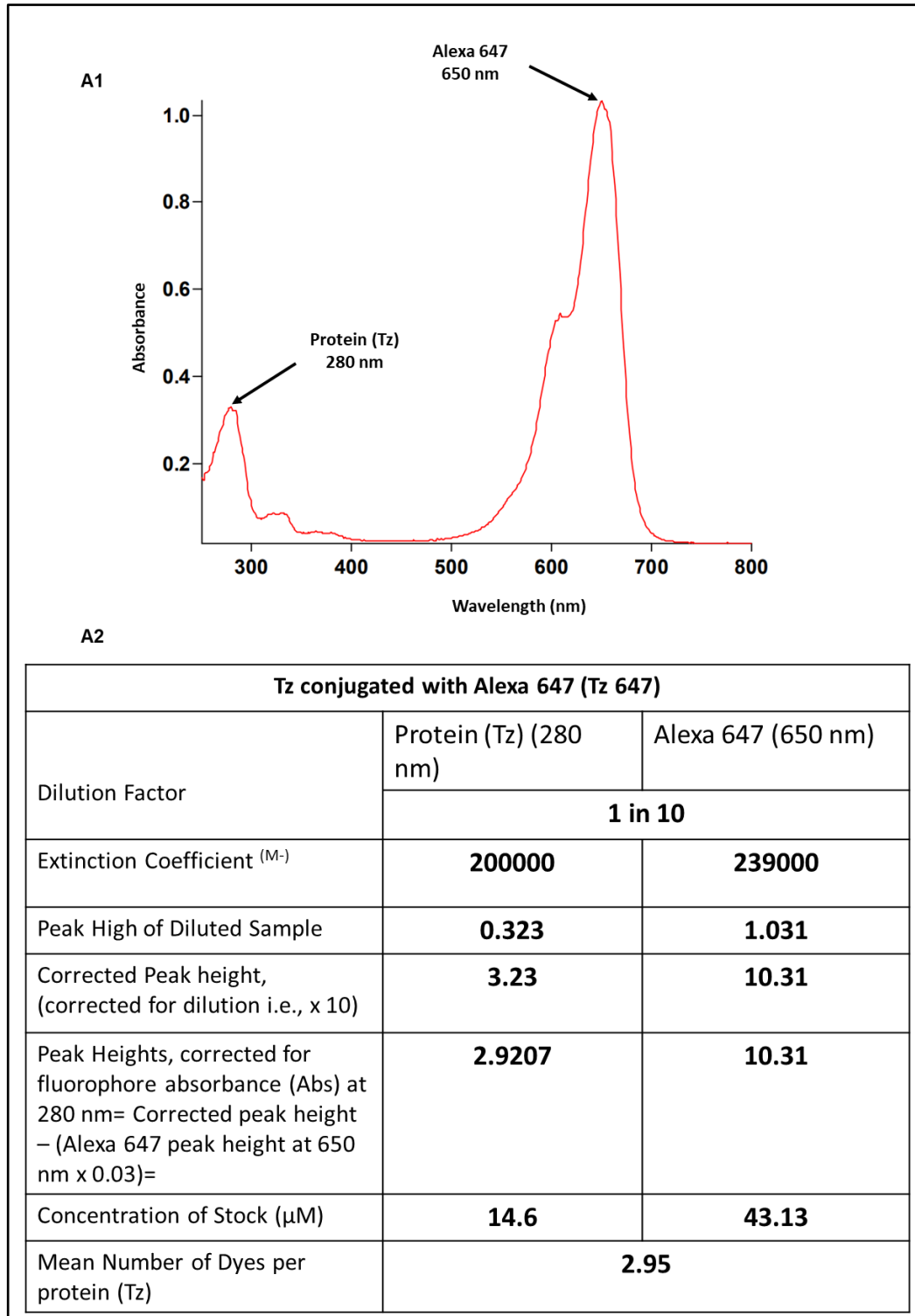


Figure 4.3: Characteristics of Tz conjugated to Alexa 647. Peak high is the absorbance of protein at 280nm and the absorbance of the fluorophore at 647nm.

4.2.2 Tz488 binding and internalisation in BC cells

Several studies have shown that Tz undergoes receptor-mediated endocytosis after binding to HER2 (Barok et al. 2014; Hunter et al. 2020). The effectiveness of the Tz on HER2 endocytosis is a topic of intense debate. Although some studies suggest Tz efficacy upon HER2 downregulation, they have not provided a clear explanation of the mechanism of action (Yang et al. 2017). In contrast, several studies also demonstrate that Tz does not affect HER2 downregulation (Bagnato et al. 2017).

Tz488 was incubated with the four BC cell lines for either 30 mins or 7hrs. Binding was very apparent on the plasma membrane of all HER2+ cells at 30 mins (Figure 4.4), and MCF7 showed very low fluorescence confirming the selectivity of the conjugate for HER2. At 30 mins, only the plasma membrane was labelled, but after 7 hrs, there was clear evidence of punctate fluorescence indicative of Tz endocytosis in SKBR3 and BT474 cells but not in Clone5 BT474 cells.

Actin polymerization at the plasma membrane can lead to the formation of ruffles and macropinocytosis (Kay 2021). In SKBR3 and BT474 cells, similar structures labelled with Tz488 were observed after 7 hrs treatment with the antibody (Figure 4.4).

An earlier study by Dokmanovic et al. (2014) investigating Tz effects on SKBR3 and BT474 cells found Tz mediated tyrosine phosphorylation at HER2-Y1248 and EGFR-Y845 was increased by Tz in both cell lines. The phosphorylation of ERK1/2 was likewise increased. It has previously been shown that Ras GTP is associated with activation of the ERK1/2 pathway (Sugden 2003), which also

activates Rac. Rac has been heavily implicated in mediating Macropinocytosis (Kay 2021); thus, the ruffling observed in figure 4.4 may be due to HER2/EGFR signalling

The same Dokmanovic et al. (2014) study also demonstrated that Tz stimulated HER2 degradation following this observed signalling process that also then suppressed HER2-mediated growth signalling.

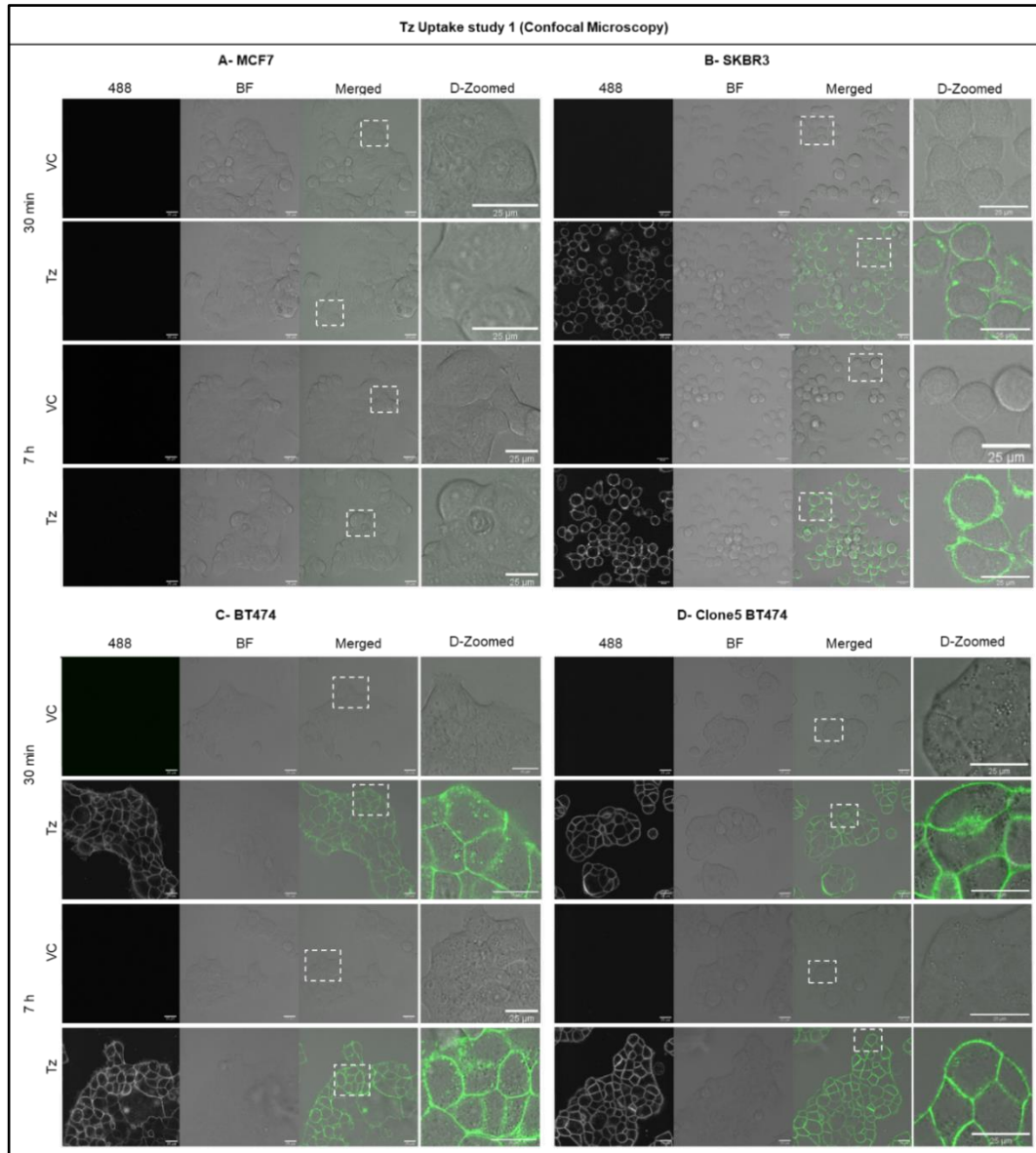


Figure 4.4: Tz488 binding and internalisation in BC cells. Tz conjugated Alexa 488 (50nM) was incubated with BC cell lines: MCF7, SKBR3, BT474, and Clone5 BT474, for 30 mins and 7 hrs before analysis by live cell confocal microscopy. D-zoomed; Digital zoomed. Scale bars 25μm, D-Zoomed; Digital zoomed, BF; Bright Field.

4.2.3 Time dependant Tz488 uptake and plasma membrane ruffling in BC cell lines.

To identify evidence of Tz endocytosis and ruffling, the conjugate was then incubated with the 4 BC cell lines for different periods of time. Data in figure 4.5 indicate the first clear evidence of Tz endocytosis after 5 hrs incubation but only in BT474 and SKBR3 cells and much less evidence of vesicular fluorescence in Clone5 BT474 cells. As expected, there was no labelling in MCF7 cells. From 5-7 hrs, more prominent vesicular labelling was observed in BT474 and SKBR3 cells, with again this being less apparent in the Clone 5 BT474 cell line

As previously mentioned, Austin et al. (2004) examined in detail the effect of Tz and HER2 endocytosis in SKBR3 and BT474. They demonstrated that HER2 receptors are constitutively internalised and recycled to the plasma membrane, and this is not affected by Tz. Although Tz is identified in internalised vesicles a few hrs after incubation with the cells, the vesicles observed in figure 4.5 may be predominantly recycling endosomes rather than endosomes destined for the lysosome, which could degrade HER2 and Tz. A separate study showed that the most of Tz and HER2 receptors were recycled to the plasma membrane. However, Dokmanovic et al. (2009) observed Tz internalisation and HER2 degradation after long SKBR3 Tz treatment for four days. Both of these studies mentioned the localization of internalized Tz attached to HER2 in early endosomes. Overall, these studies and others highlight that Tz has minimal effects on HER2 endocytosis in vitro studies (Maadi et al. 2021). Thus as previously demonstrated in our laboratory, other strategies such as HER crosslinking is needed to drive HER2 endocytosis and deliver to lysosomes for degradation (Moody et al. 2015; Wymant et al. 2020).

Data in this study clearly suggest Tz effects at plasma membrane, for example, identified as red arrowheads in figure 4.5. Interestingly Bagnato et al. (2017) observed similar structures in SKBR3 following Tz treatment and referred to them as Circular dorsal ruffles (CDRs). These are actin driven plasma membrane protrusions that combine into a single ring-shaped projection rising vertically from the dorsal cell surface. They, using similar Tz concentration, found that these structures appeared after only 10 mins incubation, and they also commented on the redistribution of HER2 and EGFR on the plasma membrane. However, they fixed the cells (for detecting HER2) before imaging, which could have led to the appearance of more pronounced effects on the plasma membrane.

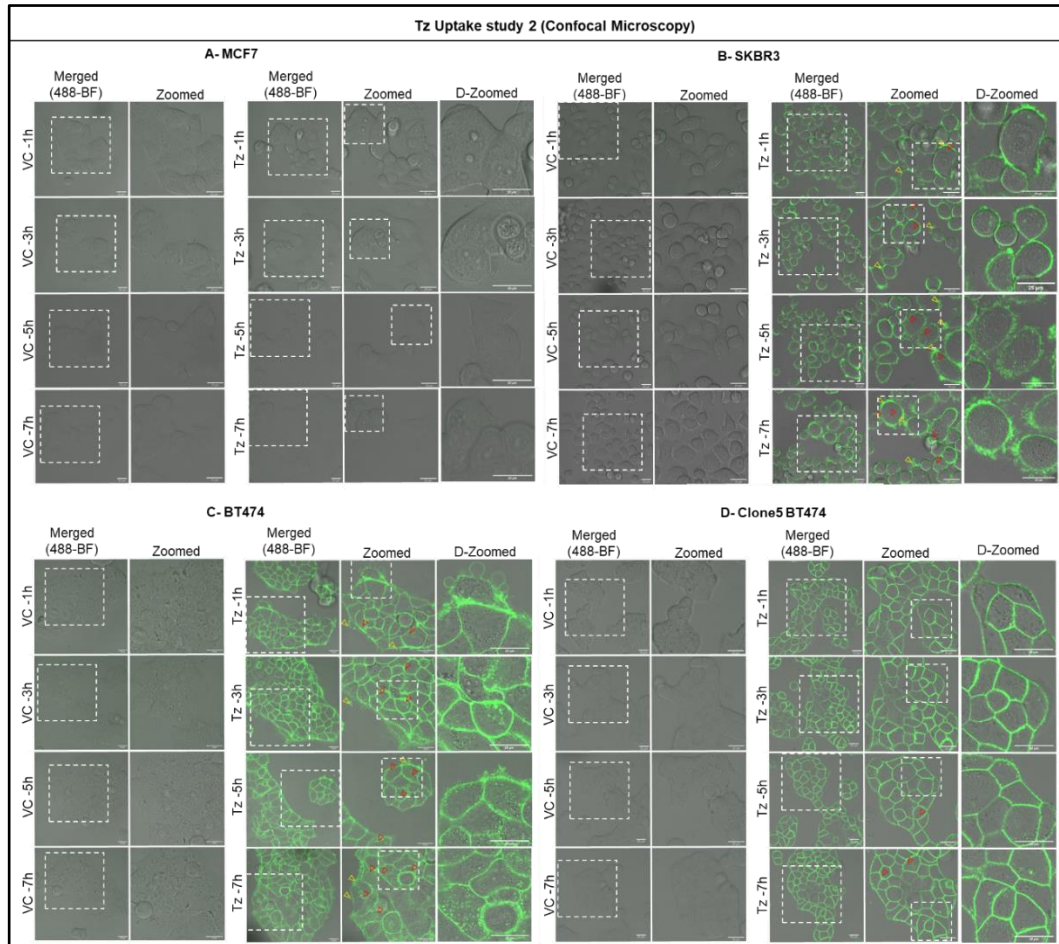


Figure 4.5: Tz treatment enhances HER2 plasma membrane ruffling in HER2 BC cells. Tz conjugated Alexa 488 (50nM) was incubated with BC cell lines: MCF7, SKBR3, BT474, and Clone5 BT474, for 1hrs, 3hrs, 5hrs, and 7hrs before analysis by live cell confocal microscopy. The yellow arrowheads indicated plasma ruffles, and red arrowheads indicated HER2 endocytosis. Scale bars 25 μ m, D-zoomed; Digital zoomed, BF; Bright Field.

4.2.4 EIPA enhances Tz488 internalisation.

4.2.4.1 Tz +/- EIPA in BC cell lines (Methods Optimized)

Methods A, B, and C were chosen to observe EIPA effects on Tz binding and internalisation. Method A includes labelling cells with Tz, followed by adding EIPA. Method B allowed EIPA to function before adding the Tz. Method C involves co-incubating the drug and antibody onto the cells. This would allow for more information on any effects that this drug may have on Tz cell dynamics. The methods of EIPA treatment of cells incubated with Tz were optimised based on findings that after 1h incubation, there was little evidence of antibody internalisation, that was clear to observe after 5h. Thus, attempts were made to investigate these two time points with the antibody incubated with the cells for 1 or 5 hrs followed by a 1 hr EIPA treatment before processing the cells for imaging (Method A). The second method B involved a 1hr or 5hrs preincubation period with EIPA and then adding Tz488 for 1 hr before imaging. In Method C, the drug and antibody were co-incubated with the cells for 2 or 5 hrs.

Surprisingly, for Methods A and B as demonstrated in figures 4.6 and 4.7, EIPA promoted Tz488 internalisation in SKBR3 and BT474 cells, but the effects were negligible in the Clone 5 BT4474 variant. This suggests a common mechanism in two of the cell lines, but for some reason, Clone 5 BT474 cells were resistant to this effect. In the 5hrs time point, there was also evidence of membrane ruffling in the same cells that showed increased internalisation, and again there was no evidence of this in the Clone 5 BT474 variant (Figure 4.6 B & C). The effects of EIPA on membrane ruffling were, however, method dependent; as with Method B, there was only evidence of membrane ruffling in SKBR3 after 1 hr and 5 hrs EIPA treatment followed by 1hr Tz treatment (Figure 4.7 -B) while having no

visible effect on the other cells. Additionally, EIPA's impact on SKBR3 is seen in Figure 4.8 as a plasma membrane blebbing emanating from cells after 5 hrs of EIPA treatment. Again, and intriguingly, EIPA had little influence on Clone5 BT474 using both Methods A and B. As expected, no fluorescence signal was detected in MCF7 cells.

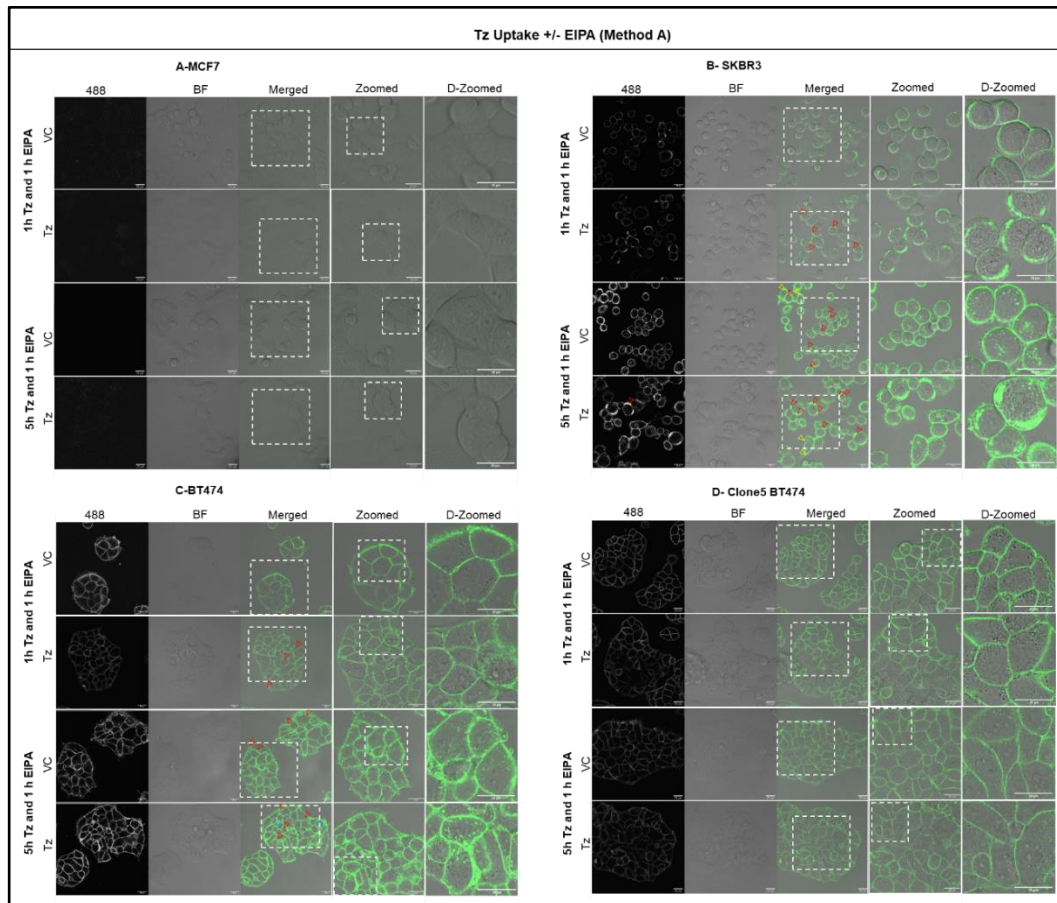


Figure 4.6: The effects of EIPA on HER2 endocytosis and Plasma ruffles in BC cells (Method A). Tz 488 (50 nM) was incubated with BC cell lines for 1hr and 5 hrs, followed by 50 μ M EIPA or MeOH for 1 hr before analysis by live cell confocal microscopy. Yellow arrowheads indicated plasma ruffles, red arrowheads indicated HER2 endocytosis, and blue arrowheads indicated vacuole like structure. Scale bars 25 μ m, D-zoomed; Digital zoomed, BF; Bright Field.

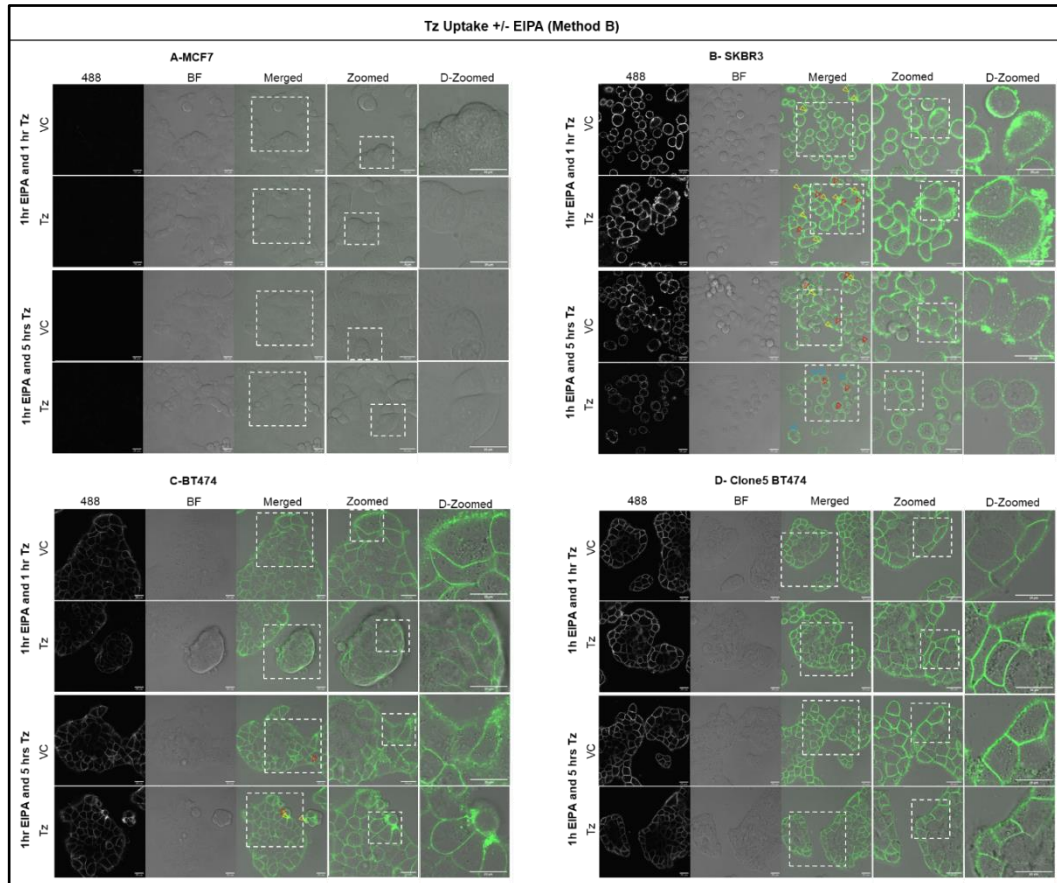


Figure 4.7: EIPA increases HER2 endocytosis and Plasma ruffles in HER2 BC cells (Method B). EIPA (50 μ M) or MeOH were incubated with BC cell lines for 1hr and 5 hrs, followed by Tz488 (50 nM) for 1 hr before analysis by live cell confocal microscopy. Yellow arrowheads indicated plasma ruffles, red arrowheads indicated HER2 endocytosis, and blue arrowheads indicated vacuole like structure. Scale bars 25 μ m, D-zoomed; Digital zoomed, BF; Bright Field.

4.2.4.2 Method C: EIPA/Tz488 co-incubation

Here the drug and antibody we co-incubated to assess whether similar effects to figures 4.6 and 4.7 were observed. Data in figure 4.8 validates previous findings with the drug causing, ruffling and blebbing but also the appearance of large Tz488 vacuole-like structures (particularly noted in SKBR3 cells Fig 4.8B). All cells did not show these structures; overall, there was quite some heterogeneity in phenotype within even a single field of view. These contradictory results may have various causes. There was also a noticeable effect on the overall shape of the cells after 5 hrs of EIPA treatment, suggesting that EIPA may have induced apoptosis. This is supported by (Acevedo-Olvera et al. 2015), which demonstrated a correlation between NHE inhibition by EIPA and the blebbing and apoptosis of cancer cells. They also found that EIPA promotes cell death via autophagy, membrane blebbing, and apoptosis in a human leukaemia cell line. Their findings suggested that the NHE exchanger is crucial to the survival of the human leukaemia cell line. They revealed that EIPA inhibited TF-1 cell survival in a dose- and time-dependent manner and the EIPA had a functional impact on mitochondria. Overall, this led to an experiment investigating the viability of these BC cells in the presence of EIPA, and the data is shown later in this chapter.

Apoptosis is characterised by the blebbing of the plasma membrane and the eventual deconstruction of cells into apoptotic bodies. Cancer cells have the exceptional capacity to create a defensive mechanism known as blebbishielding. This involves the fusion of apoptotic blebs and internal vacuoles (Jinesh and Kamat 2016). It is also stated that within blebbishields, endocytosis is activated in order to stop the apoptotic response from progressing further (Pfeffer and Singh 2018).

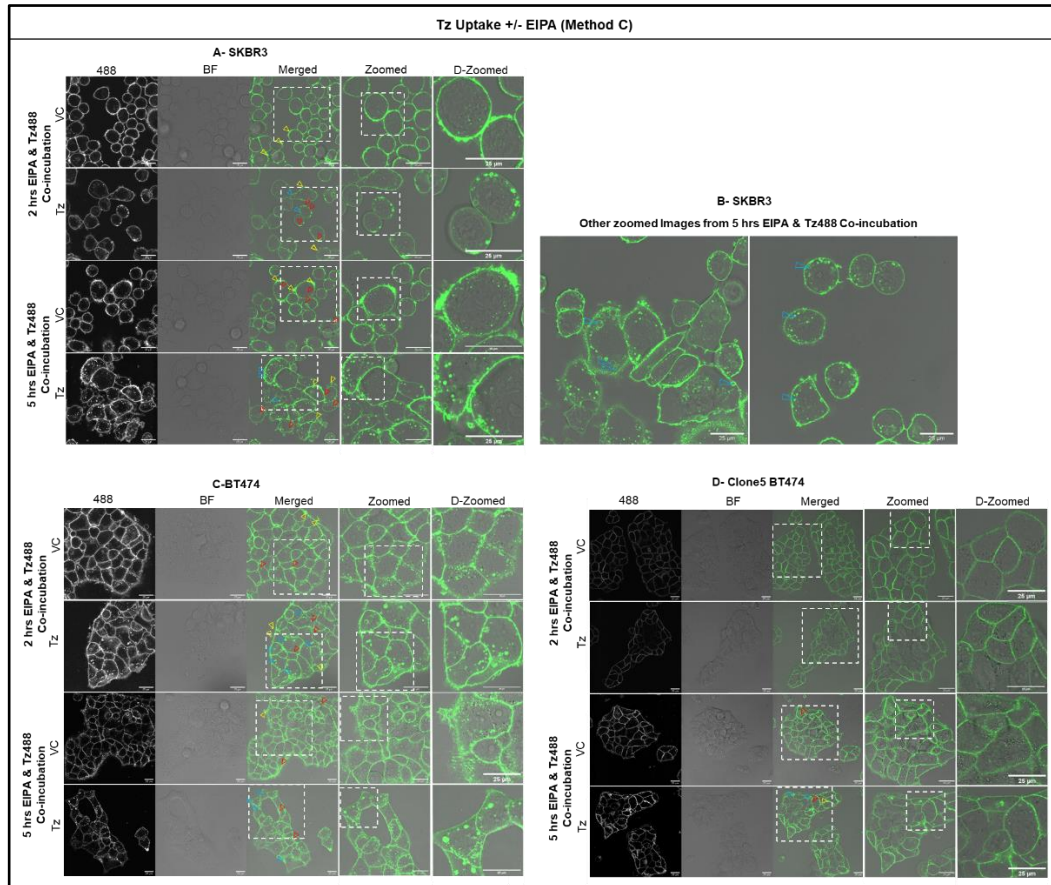


Figure 4.8: Co-incubation analysis of EIPA and TZ488 in BC cells to monitor Tz488 uptake and plasma membrane dynamics (Method C). Tz488 (50nM) and EIPA (50 μ M) or MeOH were co-incubated with BC cell lines: MCF7, SKBR3, BT474, and Clone5 BT474, for 2hrs and 5 hrs before analysis by live cell confocal microscopy. Yellow arrowheads indicated plasma ruffles, red arrowheads indicated HER2 endocytosis, and blue arrowheads indicated vacuole like structure. Scale bars 25 μ m, D-zoomed; Digital zoomed, BF; Bright Field.

NHE1 inhibitors EIPA and cariporide were introduced to 3-dimensional (3D) spheroids of BC and non-cancerous cells for 2–7 days (Rolver et al. 2020). EIPA was able to reduce the viability of BC spheroids in a dose-dependent manner, but cariporide (studied later) had no effect. Significant accumulations of EIPA were observed in spheroids, and this was associated with notable vacuolization, apparent autophagic arrest, and mitochondrial- and DNA damage, which are all signs of cell death. An earlier study suggests that EIPA at specific concentrations kills tumour cells while maintaining an acceptable degree of toxicity in normal cells (Raghuwand and Gillies 2000). Additionally, they noted that tumour cell intracellular pH acidification enhances chemotherapeutic drug efficacy. This also explains our findings, showing that inhibiting NHE with EIPA may lead to cellular acidification of the intracellular pH manifested as an increase in Tz uptake. But this remains to be investigated as results in Chapter 3 showed no EIPA effect on Tf uptake, suggesting this is not a common phenomenon.

The intracellular pH of healthy cells is tightly controlled to be very close to neutral by ion transport proteins on the plasma membrane. Normal cells have an intracellular pH of 7.2, whereas cancer cells have an alkaline intracellular pH of >7.4 as a result of an increase in NHE1 expression (Lee and Shanti 2021). Intracellular acidification can trigger apoptosis; however, an elevated cytoplasmic pH helps cancer cells avoid triggering apoptosis (Ko et al. 2020). Blocking NHE inhibits H⁺ efflux, resulting in intracellular acidification. A study by Schneider et al (2004) demonstrated that EIPA decreased intracellular pH by 0.2 - 0.3 units after one hour of treatment and that this decrease in pH resulted in cell death that in the absence of the involvement of caspases, did not seem to be due to classical

apoptosis. This further demonstrated the multiple effects on cells that EIPA can induce.

As demonstrated in figure 4.8C, the effects of EIPA are less pronounced on BT474 cells compared with SKBR3, but the observed effects are still clearly visible. Interestingly and in agreement with other EIPA methods A and B, EIPA has the least effect on Clone5 BT474, and after 5 hrs of treatment, there was, however, evidence of ruffling and Tz-488 internalisation.

4.2.5 Cellular profile of CellMask in EIPA treated BC cell lines

The commercial cell mask reagents comprise amphipathic molecules that stain the cell plasma membrane by offering a lipophilic moiety for enhanced membrane loading and a range of negatively charged hydrophilic dyes for confirming the probe's presence in the plasma membrane.

Deep Red CellMask was utilised to stain the plasma membrane, and this then allowed for a further opportunity to observe potential EIPA effects on this structure. Here as in Method C above, the dye and EIPA were co-incubated for 5 hrs. Data in figure 4.9 clearly demonstrate membrane effects in the form of ruffles/blebs in EIPA treated SKBR3 and BT474 cells. The data also show intracellular CellMask positive vacuoles similar to those observed with Tz488, especially in SKBR3 cells. The effects on MCF7 and Clone5 BT474 cells were much less pronounced, but there was a clear change in the CellMask profile with EIPA treatment.

Overall, the data are consistent for all cells with regards to EIPA effects on Tz488 and CellMask, showing higher sensitivity for BT474 and SKBR3 compared with Clone5 BT474 and MCF7. The reason for these differences is unknown but appears to be a general plasma membrane effect rather than the expression of HER2.

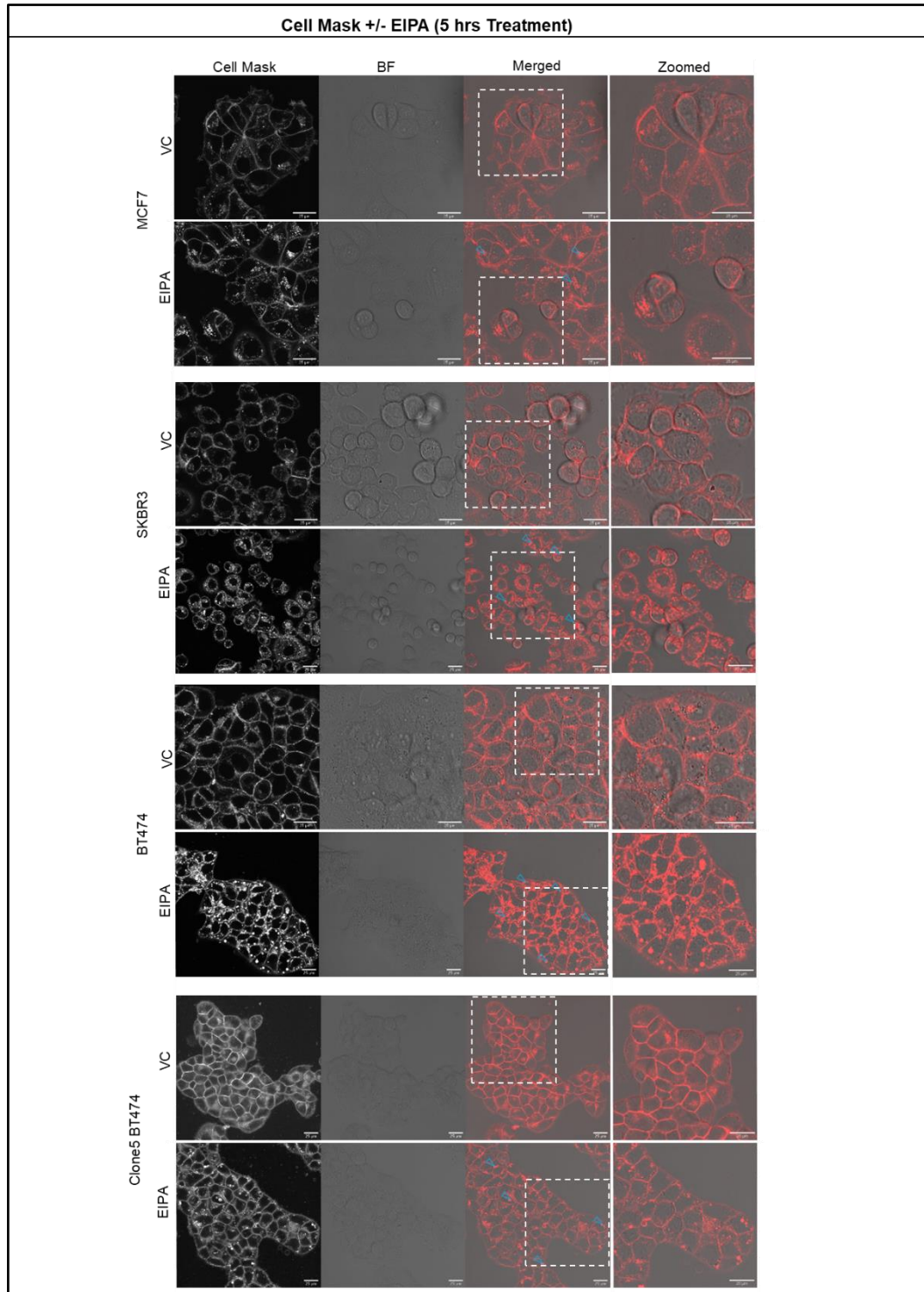


Figure 4.9: Incubation of BC cells with EIPA and CellMask Deep Red. CellMask (1 in 1000) and EIPA (50 μ M) or MeOH were co-incubated for 5 hrs with BC cell lines: MCF7, SKBR3, BT474, and Clone5 BT474 before confocal microscopy. Blue arrowheads indicate vacuole like structure. Scale bars 25 μ m, D-Zoomed; Digital zoomed, BF; Bright Field.

4.2.6 Tz +/- Amiloride or cariporide co-incubated in BC cell lines

Method C was then utilized for analysis of Tz uptake in presence of either cariporide or amiloride. In contrast to the effects seen with EIPA, data shown in figures 4.11 and 4.12 that adding amiloride or cariporide to BC cells co-incubated with Tz488 for 2 or 5 hrs has no visual effect. This finding was also consistent with Chapter 3 figures 3.2, 3.6, 3.8, and 3.10 show that they had no influence on DEX uptake compared to EIPA that, significantly increased endocytosis of this fluid phase probe.

Despite the fact that in this thesis, some positive effect of amiloride and cariporide was not investigated, it is clear that the effects of the EIPA go beyond simply inhibiting NHE and that other targets are likely to be involved in causing the observed effects. It may be that EIPA is more effective than the other compounds at inhibiting other NHE isomers or that it has an additional target or targets. Another possible reason is that, unlike other NHE1 inhibitors, EIPA has a distinct effect on cancer cells. This concept was proposed by Rolver et al. (2020), who concluded that pyrazinoylguanidine-type NHE1 inhibitors (Figure 4.10), like EIPA, effectively suppress the formation of cancer cell spheroids via several mechanisms, and they are able to do so regardless of NHE1 expression. They also show that the potency of EIPA is superior to amiloride, with no observable effects seen with the benzoylguanidine (cariporide).

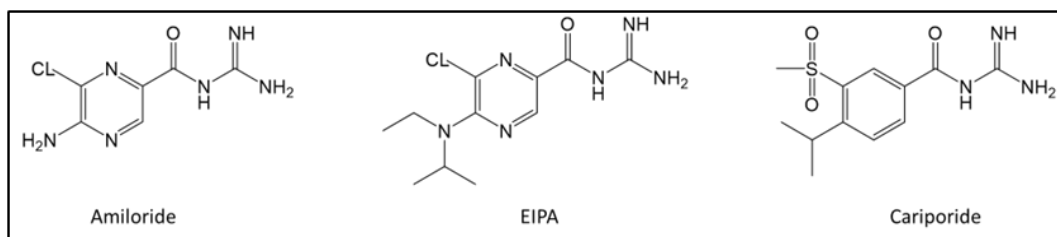


Figure 4.10: Structures of pyrazinoylguanidine (Amiloride and EIPA) and benzoylguanidine (cariporide). The structure differences between two major classes of NHE1 inhibitors, the pyrazine compounds of amiloride and EIPA 5-(N-ethyl-N-isopropyl-amiloride) and the benzoylguanidine (cariporide). Adapted from (Mondal and Ilies 2020).

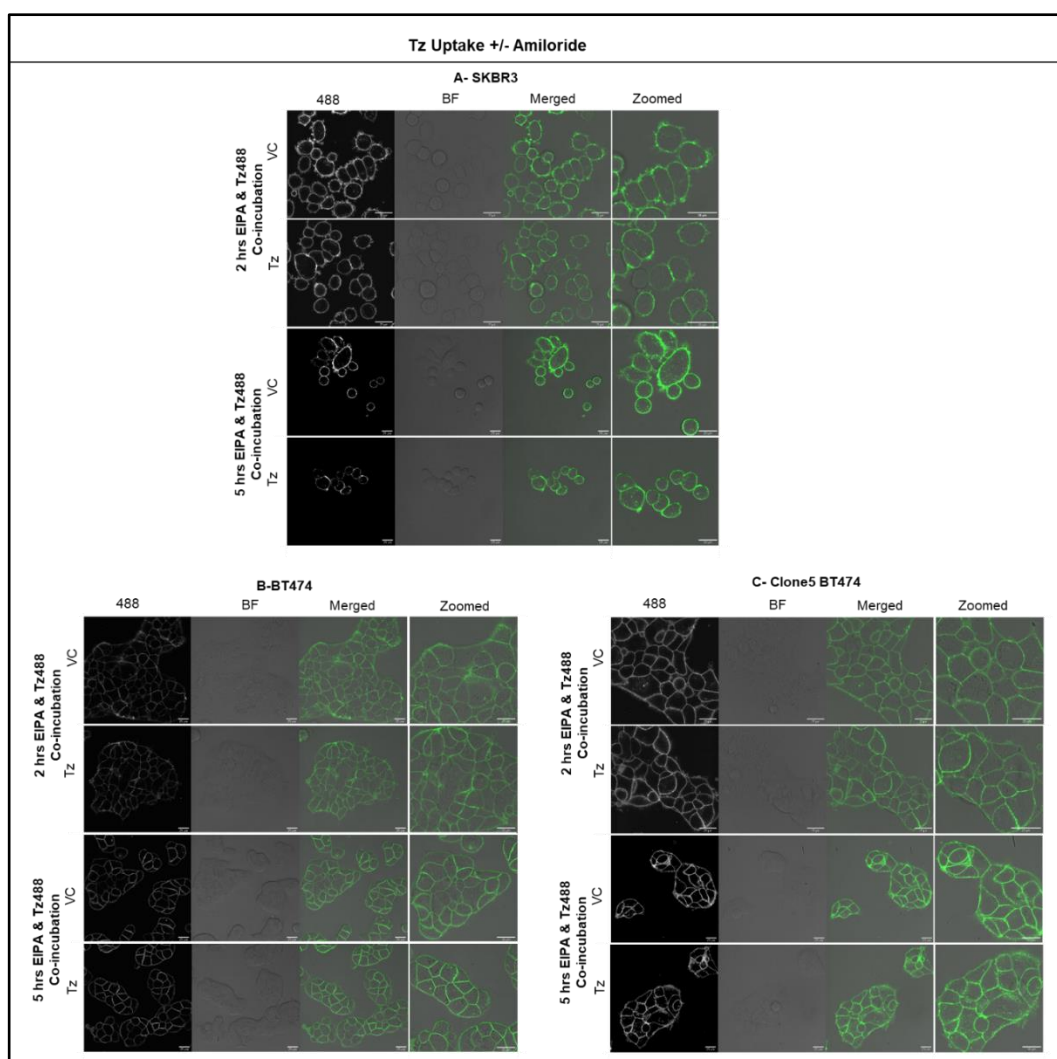


Figure 4.11: Effects of amiloride on Tz binding and internalisation in BC cells. Tz488 (50nM) and amiloride (50 μ M) or DMSO were co-incubated with BC cell lines: MCF7, SKBR3, BT474, and Clone5 BT474, for 2hrs and 5 hrs before analysis by live cell confocal microscopy. Scale bars 25 μ m, BF; Bright Field.

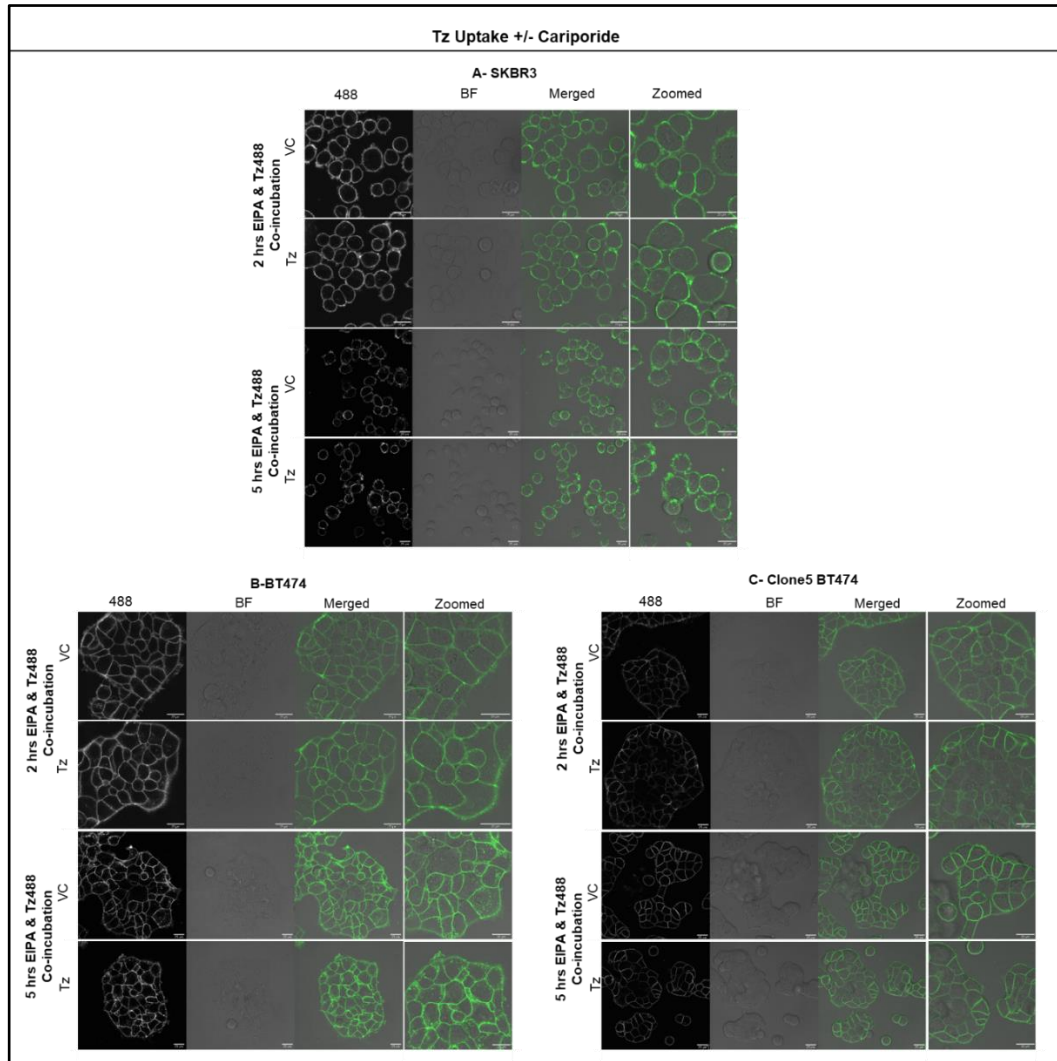


Figure 4.12: Effects of cariporide on Tz binding and internalisation in BC cells. Tz488 (50nM) and cariporide (50 μ M) or DMSO were co-incubated with BC cell lines: MCF7, SKBR3, BT474, and Clone5 BT474, for 2hrs and 5 hrs before analysis by live cell confocal microscopy. Scale bars 25 μ m, BF; Bright Field.

4.2.7 Metabolic Activity Assay (EIPA and Tz)

EIPA clearly had effects, and the next set of experiments focused on assessing the cytotoxicity of different concentrations of EIPA and Tz over a 7 hrs time period in the presence or absence of increasing concentrations of the antibody and EIPA. Figure 4.13 demonstrates some commonality with respect to the effects of the drug and/or the antibody on the four types of BC cells, but also some cell type specific effects were noted. Generally, EIPA showed toxicity in all cell lines at 150 μ M, with MCF7 and BT474 cells showing the highest toxicity (approximately 40%) at this concentration. Then there was dose-dependent toxicity and complete loss of viability in all cell lines at 500 μ M. Tz alone at 50nM showed no evidence of toxicity and generally had very little effect on the sensitivity of the cells to EIPA. The IC₅₀ values for this figure and subsequent experiment are shown in table 4.1.

Separate experiments for 24 hrs whereby the antibody concentration was maintained at 50nM with increasing concentrations of EIPA revealed no synergy between these two agents in influencing metabolic activity (Figure 4.14 and Table 4.1). However, the IC₅₀ data was very different between the two experiments showing that EIPA toxicity is highly dependent on time. Overall these studies clearly demonstrated EIPA toxicity, but there was little evidence that this was happening at 50 μ M (< 7hrs), i.e. the concentration and maximal experimental time point used for the presented analysis of EIPA effects on cell binding and uptake of Tz488 and the endocytic probes. Tormo et al. (2017) showed that BT474 cells treated with Tz at a concentration of 15 μ g/mL for 7 days, which is nearly double our concentration (7.4 μ g/mL) and much longer exposure, showing a 40% loss of viability. Tz therapy had no effect on other HER2 negative cell like

MDA-MB-231 or BT474- Tz resistant cells. It should be noted that one of the cells studied in this paper was the same as our Clone5 BT474.

A separate study by Vanderhoeven et al. (2018) agrees with findings in figure 4.14, demonstrating that Tz concentrations of 1 and 10 $\mu\text{g/mL}$ had a negligible effect on the viability of SKBR3 cells after 24 and 48 hrs. However, they revealed that Tz started to significantly affect the viability of SKBR3 and BT474 cells after 72 hrs of Tz treatment. The last study demonstrates the time-dependent susceptibility of Tz (2.4 and 4.8 $\mu\text{g/well}$) treatments to BT474 metabolic activity as a control in 72, 96 and 120 hrs (Bapat et al. 2021). Around 40% of cells were died after 120 hrs Tz treatment. Based on the literature and data presented in this thesis, it would be interesting to do further Tz analysis in these cell lines for 72 hrs with an EIPA concentration of 10 μM that initially gives evidence of toxicity in figure 4.14. This could reveal the difference between HER2 expressing and no expressing cells.

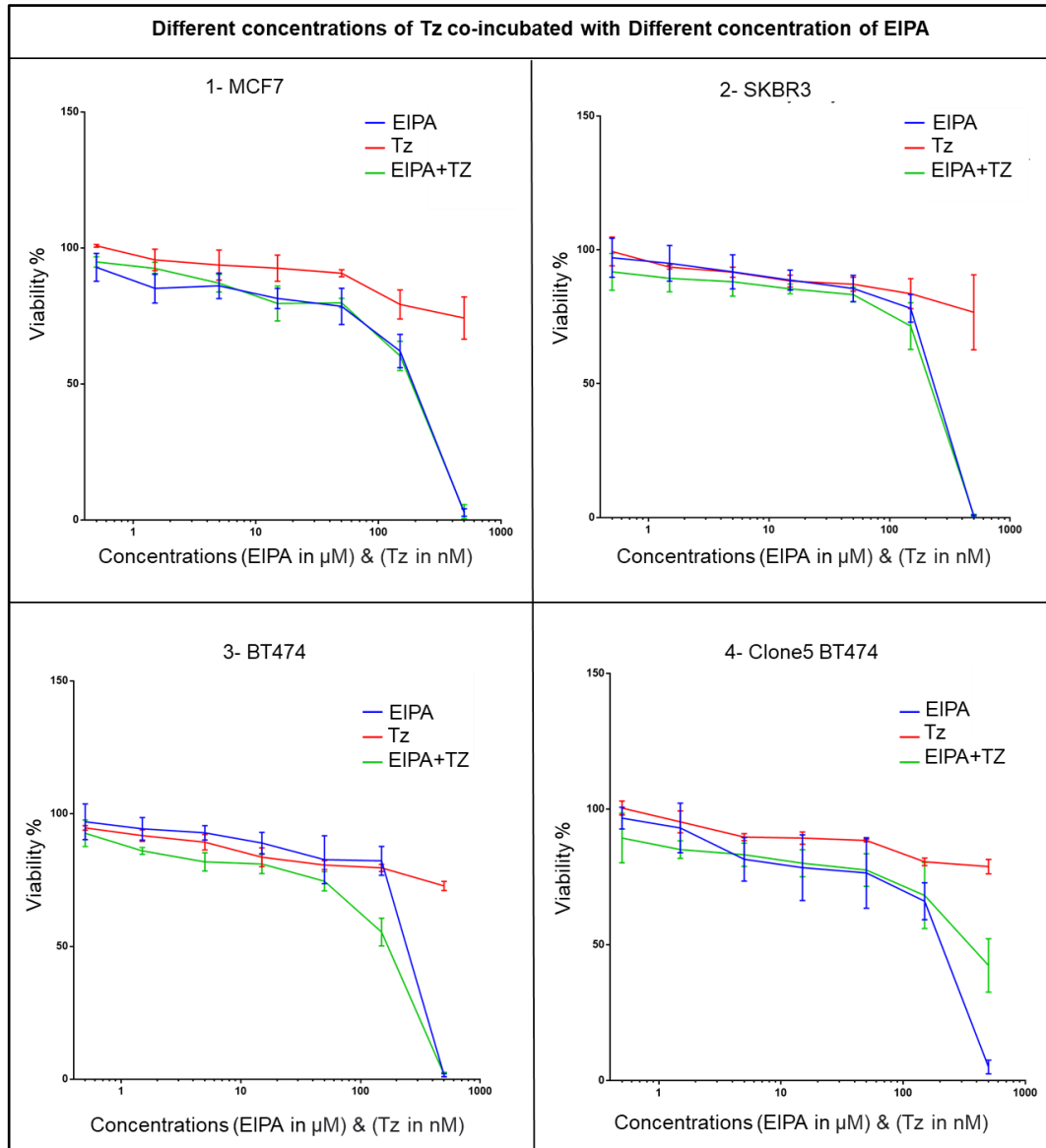


Figure 4.13: EIPA enhances BC cells toxicity with different concentrations of Tz. Cells were seeded for 48 hrs prior to co-incubation with EIPA/Tz for 7 hrs before performing viability assays. Data represent the means and standard error of the means from three independent experiments performed in triplicate.

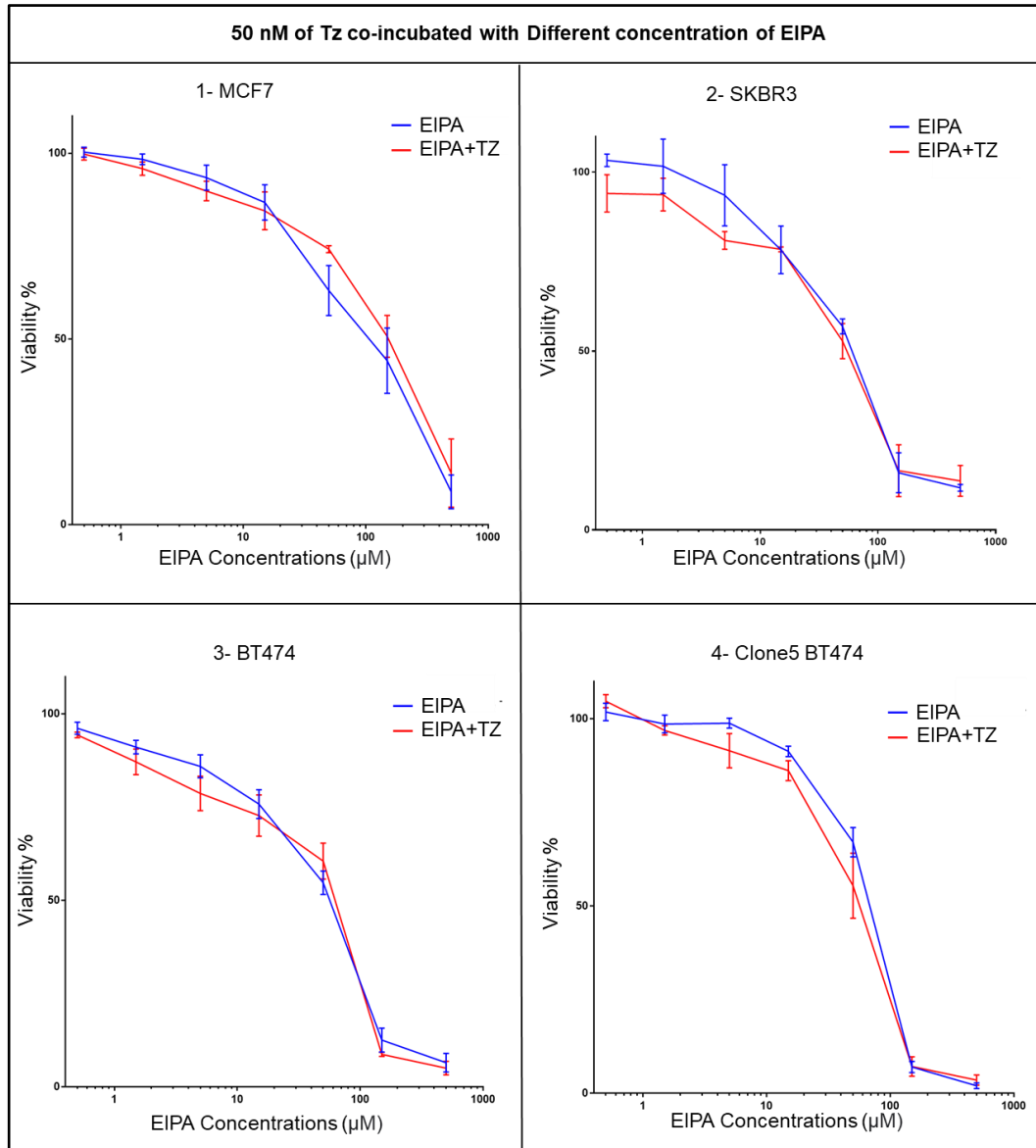


Figure 4.14: BC Metabolic Activity in the presence of different concentrations of EIPA and 50nM Tz. Cells were seeded for 48 hrs prior to co-incubation with EIPA/Tz for 24hrs, before performing viability assays. Data represent the means and standard error of the means from three independent experiments performed in triplicate.

Table 4.1: IC₅₀ calculations after cells were treated with EIPA for 7 or 24 hrs.

IC₅₀ of figure 4.13 – 7 hrs treatment		
Cell Lines	EIPA (μM)	
MCF7	181.8	
SKBR3	199.8	
BT474	205.4	
Clone5 BT474	162.9	
IC₅₀ of figure 4.14 – 24 hrs treatment		
	EIPA (μM)	EIPA(μM) +Tz (50nM)
MCF7	74.29	91.33
SKBR3	37.11	40.07
BT474	43.26	45.92
Clone5 BT474	61.17	43.29

4.3 Summary

HER2 is well characterised as being an endocytosis resistant member of this family of receptor tyrosine kinase and that this is likely to reduce the effect of Tz on breast and other cancer cells that overexpress this receptor. It is also likely to be a major determinant of Tz resistance, that is still a major clinical problem (Wu et al. 2021; Wu et al. 2022). In this chapter experiments were performed to investigate Tz internalisation in four BC cells as well as investigate the effect of macropinocytosis inhibitors on endocytic probes along with Tz binding and internalisation via HER2. After successfully conjugating Tz to Alexa 488 and Alexa 647 it was possible to study Tz488 effects on BC cell lines at much earlier time points that are usually studied and found that Tz caused ruffling specifically in HER2+ BT474 and SKBR3 cells and began showed evidence of internalisation after 5 hrs. Previous experiments in our laboratory revealed that the Clone 5 BT474 cell line was resistant to HER2 crosslinking and subsequent endocytosis and degradation in lysosomes (Wymant et al. 2020). The data from my thesis highlight another difference with respect to how this cell line interacts with Tz at the plasma membrane, but the specific reason for these differences remains to be determined as well as specific endocytic features shown in Chapter 4.

The Tz488 was treated in the presence of EIPA, and the Methods were optimized. The combination of Tz and EIPA in co-incubation with BC cells produced the most significant results compared to other methods that attempted to activate NHE protein before or after Tz treatment. After that, amiloride and cariporide were utilised to study the process of macropinocytosis with Tz co-incubation. In contrast to amiloride and cariporide, which essentially did not affect

Tz, the effect that EIPA has on HER2-Tz is significantly different. This investigation again validated the findings from Chapter 3 results, which showed that EIPA enhanced the internalisation process rather than inhibiting it. Amiloride and EIPA were the first to be suggested to investigate the HER2 internalisation that we believe follows macropinocytosis, as mentioned in our previous results by both (Moody et al. 2015; Wymant et al. 2020). This is doubted in another study that mentioned HER2 internalisation observed receptor-mediated endocytosis (Barok et al. 2014).

We have come to the conclusion that the internalisation of Tz was increased by EIPA. Another experiment was conducted using EIPA alone in BC cells, and the results demonstrated that EIPA causes a rise in BC cell blebs, which is an indication of cell apoptosis.

Lastly, a metabolic activity experiment was carried out to verify EIPA and Tz toxicity in treating BC cells. The EIPA and Tz metabolic activity experiment was initially utilised in an effort to simulate confocal microscopy, and the cells were treated for 7 hrs. It should also be noted that different concentrations of EIPA and Tz were utilised in this investigation. Through this technique, it became abundantly evident that EIPA had a significant impact on BC cells, in contrast to Tz, which only had a marginal effect on these cells. The toxicity of EIPA was further validated by the second protocol, which utilised a range of doses in conjunction with 50 nM of Tz. The experiments also showed that EIPA was extremely toxic to BC cells at high doses. Approximately one-quarter of the cells were impacted by EIPA when it was used at the concentration we were dealing with.

In the future, these findings may assist in understanding EIPA as a macropinocytosis inhibitor, particularly in cancer and HER2 BC cells. The mechanisms of action and impact of EIPA on cancer cells also need to be investigated, as well as the relationship between EIPA and NHE inhibitor mechanisms.

Chapter 5: Synthesis and in vitro analysis of Trastuzumab conjugated PLGA nanoparticles for targeting HER2

5.1 Introduction

In the past two decades, an increasing number of nanomedicines have been described for a number of different therapeutic interventions, but very few reached the clinic (Shete et al. 2022). Notable successes include nanomedicines containing doxorubicin (Doxil), cytarabine (DepoCyt), and irinotecan (Onivyde) (Abdellatif and Alsowinea 2021), but to date, no nanoparticle (NP) formulation containing ligands for specifically targeting plasma membrane receptors have been approved in the UK. NPs as nanomedicines have several potential advantages over conventional approaches that in cancer mostly involve administering small molecule drugs, including the protection of the drug from being modified or destroyed before it reaches its target site. The NP can be surface modified to provide targeting so reducing side effects and also its assistance to delivering a therapeutic to the inside of cells can overcome drug efflux proteins that can cause drug resistance. For example, it was demonstrated that polymer drug conjugates were effectively retained in multidrug-resistant (MDR) cells and that the intracellular concentrations of medications released from the polymers are much greater after the same incubation period than when the free drug is provided (Twaites et al. 2005). Typically, less than 0.01% of the injected dosage of antibodies accumulates at the target site, whereas the same value for NPs accumulates from 1 to 5% (Wilhelm et al. 2016). However, toxicities such as molecular, cellular, and tissue toxicities and immunological responses are found in certain NPs (Wolfram et al. 2015). NPs have also been utilised to deliver macromolecular therapeutics such as siRNA and mRNA, critically acting as vectors for entities that cannot cross biological membranes alone (Mokhtarzadeh et al. 2017).

Commonly, polymer nanomedicines are divided into: (a) polymer-drug conjugates for enhanced drug half-life and bioavailability or (b) degradable polymer structures for controlled release applications (Bobo et al. 2016).

5.1.1 Nanoparticles and Cancer

To maintain sufficient nutrition and oxygen for fast tumour development (angiogenesis), tumour blood vessels show a higher degree of abnormality and tortuosity than normal physiological vessels. The pore size of several tumour models has been reported to range between 380 and 780 nm (Sultan et al. 2022), which opens out the possibility of giving NP access to the tumour via the EPR effect (Shi et al. 2020), described in detail in Chapter 1. However, it has been determined that NPs have a very limited circulation period (the average half-life of typical NPs after intravenous delivery is 3–5 mins) (Brigger et al. 2012). Particles can be removed by hepatic macrophages (Kupffer cells) from the blood circulation and these cells represent the majority of tissue macrophages that are in direct contact with blood. Kupffer cells have plasma membrane receptors (including Fc, complement, scavenger, and carbohydrate receptors) that contribute to the detection and removal of particles from blood circulation (Haroon et al. 2022).

Hydrophilicity is one of the most important factors that contribute to NPs' long-term circulation. Polyethylene glycol (PEG) is a polymeric material with high hydrophilicity, and PEG coating is an important factor in prolonging the circulation duration of NPs in the body, often known as the "stealth effect" (Shi et al. 2021).

The physicochemical characteristics of NPs, such as their size, shape, and surface charge, would also have an impact on the in vivo circulation time. The

shape of non-spherical NPs compared to spherical and negatively charged or uncharged NPs have a longer circulation time in vivo (Zhao and Stenzel 2018). NPs with a size between 5 and 100 nm generally have longer circulation time (Di et al. 2021). The optimum size for long-term blood circulation is approximately 100 nm, allowing for prolonged circulation lifetimes and effective accumulation in tumour tissue through the EPR effect (Wu et al. 2018).

5.1.2 Polymeric nanoparticles

This thesis is focused on polymeric NP, which is one type of many forms of NPs. Briefly, polymeric platforms can self-assemble into NPs essentially by emulsification followed by removal of the internal phase, and the resultant NPs exist as nanocapsules or nanospheres that can encapsulate a broad range of anti-cancer medications (Bhasarkar and Bal 2021; Jiang et al. 2022). Polymeric NPs have been extensively studied for primary and metastatic BC treatments, and have a variety of other biomedical uses because to their physical flexibility, chemical characteristics, surface properties, hydrogelability, biocompatibility, biodegradability, porosity, mechanical strength, and hydrophobicity or amphiphilicity (Salari et al. 2022). Polymer NPs can provide advantages for triggered release of therapeutics, provide further control for targeting, and reduce systemic toxicity. For example, NPs can be engineered to prevent drug release unless exposed to a specific biological trigger such as pH (Mitragotri et al. 2014). Polymeric NPs can also encapsulate of different types of hydrophobic and hydrophilic drugs for treating BC (Sánchez et al. 2020).

Polymeric NPs have better shelf life (shelf life expresses the time length for which the polymeric NP remain usable, fit for consumption, or saleable) compared to many other types of NPs. The surface of Polymeric NPs can be easily

engineered/modified for targeting efficiency; they can also as an efficient sustained or controlled drug delivery system, releasing the drug slowly in a controlled fashion over a long period (Dristant et al. 2023).

This is accomplished by utilising functionality that degrades slowly, resulting in kinetically driven drug release. An example is the incorporation of leuprolide (a medication that inhibits testosterone) into polylactide-co-glycolic acid (PLGA). This medication, marketed under the brand name Eligard®, has shown to be an effective therapy for the symptoms of prostate cancer (Bobo et al. 2016).

5.1.3 Poly (lactic-co-glycolic acid) – (PLGA)

The U.S. Food and Drug Administration and the European Medicines Agency have authorised PLGA for use in drug delivery applications due to its safety profile, biocompatibility, low levels of immunogenicity and toxicity, and biodegradation during in vivo investigations. The polymer is widely employed in biosensors, drug delivery, tissue engineering, and biomimetic material design (Zielińska. et al. 2020).

PLGA is a widely investigated copolymer used in many FDA approved therapeutic devices (Iv et al. 2020). PLGA polymers are formed by ring-opening polymerization of lactide and glycolide monomers; commonly, stannous octoate is used as a catalyst to activate hydroxyl moieties to initiate ring-opening polymerization. The hydroxyl moiety is attached to the growing PLGA chain by an ester bond (Hadar et al. 2019). The ratio between poly(lactic acid) (PLA) and poly(glycolic acid) (PGA) has a significant impact on degradation and drug release rate (Pandey and Jain 2015). Hydrophobic drugs, that involve several

chemotherapeutic agents, can be easily encapsulated in PLGA (Mitragotri et al. 2014).

Spherical-shaped PLGA NPs are the most extensively used formulations (Rezvantlab et al. 2018). PEGylation of PLGA enhances the hydrophilicity of the formulation, resulting in increased blood circulation time and better pharmacokinetics by inhibiting opsonization and uptake by the mononuclear phagocyte system (MPS) (Turecek et al. 2016). However, NPs (Non-spherical) particles of various shapes, such as plug, rod, curved, vase, and conical, can be made using different methodologies. Essentially the methods were divided into two categories: (1) *ab initio* synthesis of non-spherical particles and (2) manipulation of spherical particles into non-spherical geometries. For example, elliptical PLGA disk were produced using the film-stretching method as an example of manipulation techniques (Champion et al. 2007).

This approach was utilised to synthesize PLGA NPs with various surface modifications such as PEGylation and targeted PLGA NPs for the delivery of anticancer medicines to the tumour location. Due to its hydrophilic nature, PEGylation of nanocarriers significantly increase blood circulation half-life and decreases removal of NPs by MPS, increases their stability to enzymic degradation and decreases their immunogenicity (Tashima 2018; Shi et al. 2021; Suk et al. 2016). It also enhances hydrophilicity through the use of block or branching copolymers and increases blood circulation as an approach for tumour targeting (Brigger et al. 2012).

5.1.4 PLGA conjugated Tz.

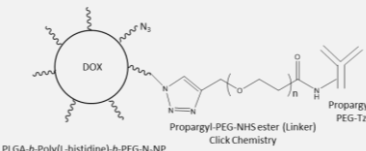
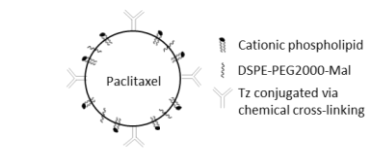
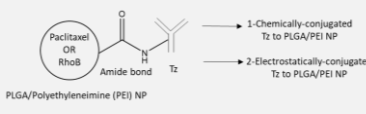
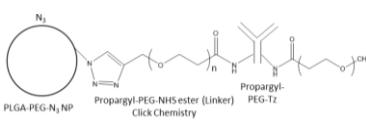
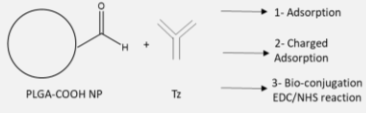
PLGA attached to Tz has previously been investigated using a variety of methods and reactions (Juan et al. 2020). Attempts have been made to modify the antibody attached to PLGA, and rather than using full length Tz, smaller Tz based fragments in the form of affibodies and nanobodies were investigated. Nanobodies are defined as “single-domain variable fragments of camelid-derived heavy-chain antibodies (hcAb)” (Schumacher et al. 2018), whilst affibodies are very small proteins in size (6.5 kDa) purified from bacteria, with similar affinity to the proteins like HER2 and are considered as a good alternative to full-length antibodies (Barozzi et al. 2020). Research on PLGA NPs conjugated to a HER2 affibody encapsulated Rose Bengal (as an anticancer agent) yielded interesting findings with substantial cell toxicity in SKBR3 cells (Shipunova et al. 2021).


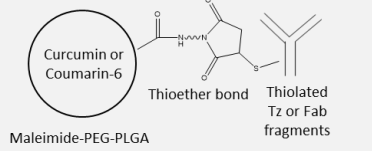
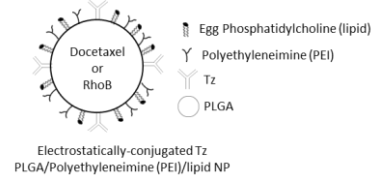
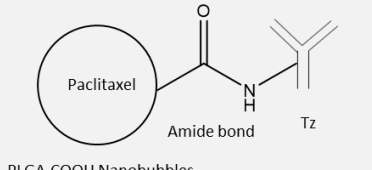
The PLGA conjugated Tz NPs were identified in another study to uptake through pinocytosis in 2h incubation time. These were localised inside SKBR3 endosome and were then transported into the lysosome. If the internalised NPs are unable to escape these acidic compartments, they may be degraded by enzymes or transferred out of the cells via exocytosis (Zhou et al. 2015).

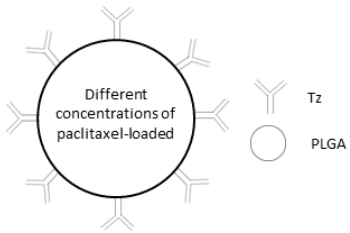
Another study stated that PLGA coated with Tz were primarily internalised by clathrin-mediated and caveolae-dependent endocytosis (Yu et al. 2016).

Table 5.1 summarises identified in vitro studies in different breast cancer models involving PLGA attached to Tz or Tz fragments; some also described in vivo studies.

Table 5.1: The table shows different studies used PLGA conjugated/Encapsulated Tz.

Studies	Cell Lines	Description	NPs Structures
(Zhou et al. 2015)	- In vitro: MCF7 SKBR3	The study attempted to produce two models of PLGA Tz, one of which is pH-sensitive and the other of which is pH-insensitive. The study indicated that Tz conjugated to PLGA had a greater uptake in BC cells when compared to Tz-free NPs. It is also demonstrated that SKBR3 has more PLGA-Tz than MCF7. PLGA-sensitivity Tz's to acidic pH is also proved to have triggered the drug release of DOX, and the size of NPs in acidic pH was detectably bigger than in high pH.	 <p>PLGA-b-Poly(L-histidine)-b-PEG-N₃ NP Propargyl-PEG-NHS ester (Linker) Click Chemistry Propargyl-PEG-Tz</p>
(Yu et al. 2016)	- In vitro: BT474 MCF7	The study included three methods for conjugating Tz to PLGA/Cationic phospholipid/DSPE-PEG2000-Mal NP. The models were then evaluated in several studies, including cellular uptake, cytotoxicity, drug loading, and encapsulation efficiency.	 <p>Paclitaxel Cationic phospholipid DSPE-PEG2000-Mal Tz conjugated via chemical cross-linking PLGA/DODMA phospholipid/DSPE-PEG2000-Mal conjugated Tz NP was prepared in three different strategies</p>
(Yu et al. 2016)	- In vitro: BT474 MCF7	Two different models were developed using PLGA that had either been chemically or electrostatically attached to Tz and then filled with paclitaxel or RhoB. They evaluated two models in vitro and found variations in cellular uptake, drug release, and cytotoxicity between the two models.	 <p>Paclitaxel OR RhoB Amide bond Tz PLGA/Polyethylenimine (PEI) NP 1- Chemically-conjugated Tz to PLGA/PEI NP 2- Electrostatically-conjugated Tz to PLGA/PEI NP</p>
(Badkas et al. 2018)	- In vitro: SKBR3 MCF7 MDA-MB-231	The study employed Tz conjugated with PLGA and PEG NPs. They attempted to determine the relationship between this model and the activation of immune cell uptake.	 <p>PLGA-PEG-N₃ NP Propargyl-PEG-NHS ester (Linker) Click Chemistry Propargyl-PEG-Tz</p>
(Choi et al. 2018)	- In vitro: BT474 SKBR3 MCF7 HaCaT	Tz was conjugated to surface modified PLGA loaded with docetaxel in three distinct ways. Comparing the effect of three models on cell internalisation, physical properties, particle morphology, particle size, surface charge, particle interaction with	 <p>PLGA-COOH NP Tz 1- Adsorption 2- Charged Adsorption 3- Bio-conjugation EDC/NHS reaction</p>

		Tz, and stability were examined.	
(Colzani et al. 2018)	- In vitro: SKBR3	PLGA-encapsulated Tz and PLGA-encapsulated Tz and DOX exhibited a lower uptake of NPs than other studies that conjugated Tz to PLGA. Nonetheless, the study demonstrates the efficacy of PLGA encapsulated Tz on HER2 signalling and its capacity to activate the ADCC pathway.	
(Duan et al. 2018)	- In vitro: BT-474 MDA-MB 231 - In vivo	The research was carried out using two different models: the first model consisted of Tz conjugated to PLGA and filled with curcumin or coumarin-6; the second model consisted of Tz Fab parts that were modified and were also attached to PLGA. The Tz Fab model was shown to have enhanced BT474 toxicity and to have produced superior outcomes in vivo experiments.	
(Zhang et al. 2019)	- In vitro: MCF7 BT474	Preparation of PLGA/ polyethyleneimine (PEI)/phosphatidylcholine NPs was achieved by the emulsion solvent evaporation/diffusion method. Encapsulated docetaxel and electrostatically attached to Tz were added to this model and evaluated in vitro. This model efficiently transported docetaxel to HER2+ BC cells, which had a cell-targeting impact and successfully inhibited cancer cell growth. They also showed an interesting uptake of this model in BT474 cells.	
(Zhong et al. 2020)	- In vitro: MCF7 - In vivo	Paclitaxel-loaded PLGA-COOH nanobubbles covalently conjugated with Tz were synthesised. This model was then evaluated in vitro, utilised as a control, and compared to the same NPs treated with ultrasound to observe the release of paclitaxel, cell uptake, and apoptosis. The approach was further evaluated in vivo (mice), and paclitaxel targeting and accumulation in breast tumours were analysed.	

(Sakhi et al. 2022)	- In vitro: MCF7 - In vivo	Paclitaxel-loaded PLGA coated with Tz were produced, Sodium Lauryl Sulfate (SLS), Poloxamer 407 and paclitaxel's different concentrations and formulations were studied. The pharmacokinetic characteristics of paclitaxel-loaded PLGA-Tz NPs indicate an increase in half-life $t_{1/2}$ and volume of distribution V_d , whereas (Clearance) CI was lowered. The findings of cytotoxicity tests indicate that cell viability decreases significantly as medication concentration and incubation period rise.	
---------------------	-------------------------------	--	---

PLGA NPs containing different targeting moieties, such as folic acid or hyaluronic acid or Tf, have also been investigated as potential BC therapies (El-Hammadi et al. 2017; Jose et al. 2019; Paswan et al. 2021). One study found that all three ligands showed a higher percentage of curcumin internalisation in MDA-MB-231 cells compared with PLGA-curcumin, leading to enhanced cancer cell killing with targeted NPs, as demonstrated by confocal microscopy and flow cytometry (Prabhuraj et al. 2020). Folic acid or hyaluronic acid-PLGA internalised curcumin more efficiently compared with Tf. It would be interesting to study if this was due to the possibility that the NP-Tf bound to the TfR is being rapidly recycled, not giving the curcumin an opportunity to reach its cellular target.

A major objective of this thesis was to test the hypothesis coming from our previous observations (Moody et al. 2015; Wymant et al. 2020) that states, NP-Tz can be engineered to induce HER2 clustering at the plasma membrane, drive its internalisation and degradation in lysosomes and at the same time release a small molecule drug.

5.2 Results and Discussion

5.2.1 Nanoparticles Preparations

The PLGA-conjugated Tz methodology was optimized based on information from these studies: (Yu et al. 2016; Prabhuraj et al. 2020; Rezvantlab et al. 2018). The procedure utilized the PLGA 50:50 that has been described in many papers for PLGA NPs formation (Zhou et al. 2015; Yu et al. 2016; Duan et al. 2018; Choi et al. 2018; Colzani et al. 2018) and uses EDC and NHS to conjugate Tz to the polymer; again a commonly used procedure (Thierry et al. 2010; Yu et al. 2016; Prabhuraj et al. 2020; Zhong et al. 2020).

To optimize the process, the amounts of PLGA, Tz, NHS, and EDC were investigated together with the lyophilization procedure and the amounts of the organic and aqueous phase.

PLGA-COOH concentrations of 10%, 50%, and 100% of total PLGA concentration were tested and the cellular uptake results with 50% PLGA-COOH combined with 50% PLGA were evaluated. Initially, 100 mg of PLGA/PLGA-COOH were investigated (Zhong et al. 2020), then 72 mg (Yu et al. 2016) and 24 mg.

First, dichloromethane (DCM) was employed as an organic solvent (Zhou et al. 2015; Badkas et al. 2018; Choi et al. 2018), and then it was substituted with acetone (Fathian et al. 2019), which enhanced PLGA solubility. The organic phase was added to the aqueous phase at a flow rate of 1 mL/min (Prabhuraj et al. 2020). NPs were also dried by lyophilization, and then this step was avoided to prevent NP aggregation. The COOH group in NPs was activated with 5mg NHS and 5mg EDC (Prabhuraj et al. 2020), and the concentration was raised to

100 mM EDC and 50 mM NHS (Thierry et al. 2010). NHS and EDC reacted with NPs and Tz in a N₂ environment at ambient temperature (Fathian et al. 2019). Tz was initially conjugated with PLGA at a concentration of 1 mg/mL (Prabhuraj et al. 2020). It was then decided to change this to 100 µg/mL (Badkas et al. 2018; Meng et al. 2018), and uptake was observed; finally, Tz was conjugated with a concentration of 500 µg/mL (Sakhi et al. 2022). The reason for the change in concentration of Tz in NPs was an attempt to observe a correlation between the number of Tz molecules loaded in NPs and the extent of cellular uptake.

From the above descriptions of the modifications performed for this procedure, Table 5-2 provides a summary of the physicochemical characterisation of the NP produced. Based on the size calculation, the acetone appeared to be a better solvent for PLGA NPs giving smaller particle sizes. However, they were significantly larger than desired sizes of less than 250 nm. Prabhuraj et al. (2020) demonstrated that much smaller PLGA-NPs with a size 85 nm showed enhanced cell uptake. Table 5.2 shows that reducing the PLGA mass from 100 (1.25%) to 24mgs (0.35%) mgs in 8 ml of Acetone affected the size of NPs with higher concentration giving much larger NPs. Astete and Sabliov (2006) showed that as the PLGA concentration increased from 1% to 4% (w/v), the average NP size also increased from 205 to 290 nm. However, a study by Fathian et al. (2019) found that increasing the PLGA mass from 50 (1%) to 60 (1.2%) mg, reduced the NPs sizes from 178 nm to 72 nm.

Tz conjugated PLGA, and cellular uptake were enhanced by increased NHS and EDC concentrations. Skipping the lyophilization step was found to prevent aggregation and decrease the size of NPs. According to Degobert and Aydin

(2021), lyophilization may cause a variety of stresses on the NPs, which might lead to their destabilisation.

Our zeta potential (mV) of NPs showed a negative charge after Tz conjugation from values of -22.3, -26.1 and -26.2 mV. This observation was also observed in a separate study (Yu et al. 2016), showing Zeta potential of their Tz-conjugated NPs were between 0.01 and -1.11 mV following Tz conjugation changing from 10.40 to 44.60 mV, in the absence of the antibody. This suggests that there would be minimal interaction between the NPs and the negative surface of the cells thus allowing for higher level of specificity for binding via Tz-HER2. However, another study observed a swing towards a positive charge after conjugation (Zhong et al. 2020). The NPs surface charge can affect the cellular uptake of NPs (Honary and Zahir 2013). The electrostatic interactions between charged nanocarriers and the cytomembrane can trigger internalisation leading to higher cellular uptake efficiency (Zhang et al. 2022). It has been found that, compared to negatively charged NPs, positively charged variants have higher cellular uptake, particularly cancer cell surfaces, are often more negatively charged than normal cells (Chen et al. 2011; Shah et al. 2021; Chen et al. 2016) Additionally, In dispersed systems, the surface charge of NPs influences the stability of particle-particle and particle-medium interactions, and the stability of the NPs, which prevents NPs from aggregating (Midekessa et al. 2020).

The Electrical Double Layer (EDL) known as the “development of a nett charge at the particle surface affects the distribution of ions in the surrounding interfacial region, resulting in an increased concentration of counter ions, ions of opposite charge to that of the particle, close to the surface” (Malvern Instruments Ltd). A charged NP surface can attract a layer of ions due to chemical and

electrochemical reactions; this layer is known as a tightly bound inner layer. This inner layer, which is either positively or negatively charged can move with the NPs, and attract another layer of ions with opposite charge - known as the stern layer (Welker 2011). The outer layer is a diffuse layer that is weakly attached to inner layer representing a notional boundary. When a particle moves (e.g., due to Brownian motion), ions within the boundary move with it, but any ions beyond the boundary do not travel with the particle. This boundary is called the surface hydrodynamic shear or slipping plane. The potential at this boundary (surface of hydrodynamic shear) is the zeta potential (Fatehah et al. 2015).

Our non-encapsulated PLGA NPs similarly exhibited a low negative charge of -7.22 mV, and this negative charge decreased to -0.05 mV after being encapsulated in PLGA along with RhoB. However, because of the DOX encapsulation, PLGA NPs displayed a zeta potential of 0.55 mV and high zeta deviation of 0.55 ± 146 mV. This finding corresponded with (Choi et al. 2020), where their PLGA-DOX conjugates showed a positive charge, and they stated that this is because the cationic drug (DOX) interacted with the anionic surface of the PLGA NPs, in addition to encapsulating itself within the hydrophobic interior space of the PLGA NPs.

Table 5.2: Nanoparticle Preparations and formulations. The results presented in this chapter relate to formulations 9, 16, 17, 18, 19, 21 and 22 that are in red bordered in the table.

Formulation Number	1	2	3
PLGA (mg)	90	64.8	18
PLGA (COOH) (mg)	10	7.2	18
Organic Phase (Solvent)	DCM	DCM	DCM
PVA (%) - Aqueous phase (mL)	1% - 7mL	1% - 7mL	1% - 7mL
PLGA Encapsulated	0.5 mg RhoB	0.5 mg RhoB	0.5 mg RhoB
Tz conjugation	No	No	No
Tz concentration	-	-	-
NHS – EDC concentration	-	-	-
Lyophilization	Yes	Yes	Yes
Cell Uptake	No	No	No
Size (nm) (\pm SD)	1729 \pm 1152	1641 \pm 733	956 \pm 346
PDI	0.4	0.1	0.2
Zeta Potential (mV)	ND	ND	ND

4	5	6	7	8
12	12	12	12	0
12	12	12	12	24
DCM	DCM	DCM	Acetone	Acetone
1% - 7mL	1% - 7mL	1% - 7 mL	2% - 14 mL	2% - 14 mL
1 mg RhoB	1 mg RhoB	1 mg RhoB	1 mg RhoB	1 mg RhoB
No	Yes	Yes	-	Yes
-	1 g/mL	100 µg/mL	-	1 g/mL
-	5 – 5 (mg/mL)	5 – 5 (mg/mL)	-	5 – 5 (mg/mL)
Yes	Yes	Yes	-	No
No	No	No	No	No
1036 ± 515	1310 ± 1264	1006 ± 321	703 ± 458	1136 ± 466
0.2	0.9	0.1	0.4	0.1
ND	ND	ND	ND	ND

9	10	11	12	13
12	12	12	12	12
12	12	12	12	12
Acetone	Acetone	Acetone	Acetone	Acetone
2% - 14 mL	2% - 14 mL	2% - 14 mL	2% - 14 mL	2% - 14 mL
1 mg RhoB	1 mg RhoB	1 mg RhoB	-	1 mg RhoB
Yes	Yes	Yes	-	-
500 µg/mL	500 µg/mL	500 µg/mL	-	-
5 – 5 (mg/mL)	50 mM - 100 mM	50 mM - 100 mM	-	-
No	No	No	No	Yes
Yes	Yes	Yes	-	-
776 ± 554	896 ± 752	623 ± 305	415 ± 208	441 ± 273
0.5	0.7	0.2	0.2	0.3
ND	ND	ND	ND	ND

14	15	16	17	18
12	12	12	12	12
12	12	12	12	12
Acetone	Acetone	Acetone	Acetone	Acetone
2% - 14 mL	2% - 14 mL	2% - 14 mL	2% - 14 mL	2% - 14 mL
1 mg RhoB	-	1 mg RhoB	-	1 mg RhoB
Yes	No	No	Yes	Yes – non-Fluorescence
500 µg/mL	-	-	500 µg/mL	500 µg/mL
50 mM - 100 mM	-	-	50 mM - 100 mM	50 mM - 100 mM
Yes	No	No	No	No
Yes	No	No	Yes- Intensive	Yes- Intensive
498 ± 306	139 ± 63	148 ± 72	243 ± 55	259 ± 89
0.3	0.2	0.2	0.05	0.1
ND	-7.22	-0.0540	-26.2	-22.3

19	20	21	22
12	12	12	12
12	12	12	12
Acetone	Acetone	Acetone	Acetone
2% - 14 mL	2% - 14 mL	2% - 14 mL	2% - 14 mL
1 mg RhoB	1 mg DOX in Organic Phase	1 mg DOX in Aqueous Phase	1 mg Dox in Organic Phase
Yes	Yes – non-Fluorescence	Yes – non-Fluorescence	No
500 µg/mL	500 µg/mL	500 µg/mL	-
50 mM - 100 mM	50 mM - 100 mM	50 mM - 100 mM	-
No	No	No	No
Yes - Intensive	Yes	Yes	-
333 ± 212	488 ± 310	574 ± 371	341 ± 225
0.4	0.4	0.4	0.4
-26.1	ND	0.55 ± 146	ND

5.2.2 Cellular uptake study

In vitro analysis of nanomedicines of the type described in this chapter is standard practice before they are then analyzed in more complex models such as organoids and spheroids through to in vivo analysis. The endocytosis of NP can be affected by NP size, shape, and surface charge (Salatin and Khosroushahi 2017). At this point in the work, there was a need to test the NPs described in this chapter and formulations 9, 17, 18, 19 were selected (Table 5.2) because cellular uptake was observed that gives full meaning to the abbreviations used to describe the conjugates studies, whether they be polymer alone, polymer with attached Tz or polymer-Tz encapsulating a drug or dye.

5.2.3 PLGA-RhoB-Tz488 binding and internalisation in BC cells

Initial studies were conducted at relatively short times of 1 hr to investigate whether binding and internalisation could be observed by confocal microscopy. Importantly there was a significant difference in the images obtained from the low HER2 MCF7 cell line compared to the other three HER2+ variants (Figure 5.1). Controls included Tz-Alexa 488 alone and PLGA-RhoB-Tz488. There was very little evidence of binding or internalisation in the negative control line but obvious distinct plasma membrane labelling on the other three cell lines. Increasing the magnification highlighted that the labels were in aggregates on the plasma membrane that was HER2 dependant. There is some evidence of localisation in endosomes (especially in BT474 cells), but most of the label was confined to the plasma membrane. This is unsurprising based on the average size of these NP (776nm) that could only have been entered by phagocytosis or macropinocytosis. The size range of this formulation was very large, and uptake may have been mediated by the smaller approximately 250 nm variants. Interestingly the Tz488

alone showed no evidence of internalisation and was almost exclusively localised to the plasma membrane; here, there was no sign of aggregation.

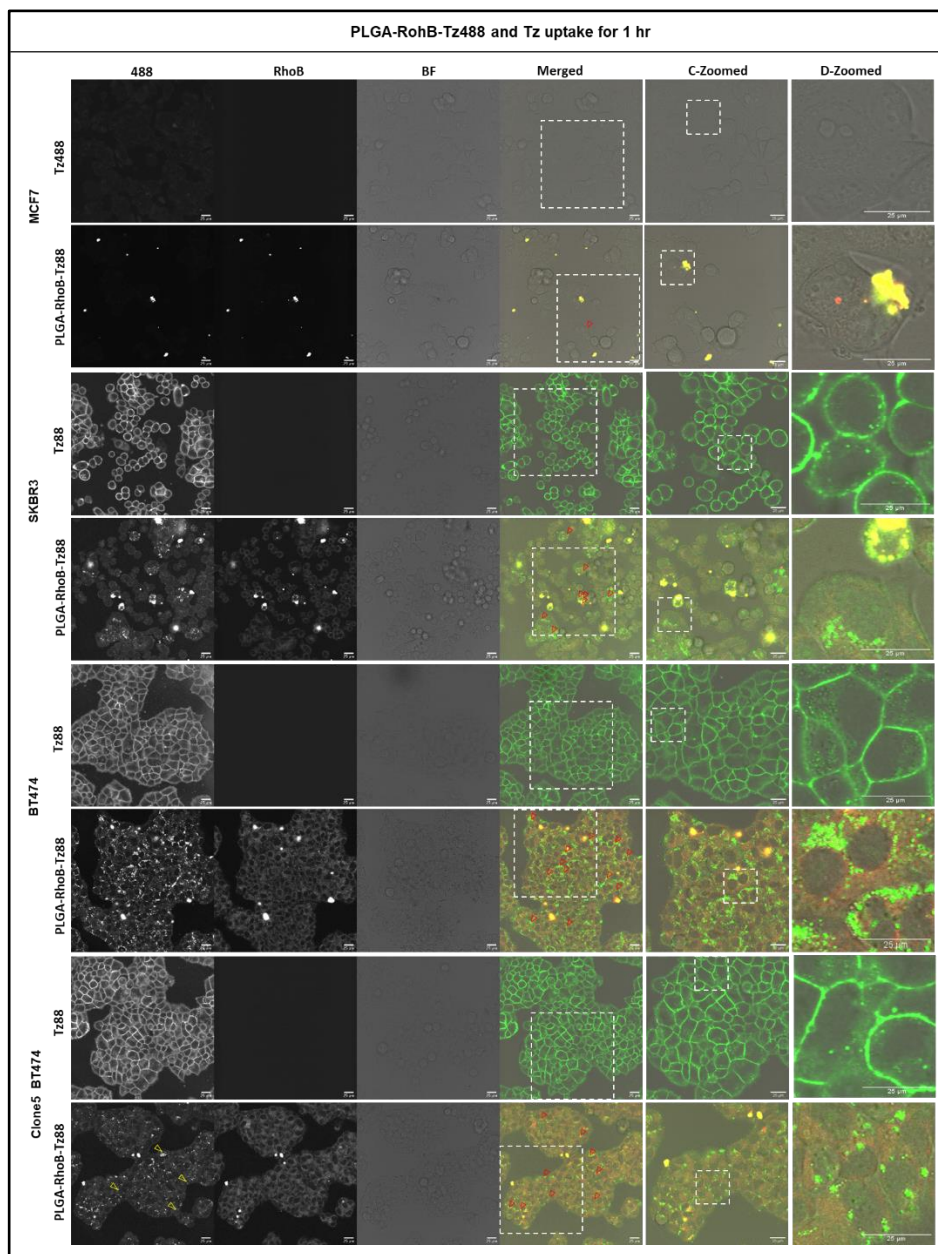


Figure 5.1: Selectivity of the Tz decorated NP for HER2 expressing BC cells . Cells were incubated with 100 $\mu\text{g}/\text{mL}$ of PLGA- RhoB-Tz488 and 50 nM of Tz488 in media for 1 hr and image by confocal microscopy. Green indicates Alexa 488, and red indicates for (RhoB). Red arrowheads indicate for internalised NPs. Scale bars 25 μm . D-zoomed; Digital zoomed. C-zoomed; Confocal zoomed, BF; Bright Field.

To investigate a separate formulation with smaller diameters, formulation 14 (mean diameter 498nm) was incubated with the SKBR3 or Clone5 BT474 cells on ice to inhibit all endocytic pathways. Tf as an Alexa488 conjugate was also studied in this experiment as a ligand that should not enter cells at this temperature (Baravalle et al. 2005). There was no evidence of NPs or Tf uptake in either cell line (Figure 5.2), but very clear evidence of plasma membrane binding with some evidence of aggregation of the NP-RhoB-Tz488.

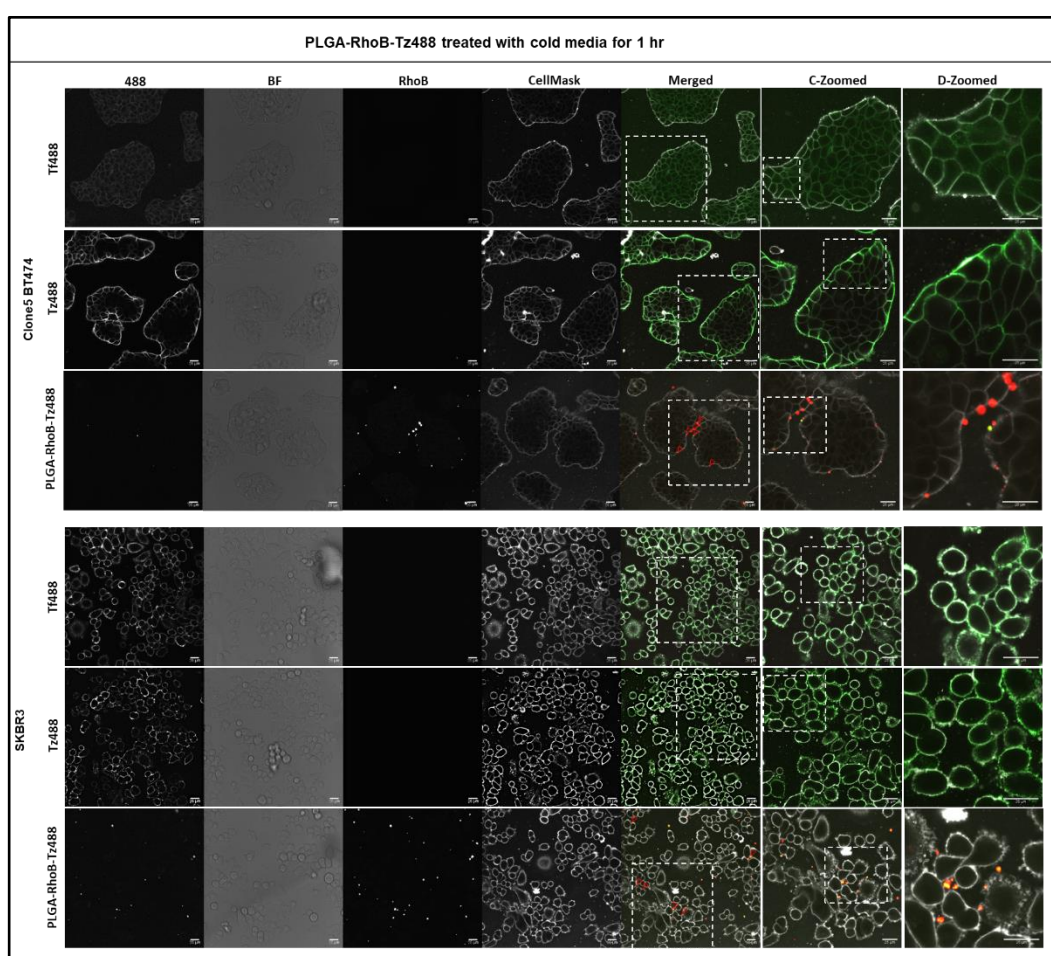


Figure 5.2: Cell binding of PLGA-RhoB-Tz488, Tz488 and Tf488 incubated with BC cells for 1 hr on Ice. Formulation 14 (PLGA-RhoB-Tz488) from table 5.2 with size of 498nm was used. Cells were incubated with 100 $\mu\text{g}/\text{mL}$ of PLGA-RhoB-Tz488 and 50 nM of Tz488, and 50 nM of Tf488 in cold media for 1 hr on ice. Cells were then imaged by live cell confocal microscopy. Green indicates Alexa 488, and red indicates for (RhoB).

Red arrowheads indicate for internalised NPs. Scale bars 25 μ m. D-zoomed; Digital zoomed, C-zoomed; Confocal zoomed, BF; Bright Field.

The next experiment investigated formulations of 15,16,17,18 and 19 and incubated them with BT474 and Clone5 BT474 for 5 hrs (Figures 5.3 and 5.4). These variants were then used throughout this study and RhoB. The first control is PLGA-Tz488, and the size was 243 ± 55 nm, with a negative charge of -26.2 mV. The second control is PLGA-RhoB, with a size of 148 ± 72 nm and a slight negative charge of -0.05 mV. This is likely due to the fact that RhoB is positively charged because of the amine groups (Liu et al. 2015). Our finding for the size of PLGA-RhoB NPs was nearly identical to that of a separate study which revealed a PLGA-encapsulated RhoB NP of 184 nm (Jonderian and Maalouf 2016). However, their NP had a more negative charge of -21.7 mV, which may be because they used 10 times less RhoB concentration in their PLGA- RhoB synthesis (1 mg/mL compared with 0.01 mg/mL). The third control is non-fluorescent Tz conjugated to PLGA-RhoB with a size of 259 nm and a charge of -22.3 mV. Tz488 was employed as the final control at a concentration of 50 nM. The rationale for 50 nM of Tz488 is to be consistent with all of our previous studies.

There was a significant degree of similarity between the images obtained using these conjugates in the BT474 and the Clone 5 BT474 variant (Figures 5.3-5.4). However, in the parental cell line, there was a higher degree of internalisation of the Tz488 compared with the Clone 5 BT474 that showed only plasma membrane labelling. This is likely to be a feature of the resistance of this cell line to Tz (Wymant et al. 2020; Kute et al. 2004). As expected, there was no fluorescence in the blue channel in the absence of Tz or fluorescent Tz and

rhodamine was observed on and in the cells when delivered by the polymer with either Tz488 or the non-fluorescent version. Interestingly there was very little difference in the uptake properties of the polymer for Tz or RhoB in the BT474 and Clone 5 BT474 cells, highlighting that polymer driven uptake was able to override the difference when the cells were incubated with Tz488 alone, showing no uptake in the Clone 5 BT474 cell line. In both cell lines, there was evidence of cell-dependent aggregation of the polymers on the plasma membrane and also vesicle like structures indicative of endosomes. The aggregation observed is highly to be a function of the polymers binding to HER2 as there was no aggregation in regions that did not contain cells. There was strong colocalization between the Tz488 and RhoB but no real evidence of different RhoB labelling indicative of the release of the dye from the polymer.

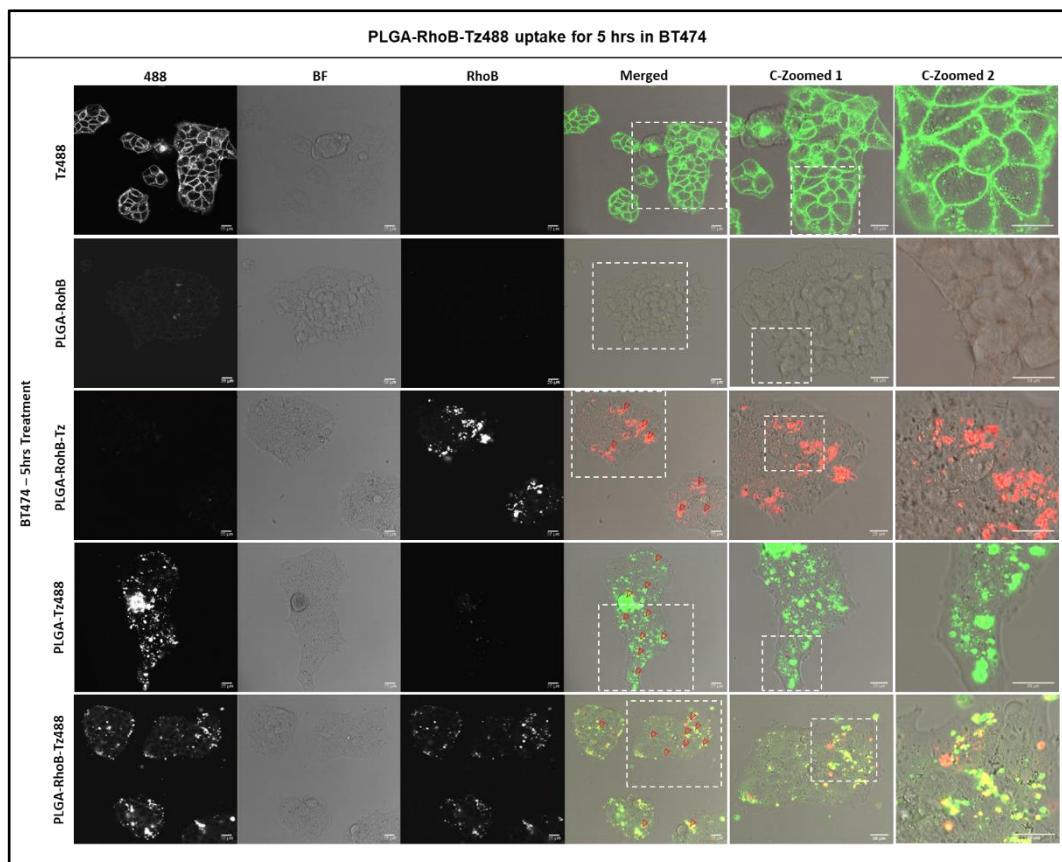


Figure 5.3: High selectivity for HER2 expression of PLGA-RhoB-Tz488 incubated with BT474 cells for 5 hrs. Formulations of 15,16,17,18 and 19 from table 5.2 with average sizes of 139nm, 148nm, 243nm, 259nm and 333 nm and Zeta Potential - 7.22mV, -0.0540mV, -26.2mV, -22.3mV and -26.1 respectively were used. Cells were incubated with 500 µg/mL of PLGA-RhoB-Tz488 and 50 nM of Tz488 for 5 hrs. Cells were then imaged by live cell confocal microscopy. Green indicates (Alexa 488), and red indicates (Rho-B). Red arrowheads indicate for internalised NPs. Scale bars 25µm. D-zoomed; Digital zoomed, C-zoomed; Confocal zoomed, BF; Bright Field.

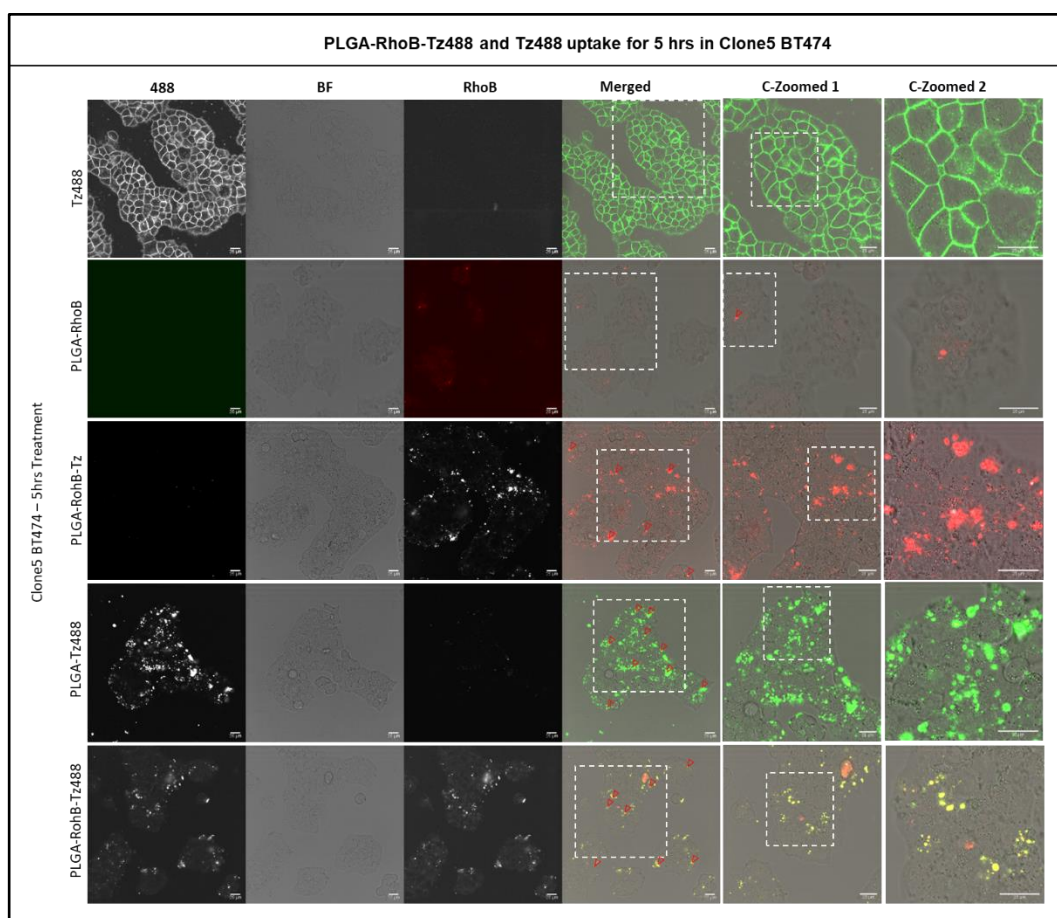


Figure 5.4: High selectivity for HER2 expression of PLGA-RhoB-Tz488 incubated with Clone5 BT474 cells for 5 hrs. Formulations of 15,16,17,18 and 19 from table 5.2 with average sizes of 139nm, 148nm, 243nm, 259nm and 333 nm and Zeta Potential - 7.22mV, -0.0540mV, -26.2mV, -22.3mV, and -26.1 respectively were used. Cells were treated with 500 µg/mL of PLGA-RhoB-Tz488 and 50 nM of Tz488 for 5 hrs. Cells were processed for analysis by confocal microscopy. Green indicated for (Alexa 488), and red indicated for (RhoB). Red arrowheads indicate for internalised NPs. Scale bars 25 µm. C-zoomed; Confocal zoomed, BF; Bright Field.

5.2.4 NP studies and plasma membrane labelling with CellMask.

CellMask deep red is a lipid dye commonly used to label the plasma membrane of cells (Zhang et al. 2019; Mu et al. 2014). In the experiments presented here, the label was incubated with the cells 10 mins before the end of the 5 hrs incubation with the NPs or Tz alone. This was to better identify the location of the NPs and confirm uptake into the cytoplasm.

Data in Figure 5.5 highlight very little Tz binding to the MCF7 cells showing clear plasma membrane labelling with CellMask. There were some similarities and differences in the labelling and the apparent internalisation of Tz488 and the conjugates in HER2+ cells (Figures 5.6, 5.7 and 5.8). Unlike data shown in figure 5.8, there was evidence of Tz488 uptake in the Clone 5 BT474 cell line suggesting that the antibody alone can enter this cell line and currently, the reason for the difference is unknown. With regards to the conjugates, there was clear evidence of plasma membrane location and internalisation of the antibody and RhoB to the cell interior. The strongest evidence of internalisation was shown in the Clone 5 BT474 line showing very strong punctate labelling of both the antibody and the dye (Figure 5.8). This may be due to receptor (HER2) clustering and the driving of macropinocytosis to generate very large ruffles on the plasma membrane (Wymant et al. 2020) that are predicted to engulf a large portion of the plasma membrane that is then shown as these structures inside the cells.

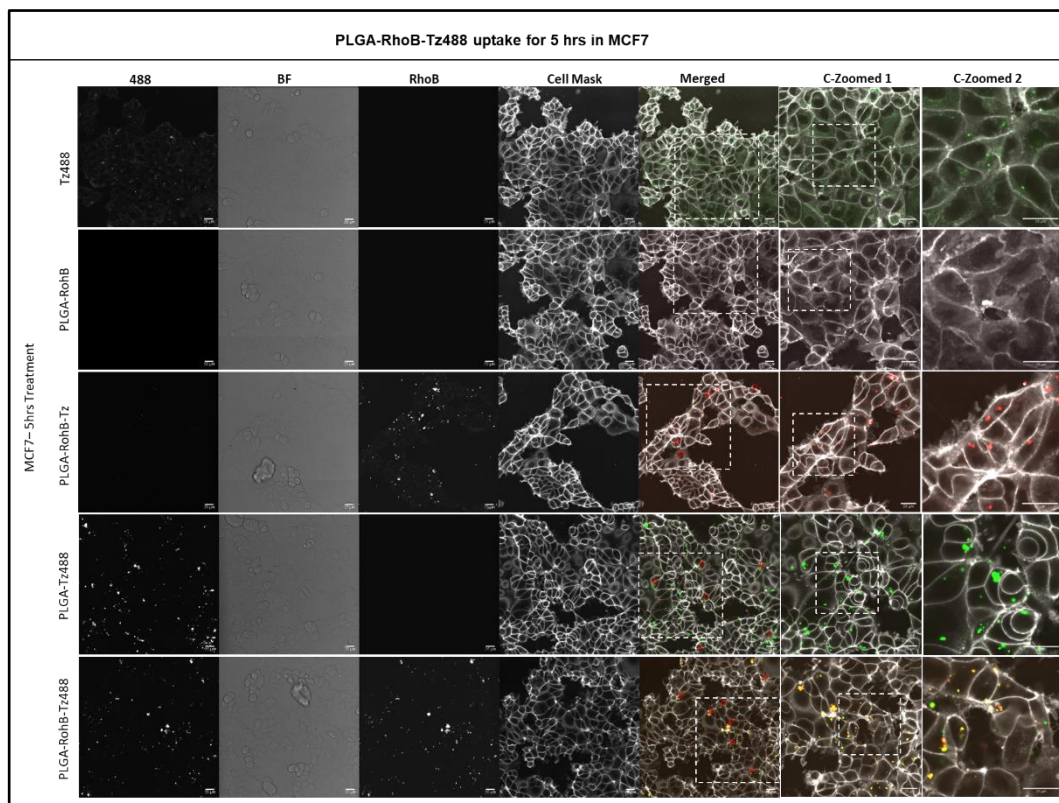


Figure 5.5: Lack of binding to MCF7 cells of PLGA-RhoB-Tz488 after 5 hrs. Formulations of 15,16,17,18 and 19 from table 5.2 with average sizes of 139nm, 148nm, 243nm, 259nm and 333 nm and Zeta Potential -7.22mV, -0.0540mV, -26.2mV, -22.3mV, and -26.1 respectively were used. Cells were incubated with 100 $\mu\text{g}/\text{mL}$ of NPs or 50 nM of Tz488 for 5 hrs. CellMask was then added for 10 mins. Cells were then imaged by live cell confocal microscopy. Green indicates (Alexa 488), white indicates (CellMask), and red indicates for (RhoB). Red arrowheads indicate for internalised NPs. Scale bars 25 μm . C-zoomed; Confocal zoomed, BF; Bright Field.

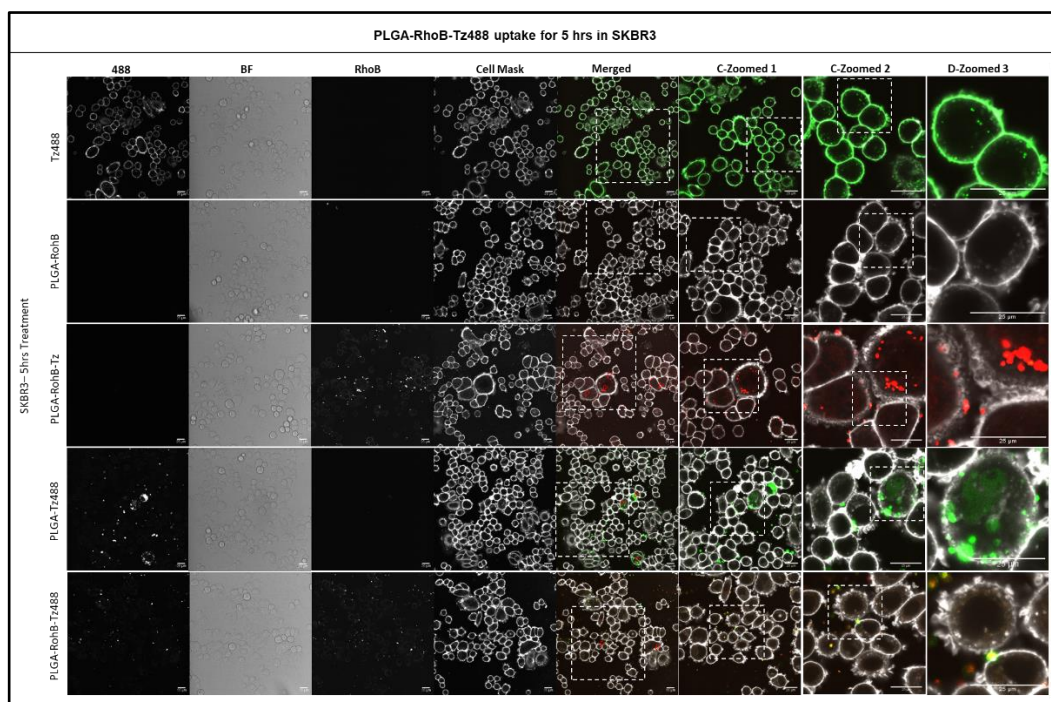


Figure 5.6: Selectivity of PLGA-RhoB-Tz488 for HER2 after incubation in SKBR3 cells for 5 hrs. Formulations of 15,16,17,18 and 19 from table 5.2 with average sizes of 139nm, 148nm, 243nm, 259nm and 333 nm and Zeta Potential -7.22mV, -0.0540mV, -26.2mV, -22.3mV, and -26.1 respectively were used. Cells were incubated with 100 $\mu\text{g}/\text{mL}$ of NPs or 50 nM of Tz488 for 5 hrs. CellMask was then added for 10 mins. Cells were then imaged by live cell confocal microscopy. Green indicates (Alexa 488), white indicates (CellMask), and red indicates for (RhoB). Red arrowheads indicate for internalised NPs. Scale bars 25 μm . D-zoomed; Digital zoomed, C-zoomed; Confocal zoomed, BF; Bright Field.

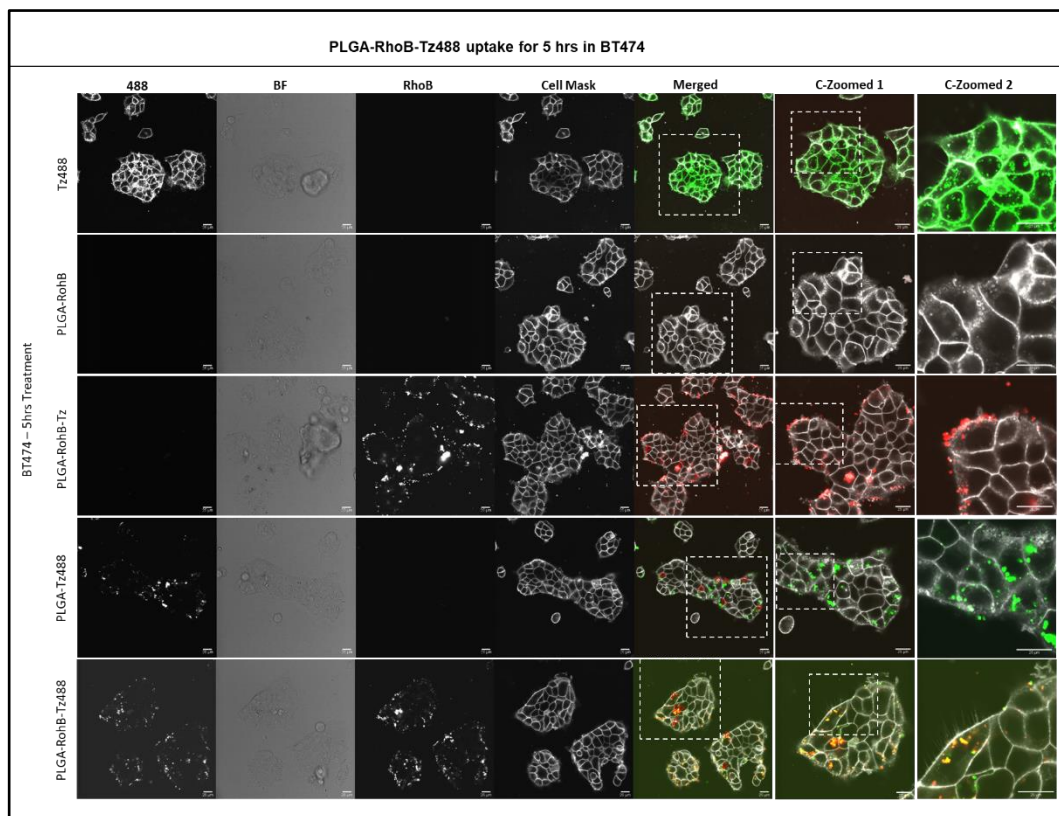


Figure 5.7: Selectivity of PLGA-RhoB-Tz488 for HER2 after incubation in BT474 cells for 5 hrs. Formulations of 15,16,17,18 and 19 from table 5.2 with average sizes of 139nm, 148nm, 243nm, 259nm and 333 nm and Zeta Potential -7.22mV, -0.0540mV, -26.2mV, -22.3mV, and -26.1 respectively were used. Cells were incubated with 100 µg/mL of NPs or 50 nM of Tz488 for 5 hrs. CellMask was then added for 10 mins. Cells were then imaged by live cell confocal microscopy. Green indicates (Alexa 488), white indicates (CellMask), and red indicates for (RhoB). Red arrowheads indicate for internalised NPs. Scale bars 25 µm. C-zoomed; Confocal zoomed, BF; Bright Field.

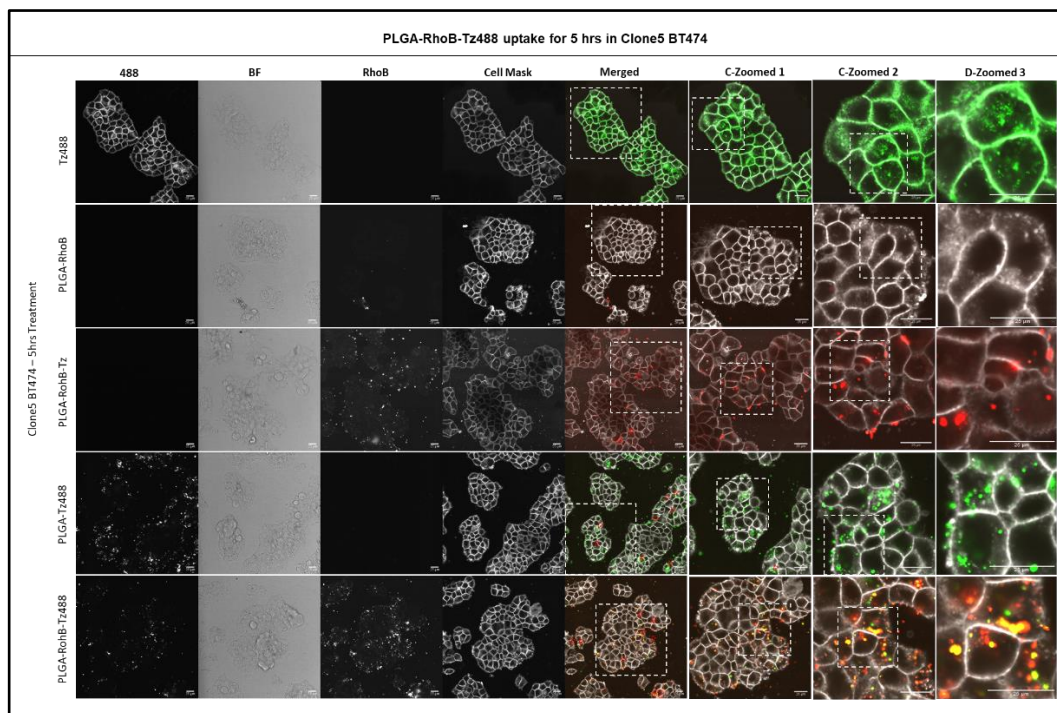


Figure 5.8: Selectivity of PLGA-RhoB-Tz488 for HER2 after incubation in Clone 5 BT474 cells for 5 hrs. Formulations of 15,16,17,18 and 19 from table 5.2 with average sizes of 139nm, 148nm, 243nm, 259nm and 333 nm and Zeta Potential -7.22mV, -0.0540mV, -26.2mV, -22.3mV, and -26.1 respectively were used. Cells were incubated with 100 $\mu\text{g}/\text{mL}$ of NPs or 50 nM of Tz488 for 5 hrs. CellMask was then added for 10 mins. Cells were then imaged by live cell confocal microscopy. Green indicates (Alexa 488), white indicates (CellMask), and red indicates for (RhoB). Red arrowheads indicate for internalised NPs. Scale bars 25 μm . C-zoomed; Confocal zoomed, D-zoomed; Digital zoomed, BF; Bright Field.

Through this study, MCF7 cells have been classified as a HER2 negative cell line, but this is open to debate and may differ between laboratories or at different passage numbers.

There is a lack of consistency in the literature regarding the status and labelling of MCF7s regarding HER2. One fairly recent study classified MCF7 as moderately HER2-expressing breast cancer cells with BT474 cells as overexpressing cells (Yu et al. 2016). They generated three different PLGA-Tz NPs based on how they were synthesised and encapsulated the conjugates with

RhoB for cell uptake analysis. Compared with the data in this thesis showing extensive differences between MCF7 and the HER2 overexpressing lines, they are only minimal in the breast NP uptake in BT474 compared with MCF7. A more recent study Zhong et al. (2020) classified MCF7 identified as a breast cancer cell line with HER2 overexpression but did not state the origin of this definition. MCF7 cells were shown to internalise PLGA-Tz nanobubbles encapsulating paclitaxel however the nanobubbles were labelled with the lipid Dil, and they were not analysed in known HER2 overexpressing cells such as BT474. However, another study (Yu et al. 2016) did compare MCF7 written as (HER-) with BT474 (HER+) and showed that after 2 hrs, the uptake in MCF7 was virtually non-existent, while in BT474 was clear but seemed to be confined to the plasma membrane. Zhang's group conducted a study demonstrating that their PLGA NPs attached to Tz encapsulating RhoB showed data comparable to this thesis showing very little uptake in MCF7 cells and uptake profiles in BT474 very similar to this thesis, including large structures inside the cells (Zhang et al. 2019). They also demonstrated that when cells were introduced to free Tz before adding NPs-Tz, to block HER2, there was no uptake.

5.2.5 Influence of PLGA-T z NPs on HER2 Degradation

Previous work from our laboratory has demonstrated that HER2 clustering by biotinylated Tz and the addition of streptavidin led to an increase in HER2 endocytosis, also its degradation (with HER3) in lysosomes (Moody et al. 2015; Wymant et al. 2020). Previous work in this chapter showed that binding and internalisation of Tz decorated NPs experiments were performed to investigate whether this also caused HER2 degradation. A similar western blotting procedure was followed by which cell lysates were collected after incubating BT474 or the

Clone 5 BT474 with Tz alone, PLGA or PLGA NPs with the omission or addition of RhoB; or from untreated cells. These were processed for SDS-PAGE, and HER2 or tubulin (loading control) were detected by western blotting (Data in Figure 5.9). The data were quantified by calculating HER2/tubulin ratios and data normalized to 100% based on the untreated control. Overall, this data was inconclusive because of time constraints; the experiments were only performed once. However, there was a suggestion common to both cell lines: a reduction in HER2 expression in all experimental points containing PLGA-Tz. This needs further analysis because our previous work showed that the Tz-resistant Clone 5 BT474 cell line was resistant to Tz-induced HER2 clustering and downregulation (Wymant et al. 2020), but these preliminary data suggest NP-Tz strategy was able to downregulate and cluster HER2 in Tz-resistant Clone 5 BT474 cell line. This added further strength to the findings presented in chapter 3, showing differences in endocytic properties between the parental and resistant cell line with respect to endocytosis and recycling of DEX/Tf. Thus, the observations in this thesis suggest the differences between them are not restricted to the dynamics of Tz binding and uptake. Data from the Kopecek laboratory showing that HPMA-Tz affibody conjugates could effectively deliver paclitaxel to HER2+ cancer cells but did not perform analysis of the HER2 status of the cells (Radford et al. 2020). These would be interesting experiments to perform as this could have enhanced the cytotoxic properties of the drug.

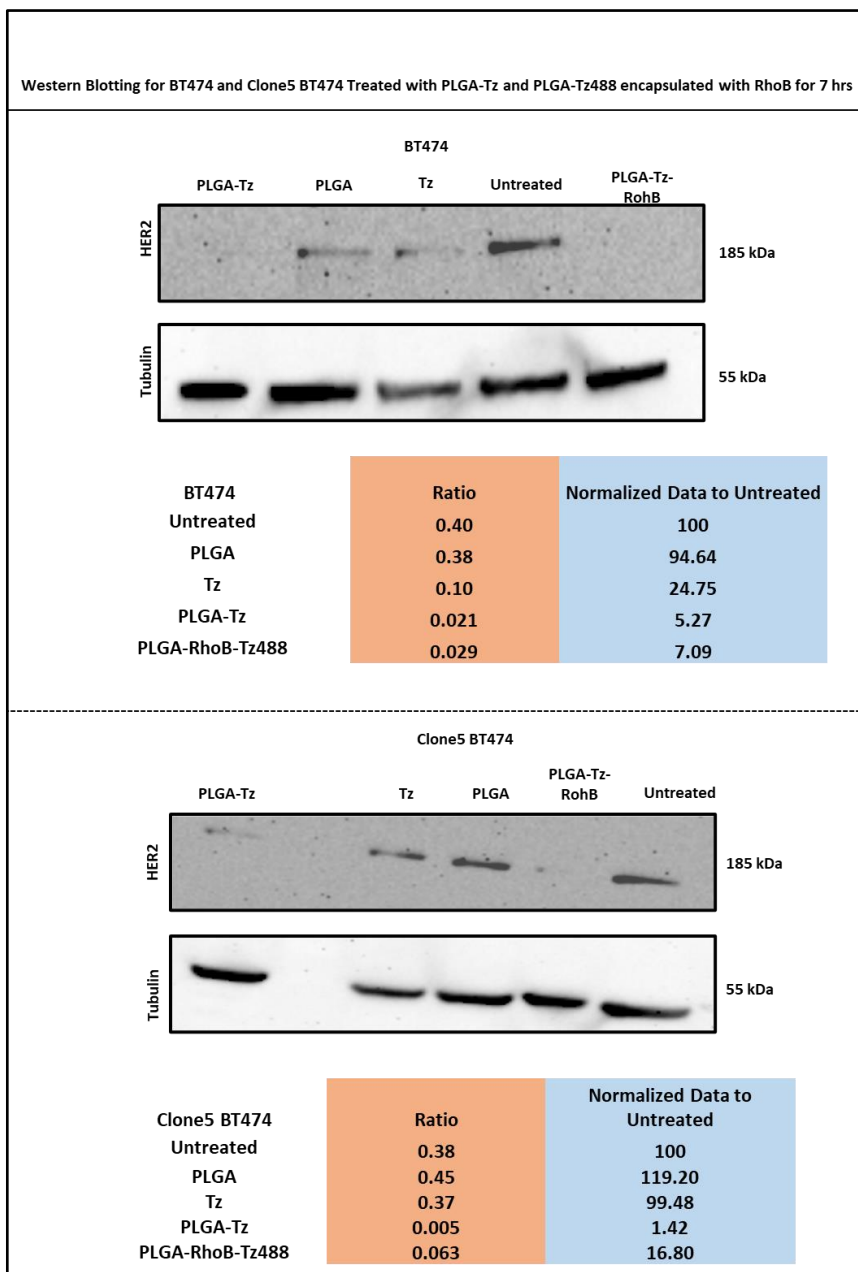


Figure 5.9: Analysis of HER 2 expression BT474 and Clone5 BT474 cells incubated for 7 hrs. Protein bands were quantified using Image J. providing quantitative analysis of HER2/Tubulin ratios.

5.2.6 Metabolic Activity assay of PLGA-Tz488

Before performing studies investigating the encapsulation of cytotoxic drugs to the PLGA-Tz NPs, it was important to assess whether they had inherent toxicity. For this, increasing concentrations of PLGA or equivalent PLGA-Tz were incubated with all four BC cell lines for 24 hrs before performing viability assays. Figure 5.10 demonstrated that all 4 cell lines have unique viability profiles.

For MCF7, the cells were viable to 70% at the highest concentration studied with the NP alone or conjugated with Tz giving very similar data. For the other three cell lines at concentration > 25 µg/mL, there was more evidence of toxicity, with a trend of the NP-Tz having a greater effect compared with NP alone. Interestingly the Clone 5 BT474 line was most sensitive to NP-Tz, resulting in 70% toxicity. The reason for this is unknown, but it was highlighted in the last experiment (figure 5.9) that the conjugate seemed to effectively degrade HER2.

Previous studies in BT474 cells Zhang et al. (2019) with PLGA-Tz conjugates showed similar metabolic activity data to those obtained in this thesis. They also incubated PLGA- Tz or blank NPs, with cells for 24 hrs at concentrations of 5, 20, 50 and 200 µg/mL. The NPs-Tz were more toxic, but at 200 µg/mL, the difference in metabolic activity between blank NPs and NPs-Tz was only 10%. In another study (Yu et al. 2016), BT474 cells were incubated with blank PLGA NPs and PLGA-Tz at 25, 50, 100 and 200 µg/mL concentrations. Blank PLGA and PLGA-Tz showed significantly higher metabolic activity than untreated controls at a concentration of ≥100 µg/mL, whereas there was no considerable difference between the blank two formulations with respect to having effects on cells. The study also compared BT474 and MCF7 metabolic activity at different times, demonstrating that the BT474 cells were more sensitive. They suggested that the

greater toxicity of NPs-Tz was related to its effects on HER2 endocytosis; its expression levels before and after the end of the experiments were not measured.

Other studies have shown that the size and zeta potential of naked PLGA NPs have a significant impact on cytotoxicity Chiu et al. (2021) for a review on this subject. Smaller PLGA NPs of between 100-200nm appear to give lower IC₅₀ values compared with those great than 200nm.

NP shape can also influence their effects on cells, as spherical PLGAs had a minimal (15%) impact on HepG2 cells at 100 µg/mL; however, needle-shaped PLGA were significantly more toxic (Zhang et al. 2017). Data obtained in the laboratory from PhD student Carwyn Hughes show that the formulation analysed here is spherical (data not shown).

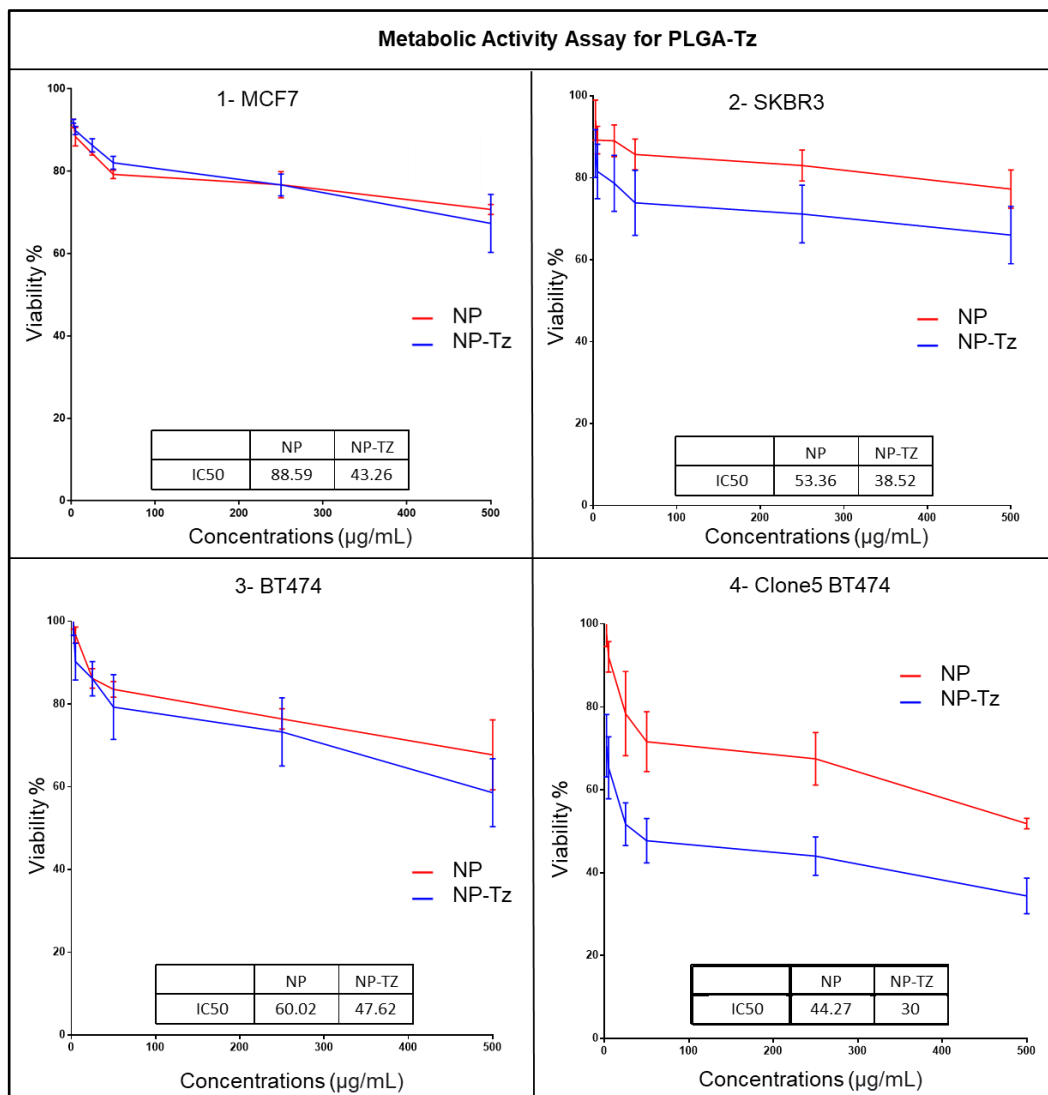


Figure 5.10: Metabolic Activity of BC cells incubated with PLGA or PLGA-Tz. Cells were seeded and cultured for 48 hrs and then incubated with the NPs for an additional 24 hrs before performing CellTiter Blue metabolic activity assays. Data show mean SEM from three independent experiments performed in triplicate.

5.2.7 PLGA encapsulated DOX attached to Tz

The previous data then allowed for analysis of the viability of these BC cells in the presence of the targeting polymer system encapsulating the therapeutic agent doxorubicin (DOX). This drug is approved to treat the early and late stages of BC (Jurcut et al. 2008). In an effort to reduce DOX cardiotoxicity, the FDA approved Doxil®, which is a PLGA PEGylated liposomal formulation (L-DOX) (known globally as Caelyx® (Ferro-Flores 2018). Doxil® was shown to lower DOX cardiotoxicity, and the PEGylated formulation prevents the liposomes (80-90nm) from detection by the MPS, permits a longer circulation period in the bloodstream while minimising free DOX exposure (Cagel et al. 2017; Prakash et al. 2022). Because of the EPR effect, Doxil® can enter tumours and give much higher DOX values (10x) compared with healthy breast tissue (Franco et al. 2018). Doxil, as a non-targeting (beyond the EPR effects), has also been approved for other cancers, including head and neck carcinoma, prostate cancer, and ovarian cancer (Soundararajan et al. 2009; Hubert et al. 2000; Pisano et al. 2013). But to date, we are still waiting for the FDA or other regulating bodies to approve a true targeting nanoformulation for BC or any other type of cancer.

In this thesis, DOX was selected as the drug to encapsulate within the PLGA NPs because of its continuous use as first-line cancer therapy and its spectral properties allowing for its microscopic visualisation in vitro analysis. Numerous studies have exploited its maximum excitation at 470nm and emission at 560nm (Shah et al. 2017). This was suitable for analysis with the SP5 confocal lasers available in the School of Pharmacy, and the Arwyn Jones group have experience in analysing DOX distribution in cells (Jin et al. 2008; Jin and Jones 2009).

DOX was encapsulated in PLGA and attached to unlabelled Tz as both would need to be excited using the argon 488 laser. As DOX has a wide excitation and emission range (Shah et al. 2017), attempts were also made to visualise the drug in cells at 546nm using the helium laser. Following the methods presented in Chapter 2, 2.3.17.5 the encapsulation efficiency was calculated to be 43% calculated from a standard curve of free DOX concentration compared with the encapsulated DOX following its release via dissolving in DMSO (see figure B in appendix B).

Cells were incubated with either 2 μ M free drug or in the NP, giving an equivalent DOX concentration from the standard curve. Initial cell analysis of this conjugate, after only one hr (Figure 5.11), showed that the DOX could be detected through the 488 laser as punctate distribution in SKBR3, BT474, and Clone5 BT474 cells but very little evidence of uptake in MCF7 cells. The signal from Ex535 was almost undetectable. The DOX alone controls showed staining of the entire cell due to its direct movement across the plasma membrane. A study in colon carcinoma CT26 cells investigating PLGA-DOX at identical 2 μ M DOX concentrations gave a similar distribution of the free drug and NP delivered drug after 1 hr, but there was more extensive punctate and nuclear labelling after 24 hrs (Choi et al. 2020). Interestingly the IC₅₀ for DOX alone was significantly lower than that encapsulated, suggesting that there was poor uptake into the cells or poor release from the NP once inside the cells.

In a separate study (Meng et al. 2018), silica-DOX-Tz NPs were investigated in MCF7 cells after only 1 hr of incubation. NPs-DOX-Tz (100 nm) were shown to stick together to make bigger particles (on the micrometre scale or above) that were easy to see by fluorescence microscopy and associated with the targeting

Tz observed as a FITC conjugate. NPs-DOX-Tz, however only had a fluorescence signal 2.21 times higher than that of NPs-DOX.

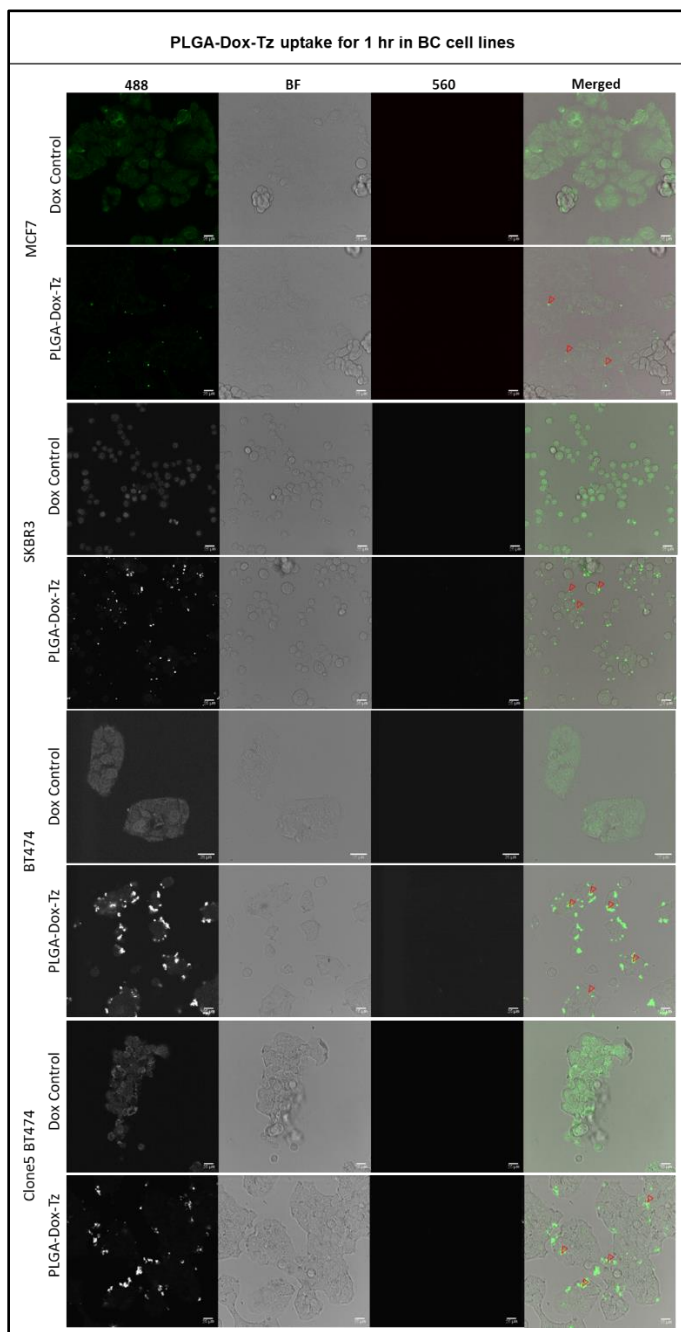


Figure 5.11: DOX distribution in PLGA-DOX-Tz incubated BC cells showing different spatial subcellular distribution compared with DOX alone. Formulation of 21 from table 5.1 with average size 574nm, Zeta Potential 0.55mV and Formulation 22 with average size 341nm were used. Cells were incubated with 2 μ M of NPs or DOX

alone for 1 hr prior to analysis by live cell confocal microscopy. Green indicates (Dox), and red arrowheads indicate for internalised NPs. Scale bars 25 μ m. BF; Bright Field.

To further investigate the previous data, the cells were incubated for a longer period of five hrs in the presence of the controls or the NPs to gain a higher level of knowledge regarding the sub-cellular distribution of the drug; the cell's nucleus and plasma membrane were also labelled 10 mins before the end of the experiment with Hoechst 33342 and CellMask respectively. As expected, with few exceptions (shown) and despite a much longer incubation time, there was very little DOX fluorescence in MCF7 cells (Figure 5.12). This would account for the low Pearson Coefficient calculated (Appendix C) as 0.12 for as a comparison of the subcellular distribution of Hoechst and DOX when the drug was delivered by the PLGA NP compared with 0.69 when the DOX was administered alone.

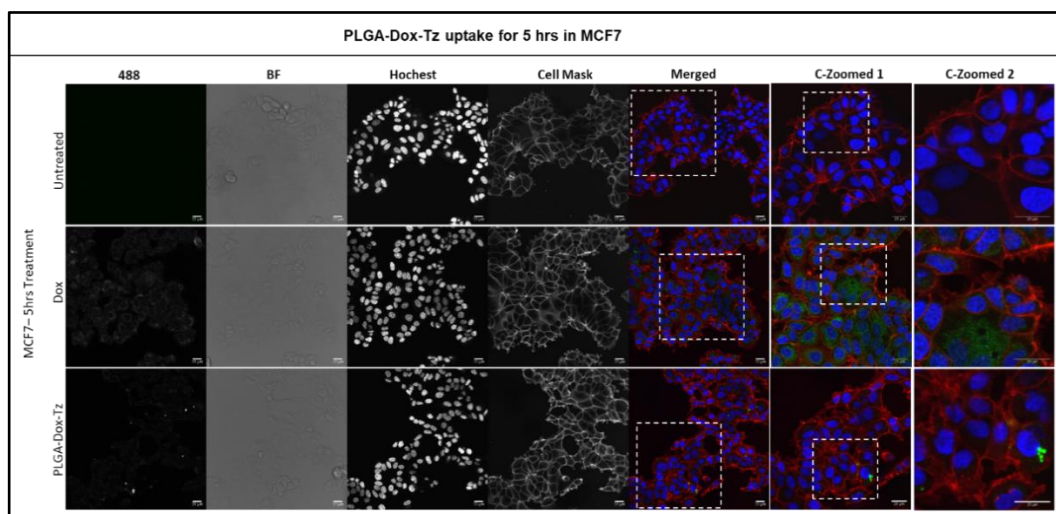


Figure 5.12: DOX distribution in PLGA-DOX-Tz incubated MCF7 cells for 5 hrs showing no evidence of vesicular labelling. Formulation of 21 from table 5.2 with average size 574nm, Zeta Potential 0.55mV and Formulation 22 with average size 341nm were used. Cells were incubated with 2 μ M of DOX/NPs-DOX-Tz prior to the addition of CellMask and Hoechst for 10 mins before the end of the experiment, and the cells were then washed and imaged by live cell confocal microscopy. Green indicates Dox, Red indicates CellMask, Blue indicates Hoechst, and red arrowheads indicate for internalised NPs. Scale bars 25 μ m. BF; Bright Field, C-zoomed; Confocal zoomed.

The same experiments in the HER2 overexpressing cell lines gave interesting data (Figures 5.13, 5.14, 5.15 and 5.16). Again, the DOX alone labelled the entire cell, including the nucleus, but all three cell lines gave a very similar profile for the drug encapsulated in the PLGA NPs. Either close to the plasma membrane or within the cytoplasm, the appearance of the drug was in quite large structures, some resembling vacuoles that seem to be unique to this PLGA conjugate. No other similar structures could be identified in the literature that mostly investigates the location of the drug or NP on or in cells after much longer incubation time points. Time did not allow for a full analysis of these structures, for example, by performing colocalization studies between them and endocytic probes such as Tf and DEX. It is, however, quite easy to hypothesise that these vacuole-like structures emanate from the ruffles observed when HER2 was cross-linked with Tz-biotin-streptavidin (Wymant et al. 2020). Similar SEM studies are now required to see if ruffling can be visualised in the NP treated cells where we would also expect to see the NPs on the surface. It was, however, difficult with this experimental set-up to clearly identify whether any of the DOX was being released into the cytosol and therefore having access to the nucleus.

Dox-PLGA-PEGylated NPs and Tz-conjugated PLGA-PEGylated NPs were synthesised to test uptake in SKBR3 and MCF7 cells after 5, 30 mins, and 2 hrs (Zhou et al. 2015). The release of the DOX from the polymer was pH dependent on the addition of the pH-sensitive ionizable histidine to the NP formulation for release in the endolysosomal pathway. They found significant increases in DOX uptake in the Tz targeted cells after 30 mins and 2 hrs of treatment, especially in SKBR3 cells incubated with NPs-Tz for 2 hrs. They also reported that the DOX

uptake efficiency in SKBR3 cells was considerably greater than that of MCF7, giving higher toxicity.

Other polymer systems have also been investigated for delivering Tz and therapeutics. MCF7 as HER2⁻ and SKOV3 as HER2⁺ cells were used as cancer models for delivery of DOX by the natural cationic polymer chitosan (Yousefpour et al. 2011). Targeted (Tz) and non-targeted NPs were generated showing entry into SKOV3 cells, but there was no significant difference in cytotoxicity profiles between the targeted and non-targeted approaches. Once again, the Pearson's coefficient for PLGA delivery of Dox to the Hoechst labelled nucleus was low in figures 5.13 to 5.15 never reaching >0.22 (Table 5.3).

Table 5.3: The Pearson correlation coefficient (r) between DOX and Hoechst in PLGA-DOX-Tz compared with DOX treatment.

Figure number	Cell line	The Pearson correlation coefficient (r) between DOX and Hoechst	
		PLGA-DOX-Tz	DOX
5.12	MCF7	0.12	0.69
5.13	SKBR3	-0.01	0.79
5.14	BT474	0.22	0.74
5.15	Clone5 BT474	0.1	0.36

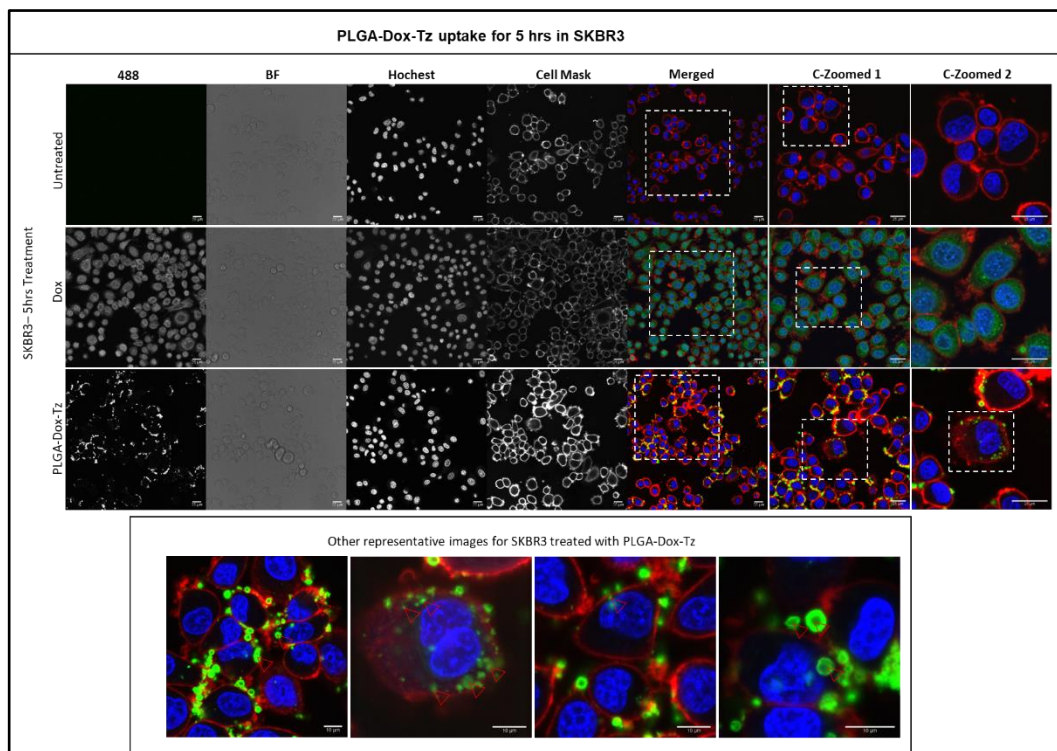


Figure 5.13: DOX distribution in PLGA-DOX-Tz incubated SKBR3 cells highlighting appearance of vacuole like structures. Formulation of 21 from table 5.2 with average size 574nm, Zeta Potential 0.55mV and Formulation 22 with average size 341nm were used. Cells were incubated with 2 μ M of DOX/NPs-DOX-Tz prior to the addition of CellMask and Hoechst for 10 mins before the end of the experiment, and the cells were then washed and imaged by live cell confocal microscopy. Green indicates Dox, red indicates CellMask, Blue indicates Hoechst, and red arrowheads indicate for internalised NPs. Scale bars top panel 25 μ m, bottom panel 10 μ m. BF; Bright Field, C-zoomed; Confocal zoomed.

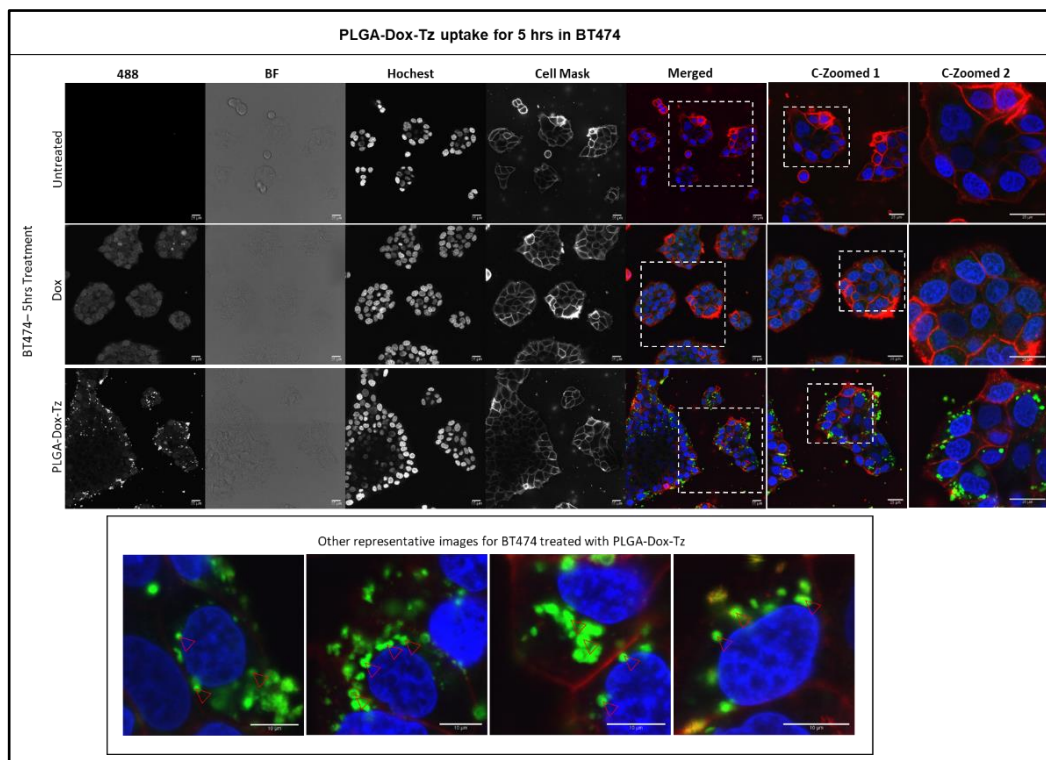


Figure 5.14: DOX distribution in PLGA-DOX-Tz incubated BT474 cells highlighting appearance of vacuole like structures. Formulation of 21 from table 5.2 with average size 574nm, Zeta Potential 0.55mV and Formulation 22 with average size 341nm were used. Cells were incubated with 2 μ M of DOX/NPs-DOX-Tz prior to the addition of CellMask and Hoechst for 10 mins before the end of the experiment, and the cells were then washed and imaged by live cell confocal microscopy. Green indicates Dox, red indicates CellMask, Blue indicates Hoechst, and red arrowheads indicate for internalised NPs. Scale bars top panel 25 μ m, bottom panel 10 μ m. BF; Bright Field, C-zoomed; Confocal zoomed.

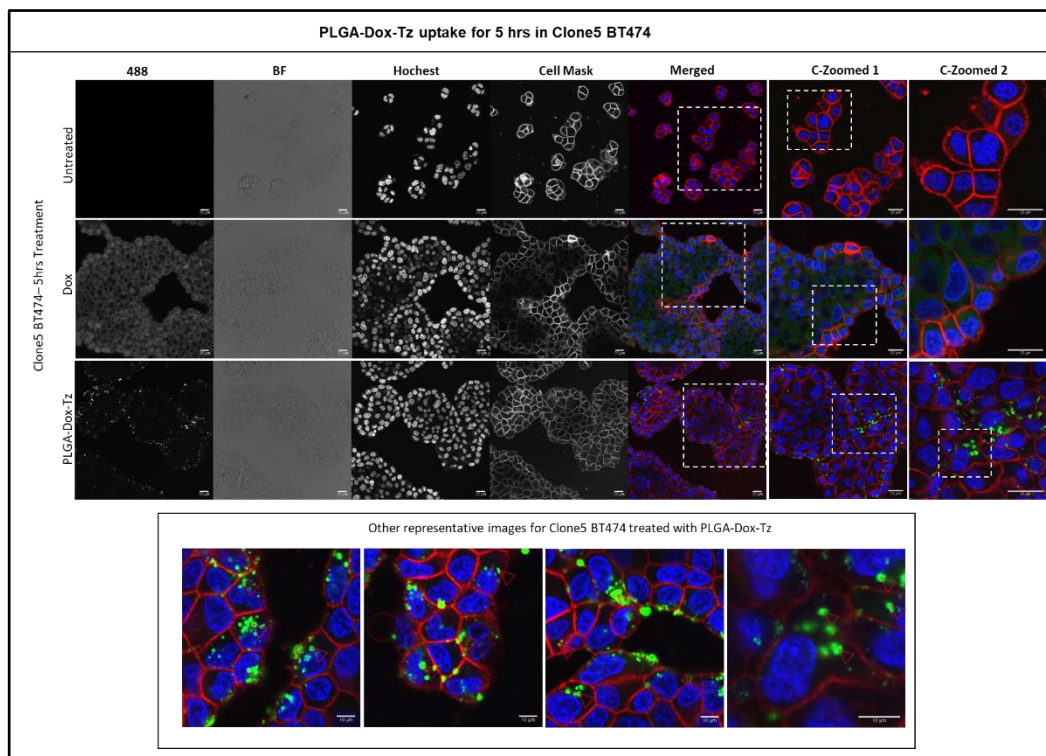


Figure 5.15: DOX distribution in PLGA-DOX-Tz incubated Clone5 BT474 cells highlighting appearance of vacuole like structures. Formulation of 21 from table 5.2 with average size 574nm, Zeta Potential 0.55mV and Formulation 22 with average size 341nm were used. Cells were incubated with 2 μ M of DOX/NPs-DOX-Tz prior to the addition of CellMask and Hochest for 10 mins before the end of the experiment, and the cells were then washed and imaged by live cell confocal microscopy. Green indicates Dox, red indicates CellMask, Blue indicates Hochest, and red arrowheads indicate for internalised NPs. Scale bars top panel 25 μ m, bottom panel 10 μ m. BF; Bright Field, C-zoomed; Confocal zoomed.

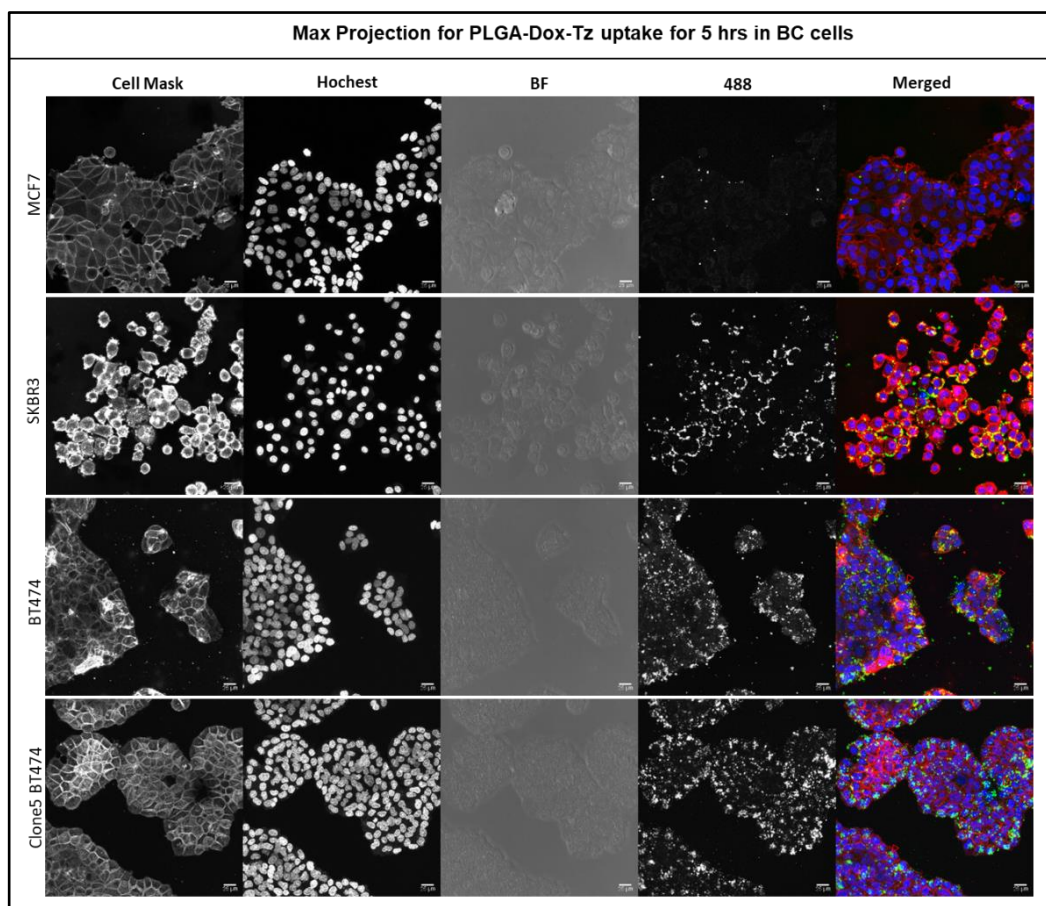


Figure 5.16: Max projection images of DOX distribution in PLGA-DOX-Tz incubated BC cells (max projection). Formulation of 21 from table 5.2 with average size 574nm, Zeta Potential 0.55mV and Formulation 22 with average size 341nm were used. Cells were incubated with 2 μ M of DOX/NPs-DOX-Tz prior to the addition of CellMask and Hochest for 10 mins before the end of the experiment, and the cells were then washed and imaged by live cell confocal microscopy. Green indicates Dox, red indicates CellMask, and Blue indicates Hochest. Scale bars top panel 25 μ m, bottom panel 10 μ m. BF; Bright Field, C-zoomed; Confocal zoomed.

In previous studies, the size and charge of NPs, such as PLGA, significantly affected the efficacy of cancer cell uptake in vitro and in vivo, often demonstrating a direct relationship between size, charge, and pharmacokinetic behaviour (Ibrahim et al. 2020; Chiu et al. 2021; Operti et al. 2019; He et al. 2010; Jiang et al. 2015). From these studies, it was difficult to identify numbers for ideal size or charge. In this thesis, there does not appear to be any significant correlation in

BC cell uptake, measured qualitatively, between size, and charge. However, vacuole like structures were noted in the three BC lines incubated with the largest NP studied (574nm) and these were selected for the cell metabolism assays that follow. Overall, the aspect of size and charge was not investigated in detail as this would have involved design, manufacture and biological characterisation of many different formulations.

5.2.8 Metabolic activity of BC cells incubated with PLGA-DOX-Tz.

The imaging data in figures 5.13-5.16 immediately led to an analysis of the capacity of the NPs to deliver DOX to affect metabolic activity. These assays were performed in all the BC cells, and the data in comparison with an equivalent amount of free DOX is presented in figure 5.17 with this time. The data shows that only in the MCF7 cells is the DOX alone better able to reduce metabolic activity compared to the NPs. Comparing the metabolic activity of PLGA-DOX-Tz to DOX in BC cells revealed no significant changes. At a high concentration of 10 μM , PLGA-DOX-Tz decreased metabolic activity to less than 10% of cells viability in SKBR3 and Clone5 BT474 with IC_{50} values of 1.49 μM and 0.91 μM , respectively, compared to BT474 and MCF7 with IC_{50} values of 1.32 μM and 1 μM , respectively. DOX had IC_{50} values of 1.04 μM , 1.79 μM , 1.49 μM , and 1.17 μM in MCF7, SKBR3, BT474, and CLONE5 BT474, respectively. The differences between DOX and PLGA-DOX-Tz could be explained by the sustained release of DOX from PLGA. This was addressed by (Choi et al. 2020), showing that after 48 hrs of treatment with DOX or non-targeting PLGA-DOX, the drug alone showed a more effective capacity to affect the viability of CT-26 tumour cells because much of the encapsulated drug was retained within the NP and could not reach its target.

Despite the fact that SKBR3 was the most sensitive cell line to single DOX treatment (Figure 5.17), it had a higher IC₅₀ value to PLGA-DOX-Tz. This may be the result of low concentrations of PLGA-DOX-Tz/DOX in SKBR3 showing no effect on metabolic activity in comparison to other cell lines before viability dropped at higher concentrations in SKBR3 cells. MCF7 exhibited significant differences between PLGA-DOX-Tz and DOX at 5 and 10 μM concentrations. In comparison to PLGA-DOX-Tz, Clone5 BT474 and BT474 exhibited nearly identical DOX-induced effects.

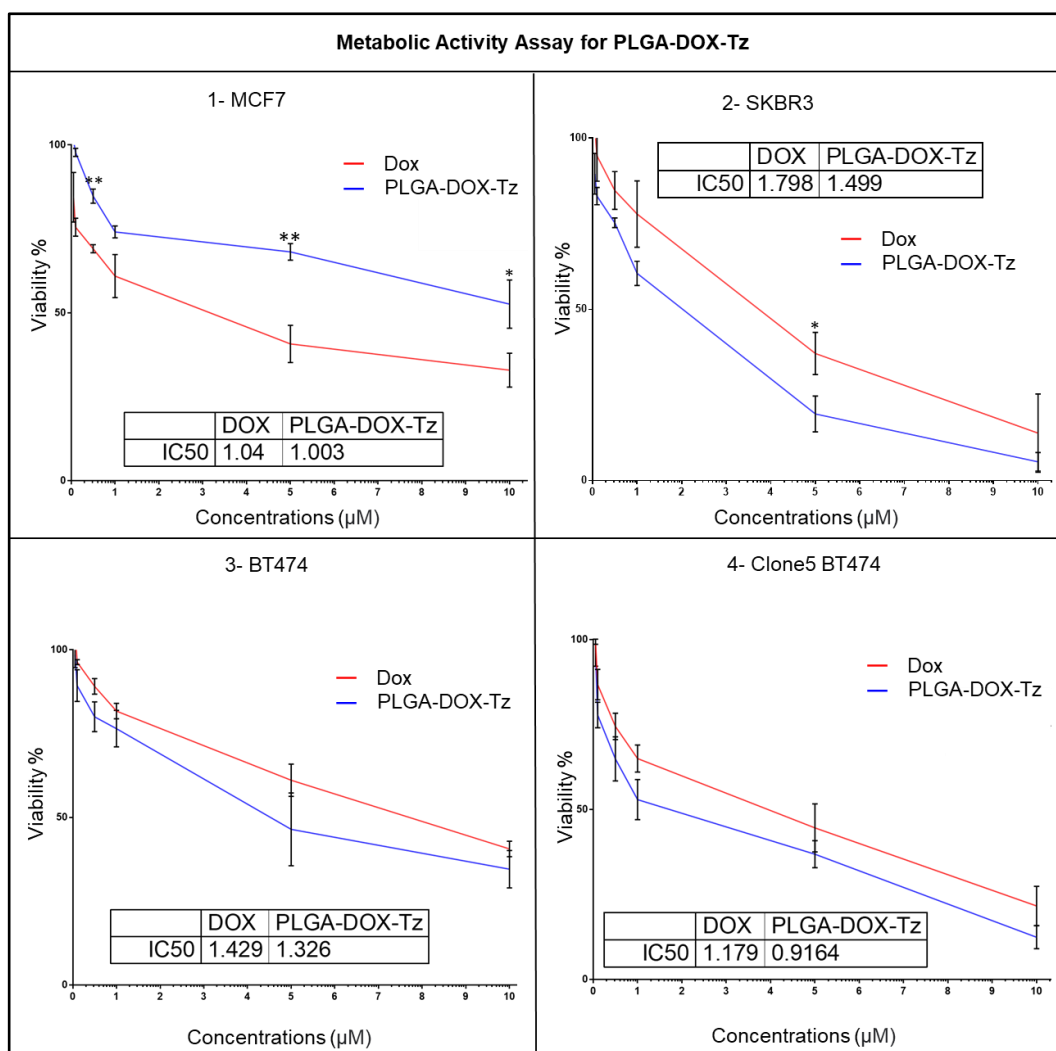


Figure 5.17: PLGA-DOX-Tz effects on Metabolic Activity of BC cells. Cells were seeded and cultured for 48 hrs and then were incubated with the NPs/DOX for an

additional 24 hrs before performing CellTiter Blue metabolic activity assays. Data show mean SEM from three independent experiments performed in triplicate. p-values for MCF7 at concentrations 1 μM (**) 0.0083, 5 μM (**) 0.0010, 10 μM (*) 0.0232, and SKBR3 at concentration 5 μM (*) 0.0479. p. Values were calculated using a two-way variance analysis ANOVA (Sidak's multiple comparisons test).

5.3 Summary

In this chapter, I was able to synthesise and perform an initial biological characterisation of a polymer drug antibody conjugate targeting an important cancer receptor. From the comparison between low HER2 expressing and HER2 overexpressing cells, the formulation gave very clear evidence of the need for the presence of HER to initiate cell binding and internalisation of both a model dye and also an anti-cancer drug. The final metabolic activity analysis demonstrated that the DOX within the NP formulation had a higher capacity to kill the three breast cancer cell lines compared with the free drug, highly suggesting that the internalised DOX was being released to the cytosol of the cell and was then able to access its target(s) in the nucleus. There is also evidence to believe that the generated formulation can downregulate HER2 expression via its delivery to lysosome.

Chapter 6: General Discussion

The motivation for this study was the need to develop more effective nanomedicines for treating HER2+ BC. Despite the benefits of administering patients with Tz as a first-line treatment, the drug's inability to drive HER2 endocytosis to lysosomes limits its effectiveness. This is especially true in using this antibody as an ADC, e.g. Kadcyla, where endocytosis and lysosomal delivery is essential to release the emtansine to the cytosol and to inhibit microtubule polymerisation (Leyton 2020) and HER2 endocytosis resistance is still not fully understood. Underpinning the work were previous experiments in the laboratory showing the potential of clustering HER2 as a therapeutic strategy and the need to further characterise this process and test the hypothesis that clustering was driving macropinocytosis very early on after adding Tz to cells (Moody et al. 2015; Wymant et al. 2020). Initial work on the thesis further analysed this endocytic process, especially with respect to characterising old and new drugs that, by virtue of their inhibition of NHE1, inhibit this process. As macropinocytosis inhibitors, we initially employed amiloride and EIPA, two substances that are widely used in drug delivery research, including NP analysis, as macropinocytosis inhibitors (Desai et al. 2019; Manzanares and Ceña 2020). However, our research unexpectedly revealed that EIPA significantly increased the uptake of the commonly used macropinocytosis probe DEX in both HER2+ cell lines (BT474, SKBR3) but not in MCF7 cells and also not in the Clone 5 BT474 line, further highlighting the difference in endocytosis between this variant and the parental line.

The metabolic activity assay was then used to evaluate the overall metabolism occurring in BC cells after NHE1 inhibitors were added. EIPA was the most toxic inhibitor in all four cell lines compared to amiloride and Cariporide. According to

the data presented in this thesis, EIPA may have other effects in addition to its effects on NHEs and macropinocytosis, and further study is necessary to examine these potential activities.

Further work in Chapter 4 with the availability of fluorescent Tz showed that EIPA increased the uptake of this antibody. These findings are difficult to interpret, especially as the drug has more than one target. More studies are needed to identify the relation between EIPA and macropinocytosis and also caution the use of this drug as a claimed inhibitor of macropinocytosis especially as recent findings demonstrate that NHE inhibition can affect the pH of cancer cells that may lead to apoptosis process (Rolver et al. 2020).

Cariporide is a separate class of NHE inhibitor as it is a more specific inhibitor of NHE1 than EIPA and amiloride. Overall, this thesis showed that this drug had no effects on the endocytosis of DEX, Tf, or Tz. This was in line with the fact that the drug was relatively non-toxic compared with EIPA. Thus, the work raises questions regarding the role of NHE1 in macropinocytosis. However, further analysis is needed to confirm (positive control) the activity of cariporide on NHE1 (Harguindey et al. 2013; Chen et al. 2019)

Tz's full mechanism of action with regard to effects on HER2 is still under scrutiny. Here, in Chapter 4, data showed that Tz caused the formation of ruffle-like structures related to those observed during macropinocytosis, but the resulting vesicles were only clearly visualised after 5-7 hrs of incubation. This is not in agreement with other studies that suggest Tz follows a CME route (García-Alonso et al. 2020). These results on Tz endocytosis also somewhat disagree

with research suggesting that Tz does not affect HER2 endocytosis (Bagnato et al. 2017).

As part of this thesis, the study of EIPA on Tz cell dynamics were investigated in detail. Compared with amiloride and cariporide that had minimal effects on Tz uptake and subcellular distribution, EIPA had major effects; as previously shown for uptake of Tf and DEX. Because of the noted effects of EIPA on Tz uptake it would also be very interesting to study the effects of this drug on HER2/3 expression. This is particularly relevant because previous studies from our laboratory have shown that clustering and endocytosis of these receptors induce their endocytosis and degradation in lysosomes (Wymant et al. 2020).

In this thesis, monolayer cultures or two-dimensional (2D) cell culture was the only method used and studied for BC cell biology, Tz and NP uptake. This method was used because: (i) (2D) cell culture is well-established and widely used method, especially in the drug screening process against cancer (Maylaa et al. 2023); (ii) 2D culture has been used since 1940s and is the most general method used in studying cell biology and molecular mechanisms because it is simple and convenient (Białkowska et al. 2020); (iii) as this is a common method, the availability of comparative literature makes it easy for researchers to compare current outcomes with past outcomes; (iv) (2D) cell culture has been the preferred method of producing disease models in vitro, is also cost-effective (Ryan et al. 2016). Cancer cell lines were used here; however, similar experiments can now be performed in patient derived cells that can also be used to generate mouse xerograph models (Aparicio et al. 2015; Dobrolecki et al. 2016).

However, 2D culture has come under scrutiny because of its low resemblance to *in vivo* cancer (Shamir and Ewald 2014). There is now significant interest and study of some experiments performed in this thesis in cancer cells that have formed 3D structures called spheroids and organoids (Van Zundert et al. 2020; Azimian Zavareh et al. 2022; Velasco et al. 2020; Fontoura et al. 2020). These allow cells to establish a connection between the cell and the extracellular matrix to form a specific 3D structure that better mimics the growing environment of cells *in vivo* (Shao et al. 2020). These also allow for analysis of the penetration of a drug delivery vector such as the NPs used in this thesis through the whole 3D space rather than allowing 100% exposure as observed in 2D. There are however some significant challenges in performing high content endocytosis analysis of drug delivery vectors in living organoids using microscopy. This is despite developments such as the availability of new developments such as Light-sheet fluorescent microscopy (Wang et al. 2019; Rennick et al. 2021).

The concept of receptor clustering has been known for quite some time, including the TfR that was partially studied here (Hopkins and Trowbridge 1983; Weissman et al. 1986; Liu et al. 2010). For example, antibodies against the TfR have been shown to increase uptake by CME and also change the intracellular traffic of the receptor, delivering it to lysosomes that it normally avoids as it is rapidly recycled out of the cells. This effect for TfR was also observed in the Jones laboratory (Moody et al. 2015), which showed similar effects for HER2 and the MHC class I receptor. Later clustering of HER2 was shown to not only lead to its uptake and degradation but also that of its referred binding partner HER3 (Wymant et al. 2020).

As proof of concept, the very well-described PLGA was chosen as the polymer backbone that was also used to provide targeting in the form of Tz. Methods need to be developed and optimised before testing the NPs in HER2 low and high expressing cells. Following this optimisation, it was very encouraging to note that the generated NPs were clearly binding to cells in a HER2 dependant manner (Chapter 5). Here, unlike most studies, we investigated NP binding and uptake after very early time points revealing extensive cell binding and evidence of NP endocytosis after only 1 hr. However, the structures on the cells and in the cells were often unlike typical endocytic structures that we see with Tf, DEX and also Tz alone. The early work encouraged loading a fluorescent dye and anti-cancer drug DOX into the NPs before adding on to the cells. Like the fluorescence of the NPs-Tz, the dye and drug were also shown to be loaded on the cell surface and enter the cells. Though there was no statistical difference between the DOX and DOX-NP in reducing metabolic activity in vitro, there may be effects in vivo as the NP will protect HER2 low expressing cells of the body from the effects of DOX that will also accumulate in the tumour via the EPR effect. Evidence for this also comes from the analysis in MCF7 cells showing statistically high DOX toxicity compared with NP-DOX. I also had the advantage of comparing the new NPs with data from studies using PLGA and other polymer-based HER2 targeting NPs in breast and other cancer research (Zhou et al. 2015; Yu et al. 2016; Sakhi et al. 2022; Colzani et al. 2018; Zhang et al. 2019; Kubota et al. 2018; Nieto et al. 2020).

Few of these studies have, as noted, looked at the cells early after adding the NPs or looked at the dynamics of the plasma membrane with tools such as CellMask. There is now ongoing work investigating how these NPs are interacting

with the plasma membrane using SEM as we have previously demonstrated with HER2 clustering caused by Tz-bi-streptavidin. It will be interesting to observe whether the very large structures on the surface of the cells represent membrane aggregates that affect the plasma membrane. Here, differences in the numbers of Tz/NP were not investigated to see if lowering to increasing the numbers affected cell binding and also uptake. This is also the subject of further work. The work could be expanded to investigate encapsulating other drugs, including nucleotides such as mRNA and also the numerous other described plasma membrane receptor targeting ligands such as folic acid (FA), sugar residues (e.g., hyaluronic acid (HA)), peptides (e.g., RGD), and proteins (e.g., cytokines, lectins, and Tf) (Morales-Cruz et al. 2019).

Unlike most studies involving NPs targeting plasma membrane receptors, the work in this thesis also performed some preliminary investigation into analysing the fate of the targeted receptor, HER2, after the addition of NPs. Time did not allow for full analysis, but there is strong and encouraging data to suggest that the NPs made here are driving the receptor into lysosomes and destruction lysosomal proteases. It will be very interesting to investigate whether HER3 is also being degraded in this way and whether this has any role in the induction of toxicity beyond that of the DOX alone. Further analysis is also required to map the punctate endosome like structures that the antibody and drug are entering into and whether they colocalize with endocytic probes such as Tf DEX and lysotracker (Zhou et al. 2015; Moody et al. 2015).

NPs as vectors for chemotherapeutics treating BC have already achieved clinical or FDA approval. For example, Abraxane®, an albumin-bound NP encapsulating paclitaxel, as first-line treatment for metastatic BC (Yuan et al. 2020). Liposomal

NPs formulations for DOX delivery such as Caelyx/Doxil® (PEGylated liposomal DOX) and Myocet® (non-PEGylated liposomal DOX) have also been approved against advanced stage BC (stage IV) and metastatic BC (Lao et al. 2013). There are also several NPs for BC treatments under phase I-III clinical trials (Table 6.1).

Table 6.1: Examples of NPs for chemotherapy delivery for BC treatment approved for clinical studies.

Drug Name	NPs formulation	Clinical trial Phase study	References
Genexol ®	Poly(D,L-lactide)-PEG-methyl ether-Docetaxel	Phase I	(Lee et al. 2011)
Bind-014 ®	PEG-PLGA-Docetaxel	Phase I	(Von Hoff et al. 2016)
Narekt-102 ®	PEG-liposome-Irinotecan	Phase III	(Li et al. 2018)
LEP-ETU ®	Liposomal-Paclitaxel	Phase I/II	(Li et al. 2018)
ThermoDox ®	Heat activated Liposomal-DOX	Phase III	(Dou et al. 2017)
Lipoplatin ®	Liposomal-Cisplatin	Phase III	(Aulic et al. 2020)
MM-302 ®	HER2-targeting antibody liposomal-DOX	Phase II	(Aulic et al. 2020)

As stated, several preclinical trials are investigating novel NPs for BC treatments. However, a view is that the most promising NPs will be those decorated with targeting ligands recognising BC surface markers (Landeros 2023).

There is a weak link between the pre-clinical studies and the results of clinical trials regarding NPs targeting BC and It is unknown why formulations with an abundance of excellent outcomes in preclinical publications fail to advance to clinical trials. Studies have shown that factors such as the human body's ability to recognise foreign bodies (Evangelopoulos et al. 2018), and concerns arising from

systemic toxicity and immune system activation (Gabizon et al. 2020), can hinder the translation of NPs into the clinic. Translation of nanotechnology to the clinic also has economic issues such as their high costs of production and generating on large scale (Bosetti and Jones 2019).

A study by Willhelm that proposed a 30-year strategy for translation of nanotechnology from bench to bedside should move focus away from NP design (size, shape and surface chemistry) and rather concentrate on studies that should focus on developing technologies to look at the effects of NP directly on tumours, and other organs such as liver, spleen, kidney and blood with the possibility of using computational strategies to predict NP performance (Willhelm et al. 2016).

In the light of FDA-approval PLGA, it is questionable whether the targeted NP developed here should enter in vivo studies to gain other information such as pharmacokinetics, systemic toxicity and biodistribution. Interestingly and very recently, in vivo rabbit experiments of paclitaxel-encapsulated Tz- targeting PLGA NPs showed encouraging results (Sakhi et al. 2022). In comparison to paclitaxel alone, the serum concentration (C_{max}), the area under the curve (AUC), the half-life ($t_{1/2}$), and the volume distribution (V_d) were increased by paclitaxel encapsulated PLGA; with reduced clearance (Cl). Intriguingly they used MCF7 cells as their only in vitro (“moderately HER2 expressing”) model.

In conclusion, although many questions remain to be answered, this project has achieved a critical exploration of NP-Tz dynamics in high and low HER2-expressing BC cells. The data shows NP-Tz specifically targeting DOX to BC cells enhances its cell toxicity compared to administering it as a free drug. The

generated targeting NPs also represent a promising new method for delivering therapies of the future such as siRNA and mRNA. As the field of NPs develops rapidly, new research is regularly published in the cancer and BC space with the hope that this work highlights how detailed cell analysis of NP cell dynamics is needed to give mechanistic information informing future NP design.

References:

Cancer Research UK. 2022. *Cancer Statistics for the UK*. [online] Available at: <https://www.cancerresearchuk.org/health-professional/cancer-statistics-for-the-uk#heading-Zero>.

Malvern Instruments Ltd. 2023. *Zeta potential - An introduction in 30 minutes*. [online] Available at: <https://www.research.colostate.edu/wpcontent/uploads/2018/11/ZetaPotential-Introduction-in-30min-Malvern.pdf>.

ProteinAtlas.org. 2022. *The Human Protein Atlas*. [online] Available at: <https://www.proteinatlas.org/>.

Who.int. 2022. *Early cancer diagnosis saves lives, cuts treatment costs*. [online] Available at: <https://www.who.int/news/item/03-02-2017-early-cancer-diagnosis-saves-lives-cuts-treatment-costs>.

Abdellatif, H. and Alsowinea, F. 2021. Approved and marketed nanoparticles for disease targeting and applications in COVID-19. *Nanotechnology Reviews* 10(1), p. 1941–1977. doi.10.1515/ntrev-2021-0115.

Acevedo-Olvera, L.F. et al. 2015. Inhibition of the Na⁺/H⁺ antiporter induces cell death in TF-1 erythroleukemia cells stimulated by the stem cell factor. *Cytokine* 75(1), p. 142–150. doi.10.1016/j.cyto.2015.06.020.

Agola, J.O. et al. 2011. Rab GTPases as regulators of endocytosis, targets of disease and therapeutic opportunities. *Clinical Genetics* 80(4), p. 305–318. doi.10.1111/j.1399-0004.2011.01724.x.

Alasvand, N. et al. 2017. Therapeutic nanoparticles for targeted delivery of anticancer drugs. *Multifunctional systems for combined delivery biosensing and diagnostics* 1(1), p. 245–259. doi.10.1016/B978-0-323-52725-5/00013-7.

Alirezaei, M. et al. 2022. Poly (lactic-co-glycolic acid) (PLGA)-based nanoparticles modified with chitosan-folic acid to delivery of *Artemisia vulgaris* L. essential oil to HT-29 cancer cells. *Process Biochemistry* 121(5), p.207-215. doi.10.1016/j.procbio.2022.06.034.

Altunay, B. et al. 2021. HER2-directed antibodies, affibodies and nanobodies as drug-delivery vehicles in breast cancer with a specific focus on radioimmunotherapy and radioimmunoimaging. *European Journal of Nuclear Medicine and Molecular Imaging* 48(5), p. 1371–1389. doi.10.1007/s00259-020-05094-1.

Alkabban, F. and Ferguson, T. 2021. Breast Cancer. *Treasure Island (FL): StatPearls Publishing* 2022, p. 1-20. PMID: 29493913.

Al Soraj, M. et al. 2012. siRNA and pharmacological inhibition of endocytic pathways to characterize the differential role of macropinocytosis and the actin cytoskeleton on cellular uptake of dextran and cationic cell penetrating peptides octaarginine (R8) and HIV-Tat. *Journal of Controlled Release* 161(1), p. 132–141. doi.10.1016/j.jconrel.2012.03.015.

Amith, S.R. et al. 2015. Na⁺/H⁺ exchange in the tumour microenvironment: Does NHE1 drive breast cancer carcinogenesis?. *International Journal of Developmental Biology* 59(7-8–9), p. 367–377. doi.10.1387/ijdb.1403361f.

- Amyere, M. et al. 2000. Constitutive Macropinocytosis in Oncogene-transformed Fibroblasts Depends on Sequential Permanent Activation of Phosphoinositide 3-Kinase and Phospholipase C. *Molecular Biology of the Cell* 11(10), p. 3453–3467. doi.10.1091/mbc.11.10.3453.
- Aparicio, S. et al. 2015. Examining the utility of patient-derived xenograft mouse models. *Nature Reviews Cancer* 15(5), p. 311–316. doi.10.1038/nrc3944.
- Araki, N. et al. 1996. A role for phosphoinositide 3-kinase in the completion of macropinocytosis and phagocytosis by macrophages. *Journal of Cell Biology* 135(5), p. 1249–1260. doi.10.1083/jcb.135.5.1249.
- Arienti, C. et al. 2019. Epidermal Growth Factor Receptor Family and its Role in Gastric Cancer. *Frontiers in Oncology* 9(11), p. 1–11. doi.10.3389/fonc.2019.01308.
- Ariyoshi, Y. et al. 2017. Na⁺/H⁺ exchanger 1 has tumor suppressive activity and prognostic value in esophageal squamous cell carcinoma. *Oncotarget* 8(2), p. 2209–2223. doi.10.18632/oncotarget.13645.
- Armstrong, G. and Olson, M.F. 2022. European Journal of Cell Biology Bending over backwards: BAR proteins and the actin cytoskeleton in mammalian receptor-mediated endocytosis. *European Journal of Cell Biology* 101(3), p. 151257. doi.10.1016/j.ejcb.2022.151257.
- Afzal, S. et al. 2022. Breast Cancer; Discovery of Novel Diagnostic Biomarkers, Drug Resistance, and Therapeutic Implications. *Frontiers in Molecular Biosciences* 9(2), p. 1–10. doi.10.3389/fmolb.2022.783450.
- Asher, C. et al. 1987. Effects of amiloride analogues on Na⁺ transport in toad bladder membrane vesicles. Evidence for two electrogenic transporters with different affinities toward pyrazinecarboxamides. *Journal of Biological Chemistry* 262(18), p. 8566–8573. doi.10.1016/s0021-9258(18)47451-0.
- Ashrafizadeh, M. et al. 2021. Biomedical application of chitosan-based nanoscale delivery systems: Potential usefulness in siRNA delivery for cancer therapy. *Carbohydrate Polymers* 260(2), p. 117809. doi.10.1016/j.carbpol.2021.117809.
- Aslantürk, Ö.S. 2018. In Vitro Cytotoxicity and Cell Viability Assays: Principles, Advantages, and Disadvantages. *Genotoxicity - A Predictable Risk to Our Actual World* 11(2), p. 1–18. doi.10.5772/intechopen.71923.
- Astete, C.E. and Sabliov, C.M., 2006. Synthesis and characterization of PLGA nanoparticles. *Journal of biomaterials science, polymer edition* 17(3), p. 247-289. doi.10.1163/156856206775997322.
- Aulic, S. et al. 2020. Breast cancer nanomedicine market update and other industrial perspectives of nanomedicine. *Nanomedicines for Breast Cancer Theranostics* 1(1), p. 371-404. doi.10.1016/b978-0-12-820016-2.00016-1.
- Austin, D. et al. 2004. Endocytosis and sorting of ErbB2 and the site of action of cancer therapeutics trastuzumab and geldanamycin. *Molecular biology of the cell* 15(12), p. 5268-5282. doi.10.1091/mbc.e04-07-0591.
- Azim, H.A. and Azim, H.A. 2012. Systemic treatment of brain metastases in HER2-positive breast cancer: Current status and future directions. *Future Oncology* 8(2), p.135-144. doi.10.2217/fon.11.149.
- Azimian Zavareh, V. et al. 2022. Three-Dimensional in Vitro Models: A Promising Tool to Scale-Up Breast Cancer Research. *ACS Biomaterials Science and Engineering* 8(11), p. 4648–4672. doi.10.1021/acsbomaterials.2c00277.

- Bachelot, T. et al. 2019. Preliminary safety and efficacy of first-line pertuzumab combined with trastuzumab and taxane therapy for HER2-positive locally recurrent or metastatic breast cancer. *Annals of Oncology* 30(5), p. 766–773. doi.10.1093/annonc/mdz 061.
- Badkas, A. et al. 2018. Modulation of in vitro phagocytic uptake and immunogenicity potential of modified Herceptin®-conjugated PLGA-PEG nanoparticles for drug delivery. *Colloids and Surfaces B: Biointerfaces* 162(1), p. 271–278. doi.10.1016/j.colsurfb.2017.12.001.
- Bagnato, P. et al. 2017. Cooperative but distinct early co-signaling events originate from ERBB2 and ERBB1 receptors upon trastuzumab treatment in breast cancer cells. *Oncotarget* 8(36), p. 60109–60122. doi.10.18632/oncotarget.17686.
- Bahrami, B. et al. 2015. Folate-conjugated nanoparticles as a potent therapeutic approach in targeted cancer therapy. *Tumor Biology* 36(8), p. 5727–5742. doi.10.1007/s13277-015-3706-6.
- Bamrungsap, S. et al. 2012. Pattern recognition of cancer cells using aptamer-conjugated magnetic nanoparticles. *ACS Nano* 6(5), p. 3974–3981. doi.10.1021/nn3002328.
- Bapat, P. et al. 2021. In vitro cytotoxicity of trastuzumab (Tz) and se-trastuzumab (se-tz) against the HER/2 breast cancer cell lines jimt-1 and BT474. *International journal of molecular sciences* 22(9), p. 4655. doi.10.3390/ijms22094655.
- Baravalle, G. et al. 2005. Transferrin recycling and dextran transport to lysosomes is differentially affected by bafilomycin, nocodazole, and low temperature. *Cell and Tissue Research* 320(1), p. 99–113. doi.10.1007/s00441-004-1060-x.
- Barok, M. et al. 2014. Trastuzumab emtansine: Mechanisms of action and drug resistance. *Breast Cancer Research* 16(2), p. 1-12. doi.10.1186/bcr3621.
- Barozzi, A. et al. 2020. Affibody-binding ligands. *International Journal of Molecular Sciences* 21(11), p. 3769. doi.10.3390/ijms21113769.
- Barros, F.F.T. et al. 2010. Understanding the HER family in breast cancer: Interaction with ligands, dimerization and treatments. *Histopathology* 56(5), p. 560–572. doi.10.1111/j.1365-2559.2010.03494.x.
- Bartholomeusz, C. and Gonzalez-Angulo, A.M. 2012. Targeting the PI3K signaling pathway in cancer therapy. *Expert Opinion on Therapeutic Targets* 16(1), p. 121–130. doi.10.1517/14728222.2011.644788.
- Bertelsen, V. and Stang, E. 2014. The mysterious ways of ErbB2/HER2 trafficking. *Membranes* 4(3), p. 424–446. doi.10.3390/membranes4030424.
- Bhagwat, G.S. et al. 2020. Formulation and Development of Transferrin Targeted Solid Lipid Nanoparticles for Breast Cancer Therapy. *Frontiers in Pharmacology* 27(11), p. 614290. doi.10.3389/fphar.2020.614290.
- Bhasarkar, J.B. and Bal, D.K. 2021. Nanomaterial-based advanced oxidation processes for degradation of waste pollutants. *Handbook of Nanomaterials for Wastewater Treatment* 1(1), p. 811–831. doi.10.1016/B978-0-12-821496-1.00003-9.
- Białkowska, K. et al. 2020. Spheroids as a type of three-dimensional cell cultures—examples of methods of preparation and the most important application. *International Journal of Molecular Sciences* 21(17), p. 1–17. doi. 10.3390/ijms21176225.
- Bitsikas, V. et al. 2014. Clathrin-independent pathways do not contribute significantly to endocytic flux. *eLife* 3(17), p. 1–26. doi.10.7554/eLife.03970.

- Blair, S. et al. 2021. Rainbow trout (*Oncorhynchus mykiss*) NA⁺/H⁺ exchangers tnhe3a and tnhe3b display unique inhibitory profiles dissimilar from mammalian nhe isoforms. *International Journal of Molecular Sciences* 22(4), p. 1–17. doi.10.3390/ijms22042205.
- Blanco, E. et al. 2015. perspective Principles of nanoparticle design for overcoming biological barriers to drug delivery. *Nature biotechnology* 33(9), p. 941-951. doi.10.1038/nbt.3330.
- Bobo, D. et al. 2016. Nanoparticle-based medicines: a review of FDA-approved materials and clinical trials to date. *Pharmaceutical research* 33(10), p. 2373-2387. doi.10.1007/s11095-016-1958-5.
- Bohdanowicz, M. and Grinstein, S. 2022. Role of phospholipids in endocytosis, phagocytosis, and macropinocytosis. 93(1), p. 69–106. doi.10.1152/physrev.00002.2012.
- Bose, R. et al. 2021. Breast cancer, HER2 mutations, and overcoming drug resistance. *New England Journal of Medicine* 385(13), p.1241-1243. doi.10.1056/NEJMci br2110552.
- Bosetti, R. and Jones, S.L. 2019. Cost-effectiveness of nanomedicine: Estimating the real size of nano-costs. *Nanomedicine* 14(11), p. 1367–1370. doi.10.2217/nnm-2019-0130.
- Braissant, O. et al. 2020. A Review of Methods to Determine Viability, Vitality, and Metabolic Rates in Microbiology. *Frontiers in Microbiology* 11(2), p. 1–25. doi.10.3389/fmicb.2020.547458.
- Bray, F. et al. 2018. Global cancer statistics 2018: GLOBOCAN estimates of incidence and mortality worldwide for 36 cancers in 185 countries. *CA: A Cancer Journal for Clinicians* 68(6), p. 394–424. doi.10.3322/caac.21492.
- Brigger, I. et al. 2012. Nanoparticles in cancer therapy and diagnosis. *Advanced Drug Delivery Reviews* 64(1), p. 24–36. doi.10.1016/j.addr.2012.09.006.
- Burugula, B. et al. 2011. Curcumin attenuates staurosporine-mediated death of retinal ganglion cells. *Investigative Ophthalmology and Visual Science* 52(7), p. 4263–4273. doi.10.1167/iovs.10-7103.
- Cagel, M. et al. 2017. Doxorubicin: nanotechnological overviews from bench to bedside. *Drug Discovery Today* 22(2), p. 270–281. doi.10.1016/j.drudis.2016.11.005.
- Cao, H. et al. 2007. Dynamin 2 mediates fluid-phase micropinocytosis in epithelial cells. *Journal of cell science* 120(23), p. 4167-4177. doi.10.1242/jcs.010686.
- Capelan, M. et al. 2013. Pertuzumab: New hope for patients with HER2-positive breast cancer. *Annals of Oncology* 24(2), p. 273–282. doi.10.1093/annonc/mds328.
- Cardone, R.A. et al. 2005. The role of disturbed pH dynamics and the NA⁺/H⁺ exchanger in metastasis. *Nature Reviews Cancer* 5(10), p. 786–795. doi.10.1038/nrc1713.
- Cardone, R.A. et al. 2015. A Novel NHE1-Centered Signaling Cassette Drives Epidermal Growth Factor Receptor–Dependent Pancreatic Tumor Metastasis and Is a Target for Combination Therapy. *Neoplasia* 17(2), p. 155–166. doi.10.1016/j.neo.2014.12.003.
- Ceresa, B.P. 2006. Regulation of EGFR endocytic trafficking by rab proteins. *Histology and Histopathology* 21(7–9), p. 987–993. doi.10.14670/HH-21.987.
- Champion, J.A. et al. 2007. Particle shape : A new design parameter for micro- and nanoscale drug delivery carriers. *Journal of controlled release* 121(1-2), p. 3-9. doi.10.1016/j.jconrel.2007.03.022.

- Chang, C.C. et al. 2014. Role of specific endocytic pathways in electrotransfection of cells. *Molecular Therapy - Methods and Clinical Development* 1(7), p. 14058. doi.10.1038/mtm.2014.58.
- Chen, B. et al. 2016. Targeting negative surface charges of cancer cells by multifunctional nanoprobe. *Theranostics* 6(11), p. 1887–1898. doi.10.7150/thno.16358.
- Chen, Q. et al. 2019. Increased NHE1 expression is targeted by specific inhibitor cariporide to sensitize resistant breast cancer cells to doxorubicin in vitro and in vivo. *BMC Cancer* 19(1), p. 1–13. doi.10.1186/s12885-019-5397-7.
- Chen, L. et al. 2011. The role of surface charge on the uptake and biocompatibility of hydroxyapatite nanoparticles with osteoblast cells. *Nanotechnology* 22(10), p. 105708. doi.10.1088/0957-4484/22/10/105708.
- Cheng, J.P.X. and Nichols, B.J. 2016. Caveolae : One Function or Many ?. *Trends in Cell Biology* 26(3), p. 177–189. doi.10.1016/j.tcb.2015.10.010.
- Chi, X. et al. 2013. Roles of Rho GTPases in Intracellular Transport and Cellular Transformation. *International journal of molecular sciences* 14(4), p. 7089–7108. doi.10.3390/ijms14047089.
- Chiasson-Mackenzie, C. et al. 2018. Merlin/ERM proteins regulate growth factor-induced macropinocytosis and receptor recycling by organizing the plasma membrane:Cytoskeleton interface. *Genes and Development* 32(17–18), p. 1201–1214. doi.10.1101/gad.317354.118.
- Chiu, H.I. et al. 2021. Cytotoxicity of targeted PLGA nanoparticles: a systematic review. *RSC Advances* 11(16), p. 9433–9449. doi.10.1039/d1ra00074h.
- Cho, K. et al. 2008. Therapeutic nanoparticles for drug delivery in cancer. *Clinical Cancer Research* 14(5), p. 1310–1316. doi.10.1158/1078-0432.CCR-07-1441.
- Choi, J.S. et al. 2018. Comparison of adsorption and conjugation of Herceptin on poly(lactic-co-glycolic acid) nanoparticles – Effect on cell internalization in breast cancer cells. *Materials Science and Engineering C* 92(1), p. 496–507. doi.10.1016/j.msec.2018.06.059.
- Choi, Y. et al. 2020. Doxorubicin-loaded plga nanoparticles for cancer therapy: Molecular weight effect of plga in doxorubicin release for controlling immunogenic cell death. *Pharmaceutics* 12(12), p. 1–18. doi.10.3390/pharmaceutics12121165.
- Colzani, B. et al. 2018. Investigation of antitumor activities of trastuzumab delivered by PLGA nanoparticles. *International Journal of Nanomedicine* 957(13), p. 957–973. doi.10.2147/IJN.S152742.
- Conti, V. and Guerrini, R. 2017. Human Mutations Associated With Brain Malformations Resulting in Hyperexcitability in Rodents. *Models of Seizures and Epilepsy* 1(1), p. 827-844. doi.10.1016/B978-0-12-804066-9/00056-0.
- Cortese, K. et al. 2008. Clathrin and LRP-1-independent constitutive endocytosis and recycling of uPAR. *PLoS ONE* 3(11), p. e3730. doi.10.1371/journal.pone.0003730.
- Cortese, K. et al. 2013. The HSP90 inhibitor geldanamycin perturbs endosomal structure and drives recycling ErbB2 and transferrin to modified MVBs/lysosomal compartments. *Molecular Biology of the Cell* 24(2), p. 129–144. doi.10.1091/mbc.E12-04-0282.
- Cossart, P. and Helenius, A. 2014. Endocytosis of viruses and bacteria. *Cold Spring Harbor Perspectives in Biology* 6(8), p. a016972. doi.10.1101/cshperspect.a016972.

- Coussens, L. et al. 1985. Tyrosine kinase receptor with extensive homology to EGF receptor shares chromosomal location with neu oncogene. *Science* 230(4730), p. 1132–1139. doi.10.1126/science.2999974.
- Cullen, P.J. and Steinberg, F. 2018. To degrade or not to degrade: mechanisms and significance of endocytic recycling. *Nature Reviews Molecular Cell Biology* 19(11), p. 679–696. doi.10.1038/s41580-018-0053-7.
- Dai, X. et al. 2015. Breast cancer intrinsic subtype classification, clinical use and future trends. *American Journal of Cancer Research* 5(10), p. 2929–2943. doi.10.2156-6976/ajcr0014158.
- Dai, X. et al. 2007. Inhibition of TRPP3 Channel by Amiloride and Analogs. *Molecular pharmacology* 72(6), p. 1576–1585. doi.10.1124/mol.107.037150.
- Davodabadi, F. et al. 2022. Breast cancer vaccines: New insights into immunomodulatory and nano-therapeutic approaches. *Journal of Controlled Release* 349(1), p. 844–875. doi.10.1016/j.jconrel.2022.07.036.
- Deeks, E.D. 2017. Neratinib: First Global Approval. *Drugs* 77(15), p. 1695–1704. doi.10.1007/s40265-017-0811-4.
- Degobert, G. and Aydin, D. 2021. Lyophilization of nanocapsules: Instability sources, formulation and process parameters. *Pharmaceutics* 13(8), p. 1112–1138. doi.10.3390/pharmaceutics13 081112.
- de Lázaro, I. and Mooney, D.J. 2020. A nanoparticle’s pathway into tumours. *Nature Materials* 19(5), p. 486–487. doi.10.1038/s41563-020-0669-9
- Deng, H. et al. 2018. General Subjects Stochastic simulations of nanoparticle internalization through transferrin receptor dependent clathrin-mediated endocytosis. *Biochimica et Biophysica Acta (BBA) - Molecular Cell Research* 1862(9), p. 2104–2111. doi.10.1016/j.bbagen. 2018.06.018.
- Derakhshani, A. et al. 2020. Overcoming trastuzumab resistance in HER2-positive breast cancer using combination therapy. *Journal of Cellular Physiology* 235(4), p. 3142–3156. doi.10.1002/jcp.29216.
- Desai, A.S. et al. 2019. Using macropinocytosis for intracellular delivery of therapeutic nucleic acids to tumour cells. *Philosophical Transactions of the Royal Society B: Biological Sciences* 374(1765). p. 20180156. doi.10.1098/rstb.2018.0156.
- Devarajan, P. V and Dandekar, P. 2019. Targeted Intracellular Drug Delivery by Receptor Mediated Endocytosis. *Springer* 39(1), doi.10.1007/978-3-030-29168-6.
- Deville, S. et al. 2015. Intracellular dynamics and fate of polystyrene nanoparticles in A549 Lung epithelial cells monitored by image (cross-) correlation spectroscopy and single particle tracking. *Biochimica et Biophysica Acta (BBA) - Molecular Cell Research* 1853(10), p. 2411–2419. doi.10.1016/j.bbamcr.2015.07.004.
- Di, J. et al. 2021. Size, shape, charge and “stealthy” surface: Carrier properties affect the drug circulation time in vivo. *Asian Journal of Pharmaceutical Sciences* 16(4), p. 444–458. doi.10.1016/j.ajps.2020.07.005.
- Dobrolecki, L.E. et al. 2016. Patient-derived xenograft (PDX) models in basic and translational breast cancer research. *Cancer and Metastasis Reviews* 35(4), p. 547–573. doi.10.1007/s10555-016-9653-x.
- Doherty, G.J. and McMahon, H.T. 2009. Mechanisms of Endocytosis. *Annual Review of Biochemistry*, p. 857–902. doi.10.1146/annurev.biochem.78.081307.110540.

- Dokmanovic, M. et al. 2009. Rac1 contributes to trastuzumab resistance of breast cancer cells: Rac1 as a potential therapeutic target for the treatment of trastuzumab-resistant breast cancer. *Molecular Cancer Therapeutics* 8(6), p. 1557–1569. doi.10.1158/1535-7163.MCT-09-0140.
- Dokmanovic, M. et al. 2014. Trastuzumab-induced recruitment of Csk-homologous kinase (CHK) to ErbB2 receptor is associated with ErbB2-Y1248 phosphorylation and ErbB2 degradation to mediate cell growth inhibition. *Cancer Biology and Therapy* 15(8), p.1029–1041. doi.10.4161/cbt.29171.
- Dou, Y. et al. 2017. To heat or not to heat: Challenges with clinical translation of thermosensitive liposomes. *Journal of Controlled Release* 249(10), p. 63–73. doi.10.1016/j.jconrel.2017.01.025.
- De Domenico, I. et al. 2008. Regulation of iron acquisition and storage: Consequences for iron-linked disorders. *Nature Reviews Molecular Cell Biology* 9(1), p. 72–81. doi.10.1038/nrm2295.
- Di Modica, M. et al. 2017. Predicting the Efficacy of HER2-Targeted Therapies: A Look at the Host. *Disease Markers* 2017(10), p. 1-14. doi.10.1155/2017/7849108.
- Donaldson, J.G. 2019. Macropinosome formation, maturation and membrane recycling: lessons from clathrin-independent endosomal membrane systems. *Philosophical Transactions of the Royal Society B* 374(1765), p. 20180148. doi.10.1098/rstb.2018.0148.
- Drago, J.Z. et al. 2022. Beyond HER2: Targeting the ErbB receptor family in breast cancer. *Cancer Treatment Reviews* 109(1), p. 102436. doi.10.1016/j.ctrv.2022.102436.
- Drebin, J.A. et al. 1986. Inhibition of tumor growth by a monoclonal antibody reactive with an oncogene-encoded tumor antigen. *Proceedings of the National Academy of Sciences* 83(23), p. 9129–9133. doi.10.1073/pnas.83.23.9129.
- Dristant, U. et al. 2023. An Overview of Polymeric Nanoparticles- Based Drug Delivery System in Cancer Treatment. *Technology in Cancer Research & Treatment* 22(1), p. 1-18. doi.10.1177/15330338231152083.
- Drumm, K. et al. 2003. Albumin and glucose effects on cell growth parameters, albumin uptake and Na⁺/H⁺-exchanger isoform 3 in OK cells. *Cellular Physiology and Biochemistry* 13(4), p. 199–206. doi.10.1159/000072422.
- Duan, D. et al. 2018. Trastuzumab-and Fab' fragment-modified curcumin PEG-PLGA nanoparticles: Preparation and evaluation in vitro and in vivo. *International Journal of Nanomedicine* 13(3), p. 1831–1840. doi.10.2147/IJN.S153795.
- Duffy, M.J. et al. 2015. Biomarkers in Breast Cancer: Where Are We and Where Are We Going?. *Advances in clinical chemistry* 71(1), p. 1-23. doi.10.1016/bs.acc.2015.05.001.
- Dutta, D. and Donaldson, J.G. 2012. Search for inhibitors of endocytosis. *Cellular Logistics* 2(4), p. 203–208. doi.10.4161/cl.23967.
- EI-Hammadi, M.M. et al. 2017. Folic acid-decorated and PEGylated PLGA nanoparticles for improving the antitumour activity of 5-fluorouracil. *International Journal of Pharmaceutics* 516(1–2), p. 61–70. doi.10.1016/j.ijpharm.2016.11.012.
- Evangelopoulos, M. et al. 2018. Trends towards biomimicry in theranostics. *Nanomaterials* 8(9), p. 1–20. doi.10.3390/nano8090637.

- Fathian, F. et al. 2019. Active targeting carrier for breast cancer treatment: Monoclonal antibody conjugated epirubicin loaded nanoparticle. *Journal of Drug Delivery Science and Technology* 53(10), p. 101136. doi.10.1016/j.jddst.2019.101136.
- Fatehah, M.O. et al. 2015. Nanoparticle Properties, Behavior, Fate in Aquatic Systems and Characterization Methods. *Journal of Colloid Science and Biotechnology* 3(2), p. 111–140. doi.10.1166/jcsb.2014.1090.
- Feng, H. et al. 2013. Role of caveolin-1 and caveolae signaling in endotoxemia and sepsis. *Life Sciences* 93(1), p. 1–6. doi.10.1016/j.lfs.2013.05.016.
- Ferreira, A.P.A. and Boucrot, E. 2018. Mechanisms of Carrier Formation during Clathrin-Independent Endocytosis. *Trends in Cell Biology* 28(3), p. 188–200. doi.10.1016/j.tcb.2017.11.004.
- Ferro-Flores, G. 2018. Targeted Nanomedicines: In the Right Route Towards Improved Therapies. *Current Cancer Therapy Reviews* 16(1), p. 3–4. doi.10.2174/1573394715666181224144500.
- Fichter, C.D. et al. 2018. A new model system identifies EGFR/HER2 and HER2/HER3 heterodimers as potent inducers of oesophageal epithelial cell invasion. *The Journal of pathology* 243(4), p. 481–495. doi.10.1002/path.4987.A.
- Fisusi, F. et al. 2020. Studies on polyethylene glycol-monooclonal antibody conjugates for fabrication of nanoparticles for biomedical applications. *Journal of nanoscience and nanomedicine* 4(2), p. 1–9. PMC7869852.
- Fontoura, J.C. et al. 2020. Comparison of 2D and 3D cell culture models for cell growth, gene expression and drug resistance. *Materials Science and Engineering C* 107(9), p. 110264. doi.10.1016/j.msec.2019.110264.
- Foulkes, W.D. et al. 2010. Triple-Negative Breast Cancer. *New England journal of medicine* 363(20), p. 1938-1948. doi.10.1056/nejmra1001389
- Francia, V. et al. 2019. Corona Composition Can Affect the Mechanisms Cells Use to Internalize Nanoparticles. *ACS Nano* 13(10), p. 11107–11121. doi.10.1021/acsnano.9b03824.
- Franco, Y.L. et al. 2018. Anticancer and cardio-protective effects of liposomal doxorubicin in the treatment of breast cancer. *Breast Cancer: Targets and Therapy* 10(11), p. 131–141. doi.10.2147/BCTT.S170239.
- Fretz, M. et al. 2006. Effects of Na⁺/H⁺ exchanger inhibitors on subcellular localisation of endocytic organelles and intracellular dynamics of protein transduction domains HIV-TAT peptide and octaarginine. *Journal of Controlled Release* 116(2), p. 247-254. doi.10.1016/j.jconrel.2006.07.009.
- Frelin, C. et al. 1988. Amiloride and its analogs as tools to inhibit Na⁺ transport via the Na⁺ channel, the Na⁺/H⁺ antiport and the Na⁺/Ca²⁺ exchanger. *Biochimie* 70(9), p. 1285–1290. doi.10.1016/0300-9084(88)90196-4.
- Frost, B. et al. 2009. Propagation of Tau Misfolding from the Outside to the Inside of a Cell. *Journal of Biological Chemistry* 284(19), p. 12845–12852. doi.10.1074/jbc.M808759200.
- Fu, X. et al. 2020. Precise design strategies of nanomedicine for improving cancer therapeutic efficacy using subcellular targeting. *Signal Transduction and Targeted Therapy* 5(1), p. 1–15. doi.10.1038/s41392-020-00342-0.

- Fuster, D.G. and Alexander, R.T. 2014. Traditional and emerging roles for the SLC9 Na⁺/H⁺ exchangers. *Pflugers Archiv European Journal of Physiology* 466(1), p. 61–76. doi.10.1007/s00424-013-1408-8.
- Furrer, D. et al. 2018. The human epidermal growth factor receptor 2 (HER2) as a prognostic and predictive biomarker: Molecular insights into HER2 activation and diagnostic implications. *Cancer Prognosis* 5, p. 11-21. doi.10.5772/intechopen.7827 1.
- Gabizon, A.A. et al. 2020. Translational considerations in nanomedicine: The oncology perspective. *Advanced Drug Delivery Reviews* 158, p. 140–157. doi.10.1016/j.addr.2020.05.012.
- Gaibar, M. et al. 2022. FGFR1 Amplification and Response to Neoadjuvant Anti-HER2 Treatment in Early HER2-Positive Breast Cancer. *Pharmaceutics* 14(2), p. 1–9. doi.10.3390/pharmaceutics14020242.
- Gajria, D. and Chandarlapaty, S. 2011. HER2-amplified breast cancer: Mechanisms of trastuzumab resistance and novel targeted therapies. *Expert Review of Anticancer Therapy* 11(2), p. 263–275. doi.10.1586/era.10.226.
- Gall, V.A. et al. 2017. Trastuzumab increases HER2 uptake and cross-presentation by dendritic cells. *Cancer Research* 77(19), p. 5374–5383. doi.10.1158/0008-5472.CAN-16-2774.
- Galvao, J. et al. 2014. Unexpected low-dose toxicity of the universal solvent DMSO. *FASEB Journal* 28(3), p. 1317–1330. doi.10.1096/fj.13-235440.
- Gao, Z. and Ijzerman, A.P. 2000. Allosteric Modulation of A 2A Adenosine Receptors by Amiloride Analogues and Sodium Ions. *Biochemical pharmacology* 60(5), p. 669–676. doi.10.1016/s0006-2952(00)00360-9.
- García-Alonso, S. et al. 2020. Trastuzumab Emtansine: Mechanisms of Action and Resistance, Clinical Progress, and Beyond. *Trends in Cancer* 6(2), p. 130–146. doi.10.1016/j.trecan.2019.12.010.
- Garcia, S.A. de B. et al. 2020. Dataset of HOXB7, HOXB8 and HOXB9 expression profiles in cell lines representative of the breast cancer molecular subtypes Luminal a (MCF7), Luminal b (BT474), HER2+ (SKBR3) and triple-negative (MDA231, MDA468), compared to a model of normal cells (MCF10A). *Data in Brief* 30(2020), p. 3–8. doi.10.1016/j.dib.2020.105572.
- Garritsen, A. et al. 1991. Receptor binding profiles of amiloride analogues provide no evidence for a link between receptors and the na⁺/h⁺ exchange, but indicate a common structure on receptor proteins. *Journal of Receptors and Signal Transduction* 11(6), p. 891–907. doi.10.3109/10799899109064686.
- Garritsen, A. et al. 1992. The mode of interaction of amiloride and some of its analogues with the adenosine A1 receptor. *Neurochemistry international* 20(2), p. 207-213. doi.10.1016/0197-0186(92)90169-r.
- Gavas, S. et al. 2021. Nanoparticles for Cancer Therapy: Current Progress and Challenges. *Nanoscale Research Letters* 16(1), p. 1-21. doi.10.1186/s11671-021-03628-6.
- Gazmuri, R.J. et al. 2019. Sodium-hydrogen exchanger isoform-1 inhibition: A promising pharmacological intervention for resuscitation from cardiac arrest. *Molecules* 24(9), p. 1765. doi.10.3390/molecules24091765.

- Gekle, M. et al. 2001. Inhibition of Na⁺-H⁺ exchanger-3 interferes with apical receptor-mediated endocytosis via vesicle fusion. *Journal of Physiology* 531(3), p. 619–629. doi.10.1111/j.1469-7793.2001.0619h.x.
- Gianni, L. 2018. Is there room for another HER2-targeting drug?. *The Lancet Oncology* 19(7), p. 847–849. doi.10.1016/S1470-2045(18)30405-4.
- Gkouvatsos, K. et al. 2012. Regulation of iron transport and the role of transferrin. *Biochimica et Biophysica Acta (BBA) - General Subjects* 1820(3), p. 188–202. doi.10.1016/j.bbagen.2011.10.013.
- Glebov, O.O. et al. 2006. Flotillin-1 defines a clathrin-independent endocytic pathway in mammalian cells. *Nature Cell Biology* 8(1), p. 46–54. doi.10.1038/ncb1342.
- Gomme, P.T. et al. 2005. Transferrin: structure, function and potential therapeutic actions. *Drug discovery today* 10(4), p. 267-273. doi.10.1016/S1359-6446(04)03333-1.
- Granja, S. et al. 2017. Value of pH regulators in the diagnosis, prognosis and treatment of cancer. *Seminars in Cancer Biology* 43(4), p. 17–34. doi.10.1016/j.semcancer.2016.12.003.
- Grossmann, A.H. et al. 2019. The small GTPase ARF6 regulates protein trafficking to control cellular function during development and in disease. *Small GTPases* 10(1), p. 1–12. doi.10.1080/21541248.2016.1259710.
- Guo, S. and Huang, L. 2014. Nanoparticles containing insoluble drug for cancer therapy. *Biotechnology Advances* 32(4), p. 778-788. doi.10.1016/j.biotechadv.2013.10.002.
- Guo, Y. et al. 2020. ERK/MAPK signalling pathway and tumorigenesis. *Experimental and Therapeutic Medicine* 19(3), p. 1997–2007. doi.10.3892/etm.2020.8454.
- Hadar, J. et al. 2019. Characterization of branched poly (lactide-co-glycolide) polymers used in injectable, long-acting formulations. *Journal of Controlled Release* 304(28), p. 75-89. doi.10.1016/j.jconrel.2019.04.039.
- Haikala, H.M. and Jänne, P.A. 2021. Thirty years of HER3: From basic biology to therapeutic interventions. *Clinical Cancer Research* 27(13), p. 3528–3539. doi.10.1158/1078-0432.CCR-20-4465.
- Hao, Y. et al. 2019. Cryo-EM Structure of HER2-trastuzumab-pertuzumab complex. *PLoS One* 14(5), p. e0216095. doi.10.2210/pdb6oge/pdb.
- Haroon, H.B. et al. 2022. A brief history of long circulating nanoparticles. *Advanced Drug Delivery Reviews* 188(5), p. 114396. doi.10.1016/j.addr.2022.114396.
- Harguindey, S. et al. 2013. Cariporide and other new and powerful NHE1 inhibitors as potentially selective anticancerdrugs - an integral molecular/biochemical/metabolic/clinical approach after one hundred years of cancer research. *Journal of Translational Medicine* 11(1), p. 1-17. doi.10.1186/1479-5876-11-282.
- Harris, C. and Fliegel, L. 1999. Amiloride and the Na⁺/H⁺ exchanger protein: Mechanism and significance of inhibition of the Na⁺/H⁺ exchanger (Review). *International Journal of Molecular Medicine* 3(3), p. 315–321. doi. 10.3892/ijmm.3.3.315.
- Hashida, M. 2022. Advocation and advancements of EPR effect theory in drug delivery science: A commentary. *Journal of Controlled Release* 346(6), p. 355–357. doi.10.1016/j.jconrel.2022.04.031.

- Hashizume, H. et al. 2000. Openings between defective endothelial cells explain tumor vessel leakiness. *American Journal of Pathology* 156(4), p. 1363-1380. doi.10.1016/S0002-9440(10)65006-7.
- Haque, S. et al. 2018. Histomorphological study of urinary bladder tumor and status of HER2/Neu and Ki67 expression in urothelial carcinoma. *Histopathol Cytopathol* 2(2), p. 99-108.
- Hayward, S.L. et al. 2016. Hyaluronic acid-conjugated liposome nanoparticles for targeted delivery to CD44 overexpressing glioblastoma cells. *Oncotarget* 7(23), p. 34158–34171. doi.10.18632/oncotarget.8926.
- Hanslick, J.L. et al. 2009. Dimethyl sulfoxide (DMSO) produces widespread apoptosis in the developing central nervous system. *Neurobiology of disease* 34(1), p. 1-10. doi.10.1016/j.nbd.2008.11.006.
- He, C. et al. 2010. Effects of particle size and surface charge on cellular uptake and biodistribution of polymeric nanoparticles. *Biomaterials* 31(13), p. 3657–3666. doi.10.1016/j.biomaterials.2010.01.065.
- Henne, W.M. et al. 2010. FCHo proteins are nucleators of Clathrin-Mediated endocytosis. *Science* 328(5983), p. 1281–1284. doi.10.1126/science.1188462.
- Hervent, A.S. and De Keulenaer, G.W. 2012. Molecular mechanisms of cardiotoxicity induced by ErbB receptor inhibitor cancer therapeutics. *International Journal of Molecular Sciences* 13(10), p. 12268–12286. doi.10.3390/ijms131012268.
- Hetzel, D.J. 1992. HER-2 / neu Expression : A Major Prognostic Factor in Endometrial Cancer. *Gynecologic oncology* 47(2), p. 179–185. doi.10.1016/0090-8258(92)90103-P.
- Hobbs, S.K. et al. 1998. Regulation of transport pathways in tumor vessels: Role of tumor type and microenvironment. *Proceedings of the National Academy of Sciences of the United States of America* 95(8), p. 4607–4612. doi.10.1073/pnas.95.8.4607.
- Honary, S. and Zahir, F. 2013. Effect of Zeta Potential on the Properties of Nano-Drug Delivery Systems - A Review (Part 1). *Tropical Journal of Pharmaceutical Research* 12(2), p. 255–264. doi.10.4314/tjpr.v12i2.20.
- Hopkins, C.R. et al. 1985. Receptor-mediated endocytosis of transferrin and epidermal growth factor receptors: A comparison of constitutive and ligand-induced uptake. *Journal of Cell Science* 1985(3), p. 173–186. doi.10.1242/jcs.1985.supplement_3.17.
- Hopkins, C.R. and Trowbridge, I.S. 1983. Internalization and processing of transferrin and the transferrin receptor in human carcinoma A431 cells. *Journal of Cell Biology* 97(2), p. 508–521. doi.10.1083/jcb.97.2.508.
- Hsu, J.L. and Hung, M.C. 2016. The role of HER2, EGFR, and other receptor tyrosine kinases in breast cancer. *Cancer and Metastasis Reviews* 35(4), p. 575–588. doi.10.1007/s10555-016-9649-6.
- Hubert, A. et al. 2000. Doxil (Caelyx): An exploratory study with pharmacokinetics in patients with hormone-refractory prostate cancer. *Anti-Cancer Drugs* 11(2), p. 123–127. doi.10.1097/00001813-200002000-00009.
- Hudis, C.A. 2007. Trastuzumab — Mechanism of Action and Use in Clinical Practice. *New England Journal of Medicine* 357(1), p. 39–51. doi.abs/10.1056/NEJMra043186.
- Hunter, F.W. et al. 2020. Mechanisms of resistance to trastuzumab emtansine (T-DM1) in HER2-positive breast cancer. *British Journal of Cancer* 122(5), p. 603–612. doi.10.1038/s41416-019-0635-y.

- Ibrahim, W.N. et al. 2020. Formulation, cellular uptake and cytotoxicity of thymoquinone-loaded plga nanoparticles in malignant melanoma cancer cells. *International Journal of Nanomedicine* 15(10), p. 8059–8074. doi.10.2147/IJN.S269340.
- Iqbal, N. and Iqbal, N. 2014. Human Epidermal Growth Factor Receptor 2 (HER2) in Cancers: Overexpression and Therapeutic Implications. *Molecular Biology International* 2014(9), p. 1–9. doi.10.1155/2014/852748.
- Iv, C.W.S. et al. 2020. Materials for Immunotherapy. *Advanced Materials* 32(13), p. 1–56. doi.10.1002/adma.201901633.
- Ivanov, A.I. 2008. Pharmacological inhibition of endocytic pathways: Is it specific enough to be useful?. *Methods in Molecular Biology* 440, p. 15–33. doi.10.1007/978-1-59745-178-9_2.
- Jahan, S. et al. 2021. Nanoparticles targeting receptors on breast cancer for efficient delivery of chemotherapeutics. *Biomedicines* 9(2), p. 1–30. doi.10.3390/biomedicines9020114.
- Janes, H. et al. 2015. The Fundamental Difficulty With Evaluating the Accuracy of Biomarkers for Guiding Treatment. *Journal of the National Cancer Institute* 107(8), p. 4–7. doi.10.1093/jnci/djv157.
- Jazayeri, M.H. et al. 2016. Various methods of gold nanoparticles (GNPs) conjugation to antibodies. *Sensing and Bio-Sensing Research* 9(1), p. 17–22. doi.10.1016/j.sbsr.2016.04.002.
- Jiang, Y. et al. 2022. Current understandings and clinical translation of nanomedicines for breast cancer therapy. *Advanced Drug Delivery Reviews* 180(1), p. 114034. doi.10.1016/j.addr.2021.114034.
- Jiang, Y. et al. 2015. The Interplay of Size and Surface Functionality on the Cellular Uptake of Sub-10 nm Gold Nanoparticles. *ACS Nano* 9(10), p. 9986–9993. doi.10.1021/acsnano.5b03521.
- Jin, J. et al. 2008. Clustering of endocytic organelles in parental and drug-resistant myeloid leukaemia cell lines lacking centrosomally organised microtubule arrays. *International Journal of Biochemistry and Cell Biology* 40(10), p. 2240–2252. doi.10.1016/j.biocel.2008.03.004.
- Jin, J. and Jones, A.T. 2009. The pH sensitive probe 5-(and-6)-carboxyl seminaphthorhodafluor is a substrate for the multidrug resistance-related protein MRP1. *International Journal of Cancer* 124(1), p. 233–238. doi.10.1002/ijc.23892.
- Jin, K.T. et al. 2020. Recent Trends in Nanocarrier-Based Targeted Chemotherapy: Selective Delivery of Anticancer Drugs for Effective Lung, Colon, Cervical, and Breast Cancer Treatment. *Journal of Nanomaterials* 2020(7), p. 1-14. doi.10.1155/2020/9184284.
- Jin, W. et al. 2012. Na⁺/H⁺ exchanger 1 inhibition contributes to K562 leukaemic cell differentiation. *Cell Biology International* 36(8), p. 739–745. doi.10.1042/cbi20100919.
- Jinesh, G.G. and Kamat, A.M. 2016. Blebbistatin emergency program: An apoptotic route to cellular transformation. *Cell Death and Differentiation* 23(5), p. 757–758. doi.10.1038/cdd.2016.26.
- Johannes, L. et al. 2015. Building endocytic pits without clathrin. *Nature reviews Molecular cell biology* 16(5), p. 311-321. doi.10.1038/nrm3968.

- Jonderian, A. and Maalouf, R. 2016. Formulation and in vitro interaction of rhodamine-B loaded PLGA nanoparticles with cardiac myocytes. *Frontiers in pharmacology* 7(458), p. 1–7. doi.10.3389/fphar.2016.00458.
- Jones, A.T. 2007. Macropinocytosis: Searching for an endocytic identity and role in the uptake of cell penetrating peptides. *Journal of Cellular and Molecular Medicine* 11(4), p. 670–684. doi.10.1111/j.1582-4934.2007.00062.x.
- Jose, S. et al. 2019. Transferrin-conjugated Docetaxel-PLGA nanoparticles for tumor targeting: Influence on MCF-7 cell cycle. *Polymers* 11(11), p. 1905. doi.10.3390/polym1111 1905.
- Joy, R. et al. 2022. Brief Outlook on Polymeric Nanoparticles, Micelles, Niosomes, Hydrogels and Liposomes: Preparative Methods and Action. *ChemistrySelect* 7(6), p. 1-18. doi.10.1002/slct.202104045.
- Juan, A. et al. 2020. An overview of antibody conjugated polymeric nanoparticles for breast cancer therapy. *Pharmaceutics* 12(9), p. 1–20. doi.10.3390/pharmaceutics120908 02.
- Julien, C. et al. 2012. Dimethyl sulfoxide induces both direct and indirect Tau hyperphosphorylation. *PLoS ONE* 7(6), p. 40020. doi.10.1371/journal.pone.0040020.
- Jurcut, R. et al. 2008. Strain Rate Imaging Detects Early Cardiac Effects of Pegylated Liposomal Doxorubicin as Adjuvant Therapy in Elderly Patients with Breast Cancer. *Journal of the American Society of Echocardiography* 21(12), p. 1283–1289. doi.10.1016/j.ech o.2008.10.005.
- Kaksonen, M. et al. 2006. Harnessing actin dynamics for clathrin-mediated endocytosis. *Nature Reviews Molecular Cell Biology* 7(6). p. 404-414. doi.10.1038/nrm1940.
- Kaksonen, M. and Roux, A. 2018. Mechanisms of clathrin-mediated endocytosis. *Nature Reviews Molecular Cell Biology* 19(5), p. 313–326. doi.10.1038/nrm.2017.132.
- Kawabata, H. 2019. Transferrin and transferrin receptors update. *Free Radical Biology and Medicine* 133(1), p. 46-54. doi.10.1016/j.freeradbiomed.2018.06.037.
- Kay, R.R. 2021. Macropinocytosis: Biology and mechanisms. *Cells and Development* 168(1), p. 203713. doi.10.1016/j.cdev.2021.203713.
- Kaźmierczak, Z. et al. 2020. Endocytosis in cellular uptake of drug delivery vectors: Molecular aspects in drug development. *Bioorganic and Medicinal Chemistry* 28(18), p. 115556. doi.10.1016/j.bmc.2020.115556.
- Khalil, H.S. et al. 2016. A novel mechanism of action of HER2 targeted immunotherapy is explained by inhibition of NRF2 function in ovarian cancer cells. *Oncotarget* 7(46), p. 75874–75901. doi.10.18632/oncotarget.12425.
- Khan, I. and Steeg, P.S. 2021. Endocytosis: a pivotal pathway for regulating metastasis. *British Journal of Cancer* 124(1), p. 66–75. doi.10.1038/s41416-020-01179-8.
- King, J.S. and Kay, R.R. 2019. The origins and evolution of macropinocytosis. *Philosophical Transactions of the Royal Society Biological Sciences* 374(1765). p. 20180158. doi.10.1098/rstb.2018.0158.
- Kim, C. et al. 2017. PTEN loss and level of HER2 amplification is associated with trastuzumab resistance and prognosis in HER2-positive gastric cancer. *Oncotarget* 8(69), p. 113494–113501. doi.10.18632/oncotarget.23054.

- Kim, S. et al. 2017. Drifts in ADCC-related quality attributes of Herceptin®: Impact on development of a trastuzumab biosimilar. *mAbs* 9(4), p. 704–714. doi.10.1080/19420862.2017.1305530.
- Kleyman, T.R. and Cragoe, E.J. 1988. Amiloride and its analogs as tools in the study of ion transport. *The Journal of Membrane Biology* 105(1), p. 1–21. doi.10.1007/BF01871102.
- Ko, M. et al. 2020. Emerging links between endosomal pH and cancer. *Cancer and Metastasis Reviews* 39(2), p. 519–534. doi.10.1007/s10555-020-09870-1.
- Kobayashi, H. et al. 2014. Improving conventional enhanced permeability and retention (EPR) effects; What is the appropriate target?. *Theranostics* 4(1), p. 81–89. doi.10.7150/thno.7193.
- Koivusalo, M. et al. 2010. Amiloride inhibits macropinocytosis by lowering submembranous pH and preventing Rac1 and Cdc42 signaling. *Journal of Cell Biology* 188(4), p. 547–563. doi.10.1083/jcb.200908086.
- Koltai, T. 2020. Targeting the pH paradigm at the bedside: A practical approach. *International Journal of Molecular Sciences* 21(23), p. 1–36. doi.10.3390/ijms21239221.
- Kon, E. et al. 2022. Principles for designing an optimal mRNA lipid nanoparticle vaccine. *Current Opinion in Biotechnology* 73(1), p. 329–336. doi.10.1016/j.copbio.202109.061.
- Korzeniecki, C. and Priefer, R. 2021. Targeting KRAS mutant cancers by preventing signaling transduction in the MAPK pathway. *European Journal of Medicinal Chemistry* 211(5), p. 113006. doi.10.1016/j.ejmech.2020.113006.
- Kreutzfeldt, J. et al. 2020. The trastuzumab era: current and upcoming targeted HER2+ breast cancer therapies. *American journal of cancer research* 10(4), p. 1045–1067. doi. ISSN:2156-6976/ajcr0109526.
- Kubota, T. et al. 2018. HER2-targeted gold nanoparticles potentially overcome resistance to trastuzumab in gastric cancer. *Nanomedicine: Nanotechnology, Biology, and Medicine* 14(6), p. 1919–1929. doi.10.1016/j.nano.2018.05.019.
- Kumar, R. et al. 2020. HER family in cancer progression: From discovery to 2020 and beyond. *Advances in cancer research* 147(1), p. 109-160. doi.10.1016/bs.acr.2020.04.001.
- Kute, T. et al. 2004. Development of Herceptin Resistance in Breast Cancer Cells. *Cytometry Part A* 57(2), p. 86–93. doi.10.1002/cyto.a.10095.
- Laeckmann, D. et al. 2002. Synthesis and biological evaluation of aroylguanidines related to amiloride as inhibitors of the human platelet Na⁺/H⁺ exchanger. *Bioorganic and Medicinal Chemistry* 10(6), p. 1793–1804. doi.10.1016/S0968-0896(02)00022-6.
- Lambies, G. and Commisso, C. 2022. Macropinocytosis and Cancer: From Tumor Stress to Signaling Pathways. *Macropinocytosis* 98(6). p.15-40. doi.10.1007/978-3-030-94004-1.
- Landeros, N. 2023. Preclinical and Clinical Trials of New Treatment Strategies Targeting Cancer Stem Cells in Subtypes of Breast Cancer. *Cells* 12(5), p. 720. doi.10.3390/cells12050720.
- Lao, J. et al. 2013. Liposomal Doxorubicin in the Treatment of Breast Cancer Patients: A Review. *Journal of Drug Delivery* 2013(5), p. 1–12. doi. 10.1155/2013/456409.

- Lazarovits, J. et al. 2015. Nanoparticle-blood interactions: The implications on solid tumour targeting. *Chemical Communications* 51(14), p. 2756–2767. doi.10.1039/C4CC07644C.
- Lee, Y.J. et al. 2017. Cariporide enhances the DNA damage and apoptosis in acid-tolerable malignant mesothelioma H-2452 cells. *Molecules and Cells* 40(8), p. 567–576. doi.10.14348/molcells.2017.0059.
- Lee, S. and Shanti, A. 2021. Effect of exogenous pH on cell growth of breast cancer cells. *International Journal of Molecular Sciences* 22(18), p. 9910. doi.10.3390/ijms22189910.
- Lee, S.W. et al. 2011. Development of docetaxel-loaded intravenous formulation, Nanoxel-PMTM using polymer-based delivery system. *Journal of Controlled Release* 155(2), p. 262–271. doi.10.1016/j.jconrel.2011.06.012.
- Lewis, W.H. 1937. Pinocytosis by malignant cells. *The American Journal of Cancer* 29(4), p. 666–679. doi.10.1158/ajc.1937.666.
- Leyton, J. 2020. Improving Receptor-Mediated Intracellular Access and Accumulation of Antibody Therapeutics—The Tale of HER2. *Antibodies* 9(3), p. 32. doi.10.3390/antib9030032.
- Li, G. et al. 2017. Biomarker studies in early detection and prognosis of breast cancer. *Advances in Experimental Medicine and Biology* 1026(1), p. 27–39. doi.10.1007/978-981-10-6020-5_2.
- Li, L. et al. 2015. The effect of the size of fluorescent dextran on its endocytic pathway. *Cell Biology International* 39(5), p. 531–539. doi.10.1002/cbin.10424.
- Li, N. et al. 2019. Herceptin-conjugated liposomes co-loaded with doxorubicin and simvastatin in targeted prostate cancer therapy. *American Journal of Translational Research* 11(3), p. 1255–1269. doi.1943-8141/AJTR0090830.
- Li, Y.X. and Pang, H.B. 2021. Macropinocytosis as a cell entry route for peptide-functionalized and bystander nanoparticles. *Journal of Controlled Release* 329(10), p. 1222–1230. doi.10.1016/j.jconrel.2020.10.049.
- Li, Y. et al. 2018. Nanoparticle-mediated therapeutic agent delivery for treating metastatic breast cancer—challenges and opportunities. *Nanomaterials* 8(6), p. 361 doi.10.3390/nano8060361.
- Lim, J.P. and Gleeson, P.A. 2011. Macropinocytosis: An endocytic pathway for internalising large gulps. *Immunology and Cell Biology* 89(8), p. 836–843. doi.10.1038/icb.2011.20.
- Listinsky, J.J. et al. 2013. Glycoengineering in cancer therapeutics: A review with fucose-depleted trastuzumab as the model. *Anti-Cancer Drugs* 24(3), p. 219–227. doi.10.1097/CAD.0b013e328359e3f4.
- Liu, A.P. et al. 2010. Local clustering of transferrin receptors promotes clathrin-coated pit initiation. *Journal of Cell Biology* 191(7), p. 1381–1393. doi.10.1083/jcb.201008117.
- Liu, C.Y. et al. 2019. Varlitinib downregulates HER/ERK signaling and induces apoptosis in triple negative breast cancer cells. *Cancers* 11(1), doi.10.3390/cancers11010105.
- Liu, J. et al. 2015. Biosensors and Bioelectronics Turn-on fluorescence sensor for the detection of heparin based on rhodamine B-modified polyethyleneimine – graphene oxide complex. *Biosensors and Bioelectronic* 64(15), p. 300–305. doi.10.1016/j.bios.2014.09.023.

- Liu, Z. and Roche, P. 2015. Macropinocytosis in phagocytes: regulation of MHC class-II-restricted antigen presentation in dendritic cells. *Frontiers in physiology* 6(1), p .1. doi. 10.3389/fphys.2015.00001.
- Loibl, S. and Gianni, L. 2017. Breast cancer 2 HER2-positive breast cancer. *The Lancet* 389(16), p. 2415–2429. doi.10.1016/ S0140-6736(16)32417-5.
- Lyu, H. et al. 2018. Understanding the biology of HER3 receptor as a therapeutic target in human cancer. *Acta Pharmaceutica Sinica B* 8(4), p. 503–510. doi.10.1016/j.apsb.2018.05.010.
- Malt, R.A. 1964. Ciba Foundation Symposium: Lysosomes. *Archives of Internal Medicine* 114(4), p. 566-567. doi.10.1001/archinte.1964.03860100148032.
- Maadi, H. et al. 2018. The effects of trastuzumab on HER2-mediated cell signaling in CHO cells expressing human HER2. *BMC Cancer* 18(1), p. 1–14. doi.10.1186/s12885-018-4143-x.
- Maadi, H. et al. 2021. Trastuzumab mechanism of action; 20 years of research to unravel a dilemma. *Cancers* 13(14), p. 1–17. doi.10.3390/ cancers13143540.
- Maeda, H. and Matsumura, Y. 1986. A new concept for macromolecular therapeutics in cancer chemotherapy: mechanism of tumortropic accumulation of proteins and the antitumor agent smancs. *Cancer Research* 46(12), p. 6387-6392. doi.10.1021/bc100070g.
- Maeda, Y. et al. 2021. Ibaraki virus enters host cells by macropinocytosis. *Virus Research* 302, p. 198492. doi.10.1016/j.virusres.2021.198492.
- Manzanares, D. and Ceña, V. 2020. Endocytosis: The nanoparticle and submicron nanocompounds gateway into the cell. *Pharmaceutics* 12(4), p. 1–22. doi. 10.3390/pharmaceutics12040371.
- Manzari, M.T. et al. 2021. Targeted drug delivery strategies for precision medicines. *Nature Reviews Materials* 6(4), p. 351–370. doi.10.1038/s41578-020-00269-6.
- Markham, A. 2021. Margetuximab: First Approval. *Drugs* 81(5), p. 599–604. doi.10.1007/s40265-021-01485-2.
- Martínez-Carmona, M. et al. 2018. Lectin-conjugated pH-responsive mesoporous silica nanoparticles for targeted bone cancer treatment. *Acta Biomaterialia* 65(1), p. 393–404. doi.10.1016/j.actbio.2017.11.007.
- Martínez-Sáez, O. and Prat, A. 2021. Current and Future Management of HER2-Positive Metastatic Breast Cancerther. *JCO Oncology Practice* 17(10), p. 594–604. doi. 10.1200/op.21.00172.
- Maruyama, I. 2014. Mechanisms of Activation of Receptor Tyrosine Kinases: Monomers or Dimers. *Cells* 3(2), p. 304–330. doi.10.3390/cells3020304.
- Masereel, B. et al. 2003. An overview of inhibitors of Na⁺/H⁺ exchanger. *European journal of medicinal chemistry* 38(6), p.547-554. doi.10.1016/S0223-5234(03)00100-4.
- Masoud, V. and Pagès, G. 2017. Targeted therapies in breast cancer: New challenges to fight against resistance. *World Journal of Clinical Oncology* 8(2), p. 120–134. doi.10.5306/wjco.v8.i2.120.
- Matsumoto, K. et al. 1984. Pathogenesis of serratial infection: Activation of the hageman factor-prekallikrein cascade by serratial protease. *Journal of Biochemistry* 96(3), p. 739-749. doi.10.1093/oxfordjournals.jbchem.a134892.

- Matthews, H. et al. 2011. Anti-tumour/metastasis effects of the potassium-sparing diuretic amiloride: An orally active anti-cancer drug waiting for its call-of-duty?. *International Journal of Cancer* 129(9), p. 2051–2061. doi.10.1002/ijc.26156.
- Mavaddat, N. et al. 2010. Genetic susceptibility to breast cancer. *Molecular Oncology* 4(3), p. 174–191. doi.10.1016/j.molonc.2010.04.011.
- Maxfield, F.R. and McGraw, T.E. 2004. Endocytic recycling. *Nature Reviews Molecular Cell Biology* 5(2), p. 121–132. doi.10.1038/nrm1315.
- Maximiano, S. et al. 2016. Trastuzumab in the Treatment of Breast Cancer. *BioDrugs* 30(2), p. 75–86. doi.10.1007/s40259-016-0162-9.
- Maylaa, T. et al. 2023. A Hierarchical Deep Learning Framework for Nuclei 3D Reconstruction from Microscopic Stack-Images of 3D Cancer Cell Culture. *Intelligent Sustainable Systems* 2, p. 225-235. doi.10.1007/978-981-19-7663-6_22.
- Mayor, S. et al. 2014. Clathrin-independent pathways of endocytosis. *Cold Spring Harbor Perspectives in Biology* 6(6), doi.10.1101/cshperspect.a016758.
- Meier, O. et al. 2002. Adenovirus triggers macropinocytosis and endosomal leakage together with its clathrin-mediated uptake. *Journal of Cell Biology* 158(6), p. 1119-1131. doi.10.1083/jcb.200112067.
- Mettlen, M. et al. 2018. Regulation of clathrin-mediated endocytosis. *Annual review of biochemistry* 87(20), p. 871-889. doi.10.1146/annurev-biochem-062917-012644.
- Meng, L. et al. 2018. Trastuzumab modified silica nanoparticles loaded with doxorubicin for targeted and synergic therapy of breast cancer. *Artificial Cells, Nanomedicine and Biotechnology* 46(3), p. S556–S563. doi.10.1080/21691401.2018.1501380.
- Merrifield, C.J. 2004. Seeing is believing: Imaging actin dynamics at single sites of endocytosis. *Trends in Cell Biology* 14(7), p. 352-358. doi.10.1016/j.tcb.2004.05.008.
- Midekessa, G. et al. 2020. Zeta Potential of Extracellular Vesicles: Toward Understanding the Attributes that Determine Colloidal Stability. *ACS Omega* 5(27), p. 16701–16710. doi.10.1021/acsomega.0c01582.
- Min, Y. et al. 2015. Clinical Translation of Nanomedicine. *Chemical Reviews* 115(19), p. 11147–11190. doi.10.1021/acs.chemrev.5b00116.
- Mitchell, M.J. et al. 2021. Engineering precision nanoparticles for drug delivery. *Nature Reviews Drug Discovery* 20(2), p. 101–124. doi.10.1038/s41573-020-0090-8.
- Mitchell, R.A. et al. 2018. Epidermal growth factor receptor: Structure-function informing the design of anticancer therapeutics. *Experimental Cell Research* 371(1), p. 1–19. doi.10.1016/j.yexcr.2018.08.009.
- Mitragotri, S. et al. 2014. Organic nanoparticles for drug delivery and imaging. *MRS Bulletin* 39(3), p. 219–223. doi.10.1557/mrs.2014.11.
- Modi, S. et al. 2020. Trastuzumab deruxtecan in previously treated HER2-positive breast cancer. *New England Journal of Medicine* 382(7), p. 610–621. doi.10.1056/NEJMoa1914510.
- Montagna, E. and Colleoni, M. 2019. Hormonal treatment combined with targeted therapies in endocrine-responsive and HER2-positive metastatic breast cancer. *Therapeutic Advances in Medical Oncology* 11(12), p.1-7. doi.10.1177/1758835919894105.

- Mondal, U.K. and Ilies, M.A. 2020. Efflux pumps, NHE1, monocarboxylate transporters, and ABC transporter subfamily inhibitors. *Elsevier Inc* 1(1). p. 95-120. doi.10.1016/B978-0-12-820701-7.00017-8.
- Mokhtarzadeh, A. et al. 2017. Biodegradable nano-polymers as delivery vehicles for therapeutic small non-coding ribonucleic acids. *Journal of Controlled Release* 245(10), p. 116–126. doi.10.1016/j.jconrel.2016.11.017.
- Momenimovahed, Z. and Salehiniya, H. 2019. Epidemiological characteristics of and risk factors for breast cancer in the world. *Breast Cancer: Targets and Therapy* 11(10), p. 151–164. doi.10.2147/BCTT.S176070.
- Montané, X. et al. 2020. Encapsulation for cancer therapy. *Molecules* 25(7), p. 1–25. doi.10.3390/molecules25071605.
- Moody, P.R. et al. 2015. Receptor Crosslinking: A General Method to Trigger Internalization and Lysosomal Targeting of Therapeutic Receptor:Ligand Complexes. *Molecular Therapy* 23(12), p. 1888–1898. doi.10.1038/mt.2015.178.
- Morales-Cruz, M. et al. 2019. Smart targeting to improve cancer therapeutics. *Drug Design, Development and Therapy* 13(30), p. 3753–3772. doi.10.2147/DDDT.S219489.
- Morris, S.A. and Schmid, S.L. 1995. Synaptic Vesicle Recycling: The Ferrari of endocytosis?. *Current Biology* 5(2), p. 113–115. doi.10.1016/S0960-9822(95)00028-5.
- Mosly, D. et al. 2018. Predictive markers of endocrine response in breast cancer. *World Journal of Experimental Medicine* 8(1), p. 1–7. doi.10.5493/wjem.v8.i1.1.
- Mu, J. et al. 2014. A Small-Molecule FRET Reporter for the Real-Time Visualization of Cell-Surface Proteolytic Enzyme Functions. *Angewandte Chemie* 126(52), p. 14585–14590. doi.10.1002/ange.201407182.
- Nahta, R. and Esteva, F.J. 2006. HER2 therapy: Molecular mechanisms of trastuzumab resistance. *Breast Cancer Research* 8(6), p. 1–8. doi.10.1186/bcr1612.
- Nami, B. et al. 2018. Mechanisms underlying the action and synergism of trastuzumab and pertuzumab in targeting HER2-positive breast cancer. *Cancers* 10(10), p. 324 doi.10.3390/cancers10100342.
- Nanda, J.S. and Lorsch, J.R., 2014. Labeling a protein with fluorophores using NHS ester derivitization. *Methods Enzymol* 536(1), p. 87-94. doi.10.1016/B978-0-12-420070-8.00008-8.
- Nazere, K. et al. 2022. Amyloid Beta Is Internalized via Macropinocytosis, an HSPG- and Lipid Raft-Dependent and Rac1-Mediated Process. *Frontiers in Molecular Neuroscience* 15(11), p. 1–11. doi.10.3389/fnmol.2022.804702.
- Neek, M. et al. 2019. Protein-based nanoparticles in cancer vaccine development. *Nanomedicine: Nanotechnology, Biology, and Medicine* 15(1), p. 164–174. doi.10.1016/j.nano.2018.09.004.
- Nguyen, S.T. et al. 2020. Comparative cytotoxic effects of methanol, ethanol and DMSO on human cancer cell lines. *Biomedical Research and Therapy* 7(7), p. 3855–3859. doi.10.15419/bmrat.v7i7.614.
- Nguyen, X. et al. 2021. A Review of Fam-Trastuzumab Deruxtecan-nxki in HER2-Positive Breast Cancer. *Annals of Pharmacotherapy* 55(11), p. 1410–1418. doi.10.1177/10600280 21998320.

- Niazi, M. et al. 2016. Nano-based strategies to overcome p-glycoprotein-mediated drug resistance. *Expert Opinion on Drug Metabolism and Toxicology* 12(9), p. 1021–1033. doi.10.1080/17425255.2016.1196186.
- Nieto, C. et al. 2020. Trastuzumab: More than a guide in her2-positive cancer nanomedicine. *Nanomaterials* 10(9), p. 1–20. doi.10.3390/nano10091674.
- Oganesyan, V. et al. 2018. Structural insights into the mechanism of action of a biparatopic anti-HER2 antibody. *Journal of Biological Chemistry* 293(22), p. 8439–8448. doi.10.1074/jbc.M117.818013.
- Ogun, S. and Adeyinka, A. 2021. Biochemistry, transferrin. *StatPearls*, p. 2–5. PMID: 30422523.
- Operti, M.C. et al. 2019. Microfluidics-assisted size tuning and biological evaluation of PLGA particles. *Pharmaceutics* 11(11), p. 1–17. doi.10.3390/pharmaceutics11110590.
- Obaid, G. et al. 2017. Activatable clinical fluorophore-quencher antibody pairs as dual molecular probes for the enhanced specificity of image-guided surgery. *Journal of Biomedical Optics* 22(12), p. 121607-121607. doi.10.1117/1.jbo.22.12.121607.
- Oh, D.Y. and Bang, Y.J. 2020. HER2-targeted therapies — a role beyond breast cancer. *Nature Reviews Clinical Oncology* 17(1), p. 33–48. doi.10.1038/s41571-019-0268-3.
- Palm, W. 2019. Metabolic functions of macropinocytosis. *Philosophical Transactions of the Royal Society B: Biological Sciences* 374(1765), p. 20180285. doi.10.1098/rstb.2018.0285.
- Pandey, A. and Jain, D.S. 2015. Poly Lactic-Co-Glycolic Acid (PLGA) Copolymer and Its Pharmaceutical Application. *Handbook of Polymers for Pharmaceutical Technologies* 2(27), p. 151–172. doi.10.1002/9781119041412.ch6.
- Park, S. et al. 2022. High Frequency of Juxtamembrane Domain ERBB2 Mutation in Gastric Cancer. *Cancer Genomics and Proteomics* 19(1), p. 105–112. doi.10.21873/cgp.20307.
- Parodi, A. et al. 2022. Anticancer Nanotherapeutics in Clinical Trials: The Work behind Clinical Translation of Nanomedicine. *International Journal of Molecular Sciences* 23(21), p. 13368. doi.10.3390/ijms232113368.
- Paroni, G. et al. 2019. HER2-positive breast-cancer cell lines are sensitive to KDM5 inhibition: definition of a gene-expression model for the selection of sensitive cases. *Oncogene* 38(15), p. 2675–2689. doi.10.1038/s41388-018-0620-6.
- Patel, S.B. et al. 2015. Profile of panitumumab as first-line treatment in patients with wild-type KRAS metastatic colorectal cancer. *OncoTargets and Therapy* 9(30), p. 75–86. doi.10.2147/OTT.S68558.
- Pelzel, H.R. et al. 2010. Histone H4 deacetylation plays a critical role in early gene silencing during neuronal apoptosis. *BMC Neuroscience* 11(1), p. 1-20. doi.10.1186/1471-2202-11-62.
- Peng, C. et al. 2019. Tuning the In Vivo Transport of Anticancer Drugs Using Renal-Clearable Gold Nanoparticles. *Angewandte Chemie* 58(25), p. 8567–8571. doi.10.1002/ange.201903256.
- Pfeffer, C.M. and Singh, A.T.K. 2018. Apoptosis: A target for anticancer therapy. *International Journal of Molecular Sciences* 19(2), p. 448. doi.10.3390/ijms19020448.

- Pillai, R.N. et al. 2017. HER2 mutations in lung adenocarcinomas: A report from the Lung Cancer Mutation Consortium. *Cancer* 123(21), p. 4099–4105. doi.10.1002/cncr.30869.
- Piccart-Gebhart P. et al. 2005. Trastuzumab after Adjuvant Chemotherapy in HER2-Positive Breast Cancer. *NEngl J Med* 353(16), p. 1659-1672. doi.10.1056/NEJMoa052306
- Pisano, C. et al. 2013. Clinical Trials with Pegylated Liposomal Doxorubicin in the Treatment of Ovarian Cancer. *Journal of Drug Delivery* 2013, p. 1–12. doi.10.1155/2013/898146.
- Pohlmann, P.R. et al. 2009. Resistance to trastuzumab in breast cancer. *Clinical Cancer Research* 15(24), p. 7479–7491. doi.10.1158/1078-0432.CCR-09-0636.
- Prabhuraj, R.S. et al. 2020. Selection of superior targeting ligands using PEGylated PLGA nanoparticles for delivery of curcumin in the treatment of triple-negative breast cancer cells. *Journal of Drug Delivery Science and Technology* 57(1), p. 101722. doi.10.1016/j.jddst.2020.101722.
- Prakash, S. et al. 2022. Bioequivalence of a hybrid pegylated liposomal doxorubicin hydrochloride injection and Caelyx®: A single-dose, randomized, multicenter, open-label, two-period crossover study in patients with advanced ovarian cancer. *European Journal of Pharmaceutical Sciences* 176(1), p. 106248. doi.10.1016/j.ejps.2022.106248.
- Prager, I. et al. 2019. NK cells switch from granzyme B to death receptor-mediated cytotoxicity during serial killing. *Journal of Experimental Medicine* 216(9), p. 2113–2127. doi.10.1084/jem.20181454.
- Preta, G. et al. 2015. Dynasore - Not just a dynamin inhibitor. *Cell Communication and Signaling* 13(1), p. 1–7. doi.10.1186/s12964-015-0102-1.
- Prichard, K.L. et al. 2022. Role of Clathrin and Dynamin in Clathrin Mediated Endocytosis/Synaptic Vesicle Recycling and Implications in Neurological Diseases. *Frontiers in Cellular Neuroscience* 15(18), p. 754110. doi.10.3389/fncel.2021.754110.
- Radford, D.C. et al. 2020. Multivalent HER2-binding polymer conjugates facilitate rapid endocytosis and enhance intracellular drug delivery. *Journal of Controlled Release* 319(10), p. 285–299. doi.10.1016/j.jconrel.2019.12.049.
- Raghav, K.P.S. 2018. The role of HER2 amplification testing in metastatic colorectal cancer. *Clinical Advances in Hematology and Oncology* 16(11), p. 720–722. doi.10.1007/s11888-018-0417-6.
- Raghunand, N. and Gillies, R.J. 2000. pH and drug resistance in tumors. *Drug Resistance Updates* 3(1), p. 39–47. doi.10.1054/drup.2000.0119.
- Rahman, A. et al. 2018. HER2 Expression in Gastric Cancer and Gastroesophageal Junction Cancer. *Journal of Surgical Sciences* 22(2), p. 79–82. doi.10.3329/jss.v22i2.44069.
- Rainone, V. et al. 2016. Immunological characterization of whole tumour lysate-loaded dendritic cells for cancer immunotherapy. *PLoS ONE* 11(1), p. e0146622. doi.10.1371/journal.pone.0146622.
- Recouvreux, M.V. and Commisso, C. 2017. Macropinocytosis: A metabolic adaptation to nutrient stress in cancer. *Frontiers in Endocrinology* 8(261), p. 1–7. doi.10.3389/fendo.2017.00261.

- Rennick, J.J. et al. 2021. Key principles and methods for studying the endocytosis of biological and nanoparticle therapeutics. *Nature Nanotechnology* 16(3), p. 266–276. doi.10.1038/s41565-021-00858-8.
- Rezaei, Z. et al. 2019. Involvement of the dysregulation of miR-23b-3p, miR-195-5p, miR-656-5p, and miR-340-5p in trastuzumab resistance of HER2-positive breast cancer cells and system biology approach to predict their targets involved in resistance. *DNA and cell biology* 38(2), p. 184–192. doi.10.1089/dna.2018.4427.
- Rezvantab, S. et al. 2018. PLGA-based nanoparticles in cancer treatment. *Frontiers in Pharmacology* 9(2), p. 1260. doi.10.3389/fphar.2018.01260.
- Richard, C. and Verdier, F. 2020. Transferrin receptors in erythropoiesis. *International Journal of Molecular Sciences* 21(24), p. 9713. doi.10.3390/ijms21249713.
- Richard, S. et al. 2016. Pertuzumab and trastuzumab: The rationale way to synergy. *Anais- da Academia Brasileira de Ciencias* 88(11), p. 565–577. doi.10.1590/0001-376520162015 0178.
- Rimawi, F. et al. 2019. Low PTEN Levels and PIK3CA Mutations Predict Resistance to Neoadjuvant Lapatinib and Trastuzumab without Chemotherapy in Patients with HER2 Over-Expressing Breast Cancer. *Journal of Adolescent Health* 65(4), p. 139–148. doi.10.1007/s10549-017-4533-9.
- Robinson, P.J. and Holloway, S.L. 2019. Effects of radiotherapy on wound healing. *Journal of the European Wound Management Association* 20(2), p. 25–29. doi.10.35279/jewma20 1910.03.
- Rolver, M.G. et al. 2020. Pyrazine ring-based Na⁺/H⁺ exchanger (NHE) inhibitors potently inhibit cancer cell growth in 3D culture, independent of NHE1. *Scientific Reports* 10(1), p. 1–17. doi.10.1038/s41598-020-62430-z.
- Roskoski, R. 2014. The ErbB/HER family of protein-tyrosine kinases and cancer. *Pharmacological Research* 79(1), p. 34–74. doi.10.1016/j.phrs.2013.11.002.
- Roth, T.F. and Porter, K.R. 1964. Yolk Protein Uptake in the Oocyte of the Mosquito *Aedes Aegypti*. L. *The Journal of cell biology* 20(2), p. 313–332. doi.10.1083/jcb.20.2.313.
- Ryan, S.L. et al. 2016. Drug Discovery Approaches Utilizing Three-Dimensional Cell Culture. *Assay and Drug Development Technologies* 14(1), p. 19–28. doi.10.1089/adt.2015.670.
- Subik, K. et al. 2010. The expression patterns of ER,PR, HER2, CK5/6, EGFR, Ki-67 and AR by Immunohistochemical analysis in breast cancer cell lines. *Breast Cancer: Basic and Clinical Research* 4, p. 35–41. doi.10.1177/117822341000400004.
- Saisana, M. et al. 2016. Importance of the type I insulin-like growth factor receptor in HER2, FGFR2 and MET-unamplified gastric cancer with and without Ras pathway activation. *Oncotarget* 7(34), p. 54445–54462. doi.10.18632/oncotarget.10642.
- Sakhi, M. et al. 2022. Design and Characterization of Paclitaxel-Loaded Polymeric Nanoparticles Decorated With Trastuzumab for the Effective Treatment of Breast Cancer. *Frontiers in Pharmacology* 13, p. 1–15. doi.10.3389/fphar.2022.855294.
- Salari, N. et al. 2022. Polymer-based drug delivery systems for anticancer drugs: A systematic review. *Cancer Treatment and Research Communications* 32(7), p. 100605. doi.10.1016/j.ctarc.2022.100605.

- Salatin, S. and Khosroushahi, A.Y. 2017. Overviews on the cellular uptake mechanism of polysaccharide colloidal nanoparticles Mechanisms of nanoparticle endocytosis. *Journal of cellular and molecular medicine* 21(9), p. 1668–1686. doi.10.1111/jcmm.13110.
- Sánchez, A. et al. 2020. Recent advances in polymeric nanoparticle-encapsulated drugs against intracellular infections. *Molecules* 25(16), p. 1–45. doi.10.3390/molecules25163760.
- Sareyeldin, R.M. et al. 2019. Gene expression and miRNAs profiling: Function and regulation in human epidermal growth factor receptor 2 (HER2)-positive breast cancer. *Cancers* 11(5), p. 646. doi.10.3390/cancers11050646.
- Satpathy, M. et al. 2014. Active targeting using HER-2-affibody-conjugated nanoparticles enabled sensitive and specific imaging of orthotopic HER-2 positive ovarian tumors. *Small* 10(3), p. 544–555. doi.10.1002/smll.201301593.
- Sayers, E.J. et al. 2022. Fluid-Phase Endocytosis and Lysosomal Degradation of Bovine Lactoferrin in Lung Cells. *Pharmaceutics* 14(4), p. 855. doi.10.3390/pharmaceutics14040855.
- Scaltriti, M. et al. 2007. Expression of p95HER2, a truncated form of the HER2 receptor, and response to Anti-HER2 therapies in breast cancer. *Journal of the National Cancer Institute* 99(8), p. 628–638. doi.10.1093/jnci/djk134.
- Schechter, A.L. et al. 1984. The neu oncogene: an erb-B-related gene encoding a 185,000-Mr tumour antigen. *Nature* 312(6), p. 513-516. doi.10.1038/312513a0.
- Schneider, D. et al. 2004. Intracellular acidification by inhibition of the Na⁺/H⁺ -exchanger leads to caspase-independent death of cerebellar granule neurons resembling paraptosis. *Cell Death and Differentiation* 11(7), p. 760–770. doi.10.1038/sj.cdd.4401377.
- Schlam, I. and Swain, S.M. 2021. HER2-positive breast cancer and tyrosine kinase inhibitors: the time is now. *NPJ Breast Cancer* 7(1), p. 56. doi.10.1038/s41523-021-00265-1.
- Schumacher, D. et al. 2018. Nanobodies: Chemical Functionalization Strategies and Intracellular Applications. *Angewandte Chemie - International Edition* 57(9), p. 2314–2333. doi.10.1002/anie.201708459.
- Seaman, M.N.J. 2004. Cargo-selective endosomal sorting for retrieval to the Golgi requires retromer. *Journal of Cell Biology* 165(1), p. 111–122. doi.10.1083/jcb.200312034.
- Shamir, E.R. and Ewald, A.J. 2014. Three-dimensional organotypic culture: Experimental models of mammalian biology and disease. *Nature Reviews Molecular Cell Biology* 15(10), p. 647–664. doi.org/10.1038/nrm3873.
- Shao, C. et al. 2020. Development of Cell Spheroids by Advanced Technologies. *Advanced Materials Technologies* 5(9), p. 1–16. doi.10.1002/admt.202000183.
- Sharma, N. et al. 2010. Various types and management of breast cancer: an overview. *Journal of advanced pharmaceutical technology & research* 1(2), p.109-126. doi. 2010/1/2/109/72251.
- Shah, S. et al. 2021. Exploring the unexplored avenues of surface charge in nanomedicine. *Colloids and Interface Science Communications* 42(3), p. 100406. doi.10.1016/j.colcom.2021.100406.

- Shah, S. et al. 2017. Fluorescence properties of doxorubicin in PBS buffer and PVA films. *Journal of Photochemistry and Photobiology Biology* 170(1), p. 65–69. doi.10.1016/j.jphotobiol.2017.03.024.
- Shete, M.B. et al. 2022. Current trends in theranostic nanomedicines. *Journal of Drug Delivery Science and Technology* 71, p. 103280. doi.10.1016/j.jddst.2022.103280.
- Shi, Y. et al. 2020. The EPR effect and beyond: Strategies to improve tumor targeting and cancer nanomedicine treatment efficacy. *Theranostics* 10(17), p. 7921–7924. doi.10.7150/thno.49577.
- Shi, J. et al. 2017. Cancer nanomedicine : progress , challenges and opportunities. *Nature Publishing Group* 17(1), p. 20-37. doi.10.1038/nrc.2016.108.
- Shi, L. et al. 2021. Effects of polyethylene glycol on the surface of nanoparticles for targeted drug delivery. *Nanoscale* 13(24), p. 10748–10764. doi.10.1039/d1nr02065j.
- Shimosaki, S. et al. 2017. Development of a complete human IgG monoclonal antibody to transferrin receptor 1 targeted for adult T-cell leukemia/lymphoma. *Biochemical and Biophysical Research Communications* 485(1), p. 144–151. doi.10.1016/j.bbrc.2017.02.039.
- Shipunova, V.O. et al. 2021. PLGA Nanoparticles decorated with anti-HER2 affibody for targeted delivery and photoinduced cell death. *Molecules*, 26(13), p. 3955. doi.10.3390/molecules26133955.
- Shramova, E.I. et al. 2018. The Cause of ErbB2 Receptor Resistance to Downregulation. *Russian Journal of Bioorganic Chemistry* 44(3), p. 279-288. doi.10.1134/S1068162018030147.
- Sikorski, A.F. et al. 2015. Toward a magic or imaginary bullet? Ligands for drug targeting to cancer cells: principles, hopes, and challenges. *International Journal of Nanomedicine* 10, p. 1316–1399. doi.10.2147/IJN.S74514.
- Sindhwani, S. et al. 2020. The entry of nanoparticles into solid tumours. *Nature Materials* 19(5), p. 566–575. doi.org/10.1038/s41563-019-0566-2.
- Sorkina, T. et al. 2013. Flotillins Regulate Membrane Mobility of the Dopamine Transporter but Are Not Required for Its Protein Kinase C Dependent Endocytosis. *Traffic* 14(6), p. 709-724. doi.10.1111/tra.12059.
- Soundararajan, A. et al. 2009. Liposomal doxorubicin (Doxil): in vitro stability, pharmacokinetics, imaging and biodistribution in a head and neck squamous cell carcinoma xenograft model. *Nuclear Medicine and Biology* 36(5), p. 515–524. doi.10.1016/j.nucmedbio.2009.02.004.
- Stack, T. et al. 2021. Enhancing subcutaneous injection and target tissue accumulation of nanoparticles: Via co-administration with macropinocytosis inhibitory nanoparticles (MiNP). *Nanoscale Horizons* 6(5), p. 393–400. doi.10.1039/d0nh00679c.
- Su, H. et al. 2022. A brightly red emissive AIEgen and its antibody conjugated nanoparticles for cancer cell targeting imaging. *Materials Chemistry Frontiers* 6(10), p. 1317–1323. doi.10.1039/d2qm00273f.
- Sugden, P.H. 2003. An overview of endothelin signaling in the cardiac myocyte. *Journal of Molecular and Cellular Cardiology* 35(8), p. 871–886. doi.10.1016/S0022-2828(03)00153-6.

- Suk, J.S. et al. 2016. PEGylation as a strategy for improving nanoparticle-based drug and gene delivery. *Advanced Drug Delivery Reviews* 99(1), p. 28–51. doi.10.1016/j.addr.2015.09.012.
- Sultan, M.H. et al. 2022. Characterization of cisplatin-loaded chitosan nanoparticles and rituximab-linked surfaces as target-specific injectable nano-formulations for combating cancer. *Scientific Reports* 12(1), p. 1–16. doi.10.1038/s41598-021-04427-w.
- Sun, T. et al. 2014. Engineered nanoparticles for drug delivery in cancer therapy. *Angewandte Chemie - International Edition* 53(46), p. 12320–12364. doi.10.1002/anie.201403036.
- Sung, H. et al. 2021. Global Cancer Statistics 2020: GLOBOCAN Estimates of Incidence and Mortality Worldwide for 36 Cancers in 185 Countries. *A Cancer Journal for Clinicians* 71(3), p. 209–249. doi.10.3322/caac.21660.
- Swanson, J.A. et al. 2019. The breadth of macropinocytosis research. *Philosophical Transactions of the Royal Society B* 374(1765), p. 20180146. doi.10.1098/rstb.2018.0146.
- Szymanska, M. et al. 2016. A combination of two antibodies recognizing non-overlapping epitopes of HER2 induces kinase activity-dependent internalization of HER2. *Journal of Cellular and Molecular Medicine* 20(10), p. 1999–2011. doi.10.1111/jcmm.12899.
- Tabuchi, M. et al. 2000. Human NRAMP2/DMT1, which mediates iron transport across endosomal membranes, is localized to late endosomes and lysosomes in HEp-2 cells. *Journal of Biological Chemistry* 275(29), p. 22220–22228. doi.10.1074/jbc.M001478200.
- Talukder, J. 2021. Role of transferrin: an iron-binding protein in health and diseases. *Nutraceuticals* 1(1), p. 1011–1025. doi.10.1016/B978-0-12-821038-3.00060-4
- Tao, Z.Q. et al. 2015. Breast Cancer: Epidemiology and Etiology. *Cell Biochemistry and Biophysics* 72(2), p. 333–338. doi.10.1007/s12013-014-0459-6.
- Tarantino, P. et al. 2021. Margetuximab for the treatment of HER2-positive metastatic breast cancer. *Expert Opinion on Biological Therapy* 21(2), p. 127–133. doi.10.1080/14712598.2021.1856812.
- Tashima, T. 2018. Bioorganic & Medicinal Chemistry Letters Effective cancer therapy based on selective drug delivery into cells across their membrane using receptor-mediated endocytosis. *Bioorganic & Medicinal Chemistry Letters* 28(18), p. 3015–3024. doi.10.1016/j.bmcl.2018.07.012.
- Tejeda-Muñoz, N. et al. 2019. Wnt canonical pathway activates macropinocytosis and lysosomal degradation of extracellular proteins. *Proceedings of the National Academy of Sciences of the United States of America* 116(21), p. 10402–10411. doi.10.1073/pnas.1903506116.
- Theos, A.C. et al. 2005. Functions of adaptor protein (AP)-3 and AP-1 in tyrosinase sorting from endosomes to melanosomes. *Molecular Biology of the Cell* 16, p. 5356–5372. doi.10.1091/mbc.E05.
- Thierry, B. et al. 2010. Herceptin functionalized microfluidic polydimethylsiloxane devices for the capture of human epidermal growth factor receptor 2 positive circulating breast cancer cells. *Biomicrofluidics*, 4(3), p. 032205. doi.10.1063/1.3480573.
- Tomas, A. et al. 2014. EGF receptor trafficking: Consequences for signaling and cancer. *Trends in Cell Biology* 24(1), p. 26–34. doi.10.1016/j.tcb.2013.11.002.

- Tormo, E. et al. 2017. The role of miR-26a and miR-30b in HER2 + breast cancer trastuzumab resistance and regulation of the CCNE2 gene. *Scientific reports* 7(1), p. 1-9. doi.10.1038/srep41309.
- Torres-López, J.E. et al. 2013. Role of NHE1 in nociception. *Pain Research and Treatment*, p. 10–13. doi.10.1155/2013/217864.
- Tomasetti, C. et al. 2017. Stem cell divisions, somatic mutations, cancer etiology, and cancer prevention. *Science* 355(6331), p. 1330-1334. doi.10.1126/science.aaf9011.
- Toporkiewicz, M. et al. 2015. Toward a magic or imaginary bullet? Ligands for drug targeting to cancer cells: principles, hopes, and challenges. *International journal of nanomedicine* 10, p. 1316–1399. doi.10.2147/IJN.S74514.
- Tortorella, S. and Karagiannis, T.C. 2014. Transferrin Receptor-Mediated Endocytosis : A Useful Target for Cancer Therapy. *The Journal of membrane biology* 247(4), p. 291–307. doi.10.1007/s00232-014-9637-0.
- Toss, A. and Cristofanilli, M. 2015. Molecular characterization and targeted therapeutic approaches in breast cancer. *Breast Cancer Research* 17(1), p. 1–11. doi.10.1186/s13058-015-0560-9
- Treffers, L.W. et al. 2019. FcγRIIIb restricts antibody-dependent destruction of cancer cells by human neutrophils. *Frontiers in Immunology* 10(9), p. 1–13. doi.10.3389/fimmu.2018.03124.
- Trenker, R. and Jura, N. 2020. Receptor tyrosine kinase activation: From the ligand perspective. *Current Opinion in Cell Biology* 63, p. 174–185. doi.10.1016/j.ceb.2020.01.016.
- Trofimenko, E. et al. 2021. The endocytic pathway taken by cationic substances requires Rab14 but not Rab5 and Rab7. *Cell Reports* 37(5), p. 109945. doi.10.1016/j.celrep.2021.109945.
- Truffi, M. et al. 2018. Multivalent exposure of trastuzumab on iron oxide nanoparticles improves antitumor potential and reduces resistance in HER2-positive breast cancer cells. *Scientific Reports* 8(1), p. 1-11. doi.10.1038/s41598-018-24968-x.
- Turecek, P.L. et al. 2016. PEGylation of Biopharmaceuticals: A Review of Chemistry and Nonclinical Safety Information of Approved Drugs. *Journal of Pharmaceutical Sciences* 105(2), p. 460–475. doi.10.1016/j.xphs.2015.11.015.
- Twaites, B. et al. 2005. Synthetic polymers as drugs and therapeutics. *Journal of Materials Chemistry* 15(4), p. 441–455. doi.10.1039/b410799n.
- Valabrega, G. et al. 2007. Trastuzumab: Mechanism of action, resistance and future perspectives in HER2-overexpressing breast cancer. *Annals of Oncology* 18(6), p. 977–984. doi.10.1093/annonc/mdl475.
- Van Zundert, I. et al. 2020. From 2d to 3d cancer cell models the enigmas of drug delivery research. *Nanomaterials* 10(11), p. 1–30. doi.10.3390/nano10112236.
- Vanderhoeven, F. et al. 2018. Synergistic antitumor activity by combining trastuzumab with retinoic acid in HER2 positive human breast cancer cells. *Oncotarget* 9(41), p. 26527–26542. doi.10.18632/oncotarget.25480.
- Vanlandingham, P.A. and Ceresa, B.P. 2009. Rab7 regulates late endocytic trafficking downstream of multivesicular body biogenesis and cargo sequestration. *Journal of Biological Chemistry* 284(18), p. 12110–12124. doi.10.1074/jbc.M809277200.

- Varshney, S. et al. 2020. Role and significance of HER-2/neu as a biomarker in the premalignant and malignant lesions of uterine cervix. *Annals of Diagnostic Pathology* 45(1), p. 151443. doi.10.1016/j.anndiagpath.2019.151443.
- Veithen, A. et al. 1996. v-Src induces constitutive macropinocytosis in rat fibroblasts. *Journal of Cell Science* 109(8), p. 2005–2012. doi.10.1242/jcs.109.8.2005.
- Velasco, V. et al. 2020. Microtechnology-based methods for organoid models. *Microsystems and Nanoengineering* 6(1). p. 76. doi.10.1038/s41378-020-00185-3.
- Verma, S. et al. 2012. Trastuzumab emtansine for HER2-positive advanced breast cancer. *The New England journal of medicine* 367(19), p. 1783-1791. doi.10.1056/NEJMoa1209124.
- Vidt, D.G. 1981. Mechanism of Action, Pharmacokinetics, Adverse Effects, and Therapeutic Uses of Amiloride Hydrochloride, A New Potassium-Sparing Diuretic. *Pharmacotherapy: The Journal of Human Pharmacology and Drug Therapy* 1(3), p. 179–187. doi.10.1002/j.1875-9114.1981.tb02539.x.
- Visovsky, C. 2014. Treatment Considerations for the Management of Patients With Hormone Receptor-Positive Metastatic Breast Cancer. *Journal of the advanced practitioner in oncology* 5(5), p. 321–330. doi.10.6004/jadpro.2014.5.5.2.
- Vollrath, A. et al. 2013. A toolbox of differently sized and labeled PMMA nanoparticles for cellular uptake investigations. *Soft Matter* 9(1), p. 99–108. doi.10.1039/c2sm26928g.
- Von Hoff, D.D. et al. 2016. Phase I study of PSMA-targeted docetaxel-containing nanoparticle BIND-014 in patients with advanced solid tumors. *Clinical Cancer Research* 22(13), p. 3157–3163. doi.10.1158/1078-0432.CCR-15-2548.
- Wahdan-Alaswad, R. et al. 2020. Targeted lapatinib anti-HER2/ErbB2 therapy resistance in breast cancer: opportunities to overcome a difficult problem. *Cancer Drug Resistance* 3(2), p. 179. doi.10.20517/cdr.2019.92.
- Waks, A.G. and Winer, E.P. 2019. Breast Cancer Treatment: A Review. *JAMA - Journal of the American Medical Association* 321(3), p. 288–300. doi.10.1001/jama.2018.19323.
- Walsh, M.F. et al. 2016. Genomic biomarkers for breast cancer risk. *Novel Biomarkers in the Continuum of Breast Cancer* 882(1), p. 1-32. doi.10.1007/978-3-319-22909-6_1.
- Wang, J. et al. 2016. Human epidermal growth factor receptor 4 (HER4) is a favorable prognostic marker of breast cancer: a systematic review and meta-analysis. *Oncotarget* 7(47), p. 76693- 76703. doi.10.18632/oncotarget.12485
- Wang, J. et al. 2018. Cellular stress response mechanisms of *Rhizoma coptidis*: A systematic review. *Chinese Medicine* 13(1), p. 1–14. doi.10.1186/s13020-018-0184-y.
- Wang, J. and Xu, B. 2019. Targeted therapeutic options and future perspectives for her2-positive breast cancer. *Signal Transduction and Targeted Therapy* 4(1), p. 34. doi.10.1038/s41392-019-0069-2.
- Wang, H. et al. 2019. Infectious bronchitis virus entry mainly depends on clathrin mediated endocytosis and requires classical endosomal/lysosomal system. *Virology* 528(1), p. 118–136. doi.10.1016/j.virol.2018.12.012.
- Wang, W. et al. 2019. HER2 decreases drug sensitivity of ovarian cancer cells via inducing stem cell-like property in an NFκB-dependent way. *Bioscience Reports* 39(3), p. 1–12. doi.10.1042/BSR20180829.

- Wang, W. et al. 2019. The impact of nanoparticle shape on cellular internalisation and transport: What do the different analysis methods tell us?. *Materials Horizons* 6(8), p. 1538–1547. doi.10.1039/c9mh00664h.
- Wang, X. et al. 2021. Prediction of BRCA Gene Mutation in Breast Cancer Based on Deep Learning and Histopathology Images. *Frontiers in Genetics* 12(7), p. 1–12. doi.10.3389/fgene.2021.661109.
- Watanabe, S. et al. 2019. Targeting of the HER2/HER3 signaling axis overcomes ligand-mediated resistance to trastuzumab in HER2-positive breast cancer. *Cancer Medicine* 8(3), p. 1258–1268. doi.10.1002/cam4.1995.
- Watanabe, S. et al. 2017. Fast and ultrafast endocytosis. *Current opinion in cell biology* 47(1), p. 64–71. doi.10.1016/j.ceb.2017.02.013.
- Wee, P. and Wang, Z. 2017. Epidermal growth factor receptor cell proliferation signaling pathways. *Cancers* 9(5), p. 1–45. doi.10.3390/cancers9050052.
- Weinberg, J. and Drubin, D.G. 2012. Clathrin-mediated endocytosis in budding yeast. *Trends in cell biology* 22(1), p. 1–13. doi.10.1016/j.tcb.2011.09.001.
- Weissenstein, U. et al. 2016. Interaction of a standardized mistletoe (*Viscum album*) preparation with antitumor effects of Trastuzumab in vitro. *BMC Complementary and Alternative Medicine* 16(1), p. 1–10. doi.10.1186/s12906-016-1246-2.
- Weissman, A.M. et al. 1986. Exposure of K562 cells to anti-receptor monoclonal antibody OKT9 results in rapid redistribution and enhanced degradation of the transferrin receptor. *Journal of Cell Biology* 102(3), p. 951–958. doi.10.1083/jcb.102.3.951.
- Wei, H. et al. 2017. Structural basis of a novel heterodimeric Fc for bispecific antibody production. *Oncotarget* 8(31), p. 51037. doi.10.18632/oncotarget.17558.
- Welker, R.W. 2011. Size Analysis and Identification of Particles. *Developments in Surface Contamination and Cleaning* 4(1). p. 179–213. doi.10.1016/B978-1-4377-7883-0.00004-3.
- West, M.A. et al. 1989. Distinct endocytotic pathways in epidermal growth factor-stimulated human carcinoma A431 cells. *Journal of Cell Biology* 109(6), p. 2731–2739. doi.10.1083/jcb.109.6.2731.
- Willhelm, S. et al. 2016. Analysis of nanoparticle delivery to tumours. *Nature Reviews Materials* 1(5), p. 16014. doi.10.1038/natrevmats.2016.14.
- Willis, O. et al. 2020. PIK3CA gene aberrancy and role in targeted therapy of solid malignancies. *Cancer Gene Therapy* 27(9), p. 634–644. doi.org/10.1038/s41417-020-0164-0.
- Wind, N.S. and Holen, I. 2011. Multidrug Resistance in Breast Cancer: From In Vitro Models to Clinical Studies. *International Journal of Breast Cancer* 2011(10), p. 1–12. doi.10.4061/2011/967419.
- Wiranowska, M. et al. 2011. Clathrin-mediated entry and cellular localization of chlorotoxin in human glioma. *Cancer Cell International* 11(1), p. 1–13. doi.10.1186/1475-2867-11-27.
- Wolfram, J. et al. 2015. Safety of nanoparticles in medicine. *Current drug targets* 16(14), p. 1671–1681. doi.10.2174/1389450115666140804124808.
- Wong, P. et al. 2002. Cytostatic potential of novel agents that inhibit the regulation of intracellular pH. *British Journal of Cancer* 87(2), p. 238–245. doi.10.1038/sj.bjc.6600424.

- Wu, G. et al. 2021. A novel humanized MUC1 antibody-drug conjugate for the treatment of trastuzumab-resistant breast cancer. *Acta biochimica et biophysica Sinica* 53(12), p. 1625–1639. doi.10.1093/abbs/gmab141.
- Wu, J. et al. 2022. Case Report: Durable Clinical Response to Third-Line Pyrotinib After Resistance to Trastuzumab in a Gastric Cancer Patient. *Frontiers in Oncology* 11(27), p. 1–4. doi.10.3389/fonc.2021.780577.
- Wu, J. et al. 2022. Trastuzumab therapies in human epidermal growth factor receptor 2 cancer. *Engineering and Technology* 8(17), p. 32-40. doi.10.54097/hset.v8i.1107.
- Wu, H.J. and Chu, P.Y. 2021. Recent discoveries of macromolecule-and cell-based biomarkers and therapeutic implications in breast cancer. *International Journal of Molecular Sciences* 22(2), p. 1–43. doi.10.3390/ijms22020636.
- Wu, W. et al. 2018. Endogenous pH-responsive nanoparticles with programmable size changes for targeted tumor therapy and imaging applications. *Theranostics* 8(11), p. 3038–3058. doi.10.7150/thno.23459.
- Wymant, J.M. et al. 2020. Strategic trastuzumab mediated crosslinking driving concomitant HER2 and HER3 endocytosis and degradation in breast cancer. *Journal of Cancer* 11(11), p. 3288–3302. doi.10.7150/jca.32470.
- Xiao, F. et al. 2021. Macropinocytosis: mechanism and targeted therapy in cancers. *American journal of cancer research* 11(1), p. 14–30. doi.2156-6976/ajcr0122379.
- Xu, Z. et al. 2019. Novel HER2-Targeting Antibody-Drug Conjugates of Trastuzumab Beyond T-DM1 in Breast Cancer: Trastuzumab Deruxtecan(DS-8201a) and (Vic-)Trastuzumab Duocarmazine (SYD985). *European Journal of Medicinal Chemistry* 183(1), p. 111682. doi.10.1016/j.ejmech.2019.111682.
- Yamaoka, T. et al. 2018. Receptor tyrosine kinase-targeted cancer therapy. *International Journal of Molecular Sciences* 19(11), p. 1–35. doi.10.3390/ijms19113491.
- Yang, L. et al. 2017. NRG1-dependent activation of HER3 induces primary resistance to trastuzumab in HER2-overexpressing breast cancer cells. *International Journal of Oncology* 51(5), p. 1553–1562. doi.10.3892/ijo.2017.4130.
- Yang, T. et al. 2022. Targeting Design of Nanoparticles in Tumor Therapy. *Pharmaceutics* 14(9), p. 1919. doi. 10.3390/pharmaceutics14091919.
- Yang, X. et al. 2010. Inhibition of Na⁺/H⁺ exchanger 1 by 5-(N-ethyl-N-isopropyl) amiloride reduces hypoxia-induced hepatocellular carcinoma invasion and motility. *Cancer Letters* 295(2), p. 198–204. doi.10.1016/j.canlet.2010.03.001.
- Yarden, Y. and Sliwkowski, M.X. 2001. Untangling the ErbB signalling network. *Nature reviews Molecular Cell Biology* 2(2), p. 127–137. doi.10.1038/35052073.
- Yeh, C.Y. et al. 2016. Peptide-conjugated nanoparticles for targeted imaging and therapy of prostate cancer. *Biomaterials* 99(1), p. 1–15. doi.10.1016/j.biomaterials.2016.05.015.
- Yerushalmi, R. et al. 2010. Ki67 in breast cancer: prognostic and predictive potential. *The Lancet Oncology* 11(2), p. 174–183. doi.10.1016/S1470-2045(09)70262-1.
- Yokoyama, D. et al. 2021. PTEN is a predictive biomarker of trastuzumab resistance and prognostic factor in HER2-overexpressing gastroesophageal adenocarcinoma. *Scientific Reports* 11(1), p. 1–12. doi.10.1038/s41598-021-88331-3.

- Yoo, D.Y. et al. 2020. Macropinocytosis as a Key Determinant of Peptidomimetic Uptake in Cancer Cells. *Journal of the American Chemical Society* 142(34), p. 14461-14471. doi.10.1021/jacs.0c02109.
- Yousefpour, P. et al. 2011. Targeted delivery of doxorubicin-utilizing chitosan nanoparticles surface-functionalized with anti-Her2 trastuzumab. *International journal of nanomedicine* 6(14), p. 1977–1990. doi.10.2147/ijn.s21523.
- Yuan, H. et al. 2020. Albumin Nanoparticle of Paclitaxel (Abraxane) Decreases while Taxol Increases Breast Cancer Stem Cells in Treatment of Triple Negative Breast Cancer. *Molecular Pharmaceutics* 17(7), p. 2275–2286. doi.10.1021/acs.molpharmaceut.9b01221.
- Yu, K. et al. 2016. Comparison of three different conjugation strategies in the construction of herceptin-bearing paclitaxel-loaded nanoparticles. *Biomaterials science* 4(8), p. 1219-1232. doi.10.1039/c6bm00308g.
- Yu, K. et al. 2016. Enhanced delivery of Paclitaxel using electrostatically-conjugated Herceptin-bearing PEI/PLGA nanoparticles against HER-positive breast cancer cells. *International Journal of Pharmaceutics* 497(1–2), p. 78–87. doi.10.1016/j.ijpharm.2015.11.033.
- Yu, X. et al. 2017. Targeting EGFR/HER2 heterodimerization with a novel anti-HER2 domain II/III antibody. *Molecular Immunology* 87, p. 300–307. doi.10.1016/j.molimm.2017.05.010.
- Zeng, C. et al. 2020. Formulation and Delivery Technologies for mRNA Vaccines. *Current Topics in Microbiology and Immunology*, p. 71-110. doi.10.1007/82_2020_217.
- Zhao, J. and Stenzel, M.H. 2018. Entry of nanoparticles into cells: The importance of nanoparticle properties. *Polymer Chemistry* 9(3), p. 259–272. doi.10.1039/c7py01603d.
- Zhang, B. et al. 2017. Shape dependent cytotoxicity of PLGA-PEG nanoparticles on human cells. *Scientific Reports* 7(1), p. 1–8. doi.10.1038/s41598-017-07588-9.
- Zhang, W. et al. 2019. Amphiphilic Tetraphenylethene-Based Pyridinium Salt for Selective Cell-Membrane Imaging and Room-Light-Induced Special Reactive Oxygen Species Generation. *ACS Applied Materials and Interfaces* 11(11), p. 10567–10577. doi.10.1021/acsami.9b00643.
- Zhang, P. et al. 2022. Charge reversal nano-systems for tumor therapy. *Journal of Nanobiotechnology* 20(1), p. 1–27. doi.10.1186/s12951-021-01221-8.
- Zhang, X. et al. 2019. Trastuzumab-Coated Nanoparticles Loaded With Docetaxel for Breast Cancer Therapy. *Dose-Response* 17(3), p. 1–12. doi.10.1177/1559325819872583.
- Zhong, S. et al. 2020. Herceptin-decorated paclitaxel-loaded poly(lactide-co-glycolide) nanobubbles: ultrasound-facilitated release and targeted accumulation in breast cancers. *Pharmaceutical Development and Technology* 25(4), p. 454–463. doi.10.1080/10837450.2019.1709500.
- Zhong, S. et al. 2020. poly (lactide- co -glycolide) nanobubbles : ultrasound-facilitated release and targeted accumulation in breast cancers. *Pharmaceutical Development and Technology* 25(4), p. 454–463. doi.10.1080/10837450.2019.1709500.
- Zhou, Z. et al. 2015. Herceptin conjugated PLGA-PHis-PEG pH sensitive nanoparticles for targeted and controlled drug delivery. *International Journal of Pharmaceutics* 487(1–2), p. 81–90. doi.10.1016/j.ijpharm.2015.03.081.

Zielińska, A. et al. 2020. Polymeric nanoparticles: production, characterization, toxicology and ecotoxicology. *Molecules* 25(16), p. 3731. doi.10.3390/molecules25163731.

Appendix

Appendix A: Routinely method for ImageJ software:

Captured images were processed using ImageJ software. The image was split into the separate channel using the following command image> color > split channels, and then merged channels were followed next command Image> color > merge channels. The images were then converted to a stack using commands stk > convert images to stack. Following commands then added scale bar analyse > tools > Scale bar. The final step is to proceed with the images by following commands Stk > Make montage.

Appendix B: Standard Curve to determine DOX encapsulation efficiency (%EE) in PLGA NPs

The concentration of DOX in PLGA was determined using a standard curve prepared with known DOX concentrations ranging from 0 mg/mL to 1 mg/mL DOX standard concentration was first dissolved in 0.5% of DMSO (5 μ L) and then added 99.5% of dH₂O (995 μ L). PLGA encapsulated DOX NPs in 1mL of dH₂O was first centrifuged at 15000 xg for 15 mins, and the supernatant was aspirated. PLGA-DOX was then dissolved in 0.5% of DMSO (5 μ L), and 99.5% of dH₂O (995 μ L) was then added. This solution (200 μ L) was added in triplicate to a 96-well transparent plate. To generate a calibration curve, absorbance readings at 488 were plotted using DOX at 0 mg/mL to 1 mg/mL The formula in figure appendix B was used to calculate the encapsulation efficiency (EE%) followed the next studies (Colzani et al. 2018; Li et al. 2019). Based on the concentration of DOX in NPs that was identified from the standard curve (0.43 mg/mL). Cells were incubated with either 2 μ M free drug or in DOX the NP (Choi et al. 2020).

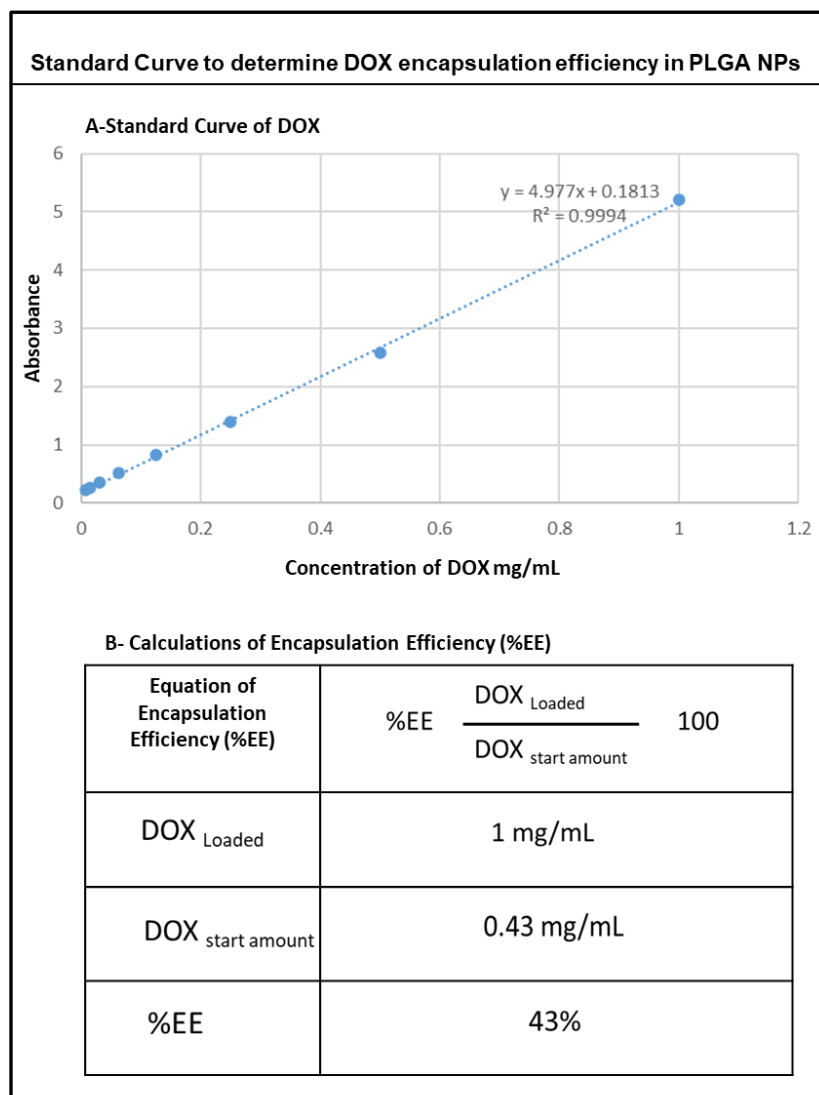


Figure B: The calculations of DOX concentration in PLGA NPs. A- Serial dilution of DOX concentration was made to develop the standard curve of DOX and to calculate the weight of DOX in PLGA NPs. B- The equation and calculation were used to figure out the DOX %EE (Encapsulation Efficiency) in PLGA NPs.

Appendix C: Calculating Pearson's coefficient for colocalisation

The image was opened using ImageJ software. The image was split into separate channels using the following command image> color > split channels. The slice of DOX and Hoechst were selected for colocalisation analysis using the next command plugins>jacop> Image A is green (DOX); Image B is blue (Hoechst)>OK. Cytofluorogram was edited and used next command More> Contents style > Change Color to black, symbol to dot >OK. Cytofluorogram was saved for reference.